Mutations in V-ATPase assembly factors cause Congenital Disorder of Glycosylation (CDG) with autophagic liver disease

Magda Cannata Serio

UNIVERSITÉ PARIS DESCARTES

École Doctorale Bio Sorbonne Paris Cité

Mutations in V-ATPase assembly factors cause Congenital Disorder of Glycosylation (CDG) with autophagic liver disease

Magda CANNATA SERIO

Defense date - 7th May 2019

Jury panel:

Prof. Thomas BRAULKE - UKE Hamburg
Dr. Frank LAFONT - University of Lille
Dr. Arnaud BRUNEEL - University Paris Sud
Dr. Fabienne FOUFELLE - University Paris Descartes
Dr. Etienne MOREL - University Paris Descartes
Dr. Matias SIMONS - University Paris Descartes

UNIVERSITÉ PARIS DESCARTES

École Doctorale Bio Sorbonne Paris Cité

Mutations in V-ATPase assembly factors cause Congenital Disorder of Glycosylation (CDG) with autophagic liver disease

Magda CANNATA SERIO

Defense date - 7th May 2019

Jury panel:

Prof. Thomas BRAULKE - UKE Hamburg
Dr. Frank LAFONT - University of Lille
Dr. Arnaud BRUNEEL - University Paris Sud
Dr. Fabienne FOUFELLE - University Paris Descartes
Dr. Etienne MOREL - University Paris Descartes
Dr. Matias SIMONS - University Paris Descartes

In life one must never resign,
never surrender to mediocrity,
but instead get out of the grey zone
in which everything is habit
and passive resignation.
One must cultivate the courage to rebel.

Rita Levi Montalcini

Table of Contents

Contents

List of Figures

List of Figures

List of Tables

List of Tables

List of Abbreviations

List of Abbreviations

4EBP1	4E-binding protein 1
ALP	Alkaline phosphatase
ALT	Alanine aminotransferase
AP-MS	Affinity-purification mass spectrometry
AST	Aspartate aminotransferase
Atg	Autophagy-related genes
ATP6AP1	ATPase H^+ transporting accessory protein 1
ATP6AP2	ATPase H^+ transporting accessory protein 2
CCDC115	Coiled-coil domain containing 115
CDG	Congenital disorder of glycosylation
CK	Creatine kinase
COP I/II	Coat protein I/II
CTSB/CTSD	Cathepsin proteases B and D
CTF	C-terminal fragment
DGAT	Diacylglycerol acyltransferase
ECD	Extracellular domain
ER	Endoplasmic reticulum
ERAD	ER-associated degradation
ERGIC	ER-Golgi intermediate compartment
ERK	Extracellular signal-regulated kinases
FL	Full-length
Fz	Frizzled
HDL	High-density lipoprotein
HPLC	High performance liquid chromatography
HRP	Handle region peptide
HSP	Heat shock protein
IEF	Isoelectric focusing
LAMP	Lysosome associated membrane protein
LC3	Microtubule-associated protein light chain 3
LDH	Lactate dehydrogenase
LDL	Low density lipoprotein

LDL-C	Low density lipoprotein (LDL) cholesterol
LDs	Lipid droplets
LRP5/6	Low-density lipoprotein receptor-related protein 5/6
MALDI	Matrix-assisted laser desorption/ionization
MAPK	Mitogen-activated protein kinases
mTORC1	Mammalian target of rapamycin complex 1
NAFLD	Non alcoholic fatty liver disease
NTF	N-terminal fragment
p62	Ubiquitin-binding protein p62
PCP	Planar cell polarity pathway
PERK	Protein kinase R (PKR)-like endoplasmic reticulum kinase
Pkr1p	Pichia farnosiakiller toxin resistance
PLZF	Promyelocytic leukaemia zinc finger protein 1
PMD	Psychomotor disease
PRR	Prorenin receptor
RAAS	Renin angiotensin-aldosterone system
RAS	Renin angiotensin system
RAVE	Regulator of ATPase of vacuoles and endosomes
s(P)RR	Soluble prorenin receptor
S6K1	S6 kinase 1
S1P	Site-1 protease
SNARE	Soluble N-ethylmaleimide-sensitive factor attachment protein receptors
SP	Signal peptide
SREBP	Sterol response-element binding protein
TGF-β1	Transforming growth factor-β1
TGN	*Trans*-Golgi network
TM	Transmembrane
TMEM199	Transmembrane protein 199
UPR	Unfolded protein response
UTR	Untranslated region
V-ATPase	Vacuolar H^+-ATPase
vma	Vacuolar membrane ATPase
Voa1p	V_0 assembly protein 1
WD	Wilson's disease
XMEA	X-linked myopathy with excessive autophagy
Y2H	Yeast two-hybrid

Abstract

Abstract

The V-ATPase is a large complex involved in the acidification of intracellular organelles. It is formed by a proton pore (V_0 domain) and an ATP hydrolysis domain (V_1 domain). Pioneering studies in *Saccharomyces cerevisiae* have shown that the assembly of the V_0 domain occurs in the endoplasmic reticulum (ER) under the guidance of five assembly factors: Vma21p, Vma12p, Vma22p, Pkr1p and Voa1p. The newly assembled V_0 sector is then escorted by Vma21p to the *cis*-Golgi, where it will bind the preassembled V_1 domain to constitute a functional holoenzyme. How the assembly works in mammalian systems is currently still unclear. Yet, it was recently shown that all the assembly factors, except Pkr1p, are conserved in mammals and that mutations in three of them, *ATP6AP1*, *TMEM199* and *CCDC115*, were identified to cause a new subgroup of congenital disorders of glycosylation (CDG) in humans. Using human genetics and functional validation, I identify in the first part of my thesis a novel mammalian assembly factor called *ATP6AP2* that causes a similar CDG-like disease when mutated. Apart from glycosylation defects, patients with missense mutations in *ATP6AP2* show steatotic liver disease, cognitive defects and immune defects. Previously exon-skipping mutations in *ATP6AP2* had been associated with a late onset cerebral disease, including Parkinsonism and epilepsy. Our work revealed that ATP6AP2 missense mutations lead to defective V-ATPase activity, subsequently causing reduced organellar acidification, lysosomal degradation and autophagic flux. Because of this, clearance of lipid droplets cannot take place in the autolysosomes, giving rise to the steatotic phenotype in the patients hepatocytes. Consistent with the similar clinical phenotype, we found that ATP6AP2 interacts with V_0 assembly factors, while the missense mutations reduced this interaction, suggesting a compromised V-ATPase assembly in the patients. By contrast, in patients with exon-skipping mutation we found normal glycosylation of serum proteins as well no effect on the interaction between ATP6AP2 and ATP6AP1, suggesting that the missense mutations have a stronger impact on overall ATP6AP2 function than the exon-skipping ones. These results shed light on the V-ATPase assembly in the ER and suggest that ATP6AP2 is an additional mammalian member of the assembly factors group.

In the second part of my thesis, I demonstrate that mutations in *VMA21* also cause CDG with liver disease. Previously, mutations of *VMA21* had been associated with a X-linked myopathy with excessive autophagy (XMEA), characterized by progressive vacuolation and atrophy of skeletal muscle. Yet, we were able to identify *VMA21* mutations

with a similar clinical phenotype compared to the other V-ATPase assembly factors deficiencies. Using patient fibroblasts, we tested the functional impact of the newly identified *VMA21* mutations on V-ATPase assembly and function, with the attempt to highlight the differences with the XMEA ones. First, we could show that VMA21 mutations are hypomorphic and reduce both VMA21 mRNA and protein expression. Second, VMA21 mutations cause autophagic defects with decreased lipid droplet degradation, similar to those observed in ATP6AP2-deficient cells. Finally, patients fibroblasts showed an accumulation of unesterified cholesterol in vesicular structures, similar to what has been reported for the lysosomal storage disease Niemann-Pick type C (NPC). The sequestration of cholesterol in lysosomes triggers lipogenic pathways mediated by the sterol response element-binding protein (SREBP), most likely leading to elevated serum cholesterol levels in the patients. Altogether, our results show that V-ATPase deficiencies are a novel group of metabolic syndromes that affect lysosomal/autophagic homeostasis. Studying these rare V-ATPase assembly disorders, that are featured by liver steatosis as a unifying pathology, may lead to a better understanding of the pathogenesis of non-alcoholic fatty liver disease (NAFLD), which is a common problem in metabolic syndrome.

Introduction

Chapter 1

The V-ATPase

The vacuolar (H+)-ATPases, or V-ATPases, are a family of ATP-dependent proton pumps, present in almost all the eukaryotic cells, involved in the acidification of intracellular compartments and in the transport of protons from the cytoplasm to the extracellular space (**Nelson, 2003; Forgac, 2007; Kane, 2012; Breton *et al.*, 2013; Sun-Wada *et al.*, 2013; Marshansky *et al.*, 2014; Cotter *et al.*, 2015**). The V-ATPases are multisubunit complexes and are composed of two different domains: the V_1 domain, a peripheral complex of 650 kDa involved in the binding and hydrolysis of the ATP, and the V_0 domain, a membrane-embedded complex of 260 kDa implicated in the translocations of protons (**Forgac, 2007; Roh *et al.*, 2018**). Both domains work together as a rotary machinery to drive proton transport across cell membranes (**Forgac, 2007**). The V-ATPases play a pivotal role in many intracellular processes that range from membrane trafficking, lysosomal protein degradation, post-translational processing and glycosylation, protein sorting as well as nutrient signalling and facilitation of ion transport (**Forgac, 2007**) (**Figure 1**).

1.1 V-ATPase structure and subunits

The V-ATPases are formed by fourteen different subunits, which are organized with different stoichiometry (**Oot *et al.*, 2017**). The standard nomenclature, used to identify the V-ATPase subunits and the V-ATPase associated genes, has been approved by the HUGO Gene Nomenclature Committee (HGNC). The symbol used is the root "*ATP6*", it is followed by the indication of the specific domain (V_1 or V_0) and then followed by the letter indicating the subunit name. To avoid any confusion, the subunits in the V_1 and the V_0 domains are named always with a capital letter, especially since the Guidelines for Human Gene Nomenclature (http://www.gene.ucl.ac.uk/nomenclature/ guidelines.html) have suggested not to use names containing lowercase letters as symbols for human genes (**Smith *et al.*, 2003**). The current nomenclature system has been implemented in 2010 to include more than forty V-ATPase variants of the fourteen subunits plus the two accessory proteins (**Miranda *et al.*, 2010**). The catalytic V_1 domain is made of eight

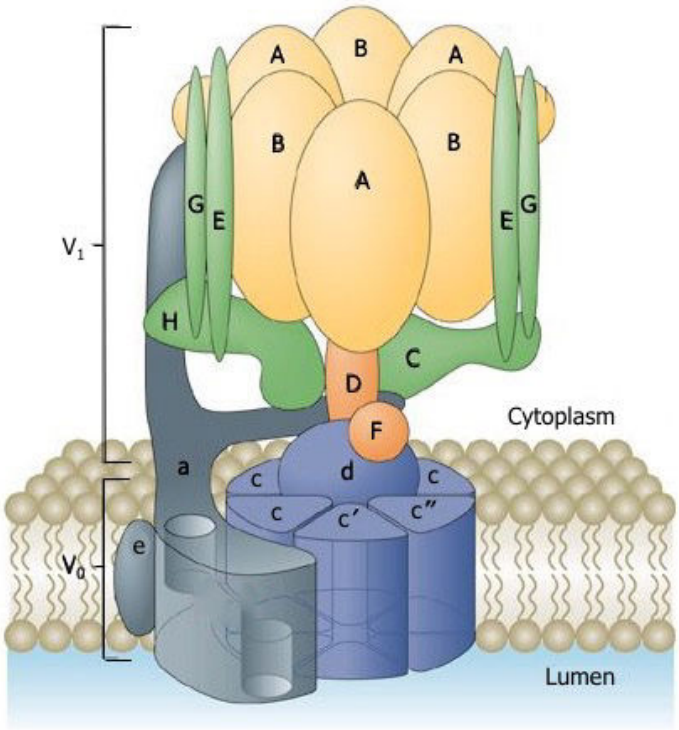

Figure 1: Structure of the V-ATPase

The V-ATPase is formed by two domains: the ATP hydrolytic domain V_1 (A-H colored yellow, orange and green) and the proton-translocator V_0 domain (*a*, *c*, *c'*, *c"* and *e*, colored blue and grey). From Forgac *et al.*, 2007.

different subunits (A-H) and the membrane embedded V_0 proton channel is composed of six-seven subunits (*a*, *d*, *e*, *f*, plus two to three proteolipid isoforms referred to as subunits *c*, (*c'*) and *c"*) (**Forgac, 2007**). The core V-ATPase complex is highly conserved from simple eukaryotes to higher animals, including humans (**Oot *et al.*, 2017**). Interestingly, biochemical purification from bovine cells has suggested that there are two subunits, which cannot be found in yeast. These two proteins do not belong to the core subunits and thus have been defined accessory subunits of the V-ATPase, ATP6AP1 and ATP6AP2 (**Getlawi *et al.*, 1994; Supek *et al.*, 1994; Ludwig *et al.*, 1998**) (see ***Chapter 3 – V-ATPase accessory subunits***).

The V-ATPase structure has been characterized extensively in the budding yeast *Saccharomyces cerevisiae*. These unicellular organisms require the proton pump to survive under specific environmental conditions, for example in alkaline conditions or toxic levels of metals (**Graham *et al.*, 2003; Eide *et al.*, 2005; Kane, 2006**). Moreover, the formation of a proton gradient generated by the V-ATPase leads to the sequestration of Ca^{2+} and Zn^{2+} ions inside the vacuole (**Klionsky *et al.*, 1990**). The deletion of any of

the V-ATPase subunits results in a number of specific growth and cellular phenotypes, which include the "*vma-* phenotype", a phenotype characterized by a failure to grow on media buffered to pH 7.5 (**Graham *et al.*, 2003; Kane *et al.*, 2006**), sensitivity to a variety of metals (including Ca^{2+} and Zn^{2+} ions) (**Eide *et al.*, 2005; Kane, 2007**) and inability to acidify the vacuoles (**Weisman *et al.*, 1987**). In *Saccharomyces cerevisiae*, the subunit *a* is expressed as two isoforms, Vph1p and Stv1p. Both have specific localizations, with Vph1p being found in the vacuole while Stv1p is present in the Golgi (**Manolson *et al.*, 2004**). In higher organisms, most of the subunits are expressed as multiple isoforms, sometimes in a tissue-specific fashion (**Toei *et al.*, 2010**), In humans, for example, there are four isoforms of the *a* subunit (*a1*, *a2*, *a3* and *a4*) with distinct vesicular and cell type distribution: V0A1 is expressed on the synaptic vesicles, V0A2 on intracellular vesicles like Golgi and early endosomes, V0A3 is on the plasma membrane of osteoclasts, whereas V0A4 is expressed on the plasma membrane of renal intercalated cells (**Nishi *et al.*, 2002; Pamarthy *et al.*, 2018**).

The V_1 domain is formed by three subdomains: the A_3B_3 cylinder, the central stalk and the peripheral stalks. The A_3B_3 subdomain is a hexamer shaped cylinder, made up of alternating A and B subunits, performing the ATP hydrolysis. There are three ATP hydrolytic sites located each one at the interface between A/B subunits (**Forgac, 2007; Maher *et al.*, 2009**). The energy derived from ATP hydrolysis is coupled to the movement of the central stalk, which acts as a rotor for the complex (**Cotter *et al.*, 2015**). The central stalk consists of single copies of subunits D, F and *d*. The last one, localized on top of the V_0 domain, provides the connection between the proteolipid ring and the central stalk in V_1 (**Forgac, 2007**). It has been shown that subunit H is essential to inhibit the ATPase activity of the V_1 domain when it is not yet attached to the V_0 domain (**Diab *et al.*, 2009**). The peripheral stalks consist of a core of EG heterodimers, connected to single copies of the subunits C, H and *a* (**Zhang *et al.*, 2008; Benlekbir *et al.*, 2012**). The peripheral stalks tether the A_3B_3 hexamer to the subunit *a*, preventing the rotation of the stator during ATP hydrolysis (**Zhang *et al.*, 2008; Benlekbir *et al.*, 2012**) (**Figure 2**).

The structure of the V_0 domain differs between yeast and humans. In *Saccharomyces cerevisiae*, it consists of six subunits: *a*, *c*, *c'*, *c"*, *d* and *e* (**Smith *et al.*, 2003; Forgac, 2007**). The mammalian V_0 domains are composed of five subunits, since the *c'* subunit is not conserved: *a* (*a1*, *a2*, *a3* and *a4* isoforms), *c*, *c"*, *d* (*d1* and *d2* isoforms) and *e* (*e1* and *e2* isoforms), respectively (**Marshansky *et al.*, 2014**). The current structural models describe the V_0 domain as composed of a proteolipid ring of *c* subunits, with adjacent a single copy of the *a* and *e* subunits (**Smith *et al.*, 2003; Forgac, 2007**). The proteolipid subunits are small highly hydrophobic proteins, containing from four to five transmembrane helices (TMs) (**Flannery *et al.*, 2004; Wang *et al.*, 2007**). Each *c* subunit contains an essential buried acidic residue that undergoes to reversible protonation during proton transport (**Hirata *et al.*, 1997; Toei *et al.*, 2010**). The *d*

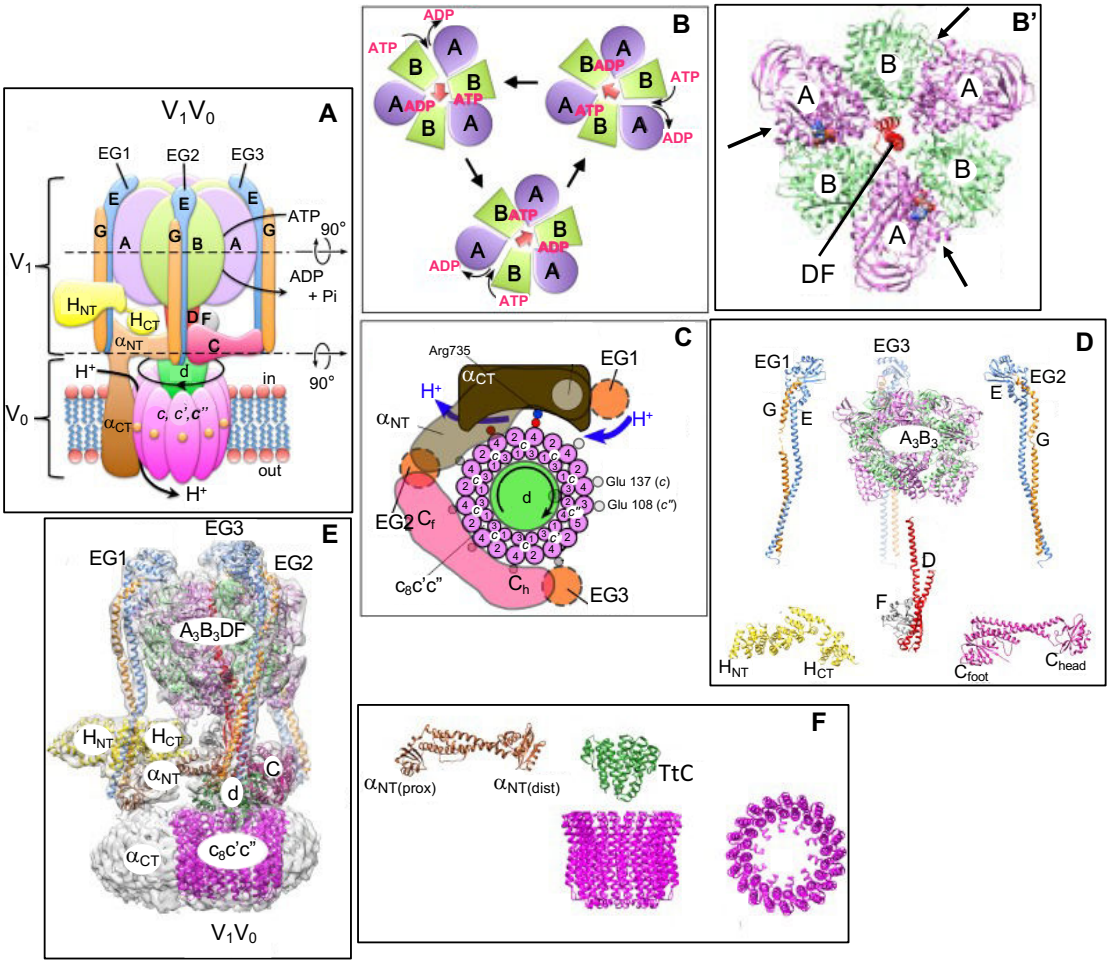

Figure 2: Subunits and domains of the V-ATPase

(**A**) The V-ATPase is formed by two domains: the ATP hydrolytic domain V_1 and the proton-translocator domain V_0. (**B**) The ATP hydrolysis occurs at three of the six AB interfaces and drives counterclockwise rotation of the central DF rotor. The A_3B_3 cylinder seen towards the cytosol. (**B'**) Crystal structure of A_3B_3DF. The arrows in (**B, B'**) show the site of the ATP hydrolysis. (**C**) The rotation of the central DF rotor drives the rotation of the proteolipid ring past the essential arginine residue in *a*. Protons enter a cytoplasmic half-channel and, after being carried 360º on lipid exposed glutamate residues on the *c* subunits, are released into the luminal half-channel. (**D**) Crystal structures of the DF subunits, stalk EGC in two conformations, H subunit and C subunit, all from *S. cerevisiae*. (**E**) CryoEM map of V_1-V_0 coordinated with the models of individual subunits and domains. (**F**) Crystal structures of the *a* subunit from *M. ruber*, *d* subunit from *T. thermophilus* and the proteolipid ring from *E. hirae*. Adapted from Oot *et al.*, 2017.

subunit is present on top of the proteolipid ring, thus providing the connection between the ring and the central stalk in V_1 (**Forgac, 2007**). The *a* subunit is a 100 kDa protein with eight transmembrane domain, with the N-terminal domain in close proximity to the H subunit (**Diepholz *et al.*, 2008; Zhang *et al.*, 2008; Benlekbir *et al.*, 2012**). Moreover, the subunit *a* possesses two hemi-channels and a crucial buried Arg residue (R735), which are required for proton translocation across the membrane (**Forgac, 2007**) (**Figure 2**).

The V-ATPase holoenzyme operates by a rotary mechanism (**Hirata *et al.*, 2003; Imamura *et al.*, 2003**). The ATP hydrolysis, occurring in the V_1 domain, causes a rotation of the entire rotary assembly, formed by subunits D, F, *d* and the ring of proteolipid subunits. Subunit *a* and the A_3B_3 hexamer are kept in fixed positions by the peripheral stators. Rotation of the proteolipid ring relative to subunit *a* leads to active transport of protons (**Forgac, 2007**). The subunit *a* provides for entry and exit of protons to the protonatable carboxyl groups of the glutamic acid (Glu) residues of the proteolipid ring. This occurs through the two aqueous hemi-channels of the subunit *a* and induces the rotation of the protonatable sites of the proteolipid ring. Following rotation, these sites are placed in contact with the hydrophobic environment and become protonated (**Forgac, 2007**). The essential TMs in both subunit *a* and in the proteolipid subunits of the V-ATPase undergo helical swivelling, meaning that they rotate about an axis through the center of the helix, relative to each other, which is possibly coupled to catalysis (**Kawasaki-Nishi *et al.*, 2003: Wang *et al.*, 2004**). Both inhibitors Bafilomycin A1 and Concanamycin A inhibit the V-ATPase activity by blocking this helical swivelling and then the proton transport (**Bowman and Bowman, 2002; Huss *et al.*, 2002**). As there are three catalytic nucleotide-binding sites in the V_1 domain and six–ten protonatable sites on the proteolipid ring of V_0 domain, the predicted H^+/ATP stoichiometry for the V-ATPases is 2–3.3 (**Kettner *et al.*, 2003**) (**Figure 3**).

For intracellular pH regulation, the excess of positive charges across the organellar membrane due to increasing of ions H^+ is counterbalanced by efflux of ions mediated by exchangers or cations efflux (**Steinberg *et al.*, 2010; Weinert *et al.*, 2010; Cang *et al.*, 2015**). Moreover, the intracellular acidity generated by the V-ATPase proton gradient is counteracted by proton back-flux called intrinsic H^+ leakage that prevents the over-acidification of the lumen of organelles (**Paroutis *et al.*, 2004**).

1.2 V-ATPase function

The V-ATPases are ubiquitously expressed in the cell and are involved in the acidification of membrane-bounded compartments, thus playing a crucial role in many intracellular processes, including membrane trafficking, protein glycosylation and sorting, protein degradation in the lysosomes or nutrient signalling.

The V-ATPases provide the acidic environment needed by the secretory pathway.

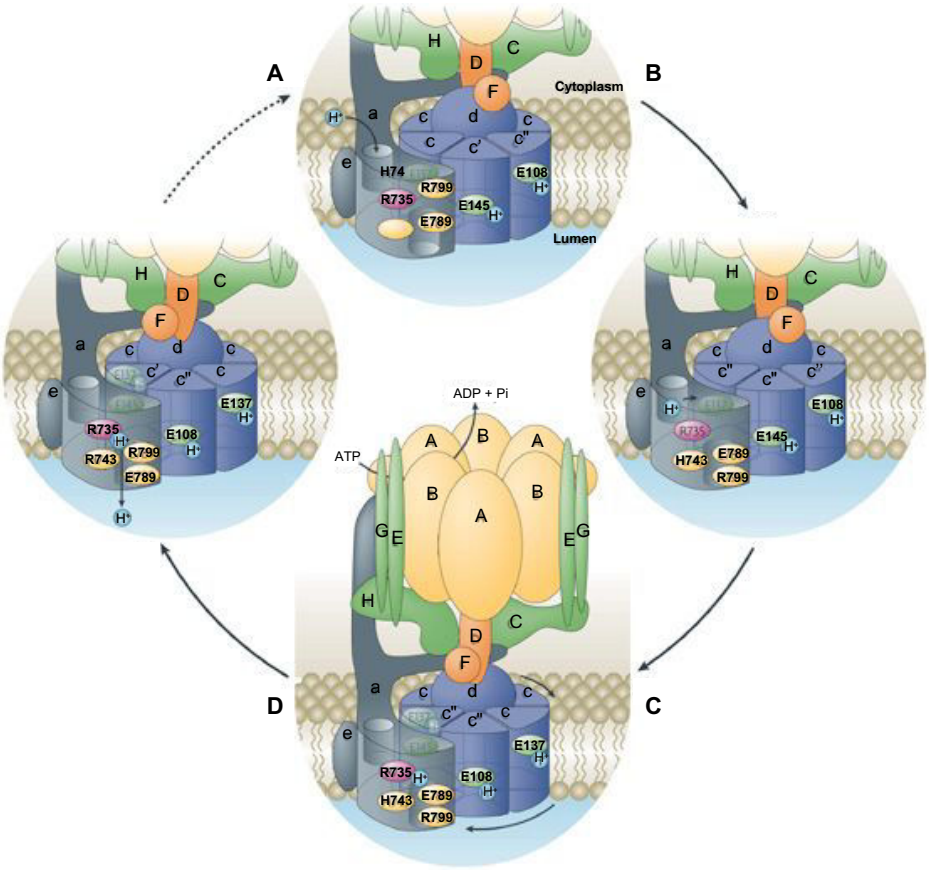

Figure 3: Rotary mechanism of the V-ATPase

(**A**) Protons enter at the cytoplasmic side of the hemi-channel in subunit *a*. (**B**) Protonation of buried Glu residues in the proteolipid ring (E137 in subunit *c*, E145 in subunit *c'* and E108 in subunit *c"*). (**C**) Forced exposure of these residues into the hydrophobic phase of the bilayer keep protonated the Glu residues. (**D**) Rotation is facilitated by ATP hydrolysis that occurs at the catalytic sites in the interface of subunits A and B. The ATP hydrolysis drives rotation of a central rotor that includes subunits D and F (colored orange) of V_1 connected to subunits *d* and the proteolipid ring of V_0 (colored blue). The subunits *a* and *e* of V_0 (colored grey) are kept fixed relative to the A_3B_3 hexamer thank to the peripheral stalks. Following rotation, protons are displaced from the proteolipid subunits into a luminal hemi-channel of subunit *a* as a result of the interaction between the glutamic acid side chains and a crucial buried arginine residue (R735) in transmembrane helix-7 (TM7) of subunit *a*. Other buried charged residues in the C-terminal domain of subunit *a* (H743, E789, R799) line the luminal hemi-channel through which protons exit the membrane. From Forgac *et al.*, 2007.

Indeed, the luminal pH is not homogeneous through the secretory pathway (**Paroutis *et al.*, 2004; Casey *et al.*, 2010; Pamarthy, *et al.*, 2018**). Since the assembly and the consequent activity of the V-ATPase start only in the Golgi, the pH of the endoplasmic reticulum (ER) is near neutral and similar to that of the cytosol, while downstream compartments, where the V-ATPase is active, become progressively more acidic. The pH of the *cis*-Golgi drops down significantly with a more acidic pH of 6.7 and the acidification becomes more marked in subsequent *cisternae* of the Golgi complex, reaching pH 6.0 in the *trans*-Golgi network (TGN). Furthermore, the pH of secretory granules has been reported to be as low as 5.2 (**Anderson and Pathak, 1985; Wu *et al.*, 2000; Paroutis *et al.*, 2004**). It has been proposed that the progressive reduction of pH along the secretory pathway depends on different isoforms of the V-ATPases, on the variation of density of V-ATPases and on the assembly of the V-ATPases (**Casey *et al.*, 2010**) (**Figure 4**).

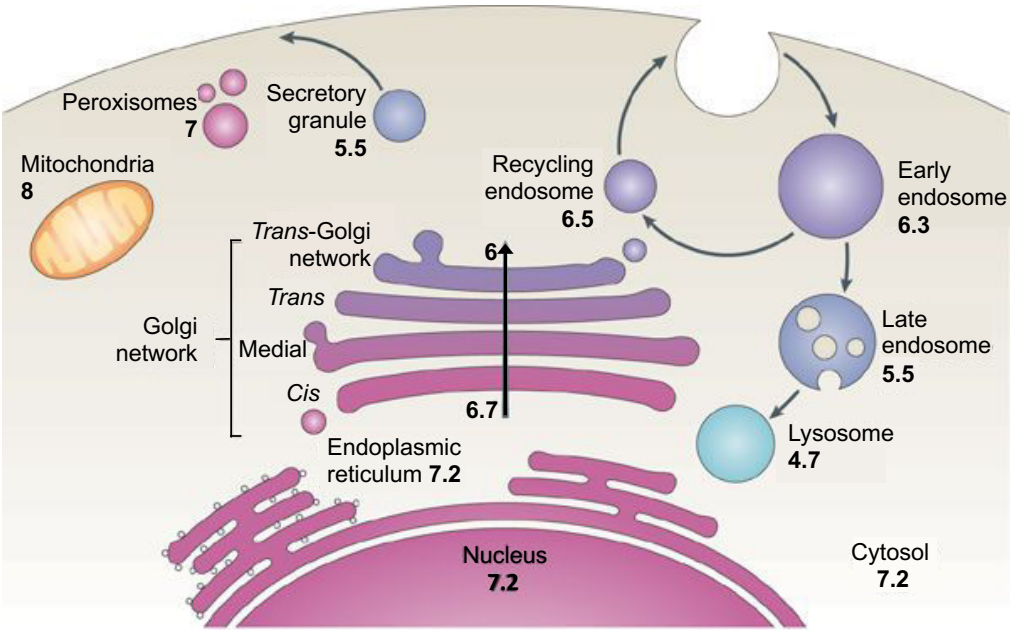

Figure 4: The pH of the secretory pathway and intracellular compartments in the mammalian cell

pH of each organelle is indicated by the numbers. Mitochondrial pH refers to the matrix. Early endosomes refer to the sorting endosomal compartment. pH of the multivesicular late endosomes refers to the bulk luminal fluid; pH of the fluid contained by the internal vesicles might differ. From Casey *et al.*, 2010.

1.2.1 Role of the V-ATPase in the Golgi: regulation of pH and glycosylation

The Golgi pH plays a pivotal role in membrane trafficking (**Griffiths *et al.*, 1983; Palokangas *et al.*, 1998**), protein sorting (**Matlin, 1986; Caplan *et al.*, 1987; Ellis and Weisz, 2006**), and glycosylation of proteins and lipids (**Kuismanen *et al.*, 1985; Thorens and Vassalli, 1986; Gawlitzek *et al.*, 2000; Axelsson *et al.*, 2001; Campbell *et al.*, 2001, Kellokumpu *et al.*, 2002**). The decrease of the luminal pH through the secretory pathway is dictated by a simultaneous increase of proton import from the luminal side and a decrease of proton export to the cytosol (**Kim *et al.*, 1996; Demaurex *et al.*, 1998; Farinas and Verkman, 1999; Schapiro and Grinstein, 2000; Wu *et al.*, 2001**). Also in the Golgi, the steady-state pH is dictated by a balance of three components: (1) V-ATPase, involved in the import of protons, (2) proton export/elimination (also called proton leaking), (3) counter-ion conductance, performed by Cl^- channel families, such as the Golgi pH regulator (GPHR) and Golgi anion channel (GOLAC1 and 2) (**Kim *et al.*, 1996; Demaurex *et al.*, 1998; Farinas and Verkman, 1999; Grabe and Oster, 2001; Wu *et al.*, 2001; Paroutis *et al.*, 2004; Thompson *et al.*, 2006; Maeda *et al.*, 2008**) (**Figure 5**).

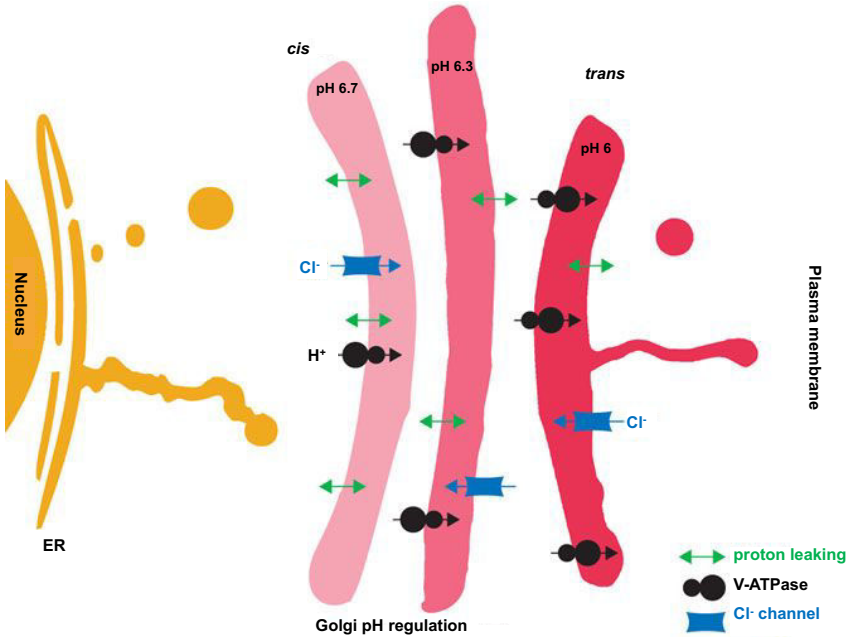

Figure 5: V-ATPase is required to regulate the Golgi pH

Processing and sorting of glycoproteins at the Golgi require a pH that becomes progressively more acidic from *cis*- to *trans*-Golgi (indicated by the color change). The gradient of pH from *cis*- to *trans*-Golgi is guaranteed by the increase in the density of V-ATPases concomitant with a decrease in the density of H^+ leaks. The chloride channels are present at low and uniform density to keep the membrane potential near zero by providing counter-ion movement to compensate for H^+ influx. The numbers indicate the pH. Adapted from Caldwell and Howell, 2008.

For the regulation of glycosylation by the Golgi pH, two different hypotheses can be proposed. One is that some glycosylation enzymes, such as sialidases, have a specific pH optimum (**Gawlitzek *et al.*, 2000**). The other is that an increased pH causes incorrect localization of glycosyltransferases within the Golgi and post-Golgi organelles (**Axelsson *et al.*, 2001**), leading to a loss of ability to execute glycosylation reactions in the correct order (**Maeda and Kinoshita, 2010**). The catalytic activity of most of the glycosyltransferases depends on the luminal pH and on the distribution of divalent cation, such as Ca^{2+}, Mg^{2+} and/or Mn^{2+}. The last ones are important to modify the conformation of the substrates that have to enter in the catalytic pocket of the glycosyltransferases (**Petrová *et al.*, 2001**). Moreover, it has been shown that already an increase in Golgi pH of only 0.2 is sufficient to inhibit a terminal sialylation of *N*-glycans and to induce selective mislocalization of the corresponding sialyltransferase. The higher pH does not affect the other glycosylation enzymes or Golgi markers, indicating that mislocalization of certain Golgi glycosyltransferases is primarily responsible for the pH-induced glycosylation defects (**Rivinoja *et al.*, 2009a, b; Maeda and Kinoshita, 2010**). Perturbation in the Golgi pH not only impairs glycosylation but also membrane trafficking and protein sorting (**Rivinoja *et al.*, 2009a, b**). Interestingly, it has been demonstrated that some glycosyltransferases can form aggregates in the more acidic environment (pH 6.3) of the *trans*-Golgi and TGN. The formation of aggregates enables their rapid movement through the Golgi stack (**Opat *et al.*, 2001a, b**).

1.2.2 Role of the V-ATPase in endolysosomes and lysosomes acidification

The progressive luminal acidification is important in various aspects of endocytosis and intracellular membrane trafficking. Indeed, the acidic pH in the endocytic compartment allows the dissociation of the ligands from their receptors complexes and the recycling of the receptors (**Forgac, 2007**). For instance, the endocytic acidification is important for the continued uptake of low density lipoprotein (LDL), a major carrier of plasma cholesterol, as well as termination of signalling from receptors such as epidermal growth factor receptor (EGFR) (**McGuire *et al.*, 2017**). Moreover, even the normal trafficking of membranes between endocytic compartments seems to be controlled by luminal acidification (**Weisz, 2003**). It has been shown that the acidification of early endosomes, due to the proton accumulation driven by the V-ATPase, recruits the small GTPase ADP-ribosylation factor 6 (Arf6) and the ARF nucleotide-binding site opener (ARNO): the two proteins are involved in endocytosis and have been implicated in vesicle-coat formation, remodelling of the actin-cytoskeleton and in lipid modification (**Hurtado-Lorenzo *et al.*, 2006**). Arf6 and ARNO interact with the V_0 subunits *a2* and *c* of the V-ATPase (**Hurtado-Lorenzo *et al.*, 2006; Recchi and Chavrier, 2006**). These observations indicate that the V-ATPase, through the *a2* subunit, can regulate membrane trafficking (**Hurtado-Lorenzo *et al.*, 2006**).

In the lysosomes, the V-ATPases provide the essential acidic environment for protein degradation, for example by promoting the activity and the proteolytic activation of acid-dependent proteases such as cathepsin B and D (CTSB and CTSD), and for the recovery of the resultant amino acids via proton-coupled amino acid transporters. Within secretory vesicles, V-ATPases both activate processing of precursor molecules and drive uptake of small molecules, such as neurotransmitters (**Breton and Brown, 2013**) (**Figure 6**).

1.2.3 Role of the V-ATPase in fusion of vesicles

The V-ATPases have also been proposed to play an important role modulating the fusion of vesicles. Pioneering studies performed in yeast uncovered a pivotal role of two V_0 subunits, the subunit *c* and *a*, in the fusion of vacuolar membranes downstream of SNARE complex assembly (**Peters *et al.*, 2001; Bayer *et al.*, 2003**). Indeed, a first evidence is suggested by the fact that deletion of the V_0 proteolipid subunit Vma3 could inhibit the traffic along the secretory pathway more severely than mutations in V_1 subunits (**Yamashiro *et al.*, 1990; Morano and Klionsky, 1994**), even if mutations in both abolish the proton pump activity (**Stevens and Forgac, 1997; Peters *et al.*, 2001**). Furthermore, Peters and Bayer suggested the formation of *trans*-complexes formed by V_0 domain from apposed vacuolar membranes, which may form a proteolipid channel spanning both membranes (**Peters *et al.*, 2001; Bayer *et al.*, 2003**). Both groups proposed that the formation of these *trans*-complexes follows the docking and pairing of

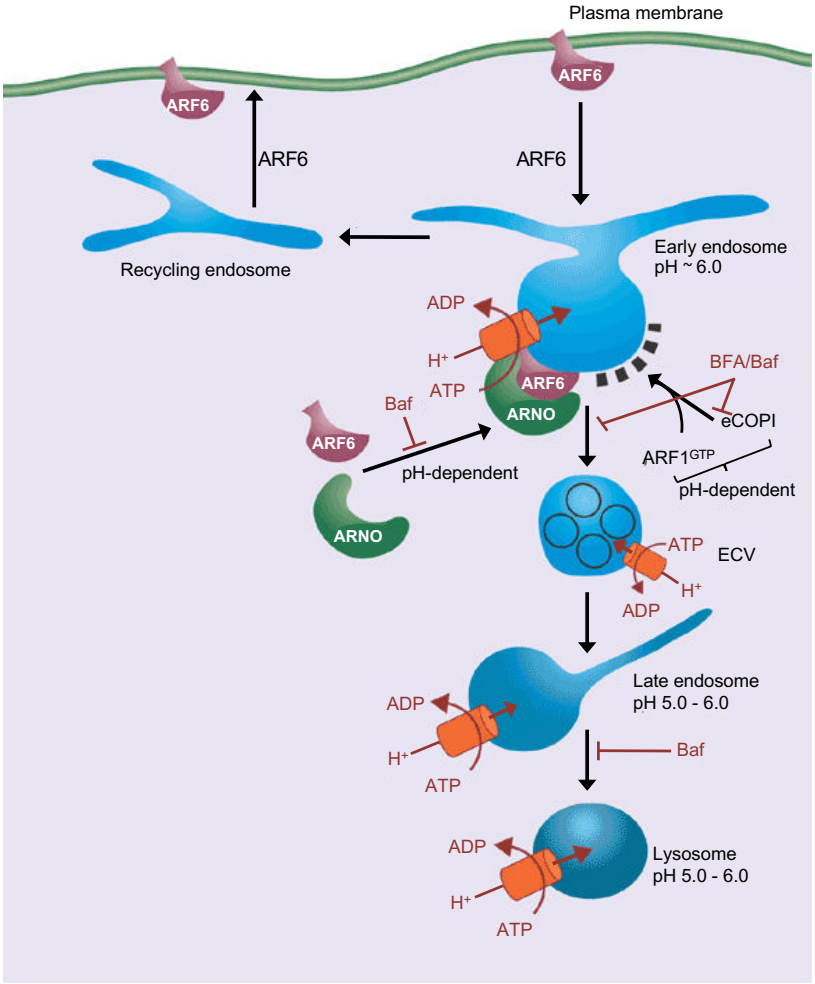

Figure 6: Distinct endocytic compartments with progressively decreasing pH

The V-ATPase (colored orange) pumps protons into the lumen of the different endosomal compartments, contributing to intra-endosomal acidification. Inhibition of V-ATPase activity by Bafilomycin A1 (Baf) or Brefeldin A (BFA) blocks endocytic trafficking at the level of early endosomes. This occurs with ARF1-dependent recruitment of the endosomal COPI coat (COPI, dashed line) and the formation of endosomal carrier vesicles (ECVs). The recruitment of ARNO and ARF6 to the early endosomal membrane is pH-dependent. The two proteins interact with the V-ATPase *a2* and *c* subunits, respectively. From Recchi and Chavrier, 2006.

the *trans*-SNARE (t-SNARE) and is independent of the proton gradient, suggesting a role of the V_0 subunits in the direct fusion of vacuoles (**Bayer *et al.*, 2003**). Moreover, Bayer *et al.* demonstrated the importance of the subunit *a* (Vph1p) on both fusion partners, suggesting a symmetric requirement of the integral multisubunit cylinders to connect the two vacuolar membranes before fusion (**Lindau and Almers, 1995; Zimmerberg, 2001**). Subsequently, a genetic screen for synaptic malfunction in *Drosophila* confirmed the role of the subunit *a1* of the V_0 domain as an essential component for synaptic transmission, also acting downstream of SNAREs (**Hiesinger *et al.*, 2005**). For this specific role, the interaction of Ca^{2+}/calmodulin with the subunit *a1* was critical and leads to spontaneous release of neurotransmitters at the neuromuscular junction (**Wang *et al.*, 2014**). Additional studies have proven the role of the subunit *a* in the regulation of vesicles fusion: the subunit *a3* regulates the secretion of insulin in pancreatic beta cells (**Sun-Wada *et al.*, 2006**), the subunit *a1* mediates the fusion lysosome-phagosome during phagocytosis in zebrafish (**Peri and Nüsslein-Volhard, 2008**), while the subunit *a* is involved in apical secretion of multivesicular bodies and in the exosome-mediated apical secretion of Hedgehog-related proteins in *Caenorhabditis elegans* (**Liégeois *et al.*, 2006; Rama *et al.*, 2018**). Although biochemical studies propose a direct interaction of the subunit *c* with several SNAREs present on synaptic vesicles (**Bennet *et al.*, 1992; O'Connor *et al.*, 1993; Galli *et al.*, 1996; Shiff *et al.*, 1996**), only in 2010 Di Giovanni *et al.* provide the first evidence of a direct interaction between a V_0 subunit and SNAREs. Indeed, the same group found in yeast two-hybrid (Y2H) that the subunit *c* binds directly the t-SNARE synaptobrevin (VAMP2) through its C-terminal. *In vivo*, they confirmed that, when this interaction is disrupted, there is a significant decrease of neurotransmission, pinpointing the importance of the interaction between V-ATPase subunits and SNARE in the vesicles fusion (**Di Giovanni *et al.*, 2010**). Conversely, subsequent studies have correlated the function of the V-ATPase with fusion of vesicles by proposing that lack of V-ATPase subunits leads to impaired vesicles acidification and thus to impaired exocytosis (**Coonrod *et al.*, 2013; Poëa-Guyon *et al.*, 2013**). Intriguingly, mutations in both V_0 (**Kornak *et al.*, 2008; Jansen *et al.*, 2016a, b, c**) and V_1 subunits (**Van Damme *et al.*, 2017; Zhao *et al.*, 2018**) have been reported to disrupt vesicular trafficking, Golgi homeostasis and post-Golgi anterograde transport.

1.2.4 Role of the V-ATPase in autophagy

Lysosomal degradation is closely related to autophagy, a catabolic pathway by which cells remove misfolded or aggregated proteins and damaged organelles. Autophagy provides the energy in response to nutrient and environmental stress and recycles macromolecules providing molecular building blocks (**Mizushima and Komatsu, 2011; Kim and Guan, 2015**). The name *autophagy* derives from the Greek and means "eating of self". It was used by Christian de Duve more than 40 years ago, with the observation of vesicles containing amorphous materials, such as mitochondria, and partially degraded

cytoplasmic organelles by electron microscopy (**Clark *et al.*, 1957; De Duve *et al.*, 1966**). In the late 1970s, it was observed that amino acid starvation was able to induce autophagy in cultured mammalian cells and in perfused rat livers (**Mitchener *et al.*, 1960; Mortimore and Schworer, 1977**). So far, more than thirty autophagy-related genes (Atg) have been described and most of them have been identified by genetic screening in yeast (**Glick *et al.*, 2010**). Many of these genes are conserved in mammals, highlighting the fundamental nature of the autophagic process (**Nakatogawa *et al.*, 2009**). There are three different types of autophagy: macroautophagy, microautophagy and chaperone-mediated autophagy (CMA). Each type of autophagy promotes the proteolytic degradation of cytosolic components inside the lysosomes. The cell uses macroautophagy to deliver cytoplasmic cargos to the lysosome through the autophagophore, a double membrane-bound vesicle that fuses with the lysosome to form an autolysosome. The cytosolic components are degraded through microautophagy: they are directly taken up by the lysosomes through invagination of the lysosomal membrane. In the last type of autophagy, the CMA, the proteins are conjugated with chaperones, such as members of the heat shock proteins, and then transported across the lysosomal membrane by the lysosomal-associated membrane protein 2A (LAMP2A) (**Saftig *et al.*, 2008; Glick *et al.*, 2010**) (**Figure 7**).

At the molecular level, autophagy occurs in five key stages: (1) formation of the phagophore (also called nucleation); (2) Atg5–Atg12 conjugation, followed by interaction with Atg16L and multimerization with other Atg at the phagophore; (3) processing of LC3 and insertion into the phagophore membrane; (4) capture of the targets for degradation; (5) formation of the autolysosome, derived by the fusion of the autophagosome with the lysosome and degradation of the cargos by the lysosomal proteases (**Glick *et al.*, 2010**) (**Figure 7**).

1. Phagophore formation. In mammalian cells, the formation of the phagophore initiates with membranes derived from the ER (the so-called omegasome) (**Hayashi-Nishino *et al.*, 2009; Yla-Anttila *et al.*, 2009**), but also from other cytosolic membranes organelles, such as the Golgi, the *trans*-Golgi, the mitochondria, the late endosomes (**Mizushima, 2007; Mizushima and Klionsky, 2007; Axe *et al.*, 2008**) and, possibly, even from the nuclear envelope under restricted conditions (**English *et al.*, 2009**). In yeast, the formation of the phagophore requires the activity of the Atg1 kinase in complex with Atg13 and Atg17. It has been proposed that the formation of this complex recruits the transmembrane protein Atg9 that promotes lipid recruitment to the expanding phagophore (**Kundu and Thompson, 2005; Klionsky, 2007; Simonsen and Tooze, 2009**). mTOR can inhibit this process phosphorylating Atg13 and preventing it from interacting with Atg1 (**Díaz-Troya *et al.*, 2008**). In mammalian cells, exist two homologues of Atg1, Ulk-1 and Ulk-2, but how they work in promoting autophagy is still not well understood (**Kundu and Thompson, 2005**). The vesicular protein sorting 34 (Vps34) class III phosphoinositide 3-kinases (PI3K) uses the phosphatidylinositol (PI)

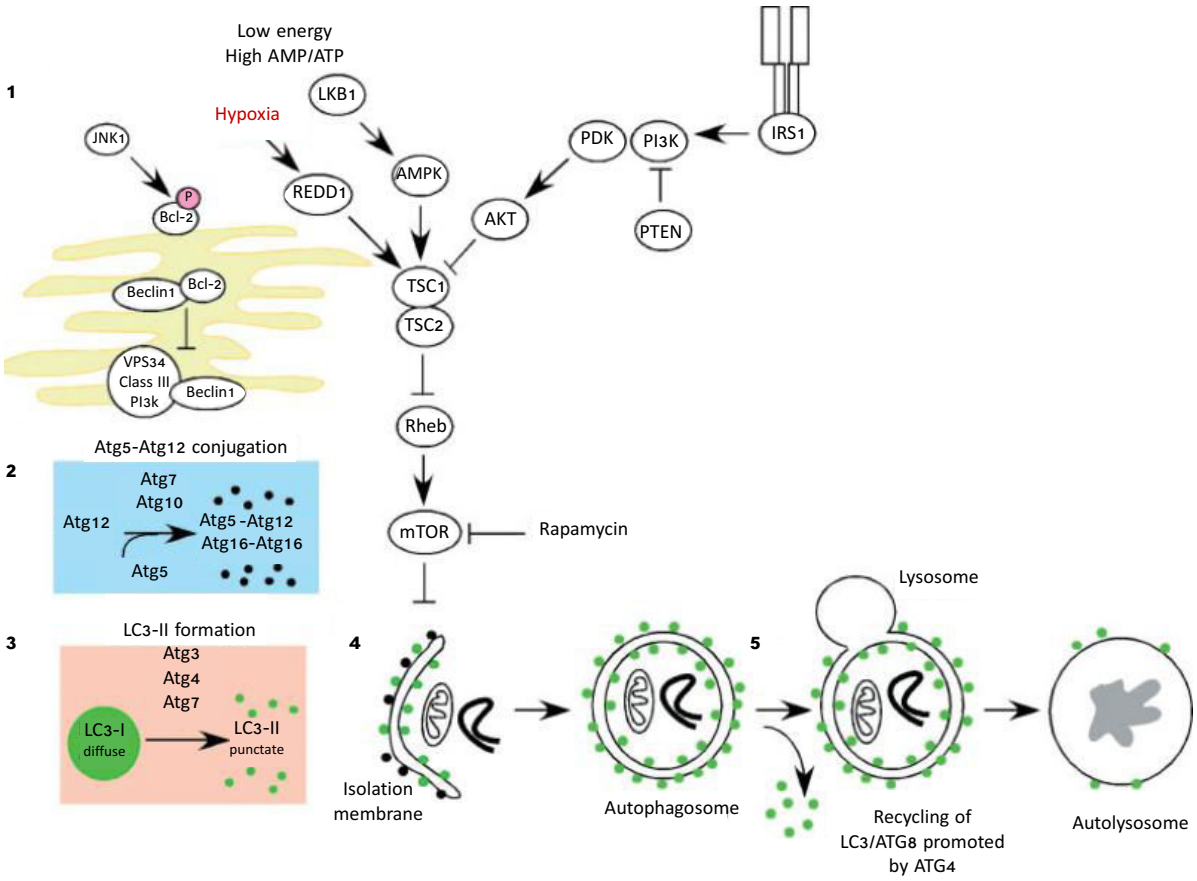

Figure 7: Signalling pathways regulating autophagy

Autophagy is a complex process that involves the following key steps: **(1)** nucleation of the phagophore in the ER initiated by Beclin-1/VPS34; **(2)** Atg5–Atg12 conjugation, interaction with Atg16L and multimerization of the Atg proteins; **(3)** processing of LC3 and insertion in the extending phagophore membrane; **(4)** capture of the targets for degradation, recycling of some LC3-II; **(5)** fusion of the autophagosome with the lysosome, proteolytic degradation by lysosomal proteases. The autophagy pathway is regulated by several signalling pathways, including JNK-1, a stress-signalling kinase that promotes autophagy by activating Bcl-2 and promoting the interaction of Beclin-1 with VPS34. Autophagy is regulated also by the mTOR kinase, via the inhibition of the ATG1/Ulk-1/-2 complexes at the earliest stages in phagophore formation. mTOR integrates metabolic, growth factors and energy signalling into autophagy. Autophagy can be induced by hypoxia and low cytosolic ATP levels. Inhibition of the autophagy can occur by the insulin receptor and its adaptor, IRS1. mTOR activity is promoted through inhibition of TSC1/TSC2 and increased Rheb GTPase activity. Adapted from Glick *et al.*, 2010.

as substrate to generate phosphatidyl inositol triphosphate (PI3P), a lipid important for phagophore elongation and involved in the recruitment of other Atg proteins (**Xie and Klionsky, 2007**). Vps34 interacts with Beclin-1 and promotes its catalytic activity increasing the levels of PI3P. Additional regulatory proteins complex can regulate positively or negatively the phagophore formation and then the autophagy induction in the ER: UVRAG, BIF-1, Atg14L and Ambra activates the autophagy (**Liang *et al.*, 2006; Fimia *et al.*, 2007; Takahashi *et al.*, 2007**), while Rubicon and Bcl-2 can inhibit it (**Pattingre *et al.*, 2005; Matsunaga *et al.*, 2009; Zhong *et al.*, 2009**). Indeed, in starvation, the interaction of Beclin-1 with Bcl-2 (and Bcl-XL) in the ER inhibits Beclin-1 activity, disrupting its interaction with Vps34 (**Pattingre *et al.*, 2005; Maiuri *et al.*, 2007; Wei *et al.*, 2008**).

2. Atg5–Atg12 conjugation. Atg7 acts as an E1 ubiquitin enzyme and activates Atg12 by binding to its carboxyterminal glycine residue, in an ATP-dependent manner. Atg12 interacts with Atg10, an E2-like ubiquitin carrier protein that potentiates covalent linkage of Atg12 to lysine 130 of Atg5 (**Glick *et al.*, 2010**). The Atg5–Atg12 complexes and dimers of Atg16L interact together to form a big complex (Atg5–Atg12–Atg16L). This complex associates with the phagophore, induces a curvature into the growing phagophore through asymmetric recruitment of LC3B-II (**Glick *et al.*, 2010**). Once the autophagosome is formed, the complex Atg5–Atg12–Atg16L dissociates from the phagophore. For that reason, the conjugated Atg5–Atg12 is a relatively poor marker of autophagy (**Barth *et al.*, 2010; Zhang *et al.*, 2016**).

3. LC3 processing. LC3B, Atg8 in yeast, is expressed in most cell types as a full-length cytosolic protein. Under autophagy induction, LC3B is proteolytically cleaved by the cysteine protease Atg4 to generate LC3B-I. After the cleavage, LC3B-I exposes a carboxyterminal glycine that is then activated by the E1-like Atg7. Activated LC3B-I is then transferred to a different E2-like carrier protein (Atg3) and the phosphatidylethanolamine (PE) is conjugated to the carboxyl glycine to generate LC3B-II. Atg5–Atg12 recruit and integrate LC3B-II in the growing phagophore. LC3B-II is found on both the internal and external surfaces of the autophagosome, where it plays a role in both hemifusion of membranes and in selecting cargos for degradation (**Glick *et al.*, 2010**). During the autophagy, the synthesis and processing of LC3 are increased, thus LC3 is the golden standard marker of autophagy (**Barth *et al.*, 2010**). During autophagy, the LC3-related protein GABARAP [γ-aminobutyric type A (GABAA)-receptor associated protein] localizes at the autophagosomes with LC3-II and undergoes to similar processing (**Kirkin *et al.*, 2009**). The role of the LC3-related molecules in autophagy is not clear, but their interactions may determine the selection of cargos engulfed in the autophagosome (**Schwarten *et al.*, 2009; Glick *et al.*, 2010; Zhang *et al.*, 2016**).

4. Selection of cargos for degradation. In general, autophagy is considered as a random process engulfing indiscriminately cytosol organelles, including mitochondria, ER and Golgi membranes (**Eskelinen, 2008**). However, there are evidence that LC3B-II

could act as a receptor on the growing phagophore membrane interacting with adaptor proteins on the target (e. g. protein aggregates, mitochondria) promoting their selective uptake and degradation. In this context, the best characterized protein is the ubiquitin-binding protein p62/sequestosome-1 (SQSTM1), an adaptor that promotes turnover of poly-ubiquitinated protein aggregates through interaction with LC3 at the autophagosome. p62 has largely used as marker for defective autophagic degradation (**Glick *et al.*, 2010; Zhang *et al.*, 2016**).

5. Fusion with the lysosome. The last step in the maturation of the autophagosome is the fusion with early and late endosomes. This happens prior to fusion with the lysosome to form the final autolysosome (**Mizushima, 2007**). When autophagosomes and endosomes fuse, the pH starts to lower acidifying the autophagic vesicle before delivery of lysosomal acid proteases (**Eskelinen, 2005**). This process requires the small G protein Ras-related protein (Rab7) bounded to GTP (**Gutierrez *et al.*, 2004; Jäger*et al.*, 2004**) and also the Presenilin protein (**Eskelinen, 2005**). The cytoskeleton is involved in the autolysosome formation since drugs against the microtubules block fusion of the autophagosome with the lysosome (**Webb *et al.*, 2004**). The CTSB and CTSD, present inside the lysosomes, are required for turnover of autophagosomes and for the maturation of the autolysosome, and can be both used as marker of lysosomal homeostasis (**Koike *et al.*, 2005; Zhang *et al.*, 2016**). LAMP1 and LAMP2 are involved in the autolysosome maturation and in the fusion of the autophagosome with the lysosomes. For instance, inactivation of LAMP2 is associated with the Danon disease in humans, an X-linked disease that leads to a pathogenic accumulation of autophagosomes in the cardiac muscle (**Tanaka *et al.*, 2000**).

As the V-ATPase is important in the acidification of the lysosomes and is necessary to activate the lysosomal acid hydrolases, it is of great importance in autolysosomal degradation (**Kissing *et al.*, 2015; Pamarthy *et al.*, 2018**). Thus, many studies point to the requirement of functional V-ATPase for autophagy (**Mijaljica *et al.*, 2011**) and Bafilomycin A1, the V-ATPase inhibitor, is also used as a classical inhibitor of autophagy (**Carr *et al.*, 2008**). However, the precise role of V-ATPase in regulating the membrane dynamics of the autophagic flux is not completely clear (**Pamarthy *et al.*, 2018**). It has been shown that the inhibition of the activity of both V-ATPase and Ca^{2+} pump SERCA via the treatment with Bafilomycin A1 leads to a block in autophagic flux, while genetic inactivation of the V-ATPase still allows fusion of lysosomes with autophagosomes (**Mauvezin *et al.*, 2015**). These results pinpoint to the involvement of V-ATPase in the degradation of autophagic cargos in lysosomes more than a function in regulating the autophagic flux (**Pamarthy *et al.*, 2018**).

1.2.5 Role of the V-ATPase in mTOR regulation

Another very exciting link between autophagy and the V-ATPase is the involvement of the V-ATPase in signalling by the master growth regulator mTORC1 activity (**Zoncu *et al.*, 2011**). The activation of mTOR occurs in presence of nutrients and is mediated by Akt kinase, PI3K and growth factor receptor signalling (**Kim and Guan, 2015**). When the amino acids are present in adequate levels, the V-ATPase interacts with the Ragulator, a scaffolding complex that anchors the Rag GTPases to the lysosomes (**Zoncu *et al.*, 2011**). Rag GTPases promote the translocation of mTORC1 to the lysosomal surface, where mTORC1 can come in contact with Rheb, an important mTOR activator (**Zoncu *et al.*, 2011; Dibble and Manning, 2013**). In *Drosophila* epithelial cells, V-ATPase/mTOR signalling is required for Rheb-stimulated protein uptake, suggesting a positive feedback loop between endocytosis and mTOR activation (**Gleixner *et al.*, 2014**). When the V-ATPase function is disrupted either genetically or pharmacologically, mTORC1 remain inactive, even when amino acids are abundant (**Zoncu *et al.*, 2011**) (**Figure 7**).

The main downstream effectors of mTORC1 are the ribosomal protein S6 kinase 1 (S6K1), the eukaryotic translation initiation factor 4E-binding protein 1 (4EBP1) and UNC-51-like kinase 1 (ULK1) (**Yoon and Choi, 2016**). When mTORC1 is activated, it phosphorylates the hydrophobic motif of S6K1 and leads to the activation of S6 inducing ribosome biogenesis (**Shimobayashi and Hall, 2014**). Instead, mTORC1 phosphorylates 4EBP1 on multiples sites inhibiting 4EBP1 and leading to translational initiation (**Shimobayashi and Hall, 2014**). In presence of nutrients, mTORC1 is activated and binds the ULK1 complex. This complex is formed by ULK1, the homolog of Atg1 in yeast, the mammalian homolog of Atg13, Atg101 and FIP2000. The binding of mTORC1 to the ULK1 complex leads to the phosphorylation of both Atg13 and ULK1, inhibiting ULK1 activity and leading to an overall inhibition of autophagosome formation (**Ueno and Komatsu, 2017**). However, in starvation, mTORC1 is inactivated and dissociates from the ULK1 complex. In this way, mTORC1 can initiate the autophagosome formation (**Rabinowitz and White, 2010**).

mTORC1 is repressed by nutrient starvation, reduced growth factors and by the drug Rapamycin (**Kim and Guan, 2015**). Moreover, mTORC1 is initially inactivated during autophagy, to ensure reduced cell growth, but the generation of energy supplied by the degradation of autolysosomal products at the end of the autophagic flux leads to the reactivation of the kinase complex. This reactivation is required for the formation of new lysosomes and highlight the important role of mTORC1 in the completion of the autophagic flux (**Kim and Guan, 2015**).

At the transcriptional level, autophagy is regulated by the transcription factor EB (TFEB) (**Settembre *et al.*, 2011, 2012, 2013; Settembre and Ballabio, 2014**). mTORC1 directly phosphorylates TFEB at Ser142 and Ser211, leading to its cytoplasmic sequestration and cytoplasm-to-nucleus shuttling (**Martina *et al.*, 2012; Settembre**

***et al.*, 2012**). TFEB's activity is inhibited by the Rag GTPases in presence of amino acids. Indeed, the Rag GTPases bind and sequester TFEB in the lysosome (**Martina and Puertollano, 2013**). The absence of Rag in RagA and RagB deficient cells leads to a constitutively activation of TFEB, regardless of nutrient availability (**Kim *et al.*, 2014**).

1.2.6 Role of the V-ATPase on the plasma membrane

A small number of cells, including renal epithelial cells, epididymal clear cells, phagocytes and osteoclasts, possess plasma membrane V-ATPases extruding protons into the extracellular space (**Nishi and Forgac, 2002; Maxson and Grinstein, 2014**). The plasma membrane V-ATPases are involved in many cellular processes: in renal cells, V-ATPases are important in the maintenance of the plasma pH homeostasis and in the secretion of acid into the urine, thus regulating the acid-base balance (**Brown and Breton, 2000; Maxson and Grinstein, 2014**). In the epididymal clear cells, the V-ATPase pumps across the membrane the H^+ to provide the required low pH for sperm maturation and storage (**Brown and Breton, 2000; Maxson and Grinstein, 2014**). In the osteoclasts, the plasma membrane V-ATPases are involved in the bone resorption, pumping H^+ in the extracellular resorption *lacuna*, and are required for the activity of secreted acid hydrolases involved in the degradation of the organic bone matrix (**Maxson and Grinstein, 2014**). By modifying tissue pH and extracellular matrix composition, plasma membrane V-ATPases are also important in the survival and invasiveness of tumor cells (**Hinton *et al.*, 2009; Capecci and Forgac, 2013; von Schwarzenberg *et al.*, 2013; Cotter *et al.*, 2015**).

1.3 Regulation of the V-ATPase

Since so many essential intracellular processes are regulated by pH, the regulation of the V-ATPase activity must be tightly controlled (**Collins and Forgac, 2018**).

One level of regulation involves a separate, and even simultaneous, assembly of the V_0 and V_1 domains. It is known that the assembly of the V_0 subunits takes place in the ER (see ***Chapter 2 – V-ATPase assembly and assembly factors***). Only later in the Golgi, the V_0 domain binds to either the almost assembled V_1 domain plus the subunit C, or to individual V_1 subunits (**Forgac, 2007**).

Another level of regulation is provided by the reversible dissociation of the V_1 and V_0 domains from each other and is thought to preserve cellular ATP stores (**Forgac, 2007; Kane, 2012**). In yeast, V-ATPase disassembly occurs upon glucose starvation. This process is rapid, reversible and does not require new protein synthesis (**Kane, 1995**). Only V-ATPases localized to the vacuole undergo disassembly in response to glucose withdrawal, while this phenomenon does not occur for the Golgi localized V-ATPases

(**Kawasaki-Nishi *et al.*, 2001**). The presence of glucose allows the reassembly of the V-ATPase and requires two glycolytic enzymes, the aldolase and the phosphofructokinase, and the presence of the heterotrimeric regulator of ATPase of vacuoles and endosomes (RAVE) complex, which binds directly the V-ATPase in a glucose-dependent fashion (**Smardon *et al.*, 2002; Lu *et al.*, 2004; Chan and Parra, 2014**). Moreover, Forgac and his collaborators could show that regulated assembly of the yeast V-ATPase is controlled by the Ras/cAMP/protein kinase A (PKA) pathway in response to changes in glucose availability (**Bond and Forgac, 2008; Collins and Forgac, 2018**).

Also in humans, the V-ATPase assembly/disassembly is a finely regulated process that responds to a plethora of stimuli. The mammalian V-ATPases respond to glucose availability and, in kidney, elevated glucose levels (20 mM; normal physiological range 3.5–5.5 mM) cause increased V-ATPase assembly and acidification of intracellular vesicles. Probably, this occurs to maintain the neutral cytosolic pH during times of increased glycolysis (**Sautin *et al.*, 2005**). The glucose-mediated assembly in mammalian cells depends on PI3K (**Sautin *et al.*, 2005**) which also controls mTORC1 (**Lemmon and Schlessinger, 2010**). It has been recently reported that, in mammalian cells, the V-ATPase assembly and activity on lysosomes is increased also during glucose starvation (**McGuire and Forgac, 2018**). This is in contrast to the yeast model, where the glucose starvation causes dissociation of the V-ATPase, probably to store the ATP for nutrient-limiting conditions (**Kane, 1995; McGuire and Forgac, 2018**). The level of amino acids inside the cell can directly regulate the V-ATPase, indeed amino acid starvation leads to a rapid and reversible increase in V-ATPase assembly and activity in lysosomes, in a PI3K and mTORC1 independent fashion (**Stransky and Forgac, 2015**). The increased V-ATPase assembly lowers the lysosomal pH values, increasing protein turnover and amino acid levels, suggesting that a regulated assembly of the V-ATPase contributes to amino acid homeostasis (**Stransky and Forgac, 2015; Collins and Forgac, 2018**) (**Figure 8**).

1.4 V-ATPase and disease

Genetic defects in V-ATPase genes have been associated with several hereditary human diseases.

Loss-of-function mutations of the ATP6V0A3 subunit (MIM: 604592) have been found to be causative for autosomal recessive osteopetrosis (ARO) (**Frattini *et al.*, 2000; Kornak *et al.*, 2000; Bhargava *et al.*, 2012**). ARO is a rare infantile malignant osteopetrosis characterized by high bone density due to a failure of bone resorption. The clinical features comprise abnormal bone remodelling, deficient hematopoiesis and neurologic impairment (**Kornak *et al.*, 2000; Balemans *et al.*, 2005**).

Mutations in ATP6V0A4 were identified in patients with recessive distal renal tubular acidosis (dRTA) (**Smith *et al.*, 2000**). The gene encodes subunit *a4* of the V-

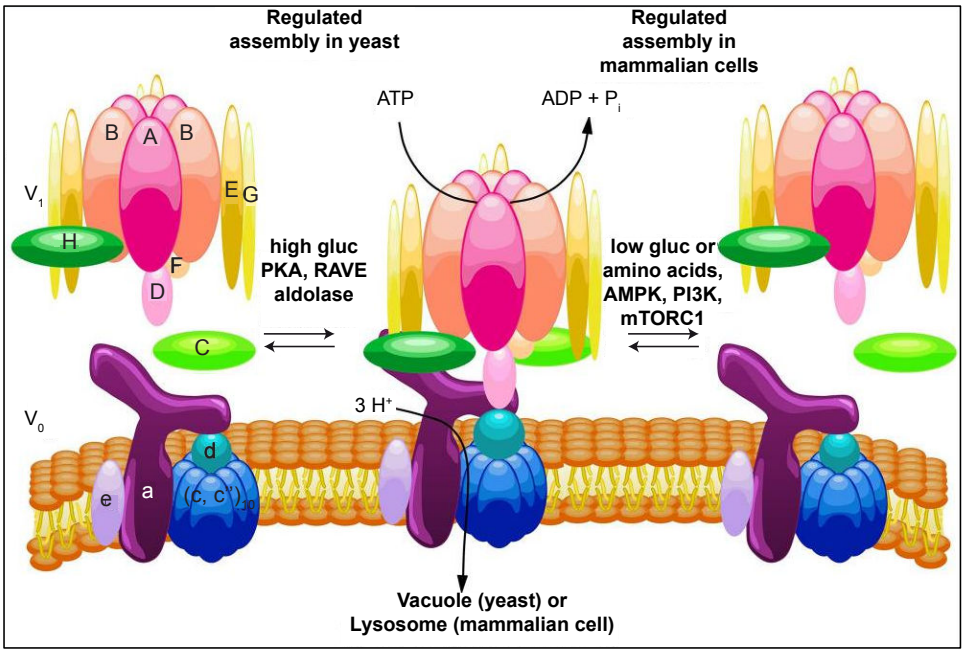

Figure 8: Regulated assembly of V-ATPases in response to nutrient availability

The assembly of the V-ATPase is a major form of V-ATPase regulation. It is a reversible process that involves the dissociation of the catalytic V_1 domain and the proton translocator V_0 domain in response to nutrient levels. On the left side of the figure, the regulated assembly in yeast. In this model, the assembly increases in high glucose conditions and is promoted by PKA, the two glycolytic enzymes aldolase and phosphofructokinase and the assembly factor RAVE. On the right side of the figure, the regulated assembly in mammalian cells, where in contrast, glucose starvation leads to increased V-ATPase assembly. This process is controlled by both the AMPK and PI3K/AKT pathways, but not PKA. Increased assembly in mammalian cells also occurs in response to amino acid starvation, and this effect is not controlled by PI3K or mTORC1. From Collins and Forgac, 2018.

ATPase, which was found to be exclusively expressed in fetal and adult kidney. Moreover, ATP6V0A4 mutations lead either to late-onset sensorineural hearing loss (SNHL) or to normal hearing (**Guillard, 2012**). Few patients developed severe hearing loss at young age (**Stover *et al.*, 2002; Guillard *et al.*, 2009**).

Mutations in ATP6V1B1 are associated with recessive dRTA, a rare genetic disease caused by failure of intercalated cells in the collecting duct to secrete the required protons for urinary acid excretion (**Guillard *et al.*, 2009; Guillard, 2012**). When untreated, this acidosis may lead to osteomalacia and rickets, with the dissolution of bones. The ATP6V1B1 mutations cause also a SNHL (**Karet *et al.*, 1999; Vargas-Poussou *et al.*, 2006**).

Mutations in both V-ATPase subunits and ER assembly factors have been associated with congenital disorders of glycosylation (CDG) type II. CDG are a group of genetic diseases with impaired synthesis/attachment of glycans to glycoproteins and glycolipids and synthesis of glycosylphosphatidylinositol (GPI) (**Freeze *et al.*, 2014**). Originally, the CDG have been classified into two groups, based on the profile of the transferrin glycoforms obtained by isoelectric focusing (IEF). This classification was mainly developed to classify deficiencies in the *N*-glycosylation pathway: (1) CDG-I covering the defects in the assembly of the *N*-glycan or its subsequent transfer to the protein, (2) CDG-II was referred to defects in the glycosylation of the proteins, either in the late ER or in the Golgi (**Aebi *et al.*, 1999**). However, the growing group of CDG caused by defects in protein *O*-glycosylation, glycolipid biosynthesis, vesicular trafficking and pH homeostasis made necessary a revision of the existing nomenclature. Nowadays, each disorder is named by the official gene symbol (not in italics), followed by the suffix "-CDG" (**Jaeken *et al.*, 2009**). The V-ATPase mutations associated with CDG can be divide into two groups:

(1) CDG with *cutis laxa*, caused by mutations in the core subunits (ATP6V0A2, ATP6V1A and ATP6V1E1);

(2) CDG with liver involvement, caused by mutations in the ER assembly factors (this group will be discussed in ***Chapter 2 – V-ATPase assembly and assembly factors*** and the ***Results*** part).

Mutations in ATP6V0A2 have been shown to cause an autosomal recessive form of *cutis laxa* type II (ARCLA2, MIM: 611716) and wrinkly skin syndrome (WSS), in combination with glycosylation defects (**Kornak *et al.*, 2008; Morava *et al.*, 2008**). *Cutis laxa* is a rare genetic disorder of the connective tissue characterized by excessive sagging of skin folds and decreased elasticity of the skin (**Guillard, 2012**). ARCLA2 is a syndromic disease, resulting in the involvement of other organs, such as the skeletal system and the central nervous system, the last one with a variable degree, either with mental retardation or without (**Morava *et al.*, 2008; Guillard *et al.*, 2009**). All the patients with ATP6V0A2 mutations show a CDG type II on transferrin IEF and abnormal IEF of apoC-III. Moreover, mass spectrometry reveals abnormal glycosylation of total serum proteins, with combined defect in *N*- and mucin-type *O*-linked glycans (**Kornak *et al.*,**

2008; Morava *et al.*, 2008). It has been suggested that the defects leading to *cutis laxa* could be due to V-ATPase related defects (**Kornak *et al.*, 2008; Guillard *et al.*, 2009**) and to abnormal function/transport of glycosyltransferases inside the Golgi (**Kornak *et al.*, 2008; Hucthagowder *et al.*, 2009**). Indeed, the most severe cases show abnormal folding/processing of the elastin in the elastic fibers (**Guillard, 2012**).

Mutations in the V-ATPase subunits ATP6V1E1 (MIM: 108746) and ATP6V1A (MIM: 607027) have been recently discovered as causative of a metabolic syndrome characterized by *cutis laxa*. Similarly to what has been shown for mutations in ATP6V0A2, these mutations affect the V-ATPase structure and assembly, leading to impaired protein glycosylation, Golgi trafficking and lysosomal function (**Van Damme *et al.*, 2017**). The patients show a variable CDG type II pattern in the transferrin IEF and abnormal transferrin glycosylation on mass spectrometry analysis. However, *N*-glycosylation is less affected than in individuals with ATP6V0A2 mutations. Even if both mutations do not affect the protein expression, they lead to reduced fully assembled V-ATPase complexes. As a consequence, the mutations lead to Golgi homeostasis defects, with abnormal swelling and Golgi fragmentation, and to compromised glycosylation of the collagen fibers. Moreover, defects in the V-ATPase lead to an accumulation of autolysosomes in the patients fibroblasts, suggesting impaired autophagy and lysosomal function (**Van Damme *et al.*, 2017**). The *cutis laxa* phenotype is less severe than the one caused by ATP6V0A2, with a generalized skin wrinkling in ATP6V1E1 mutations, and a phenotype characterized by large skin folds and abnormal fat distribution improving over time, in ATP6V1A mutations. In addition to *cutis laxa*, the seven described patients also display a multisystemic involvement, with facial features, hypotonia, joint contractures, congenital hip dysplasia and cardiopulmonary features (cardiomyopathy, congenital heart defects) (**Van Damme *et al.*, 2017**).

Chapter 2

V-ATPase assembly and assembly factors

Besides the genes encoding for the subunits of the V-ATPase complex, there are five additional proteins that are not part of the core holoenzyme but are required for the assembly of the V_0 domain in the ER. The ER assembly factors are Vma12p, Vma21p, Vma22p, Voa1p and Pkr1p (**Hirata *et al.*, 1993; Hill and Stevens, 1994, 1995; Jackson and Stevens, 1997; Malkus *et al.*, 2004; Ryan *et al.*, 2008; Davis-Kaplan *et al.*, 2006**). Each of these proteins have a human ortholog, except for Pkr1p (**Ramachandran *et al.*, 2013; Jansen *et al.*, 2016a, b, c**) (**Table 1**).

Saccharomyces cerevisiae	**Humans**
Vma21p	Vma21p
Vma12p	TMEM199
Vma22p	CCDC115
Voa1p	ATP6AP1
Pkr1p	-

Table 1: V-ATPase ER assembly factors in *Saccharomyces cerevisiae* and humans

2.1 ER assembly factors in yeast

2.1.1 Vma21p

Vma21p is a small integral protein and is one of the ER factors required for the assembly of the V_0 domain of the V-ATPase in the ER. Vma21p is evolutionarily conserved in vertebrates and invertebrates: the alignment of the protein sequences revealed that the N-terminal fragment displays high amino acid sequence identity exclusively in vertebrates while the C-terminal is highly conserved in both vertebrates and invertebrates (**Figure 9**).

Vma21p has been identified in *Saccharomyces cerevisiae* in a genetic screen designed to identify novel subunits of the V-ATPase (**Ho *et al.*, 1993; Hill and Stevens, 1994**). *Δvma21p* null mutant cells show the same phenotype of the *vma-* strains, including the inability to grow on media buffered at neutral pH, inability to acidify vacuoles, sensitivity to Ca^{2+} ions and *pet-* phenotype (inability to grow on non-fermentable carbon sources). Moreover, *Δvma21p* cells show also respiratory deficiency and a strong decreased level of V-ATPase activity (**Ho *et al.*, 1993; Hill and Stevens, 1994**).

Vma21p is formed by two hydrophobic transmembrane domains, oriented as a hairpin in the ER membrane, a 12-residue luminal loop, and N- and C-terminal domains of 12 and 16 residues, respectively, both cytoplasmically exposed (**Hill and Stevens, 1994; Malkus *et al.*, 2004**). Vma21p presents at the carboxy-terminal domain a dilysine motif KK*XX* responsible for its retention in the ER (**Hill and Stevens, 1994**) (**Figure 10**).

Failure of V_0 assembly in *Δvma21p* cells leads to decreased levels of V_0 subunits. This is particularly true for the Vph1p subunit (the ortholog of the subunit *a* in yeast), that is retro-translocated outside of the ER and degraded via the ER-associated degradation (ERAD) mechanism (**Hill *et al.*, 1994**). Conversely, in *Δvma21p* strains the levels of the V_1 subunits, whose assembly takes place in the cytosol (**Graham and Stevens, 1999**), are comparable to wild type strains. Vma21p drives the assembly of the proton translocating channel, or proteolipid ring, formed by Vma3p, Vma11p and Vma16p (the subunits *c* in humans) (**Hirata *et al.*, 1997**), interacting directly only with Vma11p (**Graham *et al.*, 1998; Malkus *et al.*, 2004**). Once the proteolipid ring is completely assembled under the help of Vma21p, Vph1p associates with Vma3p, Vma11p and Vma16p in the ER membrane (**Graham *et al.*, 1998**). In addition, the fully assembled V_0 domain is escorted outside of the ER by Vma21p, that will be then traveled back to the ER by virtue of its retrieval motif KK*XX* (**Graham *et al.*, 1998; Malkus *et al.*, 2004**). The mutagenesis of the dilysine motif KK*XX* into a diglutammic motif QQ*XX* not only lead to the mislocalization of *vma21QQp* to the vacuolar membrane, but also reduces the V-ATPase activity to almost 30% of the wild type in *Δvma21p* cells (**Hill and Stevens, 1994; Ryan *et al.*, 2008**), suggesting that the ER retrieval motif allows Vma21p to shuttle from the Golgi to the ER in order to act in multiple rounds of assembly (**Malkus *et al.*, 2004**).

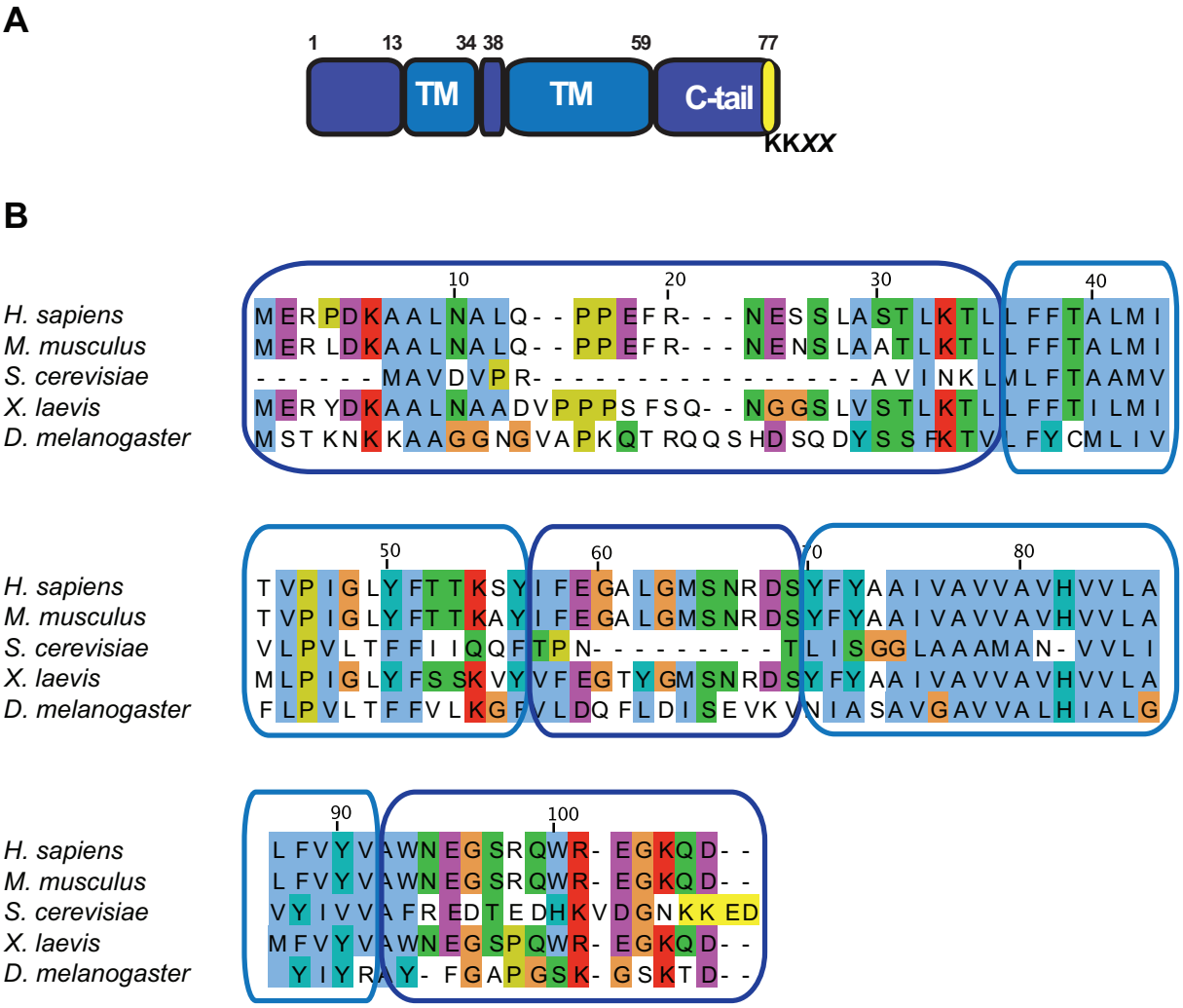

Figure 9: Structure of Vma21p and sequence alignment

Illustration showing the different domains of Vma21p. **(A)** Vma21p is a small protein of 11 kDa. It is formed by two transmembrane domains (colored light blue), with the N- and the C-terminal cytoplasmically exposed (colored dark blue). Colored in yellow, in the C-tail, is possible to observe the ER retention motif KK*XX*. **(B)** Sequence comparison of orthologs of VMA21, in humans (*H. sapiens*), mouse (*M. musculus*), yeast (*S. cerevisiae*), *Xenopus* (*X. laevis*) and *Drosophila* (*D. melanogaster*). The alignment of the sequences is displayed applying the default parameters of Clustal, highlighting the conserved position with color boxes using the Clustal X interface. The different domains are depicted by color code.

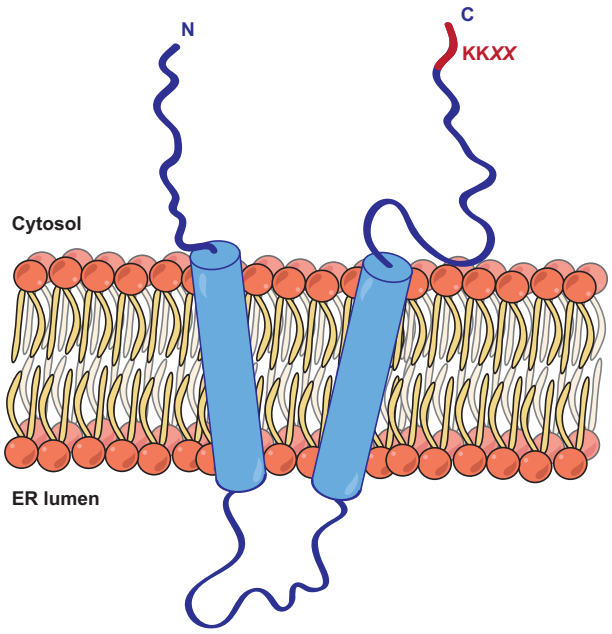

Figure 10: Structure and orientation of Vma21p in the ER

The model shows the structure and the orientation of Vma21p in the ER. Vma21p possess two transmembrane domains, with the N- and the C-terminal cytoplasmically exposed. Colored in red, in the C-terminal, the ER retention motif KK*XX*.

2.1.2 Vma12p and Vma22p

Vma12p and Vma22p are additional ER assembly factors of the V_0 domain of the V-ATPase. Vma12p, also known as Vph2p, was originally identified in a genetic screen in *Saccharomyces cerevisiae* as Ca^{2+}-sensitive mutant and initially called *cls10* (**Ohya *et al.*, 1986a, b, 1991**). Vma22p was instead identified in 1993 together with Vma21p in the genetic screen designed to identify novel genes essential for the V-ATPase (**Ho *et al.*, 1993**).

As the deletion of the *VMA12* or *VMA22* genes results in the *vma-* phenotype identical to those observed for mutant cells that lack a V-ATPase subunit, including failure to grow on media buffered to pH 7.5 and the downregulation of V_0 subunit Vph1p, both proteins Vma12p and Vma22p turned out to be involved in the V-ATPase complex (**Bachhawat *et al.*, 1993; Hirata *et al.*, 1993; Ho *et al.*, 1993; Hills and Stevens, 1995; Graham and Stevens, 1999**). Both Vma12p and Vma22p localize to the ER and do not fractionate with the purified V-ATPase indicating that they are not components of the enzyme complex but are required in the early steps of the assembly of the V_0 domain of the V-ATPase (**Hirata *et al.*, 1993; Jackson and Stevens, 1997**). Structurally, Vma12p is a 25 kDa protein with two membrane-spanning helices (**Bachhawat *et al.*, 1993; Hirata *et al.*, 1993**). Vma22p is a hydrophilic protein of 21 kDa lacking any obvious transmembrane domain (**Hill and Stevens, 1995; Graham *et al.*, 1998**). The ability of Vma22p to associate stably with ER membranes depends on the presence

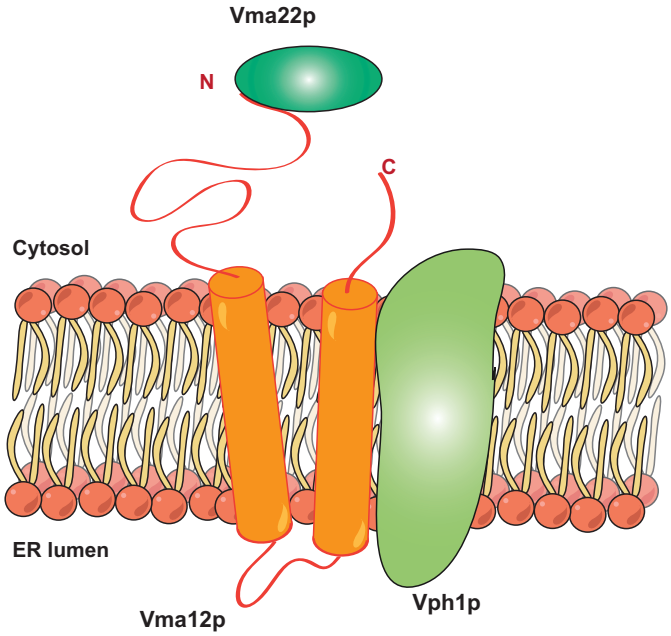

Figure 11: The complex Vma12p/Vma22p binds Vph1p in the ER

Vma12p (colored orange) binds Vma22p (colored dark green) through its cytosolic domain shortly after their synthesis and form a stable complex in the ER. The Vma12p/Vma22p complex interacts with Vph1p (colored light green). The interaction between the complex Vma12p/Vma22p and the V_0 subunit Vph1p is quite fast, reflecting that the assembly and release of the V_0 domain from the ER occurs within almost 5 minutes.

of the integral membrane protein Vma12p: Vma12p binds Vma22p through its cytosolic domain shortly after their synthesis and form a stable complex in the ER (**Graham *et al.*, 1998; Graham and Stevens, 1999**), while, in cells depleted for Vma12p, Vma22p is found to be localized in the cytosol (**Hill and Stevens, 1995; Graham *et al.*, 1998**).

The formation and stability of the Vma12p/Vma22p complex require neither ER assembly factors nor V_0 subunits (**Graham *et al.*, 1998; Graham and Stevens, 1999**). Just after forming the complex, Vma12p/Vma22p interact with Vph1p, helping its insertion in the V_0 domain, but not its translocation and/or folding (**Jackson and Stevens, 1997; Graham and Stevens, 1999**). Indeed, Vph1p is normally inserted into membranes in the absence of Vma12p, thus suggesting that the Vma12p/Vma22p complex must function at a later step aiding the assembly of the fully translocated and completely folded Vph1p into the V_0 domain (**Jackson and Stevens, 1997; Graham *et al.*, 2000; Hill and Cooper, 2000**) (**Figure 11**).

2.1.3 Pkr1p

Pkr1p is an ER-localized integral membrane protein of 14 kDa identified in a genome-wide screen in *Saccharomyces cerevisiae* (**Davis-Kaplan *et al.*, 2006**). Unlike the other ER assembly factors, the screen was performed to identify genes required for growth on low iron (**Davis-Kaplan *et al.*, 2004**). In fact, the name does not resume the implication in the *vma-* phenotype, but it has been assigned because Pkr1p is required to allow the growth on low iron medium. Indeed, when overexpressed, Pkr1p confers *P*ichia *f*arnosia *k*iller toxin resistance (**Davis-Kaplan *et al.*, 2004**).

Apart of its function in the growth of the yeast on low iron media, Pkr1p was shown to be an ER assembly factor for the V_0 domain of the V-ATPase. The deletion of Pkr1p specifically reduces the levels of Vph1p, as reflected by compromised growth in the presence of elevated Ca^{2+} (**Davis-Kaplan *et al.*, 2004**). But interestingly, unlike the other V-ATPase ER assembly factor deficiency, the strains lacking Pkr1p are still able to assemble some functional V-ATPase complexes and still have weakly acidified vacuoles (**Davis-Kaplan *et al.*, 2006**). Yet, the precise function of Pkr1p in the V_0 assembly is still unclear. It has been suggested that it may help Vma21p in stabilizing the proteolipid ring, but a direct interaction between Pkr1p and Vma21p, or other V_0 subunits, have not been proven yet (**Davis-Kaplan *et al.*, 2006**) (**Figure 12**).

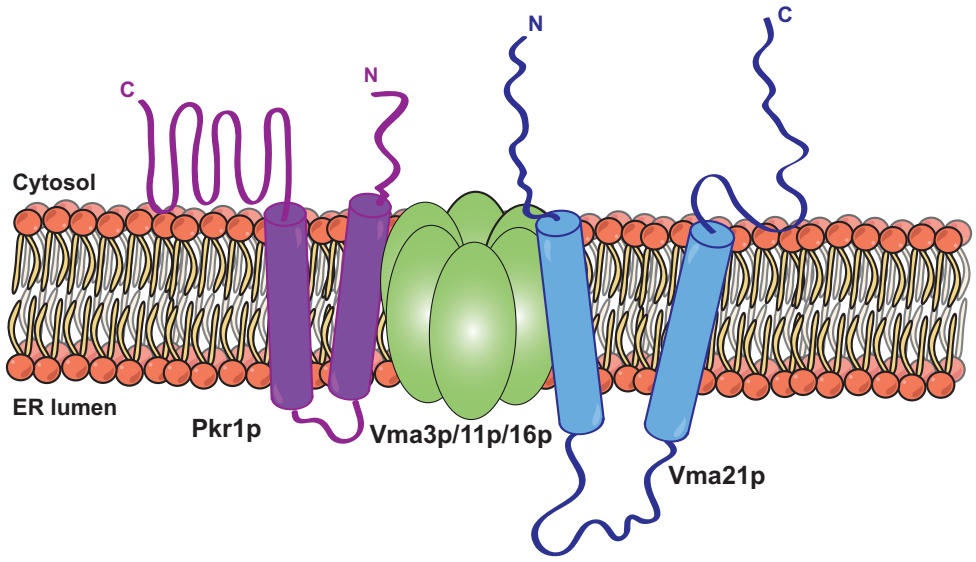

Figure 12: Model of Pkr1p and its function in the V-ATPase assembly

Pkr1p (colored purple) is a small protein of 14 kDa. Pkr1p has two transmembrane domains and is localized to the ER. The precise function of Pkr1p in the V_0 assembly is not completely clear: the proposed role is that could help Vma21p (colored blue) in stabilizing the proteolipid ring of *c* subunits (Vma3p/Vma11p/Vma16p, colored light green).

2.1.4 Voa1p

Voa1p is the fifth ER assembly factor of the V_0 domain of the V-ATPase (**Ryan *et al.*, 2008**). Voa1p was identified by Ryan and collaborators in a mass spectrometry approach designed to identify new proteins involved in the V_0/Vma21p complex in the ER membrane (**Ryan *et al.*, 2008**). The protein was called *VOA1* for *V0 a*ssembly protein 1. Voa1p is an integral glycoprotein that possesses two transmembrane segments. The N-terminal transmembrane segment is part of a predicted signal sequence that is rapidly cleaved. In addition, Voa1p possesses a cleavage site that produces a fragment anchored to the luminal side of the ER via the C-terminal transmembrane domain. This orientation results in the exposure of the dilysine ER retention motif KKNN in the cytosol and makes three asparagine residues in the luminal domain available for *N*-linked glycosylation (**Ryan *et al.*, 2008**). Voa1p deficiency reduces the V-ATPase activity to less than 25% of the wild type levels (**Ryan *et al.*, 2008**) without affecting the expression and localization of Vph1p (**Hirata *et al.*, 1993; Hill *et al.*, 1994; Hills and Stevens, 1995; Davis-Kaplan *et al.*, 2004**). However, this phenotype is only evident when it is combined with the *vma21pQQ* mutant (**Ryan *et al.*, 2008**). Voa1p associates early with the assembling V_0/Vma21p complex in the ER, interacting with the proteolipid ring. The role of Voa1p is most likely to help Vma21p in the assembly and exit of the V_0 domain from the ER (**Ryan *et al.*, 2008**) (**Figure 13**).

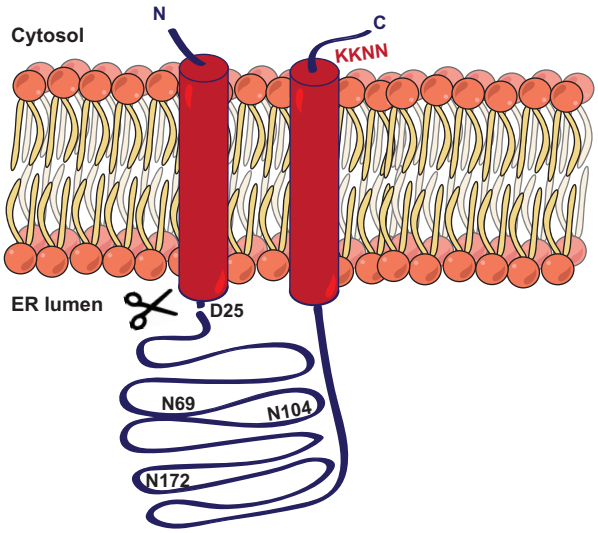

Figure 13: Schematic model of Voa1p

The model shows the structure and the orientation of Voa1p in the ER. The cleavage site of the 24 amino acids signal sequence is represented with scissors, with the Asp25 as first amino acid at the newly formed N-terminal. The bulk of Voa1p is exposed to the luminal side of the ER and consists of a globular domain anchored to the ER membrane by a transmembrane segment near the C-terminal of the protein. The three putative sites for *N*-glycosylation are indicated (N69, N104 and N172). The C-terminal contains an ER retrieval signal KKNN facing the cytosol. Adapted from Ryan *et al.*, 2008.

2.2 Regulation of V_0 assembly in yeast

The assembly of the V_0 domain is a carefully orchestrated process occurring in three steps inside the ER membrane. In the first step, the fully translocated and folded Vph1p interacts with the Vma22p/Vma12p complex (**Graham *et al.*, 1998**). In parallel, Vma21p drives the assembly of the proton translocating channel, formed by Vma3p, Vma11p and Vma16p (**Hirata *et al.*, 1997**). Vma21p interacts directly only with Vma11p (**Graham *et al.*, 1998; Malkus *et al.*, 2004**). It has been proposed that Pkr1p could stabilize the proteolipid ring to help Vma21p (**Davis-Kaplan *et al.*, 2006**). Voa1p associates early with the assembling proteolipid ring/Vma21p complex in the ER, interacting directly only with the proteolipid ring (via the *c* subunit) and with the subunits *a3* and *d* (**Ryan *et al.*, 2008**). In a second step, Vph1p is driven by the Vma22p/Vma12p complex to associate with the proteolipid ring/Vma21p complex (**Graham *et al.*, 1998**). In the third step, the subunits *d* and *e* are added to the nascent V_0 domain and both Vma12/Vma22p complex and Voa1p dissociate from the V_0/Vma21p complex. The V_0 domain is then escorted outside of the ER by Vma21p and is loaded in COPII vesicles and then transported to the Golgi (**Graham *et al.*, 1998; Malkus *et al.*, 2004**). Only in the Golgi, due to the lower pH, Vma21p dissociates from the V_0 domain and will then travel back to the ER by virtue of its retrieval motif KK*XX* (**Graham *et al.*, 1998; Malkus *et al.*, 2004**) (**Figure 14**).

2.3 ER assembly factors in humans

2.3.1 VMA21

VMA21 was identified in 1998 in screenings from bovine chromaffin granules performed to identify new V-ATPase components forming specifically the V_0 domain of the V-ATPase (**Ludwig *et al.*, 1998**). The protein was initially called M9.2 for its molecular weight after separation on blue native polyacrylamide gel electrophoresis (**Ludwig *et al.*, 1998**). The sequence similarity of human VMA21 and the yeast Vma21p proteins is not very high (45% similarity, 19% identity), but the structure is strongly conserved, with two hydrophobic transmembrane domains, a short luminal loop and a carboxy-terminal domain cytoplasmically exposed (**Ludwig *et al.*, 1998; Ramachandran *et al.*, 2013**). Interestingly, the human ortholog does not have an ER retrieval motif in the C-tail (**Figure 9 and 10**). Moreover, VMA21 has been found to associate with V_0 alone but also with V_1/V_0 holoenzymes, suggesting that the mammalian protein is not necessarily localized to the ER, as its yeast counterpart, but may even be integrated into the holoenzyme complex after having exerted its function in assembly (**Ludwig *et al.*, 1998; Ramachandran *et al.*, 2013**). Yet, it should be said that the assembly of human V-ATPase is not as well characterized as in yeast and, particularly, the VMA21 localization remains under debate. Ramachandran and his colleagues demonstrate that VMA21

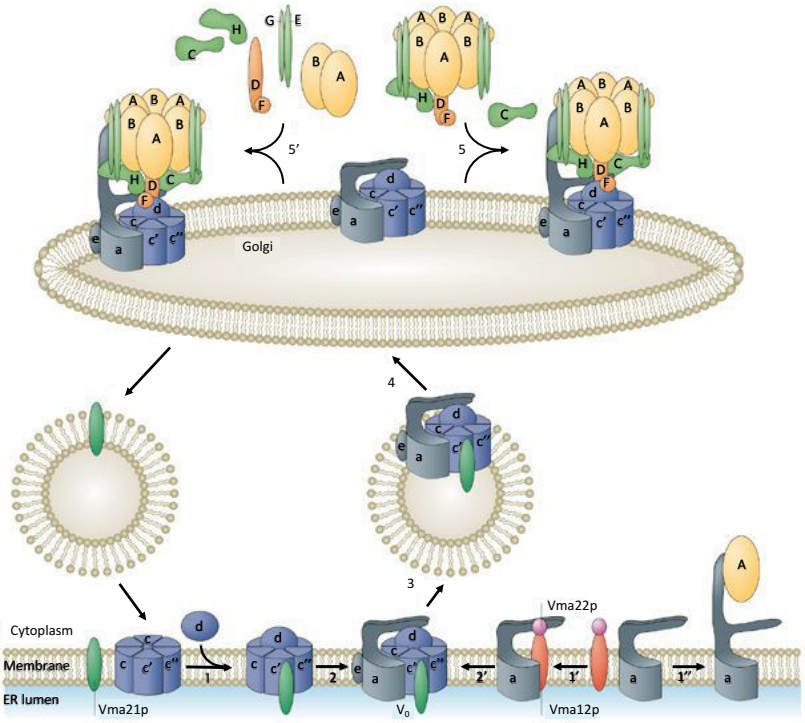

Figure 14: Assembly of the V-ATPase complex in yeast

The assembly of the V_0 domain (colored grey and blue) of the V-ATPase occurs in the ER and requires five dedicated assembly factors. Here in the figure are indicated Vma21p (colored dark green), Vma12p (colored red) and Vma22p (colored pink).
(**Step 1**) Vma21p interacts with subunit *c'* and directs the assembly of the proteolipid ring and subunit *d*. (**Steps 1', 2' and 2**) A complex formed by Vma12p/Vma22p stabilizes the subunit *a* and facilitates the assembly with the remainder of the V_0 complex. (**Steps 3 and 4**) Vma21p escortes the V_0 complex to the Golgi, where it dissociates from it and recycles to the ER by virtue of its Er retrieval motif. (**Steps 5 and 5'**) Assembly of V_0 complexes can occur either with almost fully assembled V_1 complexes (that lack subunit C) plus free subunit C or by assembly with individual V_1 subunits. (**Step 1"**) It has been suggested that assembly of the V_1 and V_0 domains can occur also in a more coordinated manner, as indicated by the complex formed between subunits A and *a*. From Forgac, 2007.

interacts with the proteolipid ring through the subunit *c"*: indeed, the subunit *c'* (the ortholog of Vma11p) does not exist in mammalian proteomes, while the V_0 domain utilizes only proteins *c* and *c"* (**Forgac, 2007**). The fully assembled V_0 domain then moves to the Golgi with the help of VMA21, but once there it does not travel back to the ER, like its yeast counterpart (**Ramachandran *et al.*, 2013**). By contrast, it has recently also been proposed that VMA21 does not remain associated with the V-ATPase, because prolonged VMA21/V_0 association reduces V_1/V_0 assembly and causes V-ATPase dysfunction (**Esmail *et al.*, 2018a, b**). In humans, mutations in *VMA21* have been associated with a rare X-linked autosomal recessive disorder (also called XMEA), characterized by myopathy with excessive autophagy (OMIM: 310440). XMEA was originally identified in 1988 in a Finnish family and, since then, additional cases have been described, with a relatively uniform clinical picture: a slowly progressive myopathy, with loss of distal and proximal muscle strength. Clinically, the skeletal muscle seems to be the only organ to be affected in the XMEA patients (**Kalimo *et al.*, 1988; Villanova *et al.*, 1995; Chabrol *et al.*, 2001**). The first muscles to be affected are shoulder, hip girdles and thigh muscles. The disease results with loss of independent ambulation after age fifty (**Kalimo *et al.*, 1988; Villanova *et al.*, 1995; Chabrol *et al.*, 2001; Ramachandran *et al.*, 2013; Dowling *et al.*, 2015**). Together with the Pompe and Danon Disease, they compose the autophagic vacuolar myopathies (AVMs), a subgroup of muscle disorders all characterized, as the name suggests, by the accumulation of autophagic vacuoles in the skeletal muscles (**Nishino, 2006; Dowling *et al.*, 2015**). Linkage analysis of the first reported XMEA family suggested that the causative gene is telomeric 10.5 cM of Xq28 (**Saviranta *et al.*, 1988; Auranen *et al.*, 2000; Saraste *et al.*, 2000; Villard *et al.*, 2000; Minassian *et al.*, 2002**). This was followed by the identification of mutations in the *VMA21* gene in 2009 (**Ramachandran *et al.*, 2013**). The diagnostic evaluation of XMEA patients revealed elevated levels of serum creatine kinase (CK) (2x to 20x normal) (**Dowling *et al.*, 2015**) (**Table 2**). Electromyography (EMG) features are variable and mostly all the patients have myopathic appearing units (**Jääskeläinen *et al.*, 2002; Munteanu *et al.*, 2005**). Interestingly, there are two cases in which it was possible to observe EMG abnormalities with myotonia also in absence of weakness (**Munteanu *et al.*, 2005**). The muscle biopsy is consistent across patients and revealed that the deficiency of VMA21 leads to the formation of autophagic vacuoles positives for lysosomal proteins (like LAMP1 and LAMP2) (**Kalimo *et al.*, 1988**) and with sarcolemmal features, mostly accumulation of sarcolemmal and T-tubule protein dysferlin on the vacuoles surface (**Kalimo *et al.*, 1988; Minassian *et al.*, 2002**). Moreover, it is possible to observe the accumulation of vacuoles enclosing partially degraded organelles and debris, which translocate to the myofiber surface and extrude their contents, forming a field of cells between multilayered basal lamina (**Kalimo *et al.*, 1988; Crockett *et al.*, 2014**). Additionally, there is deposition of complement C5b-9 (membrane attack complex) along the vacuolar and cell surface membranes (**Villanova *et al.*, 1995;**

Louboutin *et al.*, 1996; Crockett *et al.*, 2014). Fatty degeneration of muscle tissue has also been observed with magnetic resonance imaging (MRI) (**Minassian *et al.*, 2002**).

Despite the ubiquitous expression of the V-ATPase, XMEA has long been considered exclusively a skeletal muscle disease. Nevertheless, a more in-depth analysis revealed the involvement of other organs, as the heart and the liver, in few rare cases (**Munteanu *et al.*, 2015**). The members of the worst affected family, in which we talk about Congenital Autophagic Vacuolar Myopathy (CAVM), have a mild cardiac hypertrophy on echocardiography (**Munteanu *et al.*, 2015**); cardiac autopsy on one of the first cases reported revealed slight hypertrophy and cardiac vacuolation resembling exactly to the defects caused by XMEA in the skeletal muscle (**Munteanu *et al.*, 2017**). These patients have all the same mutations, c.164-6 T>G, that is just one nucleotide over from a common XMEA mutation, c.164-7T>G (**Ramachandran *et al.*, 2013; Crockett *et al.*, 2014**). This mutation removes the last pyrimidine in the polypyrimidine tract, strongly reducing the splicing efficiency, consistent with the stronger VMA21 reduction by c.164-6T>G than by c.164-7T>G (**Munteanu *et al.*, 2015, 2017**).

Interestingly, two mutations described in 3' UTR of *VMA21* revealed also a mild liver involvement (**Ruggieri *et al.*, 2015; Saraste *et al.*, 2015**). The first mutation is the c.*6A>G. This mutation was described in two different reports, in the first report in four males (aged from 25 to 48 years) having a mild plasma cholesterol increase (from 174 to 275 mg/dL) (**Saraste *et al.*, 2015**). The second report describes a patient with the same mutation, initially manifesting only skeletal muscle involvement (**Ramachandran *et al.*, 2013**) and thereafter dead due to hepatic cirrhosis (**Ackerley *et al.*, 2016**). The second mutation is a microdeletion found in one male, c.*13_*104del, associated with persistent increases in liver function tests: LDH 1499 U/L (normal range 230–460 U/L), AST 181 U/L (normal range 2–40 U/L) and ALT 438 U/L (normal range 0–40 U/L) (**Ruggieri *et al.*, 2015**) (**Table 2**, plus see **Table 3** for laboratory tests and normal values).

All the XMEA mutations are hypomorphic alleles that reduce VMA21 expression. Most of them are intronic variants that act by reducing splicing efficiency (**Table 2**) (**Ramachandran *et al.*, 2013; Crockett *et al.*, 2014; Saraste *et al.*, 2015; Ruggieri *et al.*, 2015; Munteanu *et al.*, 2015, 2017**). XMEA has an early onset, usually appearing within in the first two decades of life (**Ramachandran *et al.*, 2013; Mercier *et al.*, 2015; Munteanu *et al.*, 2015**), but there are also rare cases with adult and congenital onset (**Crockett *et al.*, 2014**). The patients with an earlier onset have more severe mutations, resulting in a greater reduction of VMA21 expression (**Munteanu *et al.*, 2015; Ruggieri *et al.*, 2015; Konialis *et al.*, 2017**).

On the muscle histology and electron microscopy, it is possible to observe accumulation of abundant clustered lysosomes. Moreover, it is possible to find vacuoles in the subsarcolemmal and intermyofibrillar space, mostly as manifestation of autophagosomes

extrusion (**Dowling *et al.*, 2015**).

Based on current knowledge, the following model for XMEA pathogenesis has been developed: (1) mutations in *VMA21* cause reduced levels of VMA21; (2) the reduced levels of VMA21 lead to V-ATPase defective assembly and reduced V-ATPase activity; (3) the reduced V-ATPase raises the lysosomal pH; (4) the increased lysosomal pH reduces the activity of lysosomal hydrolases; (5) reduced hydrolase activity leads to a partial block of the terminal steps of autophagy; (6) impaired V-ATPase activity and hydrolase function also potently induce autophagy, likely via inhibition of the mTORC1 pathway; (7) induction of autophagic flux in the setting of impaired autophagy causes a "feed forward" pathogenic loop, resulting in the accumulation of autophagolysosomes with incompletely digested contents (**Ramachandran *et al.*, 2013; Dowling *et al.*, 2015**). Although this model is rather conclusive, there are still many open questions, for example why the skeletal muscle is the most impaired despite the ubiquitous need for V-ATPase assembly and function.

Reference	Mutation	Onset	Muscle involvement	Liver involvement	Other symptoms
a. Saraste *et al.*, 2015 (previously described in **Kalimo *et al.*, 1988**); **b. Ramachandran *et al.*, 2013**; **c. Ackerley *et al.*, 2016**	c.*6A>G (3' UTR)	Childhood	Proximal and distal muscles CK: strongly elevated Absence of cardiac involvement	**a.** Cholesterol: 174–275 mg/dL **c.** Death for fatal hepatic failure	n/a
Ruggieri *et al.*, 2015	c.*13_*104 del (3' UTR)	Early neonatal	Severe muscle involvement CK: 2673 U/L Absence of cardiac involvement	LHD: 1499 U/L AST: 181 U/L ALT: 438 U/L	Congenital malformation in the right hippocampus
Ruggieri *et al.*, 2015	c.54-16_54-8 del	Early neonatal	Severe muscle involvement CK: 830–1290 U/L Absence of cardiac involvement	n/a	n/a
Ramachandran *et al.*, 2013	c.54-27 A>C c.54-27 A>T	Early childhood	Proximal muscles of the lower extremities CK: strongly elevated Absence of cardiac involvement	n/a	n/a
Mercier *et al.*, 2015	c.163+4A>G, c.163+3A>G	Early childhood	Progressive muscle weakness, fatty degeneration in MRI CK: n/a Absence of cardiac involvement	n/a	n/a
a. Ramachandran *et al.*, 2013; **b. Kurashige *et al.*, 2013**; **c. Crockett *et al.*, 2014**	c.164-7 T>G	**a.**, **b.**: Early childhood **c.** Late in adulthood	Proximal muscle weakness Absence of cardiac involvement CK: **a.** strongly elevated **b.** 450 U/L **c.** 300–400 U/L	n/a	**b.** High urinary β2 microglobulin without renal dysfunction (1.51 µg/ml)
a. Munteanu *et al.*, 2015 (previously described in **Yan *et al.*, 2005**); **b. Munteanu *et al.*, 2017** (previously described in **Morisawa *et al.*, 1998**)	c.164-6 T>G	Early childhood	Severe muscle weakness, with ventilation dependence CK: strongly elevated (10-fold) **a.** mild cardiac hypertrophy **b.** slight hypertrophy and autophagic vacuoles on myofibers	n/a	n/a
Konialis *et al.*, 2017	c.94_96 del TTC	Prenatal	Arthrogryposis CK: n/a Cardiac involvement: n/a	n/a	n/a
Ramachandran *et al.*, 2013	c.272 G>C (Gly91Ala)	Early childhood	Proximal muscle weakness CK: strongly elevated Absence of cardiac involvement	n/a	n/a

Table 2: VMA21 deficient patients: genetic, clinical and laboratory data

Test	Normal values
Creatine Kinase (CK)	Male: 171 U/L
	Female: 145 U/L
Total Cholesterol	Normal: $<$ 200 mg/dL
	Borderline: 200–239 mg/dL
	High: $>$ 240 mg/dL
LDL Cholesterol	Normal: $<$ 100 mg/dL
	Borderline: 130–159 mg/dL
	High: $>$ 160 mg/dL
Lactate Dehydrogenase (LDH)	Newborn: 100–450 U/L
	Infant: 100–250 U/L
	Child: 60–170 U/L
	Adult: 100–190 U/L
Alanine Aminotransferase (ALT)	7–55 U/L
Aspartate Transaminase (AST)	8–48 U/L
Alkaline Phosphatase (ALP)	20–140 U/L
Ceruloplasmin	20–35 mg/dL
β2 microglobulin (in urine samples)	0–0.3 μg/mL

Table 3: Laboratory tests and normal values

2.3.2 TMEM199 and CCDC115

The human ortholog of Vma12p is TMEM199 (transmembrane protein 199), a transmembrane protein with high homology to the yeast V-ATPase assembly protein Vma12p (24% sequence identity) **(Jansen *et al.*, 2016a; Miles *et al.*, 2017)**. The human ortholog of Vma22p was initially identified as a downstream gene regulated by Fibroblast growth factor 2 (FGF2) promoting cell proliferation and protecting from apoptosis (**Pellicano *et al.*, 2006, 2010**). It was initially called "coiled-coil protein 1" (ccp1) or "coiled-coil domain containing 115" (CCDC115) (**Pellicano *et al.*, 2006, 2010**). Only subsequent analysis revealed that CCDC115 is the human ortholog of Vma22p (**Kelley *et al.*, 2015; Jansen *et al.*, 2016b; Miles *et al.*, 2017**). CCDC115 is a 180 amino acids protein presenting two coiled-coil domains and a leucine-zipper structure within the first coiled-coil domain (**Pellicano *et al.*, 2006**) (**Figure 15**).

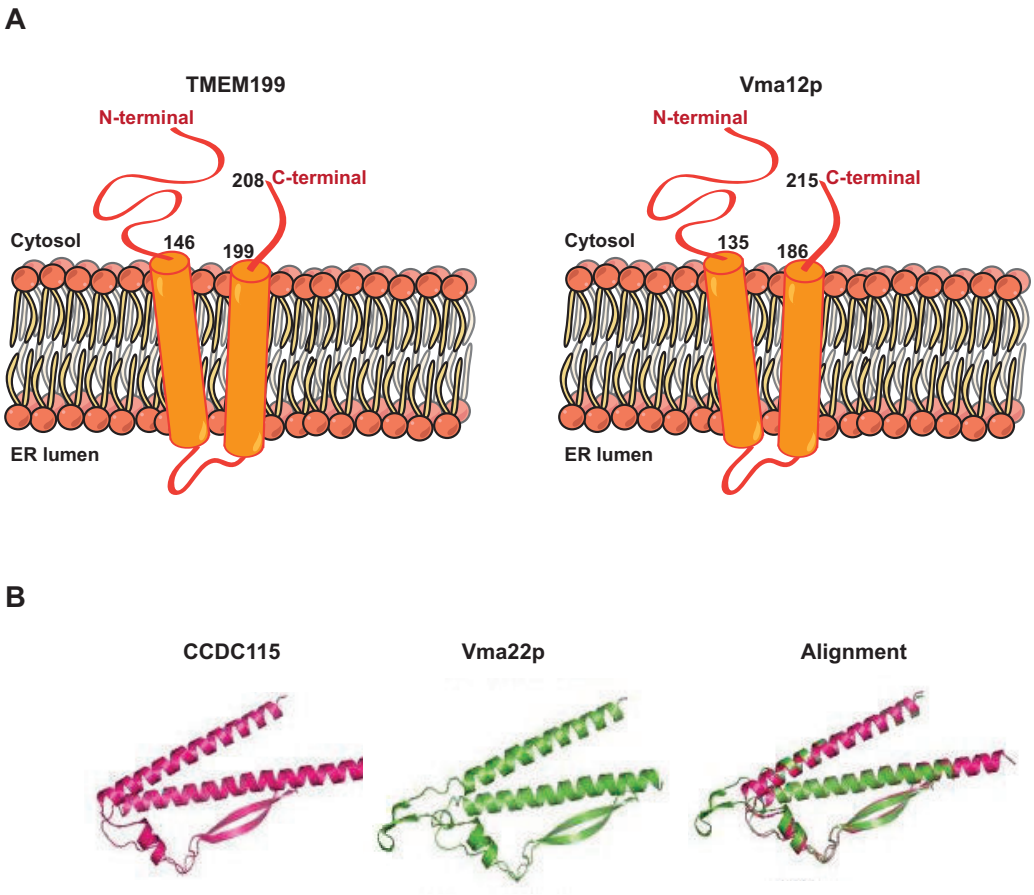

Figure 15: Schematic drawing of TMEM199 and CCDC115

(A) Schematic membrane topology of TMEM199 (left) and Vma12p (right), respectively. TMEM199 and Vma12p show 23.89% sequence identity. **(B)** Structural alignment of CCDC115 (colored pink) and Vma22p (colored green) based on Phyre2 predictions. Adapted from Miles *et al.*, 2017.

Upon transient overexpression, Jansen *et al.*, found TMEM199 to predominantly localize in the ER-Golgi intermediate compartment (ERGIC) (**Jansen *et al.*, 2016a**), while overexpressed CCDC115 localized to endo/lysosomal structures (**Pellicano *et al.*, 2006, 2010**), or ERGIC (**Jansen *et al.*, 2016b**). The analysis of the endogenous localization of both TMEM199 and CCDC115 revealed a predominant ER localization (**Miles *et al.*, 2017**). While yeast studies explain the role of the complex Vma12p/Vma22p in the V-ATPase assembly, in mammalian cells they may exert additional regulatory functions (**Miles *et al.*, 2017**). Indeed, TMEM199 and CCDC115 deficiency leads to a disturbance in Golgi homeostasis, mostly altering the lumen acidification, with an indirect effect on multiple glycosylation pathways, post-translational modification and protein secretion and sorting (**Jansen *et al.*, 2016a, b**). Moreover, TMEM199 and CCDC115 deficiency leads to V-ATPase inhibition, with reduced endosomal acidification, disturbed iron-clathrin-mediated endocytosis and reduced available pool of intracellular Fe(II) (**Miles *et al.*, 2017**). Accordingly, TMEM199 and CCDC115 mutations were found to be associated with a CDG characterized by *N*- and *O*-glycosylation abnormalities and liver disease (**Jansen *et al.*, 2016a, b; Jaeken and Péanne, 2017; Marques-da-Silva *et al.*, 2017; Girard *et al.*, 2018; Vajro *et al.*, 2018**).

The liver produces most of the glycosylated serum proteins and, indeed, defects in glycosylation can affect liver structure and function (**Blomme *et al.*, 2009**). For example, the deficiency of some glycosyltransferases [i. e. N-acetylglucosaminyltransferase V (GnT-V and α1-6 fucosyltransferase (α1-6 FT)] can lead to the development of liver cirrhosis and fibrosis (**Blomme *et al.*, 2009**). Moreover, the membrane receptors present on the hepatocytes recognize their ligand through their carbohydrate residues (**Blomme *et al.*, 2009**), thus they are not able to bind their ligands if the glycosylation is defective, leading to alteration of the hepatic functions (**Marques-da-Silva *et al.*, 2018**). Liver involvement is present in almost 20% of the CDG (**Marques-da-Silva *et al.*, 2018**).

TMEM199-CDG (MIM: 616829) is an autosomal recessive disorder characterized by the loss-of-function mutations in TMEM199 that lead to a deficiency of the ER assembly factor. All the reported patients show reduced *N*- and mucin-type *O*-glycosylation, with reduced galactose and sialic acids incorporation into the proteins (**Jansen *et al.*, 2016a; Marques-da-Silva *et al.*, 2018; Vajro *et al.*, 2018**). Based on the IEF of serum transferrin, TMEM199 is a type 2 CDG. A rising number of disorders affecting Golgi homeostasis have been implicated in metabolic syndromes with liver and brain involvement. However, TMEM199-CDG patients do not show brain problems, except for two of them, carrying the same mutation, presenting mild hypotonia and mild speech delay (**Jansen *et al.*, 2016a; Jaeken and Péanne, 2017; Marques-da-Silva *et al.*, 2017; Vajro *et al.*, 2018**). To date, there are seven patients (males and females), all showing a mild, almost subclinical, hepatic phenotype. There is no liver failure, or cholestasis or hepatomegaly and the liver disease is non-progressive over time. Electron microscopy on liver biopsy tissue showed a severe vacuolization, with the presence of large

lipid vacuoles and alteration of the mitochondria (**Jansen *et al.*, 2016a**). The biomarker of this disorder is the increase of amino transaminases (ALT and AST), serum alkaline phosphatase (ALP), cholesterol and LDL-cholesterol (**Jansen *et al.*, 2016a**). Particularly, it has been proposed that the measurement of ALP could be useful to diagnose TMEM199-CDG since all patients presented elevated levels of this enzyme. Given the low serum ceruloplasmin levels and the mild liver copper accumulation, TMEM199-CDG resembles Wilson's disease (WD) (**Jansen *et al.*, 2016a; Jaeken and Péanne, 2017; Vajro *et al.*, 2018**) (**Table 4**).

CCDC115-CDG (MIM: 616829) is an autosomal recessive disorder characterized by the deficiency of the V-ATPase assembly factor CCDC115 (**Jansen *et al.*, 2016b; Girard *et al.*, 2018**). In the last three years, eleven patients with CCDC115 deficiency have been described showing abnormal *N*- and mucin-type *O*-glycosylation of serum glycoproteins. The diagnosis based on transferrin IEF shows a CDG type 2 pattern. Unlike mutations in TMEM199, the CCDC115 deficiency causes a disorder that affects not only the liver, but displays also a neurological involvement (**Jansen *et al.*, 2016b; Jaeken and Péanne, 2017; Girard *et al.*, 2018**). Despite the patients described have the same mutations, only the group of Girard *et al.* characterized the neurological features, ranging them from mild symptoms to psychomotor disease (PMD) and hypotonia (**Girard *et al.*, 2018**). The hepatopathy in CCDC115 patients appears to be rather homogenous and can be very severe: two patients underwent liver transplantation and two patients have died for liver failure. The liver biopsy showed steatosis, focal portal inflammation and portal-to-portal bridging fibrosis classified as stage F2/F3 in the METAVIR scoring system (**Girard *et al.*, 2018**). In general, the patients show elevated ALT and AST and serum ALP, mild hypercholesterolemia and low ceruloplasmin levels (**Jansen *et al.*, 2016b; Girard *et al.*, 2018**). In few patients, it is possible to observe also elevated CK, suggesting even a muscular involvement (**Girard *et al.*, 2018**) (**Table 5**).

The deficiency of the two ER assembly factors TMEM199 and CCDC115 cause a similar metabolic syndrome, characterized by liver involvement and glycosylation defects, suggesting that the overlapping phenotype is caused by a similar defective V-ATPase assembly. However, it remains to be elucidated why mutations in the main ER assembly factor VMA21 cause a different disease, affecting the autophagic flux only in the skeletal muscle without glycosylation defects and impaired liver function.

Reference	Mutation	Glycosylation Profile	Aminotransferases	Liver	Neurological development	CK	Ceruplasmin	Cholesterol and LDL
Jansen *et al.*, 2016a	c.20 C>A (Ala7Glu)	Abnormal *N*- and *O*-glycosylation	ALT: 54 U/L AST: 73 U/L ALP: 745 U/L	Mild steatosis	Normal	n/a	11.5 mg/dL	Cholesterol: 253 mg/dL LDL-C: 188 mg/dL
Jansen *et al.*, 2016a	c.20 C>A (Ala7Glu)	Abnormal *N*- and *O*-glycosylation	ALT: 210 U/L AST: 246 U/L ALP: 1162 U/L	Mild steatosis	Normal	n/a	8.8 mg/dL	Cholesterol: 336 mg/dL LDL-C: 277 mg/dL
Jansen *et al.*, 2016a	c.40 G>C (Ala14Pro) + c.376-1 G>A (?)	Abnormal *N*-glycosylation	ALT: 190 U/L AST: 153 U/L ALP: 718 U/L	Mild steatosis and fibrosis	Normal	n/a	8.8 mg/dL	Cholesterol: 204–337 mg/dL LDL-C: 182–226 mg/dL
Jansen *et al.*, 2016a	c.92 G>C (Arg31Pro)	Abnormal *N*- and *O*-glycosylation	ALT: 36–172 U/L AST: 31–119 U/L ALP: 132–1528 U/L	Mild steatosis	Hypotonia	n/a	17–24 mg/dL	Cholesterol: 231–257 mg/dL LDL-C: 161–171 mg/dL
Vajro *et al.*, 2018	c.13-14delTT (p.Ser4Serfs*30) + c.92 G>C (Arg31Pro)	Abnormal *N*- and *O*-glycosylation	ALT: 23–329 U/L AST: 53–349 U/L ALP: 1140–1995 U/L	Slight hepatomegaly, fibrosis and focal steatosis	Normal	561–799 U/L	6–8 mg/dL	Cholesterol: 300–340 mg/dL LDL-C: 240–256 mg/dL
Vajro *et al.*, 2018	c.13-14delTT (p.Ser4Serfs*30) + c.92 G>C (Arg31Pro)	Abnormal *N*- and *O*-glycosylation	ALT: 50–221 U/L AST: 98—299 U/L ALP: 903–3990 U/L	Slight hepatomegaly, fibrosis and focal steatosis	Normal	442–142 U/L	4–6 mg/dL	Cholesterol: 220–240 mg/dL LDL-C: 176–177 mg/dL
Vajro *et al.*, 2018	c.13-14delTT (p.Ser4Serfs*30) + c.92 G>C (Arg31Pro)	Abnormal *N*- and *O*-glycosylation	ALT: 104–437 U/L AST: 156–656 U/L ALP: 713–1235 U/L	Slight hepatomegaly, fibrosis and focal steatosis	Mild delay speech	240–510 U/L	8–8.4 mg/dL	Cholesterol: 140–160 mg/dL LDL-C: 96–98 mg/dL

Table 4: TMEM199 deficient patients: genetic, clinical and laboratory data

Reference	Mutation	Glycosylation Profile	Aminotransferases	Liver	Neurological development	CK	Ceruplasmin	Cholesterol and LDL
Jansen *et al.*, 2016b	c.92 T>C (Leu31Ser)	Abnormal *N*- and *O*-glycosylation	AST: 130–158 U/L ALT: 85–101 U/L ALP: 1016–1193 U/L	Hepatomegaly	PMD, hypotonia	n/a	4 mg/dL	Normal
Jansen *et al.*, 2016b	c.92 T>C (Leu31Ser)	Abnormal *N*- and *O*-glycosylation	AST: 96–436 U/L ALT: 140–995 U/L ALP: 1070–1577 U/L	Hepatomegaly	PMD, hypotonia, muscle atrophy	n/a	4 mg/dL	Cholesterol: 289 mg/dL
Jansen *et al.*, 2016b	c.92 T>C (Leu31Ser)	Abnormal *N*- and *O*-glycosylation	AST: 1089 U/L ALT: 591 U/L ALP: 1251 U/L	Hepatomegaly	PMD	n/a	n/a	n/a
Jansen *et al.*, 2016b	c.92 T>C (Leu31Ser)	Abnormal *N*- and *O*-glycosylation	AST: 422 U/L ALT: 588 U/L ALP: 976 U/L	Hepatomegaly, copper accumulation	Mild PMD	n/a	3.3 mg/dL	Cholesterol: 381 mg/dL LDL-C: 332 mg/dL
Jansen *et al.*, 2016b	c.92 T>C (Leu31Ser)	Abnormal *N*- and *O*-glycosylation	AST: 1780 U/L ALT: 390 U/L ALP: 950 U/L	Hepatomegaly, fibrosis, steatosis, necrotic lesions	PMD, seizures hypotonia	n/a	1 mg/dL	Cholesterol: 289 mg/dL
Jansen *et al.*, 2016b	c.31 G>T (Asp11Tyr)	Abnormal *N*- and *O*-glycosylation	AST: 192–669 U/L ALT: 83–308 U/L ALP: 702 U/L	Liver failure	Normal	n/a	n/a	Mild elevated
Jansen *et al.*, 2016b	c.31 G>T (Asp11Tyr)	Abnormal *N*- and *O*-glycosylation	AST: 98–422 U/L ALT: 98–178 U/L ALP: 710-985 U/L	Liver failure (death)	Normal	n/a	n/a	Mild elevated
Jansen *et al.*, 2016b	c.92 T>C (Leu31Ser) ?_–258 (*1245_?del)	Abnormal *N*- and *O*-glycosylation	AST: 207–972 U/L ALT: 48–153 U/L ALP: 850–1031 U/L	Hepatomegaly, cirrhosis, liver failure (death)	Hypotonia	n/a	n/a	Cholesterol: 431 mg/dL LDL-C: 314 mg/dL
Girard *et al.*, 2018	c.92 T>C (Leu31Ser) c.19 C>T (Arg7*)	Abnormal *N*- and *O*-glycosylation	AST: 56 U/L ALT: 45 U/L ALP: 196 U/L	Glycogen vacuolization	Hypotonia, Delayed psychomotor development	Normal	>1 mg/dL	Cholesterol: 215 mg/dL
Girard *et al.*, 2018	c.92 T>C (Leu31Ser) c.38T>C (Leu13Pro)	Abnormal *N*- and *O*-glycosylation	AST: 154 U/L ALT: 137 U/L ALP: 218 U/L	Normal	Normal	519 U/L	>1 mg/dL	Cholesterol: 318 mg/dL
Girard *et al.*, 2018	c.92 T>C (Leu31Ser) c.19 C>T (Arg7*)	Abnormal *N*- and *O*-glycosylation	n/a	Severe fibrosis and steatosis	Hypothonia, moderate mental retardation with normal brain MRI	Elevated	9 mg/dL	Cholesterol: 386 mg/dL

Table 4: CCDC115 deficient patients: genetic, clinical and laboratory data

Chapter 3

V-ATPase accessory subunits

The biochemical purification of chromaffin granules in bovine cells have revealed the existence of two additional proteins associated with the V_1/V_0 holoenzyme. These two proteins appeared to be absent in yeast and do not seem to be part of the core subunits of the proton pump. Therefore, they have been defined accessory subunits of the V-ATPase, ATP6AP1 and ATP6AP2 (**Getlawi *et al.*, 1994; Supek *et al.*, 1994; Ludwig *et al.*, 1998).**

3.1 ATP6AP1

ATP6AP1 (ATPase H^+ transporting accessory protein 1), also known as Ac45, is a type I transmembrane protein associated with the V_0 domain of the V-ATPase (**Getlawi *et al.*, 1994; Supek *et al.*, 1994**). ATP6AP1 is composed of 468 amino acids, with an N-terminal signal sequence of 35 amino acids, a C-terminal membrane-spanning domain and several *N*-glycosylation sites (**Getlawi *et al.*, 1994**) (**Figure 13**). ATP6AP1 is synthetized as protein of 62 kDa and is then cleaved by furin between two valines (V246 and V247) early in the secretory pathway, mostly in the ER or *cis*-Golgi, where activation of the V-ATPase is necessary, and for sure before of the TGN (**Schoonderwoert *et al.*, 2002; Jansen and Martens, 2012**). The cleavage leads to the formation of a mature C-terminal (42-44 kDa) fragment of 222 amino acids and a short N-terminal fragment (20-22 kDa) (**Getlawi *et al.*, 1994; Schoonderwoert *et al.*, 2002; Louagie *et al.*, 2008**). Indeed, the cleavage of ATP6AP1 is a prerequisite for its transport to the plasma membrane (**Jansen *et al.*, 2008**). Furthermore, the cleaved form represents the naturally occurring ATP6AP1 associated with the V-ATPase in the late secretory pathway, indeed the initial name was Ac45 for its molecular weight (**Supek *et al.*, 1994**). Following passage through the Golgi, the 20-22 kDa N-terminal fragment is degraded while the C-terminal, together with the V-ATPase, is targeted to secretory granules (**Schoonderwoert *et al.*, 2002**). The C-terminal domain is highly conserved through vertebrates and invertebrates and contains a 26-amino acid domain that harbors an autonomous internalization signal, different from any previously described routing

signal. This signal drives the protein to the plasma membrane and then mediates the endocytosis of ATP6AP1 to vacuolar structures (**Jansen *et al.*, 1998; Schoonderwoert and Martens, 2002; Feng *et al.*, 2008**). Indeed, while the full-length ATP6AP1 colocalizes with the ER (**Jansen *et al.*, 2008**), the cleaved form traffics together with the V-ATPase within the secretory pathway (**Jansen *et al.*, 1998; Feng *et al.*, 2008; Yang *et al.*, 2012**). Moreover, ATP6AP1 is found associated with the ruffled border of resorbing osteoclasts, where it colocalizes with the V-ATPase subunit *a3* and F-actin (**Blair *et al.*, 1989; Nakamura *et al.*, 1997; Lee *et al.*, 1999; Holliday *et al.*, 2000; Toyomura *et al.*, 2003; Vitavska *et al.*, 2003; Feng *et al.*, 2008**). In 2016, the group of Jansen suggested ATP6AP1 to be an ortholog of Voa1p. The initial finding was based on bioinformatics analysis: upon closer inspection, the C-terminal fragment of ATP6AP1 indeed showed some sequence homology with the yeast V-ATPase assembly factor Voa1p (**Jansen *et al.*, 2016c**). To confirm that ATP6AP1 shares functions with Voa1p, Jansen *et al.* performed complementation assays in a *Saccharomyces cerevisiae* strain deficient for both Voa1p and Vma21p (*voa1::H vma21QQ* strain). This strain has a defective growth on media enriched with Ca^{2+} (*vma-* phenotype): the complementation of the *voa1::H vma21QQ* strain with the C-terminal fragment of ATP6AP1 harboring the dilysine motif KKNN rescues the yeast growth, indicating that the processed ATP6AP1 fulfils the function of Voa1p in yeast cells (**Jansen *et al.*, 2016c**). In electron and cryo-electron microscopy it has further been demonstrated that ATP6AP1 associates with the V_0 domain, with its C-terminal anchored in the membrane and the N-terminal projecting towards the luminal side (**Holthuis *et al.*, 1999; Wilkens *et al.*, 1999; Wilkens and Forgac, 2001; Muench *et al.*, 2009**). As its counterpart in yeast, ATP6AP1 tightly binds the proteolipid *c"* ring (**Wilkens and Forgac, 2001**) (**Figure 13**). In addition, the group of Feng demonstrated that ATP6AP1 also binds the subunits *a3* and *d*, mostly through its N-terminal region (**Feng *et al.*, 2008**).

3.1.1 ATP6AP1-CDG

Additional support for a functional involvement in V_0 assembly comes from patients with X-linked mutations in ATP6AP1 [ATP6AP1-CDG (MIM:300972)] with a phenotype similar to the deficiency of TMEM199 and CCDC115 (**Jansen *et al.*, 2016c; Dimitrov *et al.*, 2018**) (see ***Chapter 2 - V-ATPase assembly and assembly factors***). All patients show defects in *N*-glycosylation and in mucin-type *O*-glycosylation. The main clinical symptoms in ATP6AP1-CDG are liver involvement and immune system abnormalities (**Jansen *et al.*, 2016c; Jaeken and Péanne, 2017; Marques-da-Silva *et al.*, 2017; Dimitrov *et al.*, 2018**), leading to recurrent bacterial infections, hypogammaglobulinemia and leukopenia (**Table 6**). For instance, some patients show plantar abscesses, gastrointestinal infections, pneumonia in childhood, purulent otitis and reduced amounts of antibodies after vaccinations (**Jansen *et al.*, 2016c**). The hepatopathy described in the patients ranged from mildly elevated serum transaminases,

to cirrhosis and end-stage liver failure. Many patients show gastric problems (**Jansen *et al.*, 2016c; Dimitrov *et al.*, 2018**). Liver biopsy performed on several patients revealed steatosis, fibrosis and even micronodular cirrhosis. Moreover, the electron microscopy revealed an accumulation of autophagosomes and defects in the mitochondria (**Jansen *et al.*, 2016c**). The patients with the p.E346K substitution showed a more severe phenotype, with additional symptoms, such as splenomegaly, severe liver disease (in accordance with the early death of two patients due to liver failure) and neurological involvement, with epilepsy, mild intellectual disability and behaviour abnormalities (**Jansen *et al.*, 2016c**).

A more recently identified patient also shows *cutis laxa*, exocrine pancreatic insufficiency and changes in serum lipids. These include a significant increase of the saturated and long-chain branched pristanic and phytanic fatty acids, a reduced amount of phosphatidylcholine and phosphatidylethanolamine and an increase in cholesterol and ceramide levels (**Dimitrov *et al.*, 2018**). Also here, the laboratory tests show evidence of liver involvement, with elevated ALT and AST, elevated ALP, low serum copper and low ceruloplasmin. A few patients also had muscle weakness with mildly elevated serum CK (**Jansen *et al.*, 2016c; Jaeken and Péanne, 2017; Marques-da-Silva *et al.*, 2017; Dimitrov *et al.*, 2018**).

Reference	Mutation	Glycosylation Profile	Aminotransferases	Liver	Neurological development	CK	Ceruplasmin	Cholesterol and LDL
Jansen *et al.*, 2016c	c.1284 G>A (Met428Ile) [3 cases]	Abnormal *N*- and *O*-glycosylation	+/–	Case 1: Hepatomegaly Cases 2-3: Normal	Normal	n/a	n/a	n/a
Jansen *et al.*, 2016c	c.431 T>C (Leu144Pro)	Abnormal *N*- and *O*-glycosylation	+/–	Slight steatosis	Normal	n/a	n/a	n/a
Jansen *et al.*, 2016c	c.1036 G>A (Glu346Lys) [3 cases]	Abnormal *N*- and *O*-glycosylation	+/–	Hepatomegaly Fibrosis, steatosis and cirrhosis	Epilepsy, mild intellectual disability, behaviour abnormalities	n/a	n/a	n/a
Jansen *et al.*, 2016c	c.1036 G>A (Glu346Lys) [2 cases]	Abnormal *N*-glycosylation	+	Hepatomegaly Fibrosis, cirrhosis, choleastasis and fat liver (>60%) Death for liver failure	Epilepsy, mild intellectual disability, behaviour abnormalities	n/a	n/a	n/a
Jansen *et al.*, 2016c	c.1036 G>A (Glu346Lys)	Abnormal *N*- and *O*-glycosylation	+	Hepatomegaly	Epilepsy, mild intellectual disability, behaviour abnormalities	n/a	n/a	n/a
Jansen *et al.*, 2016c	c.938 A>G (Tyr313Cys)	Abnormal *N*- and *O*-glycosylation	+	Hepatomegaly Nodularity, fibrosis, cirrhosis and microvesicular steatosis	Normal	Mildly elevated	n/a	n/a
Dimitrov *et al.*, 2018	c.542 T>G (Leu181Arg)	Abnormal *N*-glycosylation	ALT: 69 U/L AST: 110 U/L	Hepatomegaly	Hypotonia	n/a	15 mg/dL	Cholesterol: 207 mg/dL

Table 6: ATP6AP1 deficient patients: genetic, clinical and laboratory data

3.2 ATP6AP2

The second "accessory" V-ATPase protein is ATP6AP2, or prorenin receptor (PRR) (**Ludwig *et al.*, 1998**). Since its first appearance, ATP6AP2/PRR reveals to be a protein associated with many different functions and cellular pathways. As ATP6AP1, ATP6AP2/PRR was discovered to be associated with the V_1/V_0 holoenzyme, through purification in bovine chromaffin granules. Due to its molecular weight it was termed M8-9 (**Ludwig *et al.*, 1998**). Only in 2002, the full-length was cloned revealing that M8-9 is, in fact, the C-terminal portion of ATP6AP2/PRR (**Nguyen *et al.*, 2002**). Interestingly, a yet unpublished entry in Genbank (AY038990) of a full-length clone uses the name CAPER (endoplasmic reticulum [ER]-localized type I transmembrane adaptor precursor C), highlighting its location in the ER (**Campbell *et al.*, 2008**).

Nguyen and her collaborators describe ATP6AP2/PRR as a receptor encoded by a gene composed of nine exons, localized on the X chromosome (Xp11.4). ATP6AP2/PRR is ubiquitously expressed (**Su *et al.*, 2004**), with high levels in the kidney intercalated cells (**Ichihara *et al.*, 2007; Advani *et al.*, 2009**). For a long time, the most studied function of ATP6AP2/PRR remained the one associated with the RAS system [the protein was indeed called (pro)renin receptor(PRR)] overshadowing its possible function with the V-ATPase. After a nomenclature revision, it was renamed ATP6AP2 (ATPase H^+ transporting accessory protein 2) and this is the name that will be used from now later in this chapter.

The ATP6AP2 gene is located on the X chromosome at locus p11.4 and encodes for a protein with 350 amino acids and a predicted mass of around 37 kDa. ATP6AP2 is a type I-transmembrane protein, that presents an N-terminal signal peptide (SP) for the translational transport to the ER (1-17), a large unglycosylated and highly hydrophobic extracellular domain (ECD, 17-305), a single transmembrane domain (TM, 305-327) and a short 20 amino acids long cytoplasmic domain (327-350) (**Nguyen *et al.*, 2002**) (**Figure 16**).

ATP6AP2 does not display domain homology with any known protein families or with cell surface receptors, but is an evolutionarily conserved protein in vertebrates and invertebrates (**Burcklé and Bader 2006**). Alignment of protein sequences revealed the N-terminal part of the protein, corresponding to the ECD, displays a high amino acid sequence identity exclusively in vertebrates. Conversely, the C-terminal part of the protein, the one that was originally called M8-9, is strikingly conserved in vertebrates and invertebrates (**Burcklé and Bader 2006**) (**Figure 17**).

At least in vertebrates, the two domains are linked by a cleavage site $R^{275}xxR^{278}$, which could be interpreted as a putative "pro-protein processing site" (**Figure 18**), suggesting that the two parts of the protein might have a divergent evolutionary fate and may even act separately: a recently acquired renin binding capacity for the N-terminal domain and a more conserved ancestral function for the C-terminal domain, unrelated to the RAS system (**Burcklé and Bader 2006**).

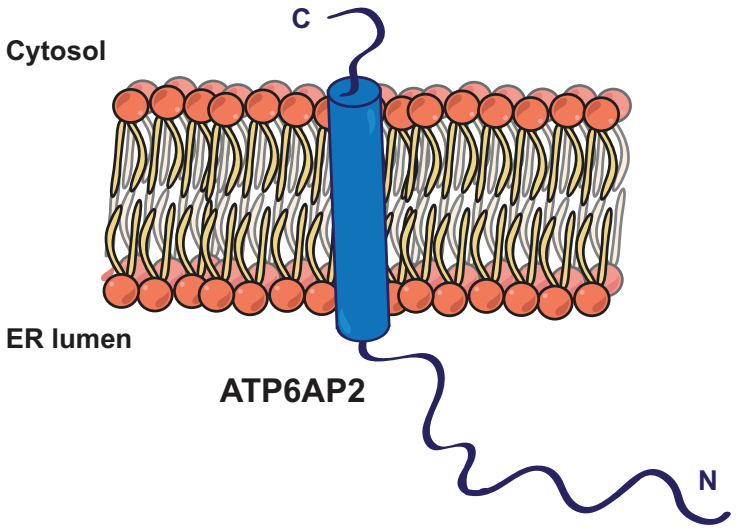

Figure 16: Schematic model of ATP6AP2

The model shows the structure and the orientation of ATP6AP2 in the ER.

Indeed, ATP6AP2 is synthesized as full-length protein (FL) in the ER and then undergoes to cleavage, which allows the generation of two different fragments: 1) the NTF, also considered as soluble (P)RR [s(P)RR], of 28-29 kDa corresponding to the first 278 amino acids, and 2) a segment including the transmembrane domain and the C-terminal tail and corresponding to the so-called M8-9 fragment (**Cousin *et al.*, 2009; Yoshikawa *et al.*, 2011**) (**Figure 18**).

Recent analyses have revealed that the cleavage of the protein is a multi-step process: the full-length ATP6AP2 (ATP6AP2-FL) is synthesized in the ER and then is transported to the Golgi, where it is cleaved by site-1 protease (S1P) at the R^{278}-T-I-$L^{281}\downarrow$ site to generate type-I NTF and the CTF (M8-9 fragment). Type-I NTF is then transported to the TGN, where it is cleaved by furin at the R^{275}-K-T-$R^{278}\downarrow$ site to generate type-II NTF [s(P)RR] that can be secreted for extracellular secretion immediately after cleavage in the TGN (**Nakagawa *et al.*, 2017**) (**Figure 18**).

Examination of the amino acid sequence of the cytoplasmic tail reveals that there are two theoretical localizations of the protein, suggested by two targeting signals. The first one is a tyrosine-based sorting signal Y^{335}DSI (generally Y$xx\emptyset$, where x is any amino acid, and $\emptyset$ is a large hydrophobic amino acid), that is used for protein sorting to endosomes and lysosomes through interaction with adaptor protein complex (**Bonifacino and Traub, 2003**). The second signal in the C-terminal of ATP6AP2 is a dibasic motif K^{346}IRMD (**Figure 17**). Conventionally dibasic signals are K(x)Kxx or R(x)Rxx and function as ER retention/retrieval signals (**Trombetta and Parodi, 2003**). Although it is optimally located, with lysine being five amino acids apart from the C-terminal of the protein,

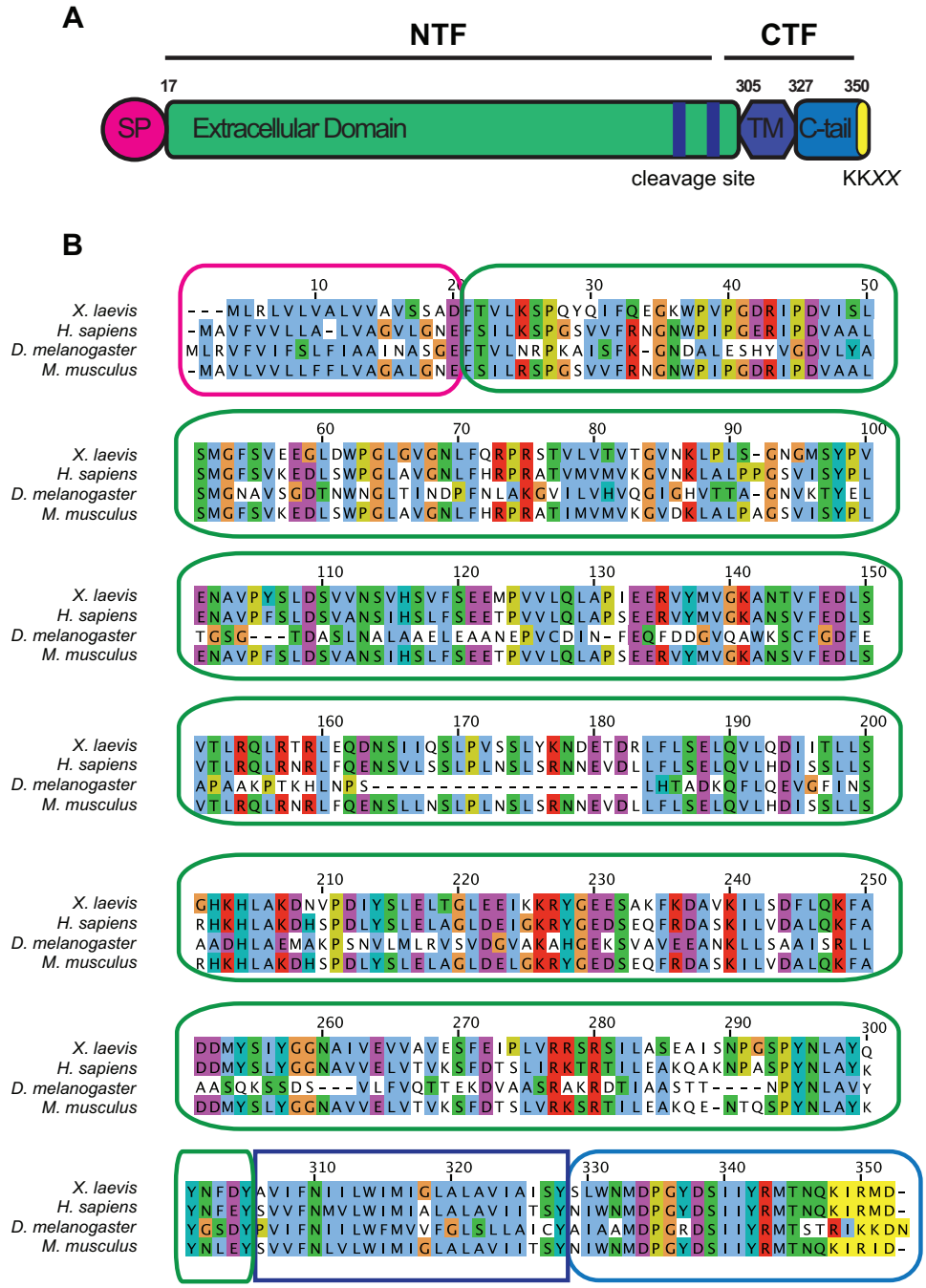

Figure 17: Structure of ATP6AP2 and sequence alignment

(A) Illustration showing the different domains of ATP6AP2. The precursor form contains a signal peptide (SP, colored fuchsia) that will be removed upon translocation of this secretory protein to the plasma membrane. After proteolytic cleavage two fragments are generated: N-terminal fragment (NTF, colored green) and C-terminal fragment (CTF, colored blue light). The cytoplasmic tail contains an ER retrieval motif, KK*XX* (colored yellow), the transmembrane protein (TM, colored blue) containing a small cytoplasmic tail (C-tail, colored light blue) and an extracellular domain that can be cleaved and secreted to the extracellular space (NTF, colored green). **(B)** Sequence comparison of orthologs of ATP6AP2, in humans (*H. sapiens*), *Xenopus* (*X. laevis*), *Drosophila* (*D. melanogaster*) and mouse (*M. musculus*). The alignment of the sequences is displayed applying the default parameters of Clustal, highlighting the conserved positions with color boxes using the Clustal X interface. The different domains are depicted by color code.

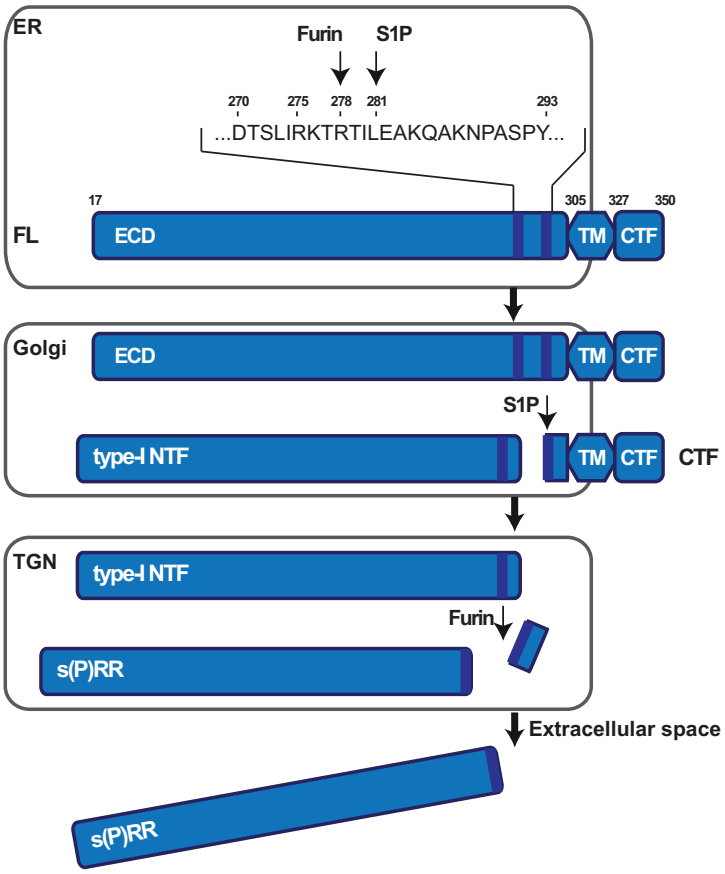

Figure 18: Sequential processing of ATP6AP2

ATP6AP2 is synthesized as a FL protein in the ER and transported to the Golgi. There, it is cleaved by S1P at the R^{278}-T-I-$L^{281}\downarrow$ site to generate type-I NTF and the CTF (also known as M8-9 fragment). Type-I NTF is transported to the TGN, where it is cleaved by furin at the R^{275}-K-T-$R^{278}\downarrow$ site to generate s(P)RR for extracellular secretion. Inspired from Nakagawa *et al.*, 2017.

in vertebrates K^{346}IRMD is an uncommon sequence (**Burcklé and Bader 2006**). In lower organisms, such as *Drosophila*, the motif is a classical KK*XX* motif. Nevertheless, the mutagenesis of the K(x)Rxx sequence by R(x)Rxx, in a tagged version of the FL receptor, was partially relocalizing the protein from its main localization in the ER to the lysosomal compartment, suggesting that the KIRMD motif is functional (**Schefe *et al.*, 2006**). Cross-linking, as well as co-immunoprecipitation studies, indicate that ATP6AP2 functions as a dimer on plasma membranes (**Nguyen *et al.*, 2002; Schefe *et al.*, 2006; Zhang *et al.*, 2011**). Furthermore, pull-down analysis showed that the ECD of ATP6AP2 is able to bind the ATP6AP2-FL indicating that the extracellular domain of ATP6AP2 participates in dimerization (**Suzuki-Nakagawa *et al.*, 2014b**).

To date, several biological functions have been proposed for ATP6AP2, some of which are still controversial and need further confirmation.

3.2.1 ATP6AP2 as a signalling receptor

The first function assigned to ATP6AP2 was the binding of the ECD to renin/(pro)renin, which activates the RAS system, suggesting that ATP6AP2 is a cell surface receptor. The RAS, or renin angiotensin-aldosterone system (RAAS), is a normal mechanism for maintaining blood pressure. Upon reduction of renal blood flow, the (pro)renin is converted in its active form, the renin, via the proteolytic cleavage of the prosegment (**Nguyen and Jan Danser, 2006**). Plasma renin will convert angiotensinogen into angiotensin I, which will subsequently be converted into angiotensin II, a potent vaso-constrincting peptide (**Fyhrquist and Saijonmaa, 2008**). Angiotensin II also stimulates the secretion of the hormone aldosterone in the adrenal cortex, causing an increase in reabsorption of Na^+ and water into the blood by the tubules of the kidney, increasing in turn the blood pressure. Excess of angiotensin is associated with deleterious cardiovascular effects (**Fyhrquist and Saijonmaa, 2008**). Initially, ATP6AP2 was reported to bind equally both renin and (pro)renin on the plasma membrane, without internalization of these proteins (**Nguyen *et al.*, 2002; Nabi *et al.*, 2006**). However, Batenburg and his collaborators argued that prorenin may be the main endogenous agonist *in vivo* (**Batenburg *et al.*, 2007**). The binding to (pro)renin and renin is supposed to occur in two different way (**Figure 19**):

1) a non-proteolytic activation of (pro)renin, leading to a conformational change, and a consequently increased generation of angiotensin peptides (**Nguyen *et al.*, 2002**). This pathway has been confirmed by *in vivo* experiments (**Nabi *et al.*, 2006; Batenburg *et al.*, 2007**) suggesting that (pro)renin binds with higher affinity to the receptor than renin, so that *in vivo* (pro)renin might be the endogenous agonist of the receptor (**Batenburg *et al.*, 2007**);

2) the induction of a signal transduction cascade angiotensin-independent. In this second pathway, the binding of (pro)renin to ATP6AP2 on the plasma membrane induces the phosphorylation of the ATP6AP2 cytoplasmic tail, mostly on the serine 337 and tyrosine 335 and 340 residues ($Y^{335}DS^{337}IIY^{340}$) (**Ichihara *et al.*, 2004**). This phosphorylation induces the activation of mitogen-activated protein kinases (MAPK) extracellular signal-regulated kinases 1 and 2 (ERK 1 and 2) (**Huang *et al.*, 2006; Huang *et al.*, 2007a; Huang *et al.*, 2007b; Krop *et al.*, 2013**). The activation of ERK1/2 leads to increased cell proliferation and stimulates the production of transforming growth factor-β1 (TGF-β1). The activation of TGF-β1 results in the upregulation of profibrotic factors, such as the plasminogen-activated inhibitor-1 (PAI-1), fibronectin and collagen (**Huang *et al.*, 2006, 2007b; Zhang *et al.*, 2008; Krop *et al.*, 2013**). Moreover, ATP6AP2 induces also MAPK activation (MAPK p42/44 and p38) and heat shock protein (HSP) 27 cascade (**Ichihara *et al.*, 2006b; Saris *et al.*, 2006**) and the phosphatidylinositol-3 kinase-p85 (PI3K-p85) pathway (**Schefe *et al.*, 2006**). An alternative pathway in response to (pro)renin binding was reported by the group of Funke-Kaiser, who proposed a specific role for the short cytoplasmic tail of ATP6AP2. Indeed, upon activation by

(pro)renin, ATP6AP2 interacts with the Promyelocytic leukaemia zinc finger protein 1 (PLZF) by its short cytoplasmic tail and stimulates PLZF translocation from the cytoplasm into the nucleus where, depending on the promoter context, PLZF can modulate the transcription of PI3K-p85 and, in a negative feedback, to repress the gene expression of ATP6AP2 (**Schefe *et al.*, 2006, 2008a, b; Funke-Kaiser *et al.*, 2010**). However, also this mechanism has to be taken with caution for two reasons: first, it is not clear whether (pro)renin binding takes place at the cell surface or directly in the cytoplasm, as ATP6AP2 is described to be mainly overlapping with the ER (**Schefe *et al.*, 2006**), and second, Krebs and his collaborators have described that an increase in renal (pro)renin actually upregulates ATP6AP2, arguing conversely for a positive feedback loop (**Krebs *et al.*, 2007**) (**Figure 19**). For all these reasons, ATP6AP2 became an interesting target in the pathophysiology of hypertension (**Burcklé *et al.*, 2006**), cardiovascular and renal diseases (**Kaneshiro *et al.*, 2007; Krebs *et al.*, 2007**), ocular inflammation (**Satofuka *et al.*, 2006, 2007**), diabetes (**Ichihara *et al.*, 2004, 2006a, 2006b; Takahashi *et al.*, 2007**) and inflammatory pathologies (**Satofuka *et al.*, 2008**). Nevertheless, despite the ability of renin/(pro)renin to bind ATP6AP2 has been extensively demonstrated in *in vitro* studies (**Saris *et al.*, 2006; Du *et al.*, 2008; Feldt *et al.*, 2008a; Zhou *et al.*, 2010**) its function as a (pro)renin receptor is still controversial, especially when it comes to *in vivo* experiments.

For instance, complete *ATP6AP2* deletion in zebrafish and rodents leads to embryonic lethality (**Amsterdam *et al.*, 2004; Contrepas *et al.*, 2007**), while tissue-specific knockouts mice die soon after birth due to massive tissue degeneration and defective cellular autophagy (**Oshima *et al.*, 2011; Wendling *et al.*, 2017**). Not only these phenotypes do not correlate with those of the knockouts of the various RAS components, which mainly display cardiovascular and metabolic syndromes (**Bader *et al.*, 2000; Yanai *et al.*, 2000; Bader, 2005**), but suggest that ATP6AP2 has functions essential for cell survival and proliferation that are unrelated to the RAS. Another reason why the proposed RAS function is controversial is related with the development of ATP6AP2 blockers, also known as "handle region peptide" (HRP) to inhibit local activation of (pro)renin (and not renin) (**Suzuki *et al.*, 2003**). While initially showing beneficial effects, *in vitro* and *in vivo* studies could not achieve the establishment of ATP6AP2 as a major player in hypertension, diabetes or in organ damage (**Batenburg *et al.*, 2007; Muller *et al.*, 2008**). For instance, experiments conducted in rodent models, using a decoy peptide designed to block (pro)renin/ATP6AP2 interaction, led to contradictory and inconsistent conclusions about the involvement of ATP6AP2 in cardiovascular pathophysiology (**Ichihara *et al.*, 2004, 2006a, b; Kaneshiro *et al.*, 2007; Feldt *et al.*, 2008b; Müller *et al.*, 2008; Wilkinson-Berka *et al.*, 2010**).

Finally, the ubiquitous expression pattern and the embryonic lethality of *ATP6AP2* knockout in mice argues against a role in the RAS system (**Kaneshiro *et al.*, 2006**), that mainly plays a role in cardiovascular physiology (**Bader *et al.*, 2000; Yanai *et al.*,**

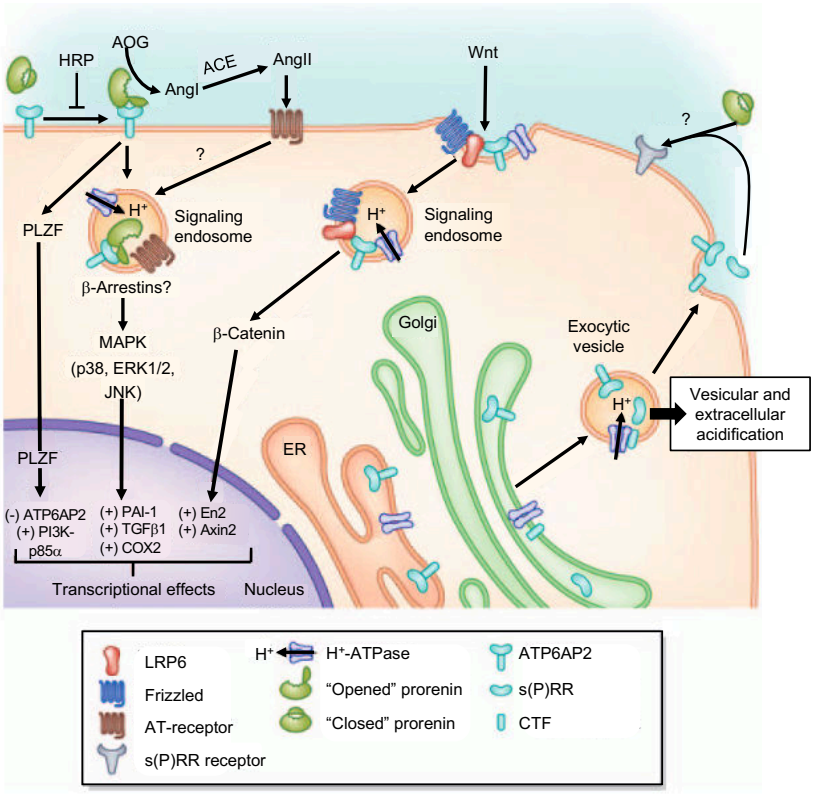

Figure 19: Functions of ATP6AP2

Several biological functions have been proposed for ATP6AP2: ATP6AP2 is involved in the renin angiotensin system (RAS) (left side); ATP6AP2 is involved in the canonical Wnt pathway (middle); ATP6AP2 is working as a soluble protein (right side). For details see text. From Sihn *et al.*, 2010.

2000; Bader, 2005). The RAS system is also not present in lower organisms such as the worm *C. elegans* and the insect *Drosophila* (**Salzet *et al.*, 2001**), both of which have a ATP6AP2 ortholog. In these specific organisms, the homology of ATP6AP2 is confined to the transmembrane and cytosolic portion of the protein, suggest that ATP6AP2 in mammals derive from the fusion of two different proteins (the N-terminal involved in the prorenin binding and the C-terminal in the V-ATPase function) (**Bader, 2007**).

3.2.2 ATP6AP2 and the V-ATPase

As mentioned above, the first indication of the involvement of ATP6AP2 in the V-ATPase came from its identification as a membrane associated protein (M8-9) of the V-ATPase in bovine chromaffin granules (**Ludwig *et al.*, 1998**). Afterward, developmental studies in zebrafish, *Xenopus* and *Drosophila* suggested an important role in the development and more specifically a role of ATP6AP2 as an accessory protein of V-ATPase. Indeed, in zebrafish, mutants of ATP6AP2 displayed phenotypes similar to that for the deletion of specific V-ATPase subunits, ATP6V0D1 and ATP6AP1, characterized by early developmental abnormalities, eye and body hypopigmentation, neuronal cell death and early death in development (**Amsterdam *et al.*, 2004; Gross *et al.*, 2005; Wang *et al.*, 2008; Nuckels *et al.*, 2009; Ichihara and Kinouchi, 2011**). In *Xenopus*, deletion of *ATP6AP2* in embryos causes the death of the embryo, neuronal malformations, defects in melanocyte and eye pigmentation (**Cruciat *et al.*, 2010**). Moreover, ATP6AP2 colocalized with the V-ATPase at the lumen of intercalated cells and at the Z-disc and dyad in cardiomyocytes (**Connelly *et al.*, 2011; Krops *et al.*, 2013**). Since a full animal *ATP6AP2* knockout is lethal in mice (**Li *et al.*, 2012; Sihn *et al.*, 2013**), the generation of tissue-specific knockouts was necessary. A specific knockout in cardiomyocyte resulted in a lethal phenotype, with mice dying for heart failure within three weeks (**Kinouchi *et al.*, 2010**). Instead, the specific knockout in podocytes resulted in massive foot process effacement, proteinuria and nephrotic syndrome, with severe alteration of the actin cytoskeleton (**Oshima *et al.*, 2011; Riediger *et al.*, 2011**). Moreover, Riediger *et al.* found that, upon ATP6AP2 ablation, the accumulation of undigested proteins leads to ER stress (**Riediger *et al.*, 2011**). The smooth muscle cell-specific ablation of ATP6AP2 resulted in nonatherogenic sclerosis in the abdominal aorta (**Kurauchi-Mito *et al.*, 2014**). All these cellular systems show impaired autophagy, with an accumulation of less acidified vesicles, which is caused by impaired assembly of the V-ATPase, mostly due to selective downregulation of the ATP6V0C subunit (**Kinouchi *et al.*, 2010; Oshima *et al.*, 2011; Kurauchi-Mito *et al.*, 2014**).

3.2.3 ATP6AP2 in canonical and non-canonical Wnt pathways

Additional studies in *Xenopus*, *Drosophila* and zebrafish have elucidated a different role of ATP6AP2 in both canonical and non-canonical Wnt pathways (**Amsterdam *et***

***al.*, 2004; Buechling *et al.*, 2010; Cruciat *et al.*, 2010; Hermle *et al.*, 2010, 2013**) (**Figure 19**). Wnts are a superfamily of secreted glycoproteins which signal through various receptors and co-receptors. The Wnt receptor activates three different pathways: (1) the canonical Wnt/β-catenin cascade, (2) the non-canonical planar cell polarity (PCP) pathway, (3) the Wnt/Ca^{2+} pathway (**Clevers, 2006**).

The canonical Wnt/β-catenin signalling pathway plays an important role in embryonic development and tissue homeostasis. Moreover, it has been implicated in certain pathologies, such as diabetes and cancer (**Krop *et al.*, 2013**). The initiation of the Wnt/β-catenin signalling pathway requires the formation of a complex composed of three proteins: the soluble Wnt ligand, the receptor Frizzled (Fz) and the co-receptor low-density lipoprotein receptor-related protein 5/6 (LRP5/6) (**Rousselle *et al.*, 2014**). The formation of this complex leads to the stabilization of β-catenin, which translocates into the nucleus where it complexes with the T cell factor/lymphocyte enhancer binding factor (TCF/LEF) to induce transcription of downstream genes and the expression of Wnt target genes (**Clevers, 2006; MacDonald *et al.*, 2009; Niehrs, 2012**). The aggregation of LRP5/6 and the formation of a signalosome (or signalling endosome) at the plasma membrane play an important role in the initiation of this cascade (**Bilic *et al.*, 2007**). After the phosphorylation of LRP5/6, the complex is internalized in vesicles via endocytosis, leading to transduction of the signal (**Blitzer and Nusse, 2006; Yamamoto *et al.*, 2006; Niehrs, 2012**). ATP6AP2 interacts by its extracellular domain with the seven transmembrane receptor Frizzled 8 (Fz8) and the co-receptor LRP5/6, acting as a physical adaptor between the Fz/LDL receptor-related protein complex and V-ATPase (**Cruciat *et al.*, 2010; Hermle *et al.*, 2010**). The complex Fz/LRP5/6 is then internalized into the signalosomes. The correct assembly of V-ATPase and its presence on the signalosomes, allows the subsequent acidification of these signalling endosomes. After the internalization of the Fz/LRP5/6 complex, LRP5/6 is phosphorylated leading to the activation of the signalling. At the molecular level, the ECD of ATP6AP2 is sufficient to bind Fz8 and LRP5/6, but the transmembrane domain is necessary to transduce the signal (**Cruciat *et al.*, 2010; Rousselle *et al.*, 2014**). Absence of ATP6AP2 resulted in abnormal frog embryos with small heads, shortened tails and hypopigmentation as described in *ATP6AP2* mutant zebrafish embryos (**Amsterdam *et al.*, 2004; Nuckels *et al.*, 2009; Cruciat *et al.*, 2010**). Decreased acidification following inhibition of V-ATPase by RNAi or pharmacological treatment, impaired LRP6 phosphorylation and Wnt signalling. All these observations suggest that *ATP6AP2* ablation disrupts the formation of proton gradient by the V-ATPase, subsequently preventing the phosphorylation of LRP5/6 and the initiation of Wnt signal transduction (**Amsterdam *et al.*, 2004; Nuckels *et al.*, 2009; Cruciat *et al.*, 2010**) (**Figure 19**).

The PCP is a pathway involved in the polarization of cells in the plane of a tissue in a cell-autonomous and non-autonomous manner. It is well characterized in *Drosophila*, where it regulates several morphogenetic processes. For instance, in the eye PCP reg-

ulates the precise arrangement of the ommatidia, in wings and notum coordinates the orientation of hairs and bristles. Because it shares molecular components such as Fz with the canonical Wnt pathway, it is also named the non-canonical Wnt pathway (**Hermle *et al.*, 2010**). Our group studied the role of ATP6AP2 in the PCP in the *Drosophila* pupal wing (**Hermle *et al.*, 2010, 2011, 2013**). So far, six proteins have been identified to be involved in the PCP: the transmembrane proteins Fz, Strabismus (Stbm) and Flamingo (Fmi). In *Drosophila* pupal wing, Fz and Fmi travel in vesicles along proximo-distally oriented microtubules to assume their asymmetric localization at the distal plasma membrane (**Hermle *et al.*, 2010, 2011**). The depletion of ATP6AP2 leads to strong PCP defects, with altered wing-hair polarity and reduced presence of PCP proteins, such as Fz and Fmi, at apical junctions of epithelial cells (**Hermle *et al.*, 2013**). Instead, these proteins were seen to localize together in vesicular compartments. The association of ATP6AP2 with the V-ATPase in proton transport suggested that acidification of vesicles may promote Fz trafficking (**Hermle *et al.*, 2011**). Moreover, a direct association of ATP6AP2 with Fmi was observed, suggesting two roles for ATP6AP2, one as a PCP core protein and another in endosomal pathway (**Hermle *et al.*, 2011**).

3.2.4 ATP6AP2 as soluble protein: s(P)RR/ATP6AP2

A last, again controversial, aspect of ATP6AP2 concerns the role of the cleaved extracellular domain. The cleavage of ATP6AP2, occurring during its passage through the Golgi, allows the release of a 28 kDa fragment, which could be detected in the supernatant of several cell types expressing the protein (**Cousin *et al.*, 2009**). As this molecular form of ATP6AP2 was found in the conditioned medium of cells, it was named s(P)RR (**Cousin *et al.*, 2009**). s(P)RR/ATP6AP2 could be found in plasma, where it is able to bind renin (**Cousin *et al.*, 2009**), and also in urine (**Ichihara *et al.*, 2010**). Bader has speculated that (pro)renin might bind to this soluble form of ATP6AP2 and act through an unknown receptor on cells (**Bader, 2007**). Interestingly, s(P)RR is found to be secreted in *Drosophila* and shows ability to bind the PCP domain in a non-autonomous fashion (**Hermle *et al.*, 2013**) (**Figure 19**). To correlate the levels of the concentrations of s(P)RR/ATP6AP2 in the plasma and urine of patients with pathophysiology, an ELISA test was designed (**Maruyama *et al.*, 2012**). Indeed, multiple clinical studies have revealed the association between serum/plasma s(P)RR/ATP6AP2 levels and certain diseases, thereby suggesting a potential role for s(P)RR/ATP6AP2 as a disease biomarker. High circulating levels of s(P)RR/ATP6AP2 were found associated with preeclampsia (**Watanabe *et al.*, 2012**), at early pregnancy could predict a subsequent gestational diabetes mellitus (GDM) (**Watanabe *et al.*, 2013b**), could be associated with renal dysfunction in patients with heart failure or essential hypertension (**Fukushima *et al.*, 2013; Morimoto *et al.*, 2014**), could be even associated with lower small for gestational age (SGA) birth (**Watanabe *et al.*, 2013a**), and finally associated with pancreatic ductal adenocarcinoma (**Shibayama *et al.*, 2015**). Serum

levels of s(P)RR were proposed to be involved in renal injury and to correlate also with the stage of chronic kidney disease (CKD) (**Hamada *et al.*, 2013**). Recently, it was proposed that elevated levels of s(P)RR/ATP6AP2 could be found in patients affected by obstructive sleep apnea syndrome (OSAS) as consequence of oxidative stress due to loss of V-ATPase activity (**Takahashi *et al.*, 2017**). Nevertheless, Nguyen and collaborators could not correlate the s(P)RR/ATP6AP2 concentrations with pathological conditions (**Nguyen*et al.*, 2014**). Moreover, the production of a soluble form of ATP6AP2 could not be reproduced *in vitro*: indeed, the overexpression of a ECD-tagged form of ATP6AP2 in mammalian cells has been found retained inside the cell through membrane association, suggesting the existence of regulatory mechanism of s(P)RR secretion, which may play a role in the biology and physiology of ATP6AP2 (**Suzuki-Nakagawa *et al.*, 2014a**).

3.2.5 ATP6AP2 and pathology in humans

Ramser *et al.* identified the first mutation in *ATP6AP2* associated with X-linked mental retardation and epilepsy (XMRE) in males of a large family with no apparent cardiovascular and renal dysfunction. It is a translationally silent C to T mutation in the exon 4 of ATP6AP2 (c.321C > T, p.D107D), in a putative exonic splice enhancer (ESE) site. This mutation is causing a partial deletion of exon 4 (Δ4-ATP6AP2) and an overall reduction of the functional protein (**Ramser *et al.*, 2005**). Further analysis suggested that ATP6AP2 dimerized with itself and with Δ4-ATP6AP2, suggesting that the XLMR and epilepsy phenotype might result from a dominant-negative effect of the Δ4-ATP6AP2 protein (**Contrepas *et al.*, 2009**).

Another mutation also causing exon 4 skipping was found in patients with X-linked parkinsonism with spasticity (XPDS). The authors showed that reduction of ATP6AP2 in HEK293 cells leads to impaired autophagy and lysosomal clearance, which was also observed in XPDS brain sections (**Korvatska *et al.*, 2013**).

In addition, a splice site mutation in ATP6AP2 was reported to cause X-linked intellectual disability, epilepsy and parkinsonism (**Gupta *et al.*, 2015**). Moreover, a meta-analysis of genome-wide association studies and gene expression data revealed significantly reduced expression of the *ATP6AP2* gene in case of Alzheimer's disease (**Goldstein *et al.*, 2016**). These data suggest that the lack of functional ATP6AP2 in the brain is very harmful.

These publications, suggesting an important function of ATP6AP2 in brain development and neurophysiology, are to date the only reports of ATP6AP2 deficiency in humans (**Bracke and von Bohlen Und Halbach, 2018**).

Aim of the Study

Aim of the study

The first part of the thesis was aimed at functionally validating missense mutations of ATP6AP2 in syndromic liver disease and at exploring what ATP6AP2 (dys)function could be responsible for the patients phenotypes. This work was a joint project with a postdoc in the lab, Maria Alexandra Rujano, who addressed these questions by using the fruit fly *Drosophila melanogaster*, while I used imaging and biochemistry approaches in patient fibroblasts and other cell culture models. The results have been published as a shared first-author paper (**Rujano and Cannata Serio *et al.*, 2018**).

The second part dealt with another V_0 assembly factor, VMA21, whose mutations have so far only been associated with a specific muscle disease (XMEA). In this project, I functionally validated mutations in *VMA21* that are responsible for similar liver phenotypes as in ATP6AP2 deficiency. The manuscript will soon be submitted as a shared first-author paper (**Cannata Serio, Graham *et al.*, 2019, *in preparation***).

Results

PART I

Mutations in the V-ATPase assembly factor ATP6AP2 cause a glycosylation disorder with autophagic defects

Article

Mutations in the X-linked *ATP6AP2* cause a glycosylation disorder with autophagic defects

Maria A. Rujano[#], Magda Cannata Serio[#], Ganna Panasyuk, Romain Péanne, Janine Reunert, Daisy Rymen, Virginie Hauser, Julien H. Park, Peter Freisinger, Erika Souche, Maria Clara Guida, Esther M. Maier, Yoshinao Wada, Stefanie Jäger, Nevan J. Krogan, Oliver Kretz, Susana Nobre, Paula Garcia, Dulce Quelhas, Tom D. Bird, Wendy H. Raskind, Michael Schwake, Sandrine Duvet, Francois Foulquier, Gert Matthijs*, Thorsten Marquardt*, Matias Simons*

J Exp Med. 2017 Dec 4; 214(12): 3707-3729. doi: 10.1084/jem.20170453. Epub 2017 Nov 10.

Autorship note:

[#] Maria A. Rujano and [#] Magda Cannata Serio contributed equally to this work.

Published Online: 10 November, 2017 | Supp Info: http://doi.org/10.1084/jem.20170453

JEM

Article

Mutations in the X-linked *ATP6AP2* cause a glycosylation disorder with autophagic defects

Maria A. Rujano,[1,2]* Magda Cannata Serio,[1,2]* Ganna Panasyuk,[3,4] Romain Péanne,[5] Janine Reunert,[6] Daisy Rymen,[5] Virginie Hauser,[1,4] Julien H. Park,[6] Peter Freisinger,[7] Erika Souche,[5] Maria Clara Guida,[1,4] Esther M. Maier,[8] Yoshinao Wada,[9] Stefanie Jäger,[10] Nevan J. Krogan,[10] Oliver Kretz,[11] Susana Nobre,[12] Paula Garcia,[12] Dulce Quelhas,[13] Thomas D. Bird,[14,16] Wendy H. Raskind,[15] Michael Schwake,[17] Sandrine Duvet,[18] Francois Foulquier,[18] Gert Matthijs,[5]** Thorsten Marquardt,[6]** and Matias Simons[1,2]**

[1]Laboratory of Epithelial Biology and Disease, Imagine Institute, Paris, France
[2]Université Paris Descartes—Sorbonne Paris Cité, Imagine Institute, Paris, France
[3]Institut Necker-Enfants Malades, Paris, France
[4]Institut National de la Santé et de la Recherche Medicale U1151/Centre National de la Recherche Scientifique UMR 8253, Paris, France
[5]University of Leuven (KU Leuven), Center for Human Genetics, Leuven, Belgium
[6]Universitätsklinikum Münster, Klinik für Kinder- und Jugendmedizin, Münster, Germany
[7]Kreiskliniken Reutlingen, Klinik für Kinder- und Jugendmedizin, Klinikum am Steinenberg, Reutlingen, Germany
[8]Dr. von Haunersches Kinderspital der Universität München, München, Germany
[9]Osaka Medical Center and Research Institute for Maternal and Child Health, Osaka, Japan
[10]Department of Cellular and Molecular Pharmacology, University of California, San Francisco, San Francisco, CA
[11]Centre for Biological Signaling Studies BIOSS, University of Freiburg, Freiburg, Germany
[12]Metabolic Reference Center, Coimbra University Hospital Center, Coimbra, Portugal
[13]Biochemical Genetics Unit, Centro de Genética Médica Doutor Jacinto Magalhães, Centro Hospitalar do Porto, Abel Salazar Institute of Biomedical Sciences, University of Porto, Porto, Portugal
[14]Department of Neurology and [15]Department of Medicine, University of Washington, Seattle, WA
[16]Geriatric Research Center, Veterans Administration Medical Center, Seattle, WA
[17]Faculty of Chemistry/Biochemistry III, University Bielefeld, Bielefeld, Germany
[18]Université Lille, Centre National de la Recherche Scientifique UMR 8576, Unité de Glycobiologie Structurale et Fonctionnelle, Lille, France

The biogenesis of the multi-subunit vacuolar-type H$^+$-ATPase (V-ATPase) is initiated in the endoplasmic reticulum with the assembly of the proton pore V0, which is controlled by a group of assembly factors. Here, we identify two hemizygous missense mutations in the extracellular domain of the accessory V-ATPase subunit ATP6AP2 (also known as the [pro]renin receptor) responsible for a glycosylation disorder with liver disease, immunodeficiency, cutis laxa, and psychomotor impairment. We show that *ATP6AP2* deficiency in the mouse liver caused hypoglycosylation of serum proteins and autophagy defects. The introduction of one of the missense mutations into *Drosophila* led to reduced survival and altered lipid metabolism. We further demonstrate that in the liver-like fat body, the autophagic dysregulation was associated with defects in lysosomal acidification and mammalian target of rapamycin (mTOR) signaling. Finally, both *ATP6AP2* mutations impaired protein stability and the interaction with ATP6AP1, a member of the V0 assembly complex. Collectively, our data suggest that the missense mutations in *ATP6AP2* lead to impaired V-ATPase assembly and subsequent defects in glycosylation and autophagy.

INTRODUCTION

The multi-subunit vacuolar-type H$^+$-ATPase (V-ATPase) acidifies intracellular organelles, thereby controlling several events in the secretory and endocytic pathway, such as proteolytic processing, protein degradation, autophagy, and glycosylation. Structurally, it consists of a proton pore (V0 sector) and ATP hydrolysis domain (V1 sector), each composed of several core subunits (Forgac, 2007). In addition, there are two accessory subunits named ATP6AP1 and ATP6AP2.

ATP6AP1 has recently been shown to be the orthologue of the yeast V-ATPase assembly factor Voa1 (Jansen et al., 2016a). Voa1 cooperates with four other chaperones (Vma21, Vma12, Vma22, and Pkr1) to assemble the V0 sector in the ER (Ryan et al., 2008). The newly assembled

*M.A. Rujano and M. Cannata Serio contributed equally to this paper.

**G. Matthijs, T. Marquardt, and M. Simons contributed equally to this paper.

Correspondence to Matias Simons: matias.simons@institutimagine.org

M. Schwake's present address is Dept. of Neurology, Northwestern University Feinberg School of Medicine, Chicago, IL.

Abbreviations used: AD, activation domain; ALT, alanine transaminase; AP-MS, affinity purification coupled to MS; AST, aspartate transaminase; CDG, congenital disorder of glycosylation; coIP, coimmunoprecipitation; CT, C-terminal fragment; Dpn, Dead-pan; Endo H, endoglycosidase H; ERAD, ER-associated degradation; FL, full-length; MALDI-TOF, matrix-assisted laser desorption/ionization time-of-flight; MS, mass spectrometry; mTOR, mammalian target of rapamycin; NT, N-terminal fragment; p4E-BP, phospho-4E-BP; PNGase F, peptide-*N*-glycosidase F; TAG, triglyceride; V-ATPase, vacuolar-type H$^+$-ATPase; Y2H, yeast two-hybrid.

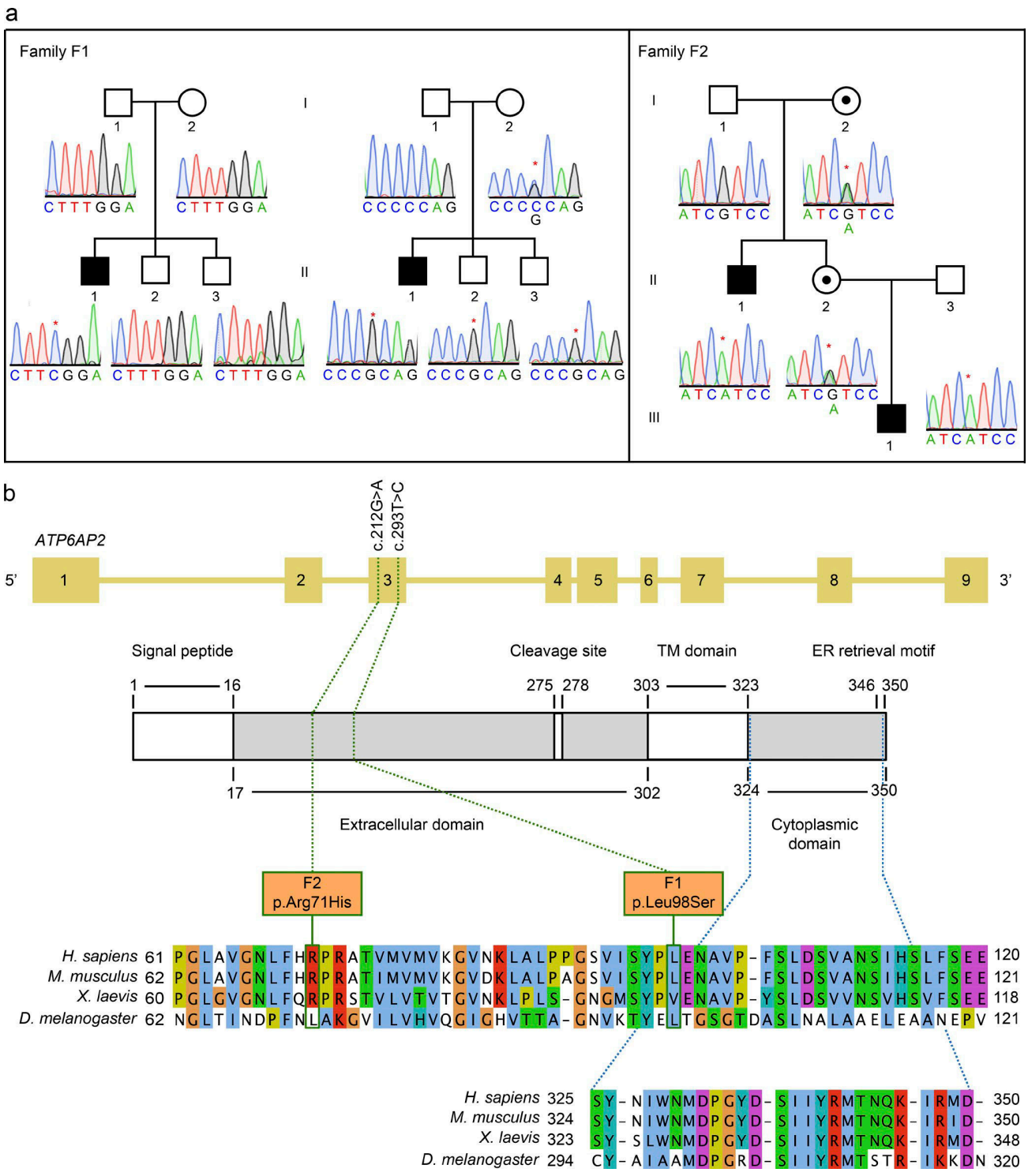

Figure 1. ***ATP6AP2* mutations cause a novel glycosylation disorder.** (a) Pedigrees and sequence profiles of *ATP6AP2* mutations in families F1 and F2. Whole exome sequencing identified two mutations in three patients from two different families. Partial chromatograms show X-linked segregation for all patients. Family F1 shows on the left side the segregation of the de novo missense pathogenic mutation (c.293T>C) identified in patient P1 (F1-II.1), and on the right side the segregation of the maternally inherited SNP (c.268C>G) to patient P1 and healthy siblings (F1-II.2 and F1-II.3). Pedigree for family F2 shows the segregation of the maternally inherited missense mutation (c.212G>A) to patient P2 (F2-II.1) and a healthy female sibling (F2-II.2). Patient P3 (F2-III.1) inherited the same mutation as P2 from healthy individual F2-II.2. Black-filled squares indicate affected males, whereas black dots in white-filled

proton pore is then transported to the Golgi, where the preassembled V1 sector is added from the cytoplasm to constitute a functional holoenzyme (Forgac, 2007). Mutations in *ATP6AP1* lead to a congenital disorder of glycosylation (CDG), which is a rapidly growing disease group caused by the deficiency in components of the glycosylation machineries and, more generally, in factors important for ER and Golgi homeostasis (Freeze et al., 2014; Scott et al., 2014; Hennet and Cabalzar, 2015). ATP6AP1 deficiency manifests with hypogammaglobulinemia as well as liver and cognitive abnormalities (Jansen et al., 2016a). Similar clinical phenotypes occur in patients with mutations in either one of the two other putative orthologues of yeast assembly factors TMEM199 (Vma12) and CCDC115 (Vma22; Jansen et al., 2016b,c), suggesting that V0 misassembly is the common pathogenic process in these syndromes.

The other accessory subunit ATP6AP2 has so far not been associated with CDG. In contrast, exon-skipping mutations in *ATP6AP2* have been associated with cognitive disorders with Parkinsonism, spasticity, epilepsy, and intellectual disability (Ramser et al., 2005; Korvatska et al., 2013). Functionally, the protein has been suggested to act as a (pro)renin receptor (Nguyen et al., 2002) and in several signaling pathways (Buechling et al., 2010; Cruciat et al., 2010; Hermle et al., 2010, 2013; Schafer et al., 2015). The involvement of ATP6AP2 in V-ATPase function has been demonstrated in various cell culture and animal studies (Kinouchi et al., 2010, 2013; Riediger et al., 2011; Hermle et al., 2013; Trepiccione et al., 2016). In mice, the deletion of *Atp6ap2* in cardiomyocytes, hepatocytes, or podocytes results in a significant decrease of V0 subunits and autophagy defects (Kinouchi et al., 2010, 2013; Kissing et al., 2017). Yet how ATP6AP2 mechanistically contributes to V-ATPase function remains to be determined.

Here, we identify missense mutations in *ATP6AP2* that cause a metabolic disorder with phenotypic similarity to the deficiency of other V0 assembly factors. Using complementary in vitro and in vivo approaches, we show that ATP6AP2 interacts with members of the ER-based V0 assembly complex. The interaction is impaired by the identified missense mutations in *ATP6AP2*, causing reduced V-ATPase activity, defective autophagy, and ultimately, compromised cellular and organismal homeostasis. Our results suggest that ATP6AP2 has a crucial role in V-ATPase assembly, both in invertebrates and vertebrates.

RESULTS

Mutations in X-linked *ATP6AP2* cause immunodeficiency, liver disease, psychomotor impairment, and cutis laxa

Two hemizygous mutations in *ATP6AP2* were identified by whole exome sequencing in three male individuals from two unrelated families included in cohorts of unsolved CDG cases. A Portuguese boy (P1) was shown to carry a hemizygous missense mutation c.293T>C (p.L98S) in exon 3 (Fig. 1, a and b). The mutation was absent in the parents and the two brothers. In contrast, the neighboring polymorphism c.268C>G was transmitted by the heterozygous mother to all sons. Together, this suggested that p.L98S, which is evolutionary conserved between vertebrates and invertebrates, is a de novo mutation. Another hemizygous missense mutation, c.212G>A (p.R71H), was found in the same exon in two individuals (P2 and P3) of a German family (Fig. 1, a and b). Both mutations were absent from more than 60,000 control individuals in the ExAC server (http://exac.broadinstitute.org/).

The predominant symptoms of the patients are hepatopathy and immunodeficiency. For P1, ascites, collateral vascularization, and hepatosplenomegaly and increased liver transaminases aspartate transaminase (AST) and alanine transaminase (ALT) led to a liver biopsy at 16 mo of age showing micronodular cirrhosis and steatosis (Table 1 and Fig. 2, a and b). Recurrent infections initiated immunological analysis that showed low levels of Igs, poor polysaccharide antibody response, decreased level of CD4+, and increased levels of CD8+ lymphocytes (Table 1). Treatment with weekly subcutaneous Ig led to decreased infection frequency. P2 suffered from recurrent pulmonary and upper respiratory tract infections throughout infancy and childhood. Plasmaelectrophoresis revealed hypogammaglobulinemia, and further investigation led to the diagnosis of IgG subclass deficiency with reduced IgG1 and IgG3. IgG substitution was consequently initiated, under which the patient's general health status improved. Repeated ultrasounds showed hepatosplenomegaly with inhomogeneous and hyperechogenic structure. Serum cholesterol and the transaminase enzymes AST and ALT were mildly elevated (Table 1). P3 developed severe liver failure at 5 mo of age. Liver biopsy revealed lipid accumulation and enlarged vacuolar structures within hepatocytes (Fig. 2, c and d). Similar to the other two patients, he has repeatedly suffered from infections, but his immunological status has so far been normal. Additional clinical features for all pa-

circles indicate healthy carrier females. The asterisk indicates the respective nucleotide change. (b) Schematic representation of the intron–exon structure of *ATP6AP2* and the encoded protein. Numbers from 1–9 represent the different exons of the *ATP6AP2* gene. The domain structure of the protein is schematized underneath, and the numbers delimiting the different domains refer to amino acids positions. In white are depicted the signal peptide, the cleavage site, the transmembrane (TM) domain, and C-terminal ER retrieval motif. The green dotted lines indicate the positions of the missense mutations within the families, both at the nucleotide and the protein level (green boxes). The blue dotted lines indicate the position of the cytoplasmic domain. The conservation of the affected amino acids is illustrated by the sequence alignments of the region containing the missense mutations (upper) and the cytoplasmic tail (lower) from *Homo sapiens* ATP6AP2 in *Mus musculus*, *Xenopus laevis*, and *D. melanogaster*, respectively. Although p.L98S is conserved in *Drosophila*, p.R71H is not. The ER retrieval motif is KxRxx in vertebrates and KKxx in *Drosophila*.

Table 1. **Clinical data of patients with ATP6AP2 mutations**

Parameter	Patient 1	Patient 2	Patient 3
Sex	Male	Male	Male
Current age	17 yr	21 yr	10 mo
Consanguinity	None	None	None
Ethnicity	Caucasian	Caucasian	Caucasian
Mutation cDNA	c.293C>T	c.212G>A	c.212G>A
Mutation protein	p.Leu98Ser (L98S)	p. Arg71His (R71H)	p. Arg71His (R71H)
Glycosylation defect	IEF: tetrasialotransferrin: 34.2% (norm: 48.5–65.3%); trisialotransferrin: 28.9% (norm: 5.5–15.1%); disialotransferrin: 15% (norm: 2.0–6.1%); monosialotransferrin: 3.3% (norm: 0.0–3.7%); asialotransferrin: 1.5% (norm: 0%)	HPLC: tetrasialotransferrin 55.17% (norm: 85.7–94.0%); trisialotransferrin 33.11% (norm: 1.16–6.36%); disialotransferrin 8.92% (norm: 0.38–1.82%); monosialotransferrin 1.68% (norm: 0%)	HPLC: tetrasialotransferrin 35.7% (norm: 85.7–94.0%); trisialotransferrin 36.4% (norm: 1.16–6.36%); disialotransferrin 18.7% (norm: 0.38–1.82%); monosialotransferrin 9.0% (norm: 0%)
Onset of symptoms	5 mo	Directly after birth	Directly after birth
Liver	Prolonged neonatal jaundice and persistent hepatosplenomegaly with recurrent episodes of hypoalbuminemia and ascites	No hepatomegaly in childhood, but liver parenchyma of an inhomogeneous, hyperechoic structure. Today: hepatomegaly, mild elevation of liver enzymes	Prolonged neonatal jaundice and hepatosplenomegaly. Cholestasis. Irregular liver parenchyma with portosystemic shunts and ascites. Hypoalbuminemia, hyperammonemia. Coagulopathy. Listed for liver transplantation.
Liver biopsy	Micronodular hepatic cirrhosis with moderate macrovesicular steatosis (biopsy at 8 mo), elevated copper	Not available	Diffuse micronodular hepatic cirrhosis Elevated copper
Neonatal icterus	+	-	+
Splenomegaly	+	+	+
Infections	Recurrent severe infections (e.g., sepsis, peritonitis)	Recurring pulmonary and upper respiratory tract infections throughout infancy and childhood	Recurring upper respiratory tract infections, positive blood cultures with pneumococcus at one occasion
Neurological symptoms	Mild cognitive impairment	Ataxic gait, mild cognitive impairment	Normal
Cutis laxa	Mild to moderate	Pronounced, improvement over time	Pronounced
Hypogammaglo-bulinemia	+	+	-
IgG	2.31 g/L (reference: 5.6–13.8 g/L)	Reduced IgG1 and IgG3	-
IgM	<0.17 g/L	18 mg/dl (reference: 40–230 mg/dl)	-
IgA	<0.08 g/L	<15 mg/dl (reference: 70–400 mg/dl)	-
Increased transaminases	At 17 yr, mild elevation of transaminases (AST 61 U/l [reference: 15–46 UI/l], ALT 51 U/l [reference: 10–40 U/l])	Ranging from mild elevation at age 9 yr: AST 92 U/l (reference: 8–60 U/l), ALT 59 U/l (reference: <44 U/l) to pronounced hepatic affection (AST 135 U/l)	Within the first year: AST 100–160 U/l, (reference: <71 U/l)
Serum copper	Not available	At 1 yr: 1.5 µmol/l (reference: 10–30 µmol/l) Normalized over the following months	Normal serum copper at the age of 4 mo: 89 µg/dl (reference: 65–165 µg/dl)
Serum lipids	At age 17 yr (liver normal): Cholesterol: 172 (reference: 200 mg/dl) LDL-cholesterol: 90 (reference: 50–130 md/dl)	At age 20 yr: Cholesterol: 199 (reference: 200 mg/dl) LDL-cholesterol: 149 (reference: 50–130 md/dl)	At age 5 mo: Cholesterol: 254 (reference: 81–147 mg/dl)
Other laboratory findings	Low factor V and VI Factor V: 30% (reference: 65–148%), factor VII: 24% (reference: 58–115%)	Low factor XI (58% [reference: >70%]) and free protein S (57.5% [reference: 60–140%])	Low factors II (27.7% [reference: 60–120%]), V (35.9% [reference: 55–130%]), VII (21.9% [reference: 47–130%]), IX (17.27% [reference: 36–136%]), and XI (23.9% [reference: 49–134%])
Other clinical findings	Mild dysmorphic features	Low-set ears, micrognathia, a flat and wide-set chest, laterally facing nipples, and hypospadia	

IEF, isoelectric focusing.

tients were cutis laxa (P1, P2, and P3), dysmorphic features (P1 and P2), mild intellectual disability (P1 and P2), and mild ataxia (P2; Table 1).

Collectively, missense mutations in ATP6AP2 cause a new syndrome, predominantly affecting the liver, immune system, central nervous system, and skin connective tissue.

ATP6AP2 deficiency causes hypoglycosylation of serum proteins in patients and mice

Analysis of protein N-glycosylation showed that all patient sera had abnormal transferrin glycosylation profiles with decreased tetrasialotransferrin and increased tri-, di-, and monosialotransferrin (Fig. S1, a and b; and not depicted).

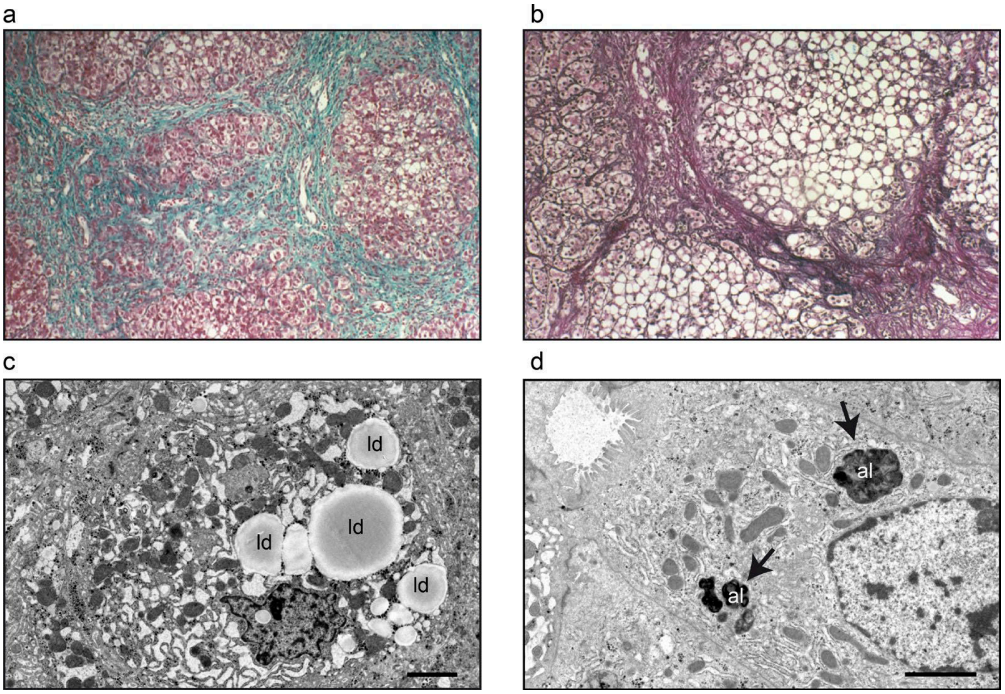

Figure 2. **Liver histology and fibroblasts of patients.** Immunohistochemistry and transmission electron microscopy of liver tissue from patient 1 (P1) and patient 3 (P3). (a and b) Liver biopsy from P1 displays micronodular cirrhosis (a; Masson's trichrome staining, 100×) and macro- and microvacuolar steatosis (b; Gordon and Sweet's staining, 200×). (c and d) Electron micrographs from single hepatocytes in liver biopsies from P3 with accumulations of autolysosomes (al; arrows) and lipid droplets (ld). Bars: (c) 5 µm; (d) 2 µm.

HPLC analysis confirmed that only half of the transferrin molecules (53.3% in patient 2 and 50.28% in P3) were present as the correctly glycosylated tetrasialo-transferrin (Fig. S1, a and b). N-linked glycans on total plasma glycoproteins were analyzed using matrix-assisted laser desorption/ionization time-of-flight (MALDI-TOF) mass spectrometry (MS), which showed a relative increase in the undersialylated glycans in patient 1 (Fig. 3 a).

So far, ATP6AP2 has not been implicated in any glycosylation disorder. Moreover, analysis of protein glycosylation in a patient carrying one of the previously described exon-skipping variants in *ATP6AP2* (Korvatska et al., 2013) showed a normal transferrin glycosylation profile and only a slight undersialylation of total serum proteins (Fig. S2, a and b). Therefore, we tested whether *ATP6AP2* deficiency was sufficient to cause serum glycosylation abnormalities. Mice carrying a floxed allele of *ATP6AP2* (Riediger et al., 2011) were injected with adeno-CRE (or adeno-GFP as a control) to induce an acute reduction of ATP6AP2 in the liver (Fig. S3 a). Serum analysis showed elevation of the liver enzymes AST and ALT and high levels of cholesterol in the Cre-injected mice, suggesting liver damage and metabolic abnormalities (Fig. S3, b and c). MALDI–TOF MS showed an increase of unsialylated and mono-sialylated N-glycans and a decrease in tri-sialylated N-glycans compared with adeno-GFP–injected mice (Fig. 3 b and Fig. S3 d). Thus, reduced ATP6AP2 expression in the liver is sufficient to recapitulate the glycosylation defects of the patients.

Disease-associated mutations target ATP6AP2 for degradation

ATP6AP2 is a type I transmembrane protein that undergoes two proteolytic cleavages in the Golgi to generate a luminal or extracellular N-terminal fragment (NT) and a C-terminal fragment (CT) harboring a transmembrane domain and a short cytoplasmic tail (Fig. 1 b; Cousin et al., 2009; Nakagawa et al., 2017). The cytoplasmic tail contains an RxKxx ER retrieval motif that mediates retrograde transport to the ER (Nilsson et al., 1989; Schefe et al., 2006; Sihn et al., 2013). To investigate the effect of the missense mutations on expression and cleavage of ATP6AP2, we performed Western blotting in fibroblasts derived from patients P1 ($ATP6AP2^{L98S}$) and P3 ($ATP6AP2^{R71H}$). Steady-state levels of full-length (FL) ATP6AP2 were significantly reduced in $ATP6AP2^{L98S}$ but not $ATP6AP2^{R71H}$ fibroblasts, in comparison to $ATP6AP2^{WT}$ from two different healthy controls (Fig. 4, a and b). In contrast, mRNA levels of $ATP6AP2^{R71H}$ but not of $ATP6AP2^{L98S}$ were elevated (Fig. 4 d). Moreover, upon transient overexpression of HA-tagged $ATP6AP2^{L98S}$ and $ATP6AP2^{R71H}$ in HEK293T cells, the levels of both mutant proteins were decreased in comparison to the WT (Fig. 4, e and f). To understand whether the reduced levels of the overexpressed mutants

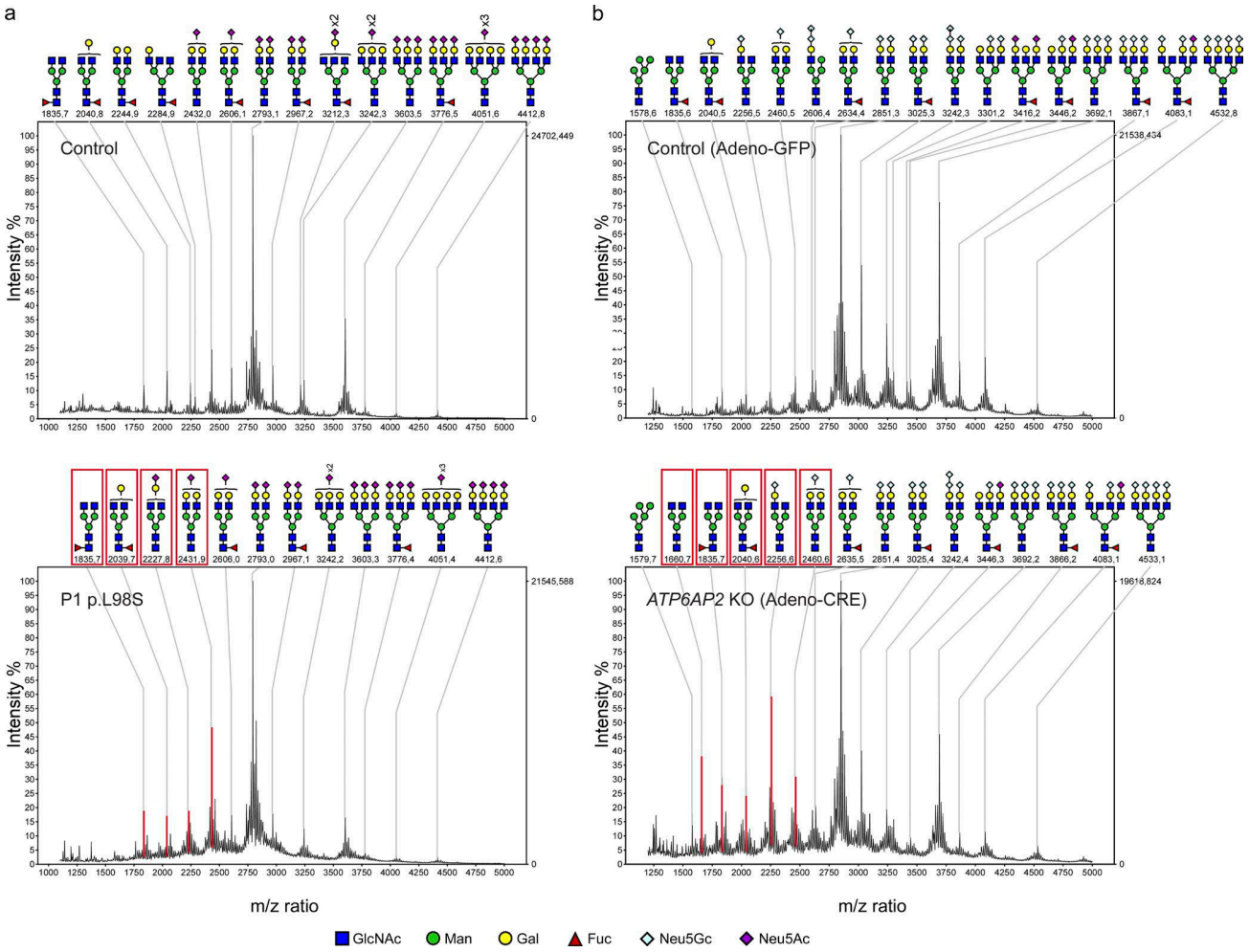

Figure 3. **Hypoglycosylation of serum proteins in patient and mouse samples.** (a) N-linked glycans of serum from a healthy individual (top) and from P1 with the L98S mutation in *ATP6AP2* (bottom) were analyzed by MALDI-TOF MS. (b) Representative MALDI-TOF MS profiles of adeno-GFP- (n = 7) and adeno-CRE- (n = 5) injected mice (complete data can be found in Fig. S4). Red boxes and peaks in the lower panels of a and b indicate the increase of biantennary glycans (compared with most extensively branched N-glycans in the control), which also contain less undersialylated structures.

were a result of decreased stability, we performed a cycloheximide chase assay in HEK293T cells. Whereas ATP6AP2^{WT} was still present after 18 h of cycloheximide pretreatment, ATP6AP2^{L98S} and ATP6AP2^{R71H} were barely detectable after 3 h, indicating that both mutant proteins have a shorter half-life and are targeted for degradation (Fig. 4, h–j).

Additionally, endogenous and overexpressed ATP6AP2^{L98S} showed reduced levels of the cleavage products NT and CT (Fig. 4, a, c, e, and g), which suggested a defect in the export out of the ER. Therefore, we asked whether degradation of this mutant involved the ER-associated degradation (ERAD) pathway, by which misfolded transmembrane proteins are targeted for proteasomal degradation via retrotranslocation into the cytoplasm. To inhibit ERAD, we coexpressed WT and dominant-negative versions of p97 (p97^{WT} and p97^{QQ}, respectively), a crucial component of the retrotranslocation machinery (Ye et al., 2001). Whereas p97^{QQ} but not p97^{WT} caused a significant accumulation of ATP6AP2^{L98S}, ATP6AP2^{WT} and ATP6AP2^{R71H} steady-state levels were unchanged (Fig. 4, k and l). Importantly, a version of ATP6AP2 with mutations in the C-terminal ER retrieval motif (ATP6AP2^{QxQxx}) not only was unaffected by both p97 constructs (Fig. 4, k and l) but also showed more cleavage (Fig. 4, e and g) and the longest half-life (Fig. 4, h–j). These findings were confirmed by localization studies of the different constructs in HeLa cells (Fig. S4, a and b). Whereas ATP6AP2^{WT} and ATP6AP2^{R71H} showed both ER and Golgi localization, ATP6AP2^{L98S} localized primarily to the ER. ATP6AP2^{QxQxx} showed an exclusive Golgi localization. Altogether, these results suggest that although the reduced retrograde transport of ATP6AP2^{QxQxx} causes more protein stability, the increased ER localization of ATP6AP2^{L98S} promotes its targeting for

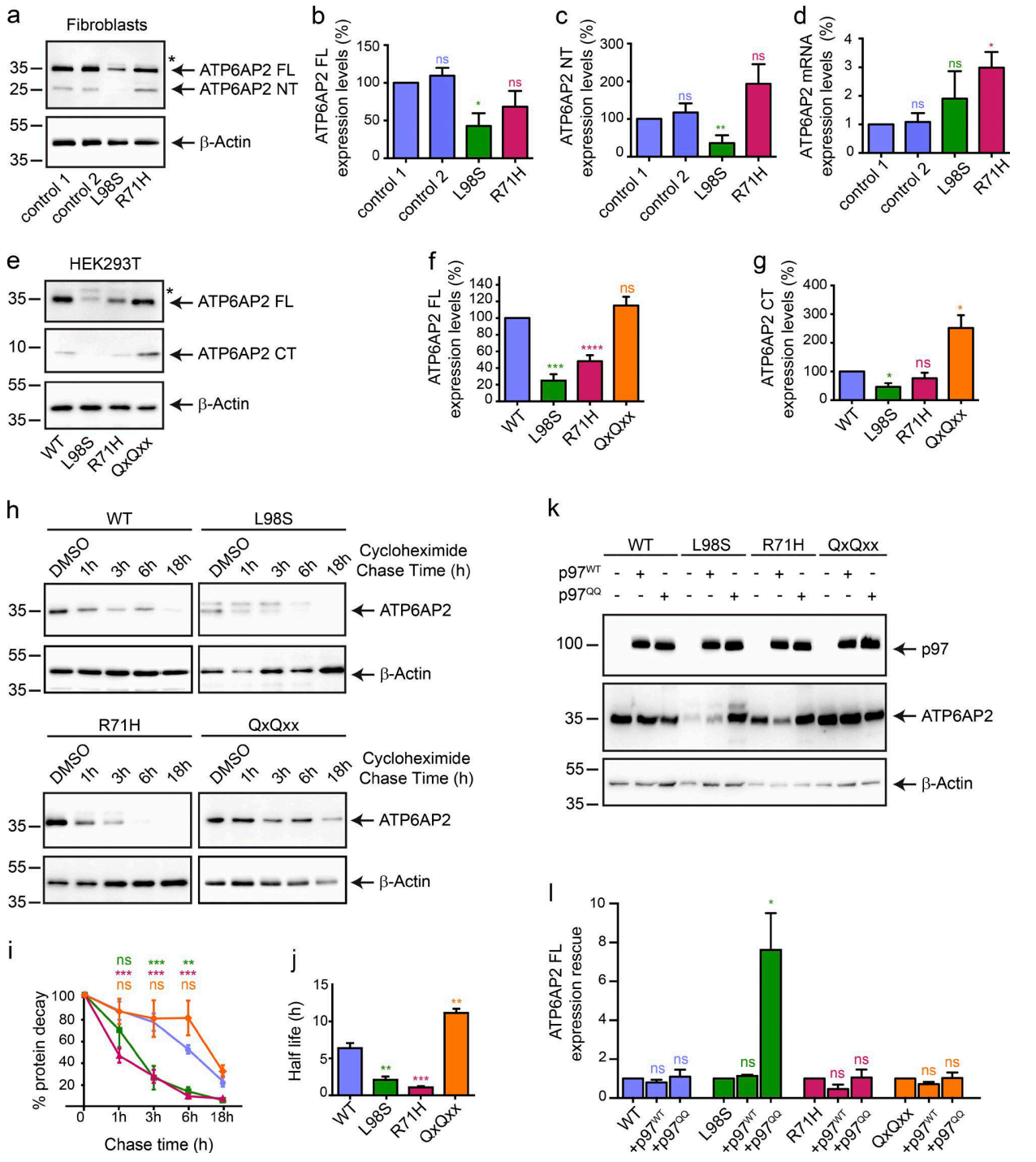

Figure 4. **ATP6AP2 mutants p.L98S and p.R71H are degraded via ERAD.** (a) Endogenous levels of ATP6AP2 FL and NT in control and patient fibroblasts using anti-ATP6AP2-NT. The asterisk * indicates glycosylated form of ATP6AP2^{L98S}. (b and c) Expression levels of ATP6AP2 FL and NT relative to those of β-actin were calculated. All data are mean ± SEM of three independent experiments. ns, not significant; *, $P < 0.05$; **, $P < 0.01$. The statistical significance was determined by an unpaired Student's *t* test. (d) ATP6AP2 mRNA quantification in control and patient fibroblasts. All data are mean ± SEM of three independent experiments. ns, not significant; *, $P < 0.05$. The statistical significance was determined by an unpaired Student's *t* test. (e) Steady-state levels of overexpressed ATP6AP2^{WT}-HA, ATP6AP2^{L98S}-HA, ATP6AP2^{R71H}-HA, and ATP6AP2^{QxQxx}-HA at 48 h after transfection in HEK293T cells. Anti-HA reveals FL and CT. The asterisk indicates glycosylated form of ATP6AP2^{L98S}. (f and g) Expression levels of ATP6AP2 FL and CT relative to those of β-actin were calculated. All data are mean ± SEM of five independent experiments. ns, not significant; *, $P < 0.05$; ***, $P < 0.001$; ****, $P < 0.0001$. The statistical significance was deter-

ERAD. For ATP6AP2^{R71H}, which showed higher endogenous steady-state levels and more Golgi localization than ATP6AP2^{L98S}, the precise degradation pathway remains unclear.

ATP6AP2^{L98S} is posttranslationally modified by N-glycan addition

Apart from lower expression levels, overexpressed ATP6AP2^{L98S} in HEK293T cells and endogenous ATP6AP2^{L98S} in patient fibroblasts also exhibited an additional slower migrating band in immunoblots (Fig. 4, a and e; and Fig. 5, a and b). As the majority of proteins synthesized in the ER undergo glycosylation, we tested whether this band was the result of glycan addition. For this, we treated protein lysates with different deglycosylation enzymes. Whereas *O*-glycosidase and sialidase A treatment did not affect the mobility of the upper band, addition of the N-glycosidases endoglycosidase H (Endo H) and peptide-*N*-glycosidase F (PNGase F) completely eliminated it (Fig. 5, a and b), suggesting that a fraction of ATP6AP2^{L98S} is N-glycosylated and localized in the ER.

N-glycosylation in the ER typically occurs cotranslationally through oligosaccharyltransferases complexes harboring the STT3A subunit (Cherepanova et al., 2016). However, when glycosylation sites are skipped or when proteins are misfolded, N-glycans can also be added posttranslationally by STT3B-containing oligosaccharyltransferase complexes (Sato et al., 2012; Cherepanova et al., 2016). To investigate whether the N-glycan addition in ATP6AP2^{L98S} occurred co- or posttranslationally, we expressed ATP6AP2^{L98S} in *STT3A* and *STT3B* KO cells (Cherepanova and Gilmore, 2016). We found that the slower migrating band ATP6AP2^{L98S} was present in *STT3A* but not in *STT3B* KO cells (Fig. 5 d), suggesting that ATP6AP2^{L98S} is subject to posttranslational N-glycosylation in the ER. Given that this mutant protein is targeted for ERAD, the results suggest that the N-glycan is added as a result of misfolding.

The p.L98S mutation causes developmental defects and decreased protein stability in *Drosophila*

To better understand the consequences of the p.L98S mutation on animal development and homeostasis, we turned to *Drosophila*, where the leucine residue at position 98 is conserved (Fig. 1 b). Null alleles of the *Drosophila* orthologue of ATP6AP2 (also known as VhaM8.9 or VhaPRR) are early lethal (Hermle et al., 2013). Thus, we generated an ATP6AP2 transgene carrying the p.L98S mutation and used a genetic rescue approach in which we expressed *ATP6AP2^{L98S}* mutant under the *ATP6AP2* promoter and in the background of the *ATP6AP2$^{\Delta 1}$* null allele (hereafter referred to as *ATP6AP2^{L98S}*; see Table S1 for precise genotypes; Hermle et al., 2013). In parallel, we analyzed versions of WT ATP6AP2 with and without a C-terminal Myc tag (*ATP6AP2$^{WT\text{-}Myc}$ and ATP6AP2^{WT}*, respectively), a deletion of the ER retrieval motif (*ATP6AP2$^{\Delta KKxx}$*), and a mutant of the furin cleavage site (*ATP6AP2^{AxxA}*) to assess the importance of ATP6AP2 proteolytic cleavage in the function of ATP6AP2. Expression of *ATP6AP2^{WT}* and *ATP6AP2^{AxxA}* led to full restoration of viability into adulthood (Fig. 6, a and b). In contrast, *ATP6AP2^{L98S}* mildly impaired larval-to-pupal transition (Fig. 6 a), and both *ATP6AP2^{L98S}* and *ATP6AP2$^{\Delta KKxx}$* significantly reduced the percentage of adults eclosing from the pupal case (Fig. 6 b). These adult survivors demonstrated poor mobility, decreased or absent climbing capabilities, blistered wings, and reduced head size and died 3–4 d after eclosion (not depicted).

Next, we analyzed ATP6AP2 protein expression and processing by Western blotting in whole larval extracts. Compared with endogenous ATP6AP2, *ATP6AP2$^{WT\text{-}Myc}$* showed reduced levels of FL protein and similar levels of cleaved NT. In *ATP6AP2$^{\Delta KKxx}$* larvae, FL and NT levels were higher compared with endogenous control (Fig. 6, c and d), indicating enhanced cleavage and stability of the protein as found for ATP6AP2^{QxQxx} overexpression in HEK293T cells. As expected, proteolytic cleavage was suppressed in *ATP6AP2^{AxxA}* with a concomitant increase of the FL protein. Importantly, in *ATP6AP2^{L98S}* larvae, the levels of both FL and NT were reduced compared with WT controls in whole larval lysates (Fig. 6, c and d), confirming the decreased stability observed for the mutant proteins in patient fibroblasts and HEK293T cells. Although glycosylated forms of *ATP6AP2^{L98S}* were not seen when expressed under its own promoter (Fig. 6, c and e), *ATP6AP2^{L98S}* was also N-glycosylated in *Drosophila* upon overexpression with the UAS-Gal4 system (Fig. 5 c). Collectively, the p.L98S mutation in *Drosophila* impairs ATP6AP2 protein stability and is sufficient to cause developmental defects.

Flies with the p.L98S mutation present brain developmental defects and impaired lipid homeostasis

To understand the cause of the compromised viability of the *ATP6AP2^{L98S}* flies, we turned to two tissues affected in the patients: the central nervous system and the fat body, a liver-like tissue. We first examined whether differences in expression

mined by an unpaired Student's *t* test. (h–j) Turnover of ATP6AP2 WT, L98S, R71H, and QxQxx was determined by cycloheximide (100 µM) chase experiments. The chase started 24 h after transfection and was allowed for the indicated time. The percentage of the protein decay was graphically reported (i), and the difference of the in cellulo half-life between the WT, L98S, R71H, and QxQxx was analyzed in j. Blots are representative of four individual experiments. All data are mean ± SEM of four independent experiments. ns, not significant; **, P < 0.01; ***, P < 0.001. The statistical significance was determined by a regular two-way ANOVA followed by a Bonferroni multiple comparisons test in i and an unpaired Student's *t* test in j. (k) HEK293T cells were transiently cotransfected with the CT-tagged construct ATP6AP2 WT, L98S, R71H, and QxQxx and p97-WT-His or p97-QQ-His. Samples were analyzed with anti-HA and anti-His antibodies. (l) Expression levels of ATP6AP2 FL in the presence of p97^{WT} or p97^{QQ} relative to those of β-actin were calculated. All data are mean ± SEM of three independent experiments. ns, not significant; *, P < 0.05. The statistical significance was determined by an unpaired Student's *t* test. Molecular mass is indicated in kilodaltons.

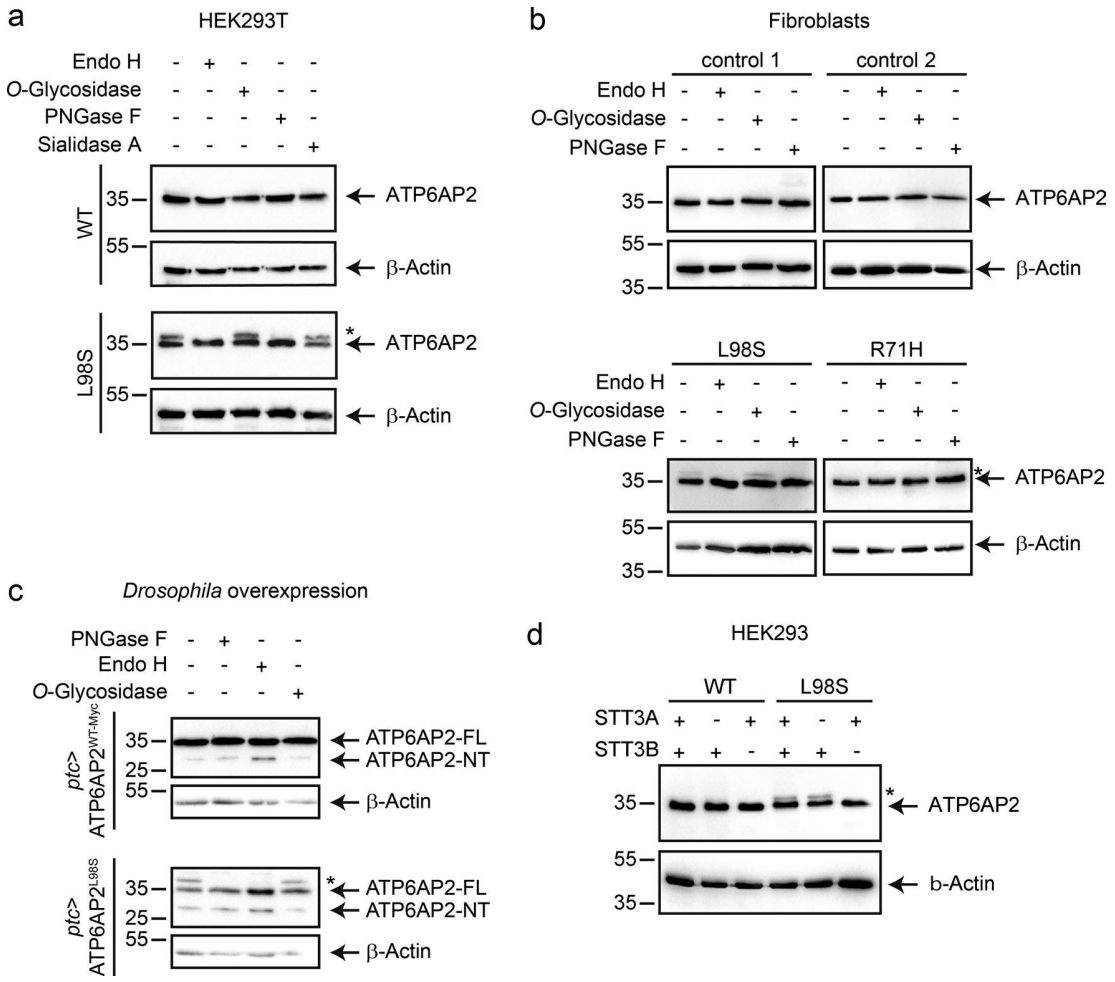

Figure 5. **The mutant ATP6AP2^{L98S} migrates as a double band as a result of posttranslational N-glycosylation.** (a) HEK293T cells were transiently transfected with C-terminally HA-tagged constructs of WT and L98S. Protein extracts were immunoblotted with anti-HA antibody after incubation with (+) and without (-) Endo H, *O*-glycosidase, PNGase F, or sialidase A. Asterisk indicates slower migrating band for ATP6AP2^{L98S}. (b) The expression of endogenous ATP6AP2 was analyzed in two different control fibroblasts from healthy donors and fibroblasts from P1 (p.L98S) and P3 (p.R71H). Cell lysates were separated by SDS-PAGE after incubation with (+) or without (-) Endo H, *O*-glycosidase, or PNGase F, and the proteins were revealed with anti-ATP6AP2-NT antibody. (c) *ATP6AP2^{WT}* and *ATP6AP2^{L98S}* were overexpressed with *patched(ptc)*-GAL4 in flies, and lysates were analyzed by immunoblot with anti-ATP6AP2-NT antibody after incubation with (+) and without (-) Endo H, *O*-glycosidase, or PNGase F. (d) Parental HEK293, *STT3A* KO, and *STT3B* KO cells were transiently transfected with ATP6AP2^{WT} or ATP6AP2^{L98S}. Cell lysates were analyzed by immunoblotting and revealed with anti-HA antibody. β-Actin served as a loading control. Data in a–d are representative of three, three, two, and five experiments, respectively. Molecular mass is indicated in kilodaltons.

levels and processing could be observed for ATP6AP2 in these tissues. We found that FL endogenous ATP6AP2 and FL transgenic *ATP6AP2^{WT}* were similarly expressed in whole larval extracts, fat body, and larval brain (Fig. 6 e). In contrast, FL *ATP6AP2^{L98S}* expression was highly reduced, especially in fat body tissue. Furthermore, minimal cleavage of ATP6AP2 was observed in fat body for both endogenous and transgenic constructs, which could indicate a higher need for the FL form of ATP6AP2 in the fat body (Fig. 6 e).

To assess the consequences of the p.L98S mutation in central nervous system development, we examined the developing brain in *ATP6AP2^{L98S}* third instar larvae. Using immunolabeling, we found that the p.L98S mutation strongly affected the optic lobes, which are one of the major structures of the *Drosophila* brain (Fig. 6, f and g). The optic lobes develop from neuroepithelial cells, which first increase in number through symmetric divisions and are later converted into optic lobe neuroblasts (Yasugi et al., 2008; Egger et al., 2010). These neuroblasts divide asymmetrically to self-renew and to generate neurons. We observed that in *ATP6AP2^{L98S}* brains there is an expansion of optic lobe neuroblasts, marked by the expression of Deadpan (Dpn; Fig. 6 g). Whereas in WT mid third instar larval brains, only three to four cell rows of optic lobe neuroblasts could be observed, in *ATP6AP2^{L98S}* mutant

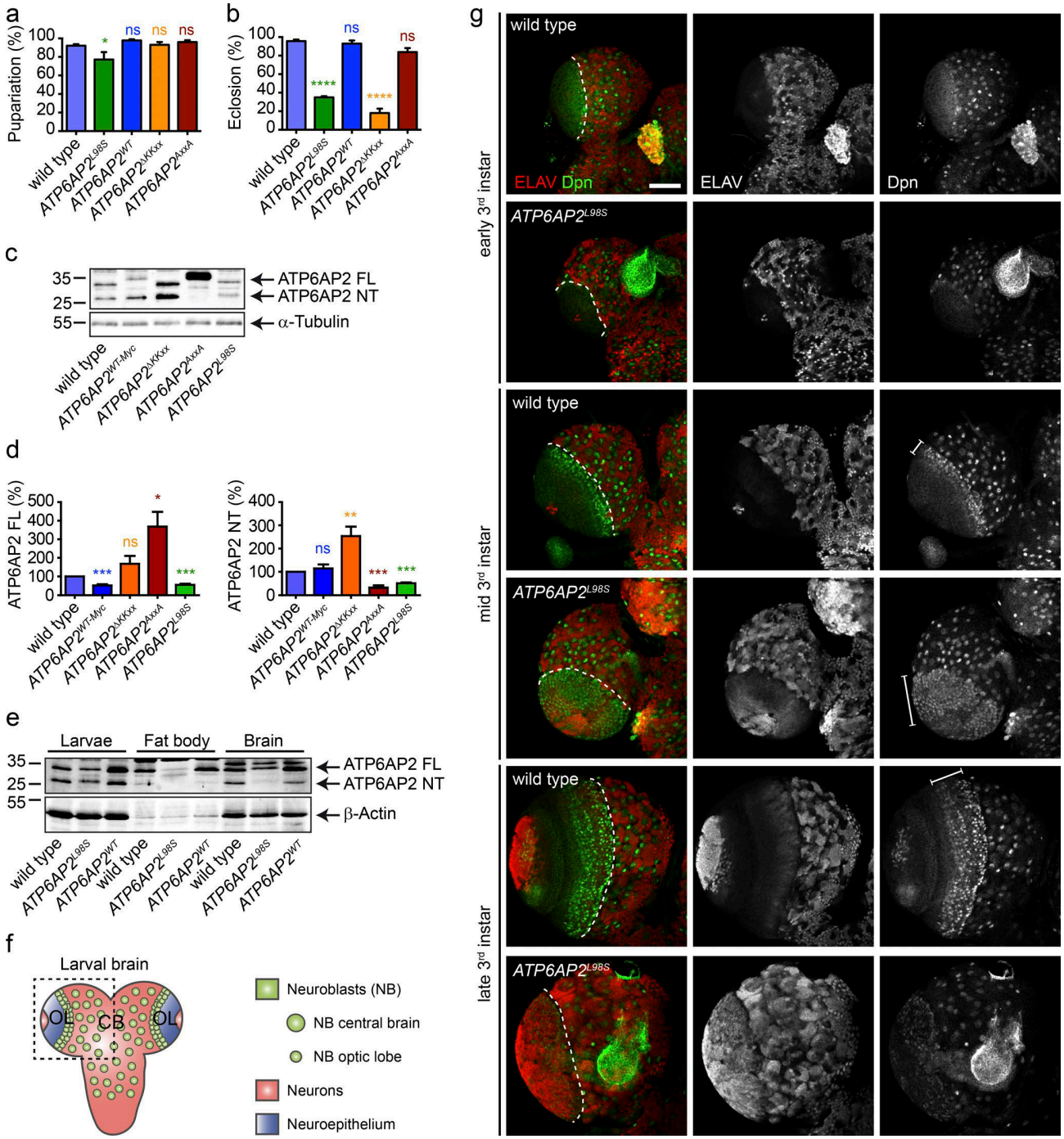

Figure 6. **L98S mutation causes decreased viability and premature differentiation of neural progenitors in *Drosophila*.** (a) Percentage of pupariation of the different *ATP6AP2* mutants used in this study. (b) Percentage of eclosion of adult flies. All data are mean ± SEM of three to five independent experiments (50–100 animals per genotype per experiment). *, $P < 0.05$; ****, $P < 0.0001$. Significance was determined by one-way ANOVA followed by a Bonferroni multiple comparisons test. (c) Western blot of ATP6AP2 in whole larvae extracts from WT and rescued flies showing expression levels and cleavage pattern of endogenous ATP6AP2 and the different rescue transgenes. α-Tubulin is used as loading control. (d) Relative levels of FL (left) and NT (right) *ATP6AP2* mutants compared with endogenous ATP6AP2. All data are mean ± SEM of seven independent experiments (5 animals per genotype per experiment). ns, not significant; *, $P < 0.05$; **, $P < 0.01$; ***, $P < 0.001$. The statistical significance was determined by a paired Student's *t* test. (e) Western blot of ATP6AP2 in whole larvae, fat body, and brain extracts of WT, $ATP6AP2^{L98S}$, and $ATP6AP2^{WT}$ rescue flies. β-Actin is used as loading control. Blot is representative of four independent experiments (5, 15, and 50 animals per genotype per experiment [larval, fat body, and brain extracts, respectively]). (f) Schematic

brains, most of the optic lobe was occupied by Dpn-positive cells, indicating a premature conversion to neuroblasts possibly at the expense of neuroepithelial cells. Consistent with a premature and increased neurogenesis, we found an increase in cells positive for the pan-neuronal marker ELAV in the optic lobes and the central brain of mid and late third instar *ATP6AP2*^{L98S} larvae (Fig. 6 g). These observations suggest that ATP6AP2 plays an important role in *Drosophila* neural development, which is altered by the patient's missense mutation.

The larval fat body is featured by a high amount of lipid droplets, which are storage organelles for triglycerides (TAGs) and cholesteryl esters (Ugur et al., 2016). Compared with WT, we found an increase in the size of lipid droplets in *ATP6AP2*^{L98S} mutant fat body cells (Fig. 7, a and b) as well as an increase in the number of small and large lipid droplets with a concomitant decrease of medium-sized droplets (Fig. 7 c). The increase in lipid droplets was accompanied by an increase in the levels of total TAGs in *ATP6AP2*^{L98S} mutant larvae (Fig. 7 d). An increase in TAGs was also observed in *ATP6AP2*$^{\Delta KKxx}$ but not in *ATP6AP2*^{AxxA} or *ATP6AP2*$^{WT\text{-}Myc}$ animals. Furthermore, in clones expressing *ATP6AP2*^{L98S} in the null background, we found a strong increase in lipid droplet size compared with the surrounding *ATP6AP2*$^{WT\text{-}Myc}$ tissue (Fig. 7 e, and see Table S1 for precise genotype). A similar phenotype was seen in clonal populations of cells in which ATP6AP2 was down-regulated using RNAi (Fig. 7 f), suggesting that *ATP6AP2*^{L98S} is a loss-of-function mutation. Furthermore, RNAi-mediated knockdown of ATP6AP2 also provoked lipid droplet accumulation in other tissues, such as Malpighian tubules (Fig. 7 g) and pupal wings (see Fig. 9 h).

Finally, we tested whether the down-regulation of other V-ATPase–associated genes could cause the same phenotype. Indeed, we found increased lipid droplet size in fat body and Malpighian tubules upon knockdown of ATP6V1C1 and ATP6AP1 (also known as Vha44 and VhaAC45, respectively; Fig. 7, f and g), suggesting that lipid accumulation in *ATP6AP2*^{L98S} cells is a general V-ATPase–dependent phenotype.

ATP6AP2 forms a complex with other V-ATPase assembly factors

Given the phenotypic overlap between the *ATP6AP2*^{L98S} mutant and ATP6V1C1 and ATP6AP1 knockdown in flies, we analyzed whether ATP6AP2 could interact with V-ATPase subunits and assembly factors and, if yes, whether the missense mutations could affect these interactions. We performed affinity purification coupled to MS (AP-MS) in HEK293T cells transiently overexpressing ATP6AP2^{WT}. Among the top-ranking interactors, we found assembly factors for the V0 sector of the V-ATPase (ATP6AP1, VMA21, and TMEM199) and V0 subunits themselves (ATP6V0A2 and ATP6V0D1; Fig. 8 a), three of which have been implicated in CDG (ATP6AP1, TMEM199, and ATP6V0A2; Kornak et al., 2008; Jansen et al., 2016a,c). For the top candidates ATP6AP1 and VMA21, the interaction was confirmed by coimmunoprecipitation (coIP) of overexpressed tagged proteins in HEK293T cells (Fig. 8 b), and for ATP6AP1 also by endogenous coIP (Fig. 8 c). Moreover, in a yeast two-hybrid (Y2H) screen on a mouse cDNA library, we found ATP6AP1 as a binding partner of ATP6AP2. Mapping experiments with different truncated constructs suggested that the interaction requires the N-terminal luminal domains of both proteins, which in the case of ATP6AP2 harbors both amino acids mutated in our patients. Accordingly, both mutations impaired the interaction with ATP6AP1 in Y2H (Fig. S5) and in reciprocal coIP experiments (Fig. 8, d and e). In contrast, a construct with a deletion of exon 4 mimicking the effect of the exon-skipping mutation in P4 bound with similar strength to ATP6AP1 as ATP6AP2^{WT} (Fig. S2 c). Together, these results suggest that ATP6AP2 forms a complex with other V-ATPase assembly factors, and that this interaction is impaired by the CDG-associated missense mutations.

ATP6AP2 mutations leads to defects in autophagy

To address the functional consequences of the decreased interactions with V-ATPase assembly factors, we analyzed V-ATPase activity in *ATP6AP2*^{L98S} fat body cells by staining with the acidotropic dye Lysotracker. *ATP6AP2*^{L98S} mutant clones showed a reduction in Lysotracker-positive organelles compared with the WT surrounding tissue, indicating reduced acidity (Fig. 9 a). In accordance with the importance of V-ATPase–mediated acidification for autophagic degradation (Mauvezin et al., 2015), we found a correlation between lipid droplet size increase in knockdown cells and impaired lysosomal activity as determined using the GFP-LAMP reporter that accumulates when lysosome function is impaired (Fig. 9 b; Pulipparacharuvil et al., 2005). Moreover, we observed an accumulation of the autophagosomal marker Atg8a-mCherry (LC3 in mammals) in fat body cells expressing *ATP6AP2* RNAi (Fig. 9 c) as well as an increase of endogenous Atg8a in *ATP6AP2*^{L98S} clones in fat body (Fig. 9 d).

To further characterize the autophagy defect, we analyzed the processing of Atg8a by Western blotting. Atg8a can be visualized as one or two forms: a nonprocessed cytosolic form (Atg8a-I) and a faster migrating membrane-associated lipidated form (Atg8a-II), which is the active form involved in autophagosome formation. We detected an increase in

representation of the larval *Drosophila* brain. CB, central brain; OL, optic lobe. (g) Representative micrographs (out of three independent experiments; 5–10 brains per genotype per experiment) for WT and *ATP6AP2*^{L98S} brain lobes from early (top) mid (middle) and late (bottom) third instar (third) larvae stained with the pan-neuronal marker ELAV (red in the merged panels) and the neuroblasts marker Deadpan (Dpn, green in the merged panels). Bar, 50 µm. Dashed lines in the merged panel separate the optic lobe (left) from the central brain (right). The region occupied by optic lobe neuroblasts is indicated with lines in mid and late third instar larvae. Molecular mass is indicated in kilodaltons.

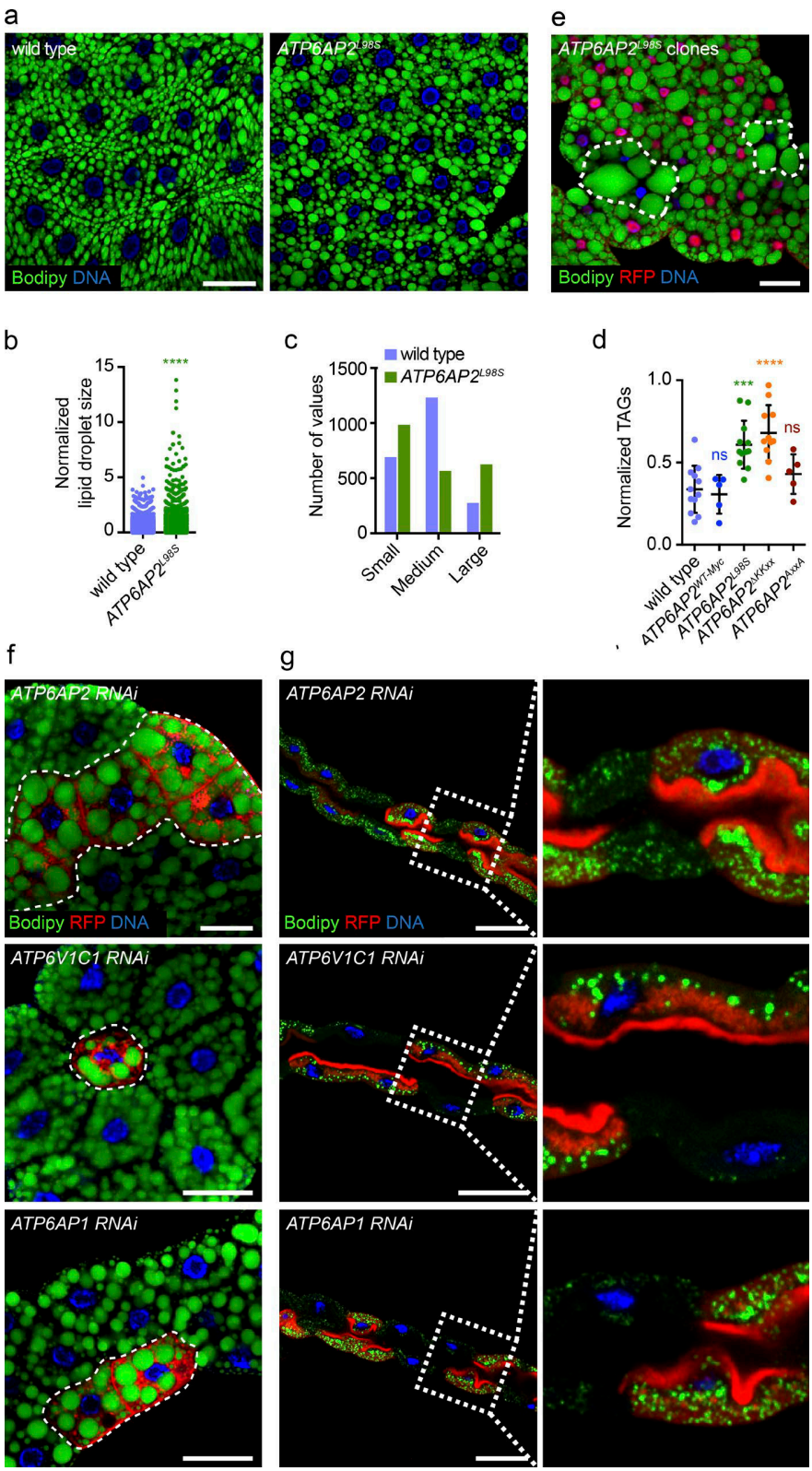

Figure 7. **L98S mutation in *Drosophila* ATP6AP2 causes impaired lipid metabolism.** (a) Bodipy (green) staining of wandering third instar larval fat bodies of WT and *ATP6AP2*^{L98S} rescue. (b) Quantification of lipid droplet size in WT and *ATP6AP2*^{L98S} third instar larval fat bodies. Each dot represents one lipid droplet. Data are from four independent experiments (5–10 animals per genotype per experiment) in which a total of 28 and 34 fat bodies were analyzed for WT and ATP6AP2^{L98S}, respectively. ****, P < 0.0001. Significance was determined by a Kolmogorov-Smirnov test. (c) Binning of data from (b) showing the distribution of lipid droplets by size category (small, medium, large). (d) Total TAG levels assayed enzymatically in WT, *ATP6AP2*$^{WT\text{-}Myc}$, *ATP6AP2*^{L98S}, *ATP6AP2*$^{\Delta KKxx}$, and *ATP6AP2*^{AxxA} wandering third instar larvae. Lines represent the mean ± SD of 5–10 independent experiments (5 animals per genotype per experiment). ns, not significant; ***, P = 0.0001; ****, P < 0.0001. Significance was determined by one-way ANOVA followed by a Bonferroni multiple comparisons test. (e) Analysis of lipid droplets in clonal populations of fat body cells expressing *ATP6AP2*^{L98S} (RFP-negative) surrounded by *ATP6AP2*$^{WT\text{-}Myc}$ cells (RFP-positive). Lipid droplets stained with Bodipy (green). DNA stained with Hoechst (blue). (f) Analysis of lipid droplets (green) in clonal populations of fat body cells and expressing RNAi against *ATP6AP2*, *ATP6V1C1*, and *ATP6AP1* (RFP-positive) surrounded by WT cells (RFP-negative). (g) Analysis of lipid droplets (green) in clonal populations of Malpighian tubule cells expressing RNAi against *ATP6AP2*, *ATP6V1C1*, and *ATP6AP1* (RFP-positive) surrounded by WT cells (RFP-negative). Right panels are magnifications of the insets demarked in left panels. (a and e–g) Bars, 50 µm. Micrographs of clonal analyses are representative of at least three independent experiments (10–15 animals per genotype per experiment).

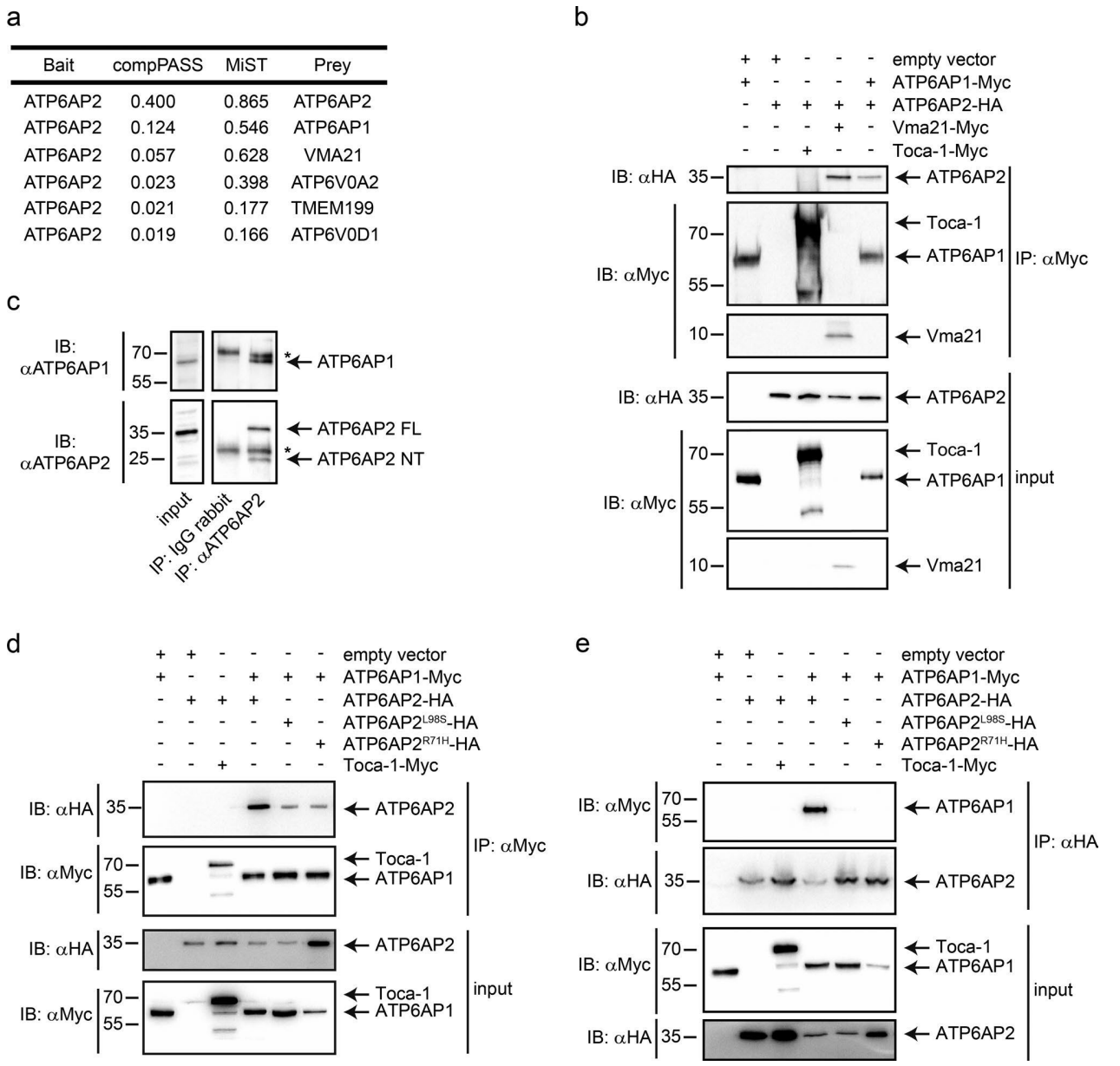

Figure 8. **ATP6AP2 interacts with V-ATPase assembly factors.** (a) Table showing the list of top-ranking interactors of ATP6AP2 based on two different score systems (CompPASS and MiST; Jäger et al., 2011). (b) CoIPs in HEK293T cells using the indicated constructs. Proteins were immunoprecipitated with anti-Myc antibody, and cell lysates were subjected to immunoblotting with anti-HA and anti-Myc antibodies. (c) Endogenous immunoprecipitation of ATP6AP2 in HEK293T cells using anti-ATP6AP2 (NT) antibody or control IgG. Immunoprecipitates were analyzed with anti-ATP6AP2 and anti-ATP6AP1. Lysate inputs of both proteins are on the left. The asterisks indicate heavy and light chains of the antibodies. (d) CoIPs in HEK293T cells using the indicated constructs. Proteins were immunoprecipitated with anti-Myc antibody, and cell lysates were subjected to immunoblotting with anti-HA and anti-Myc antibodies. (e) Reciprocal coIP experiment using anti-HA antibodies for immunoprecipitation. Toca-1-Myc is a negative control. Data are representative of eight (b), three (c), five (d), and two (e) independent experiments. Molecular mass is indicated in kilodaltons.

Atg8a-II in *ATP6AP2*^{L98S} larval lysates compared with WT and *ATP6AP2*$^{WT\text{-}Myc}$ (Fig. 9 e). To distinguish between increased autophagosome formation or decreased autophagic degradation (or a combination of both), we tested the levels of Ref(2)p (p62 in mammals). Consistent with decreased autophagic degradation, Ref(2)p was increased in *ATP6AP2*^{L98S} clones (Fig. 9 d) and *ATP6AP2*^{L98S} whole larval lysates (Fig. 9 e). Importantly, this is in agreement with the increased LC3-II, p62, and LAMP1/2 levels in mouse liver tissue acutely depleted of ATP6AP2 (Fig. S3 a; Kissing et al.,

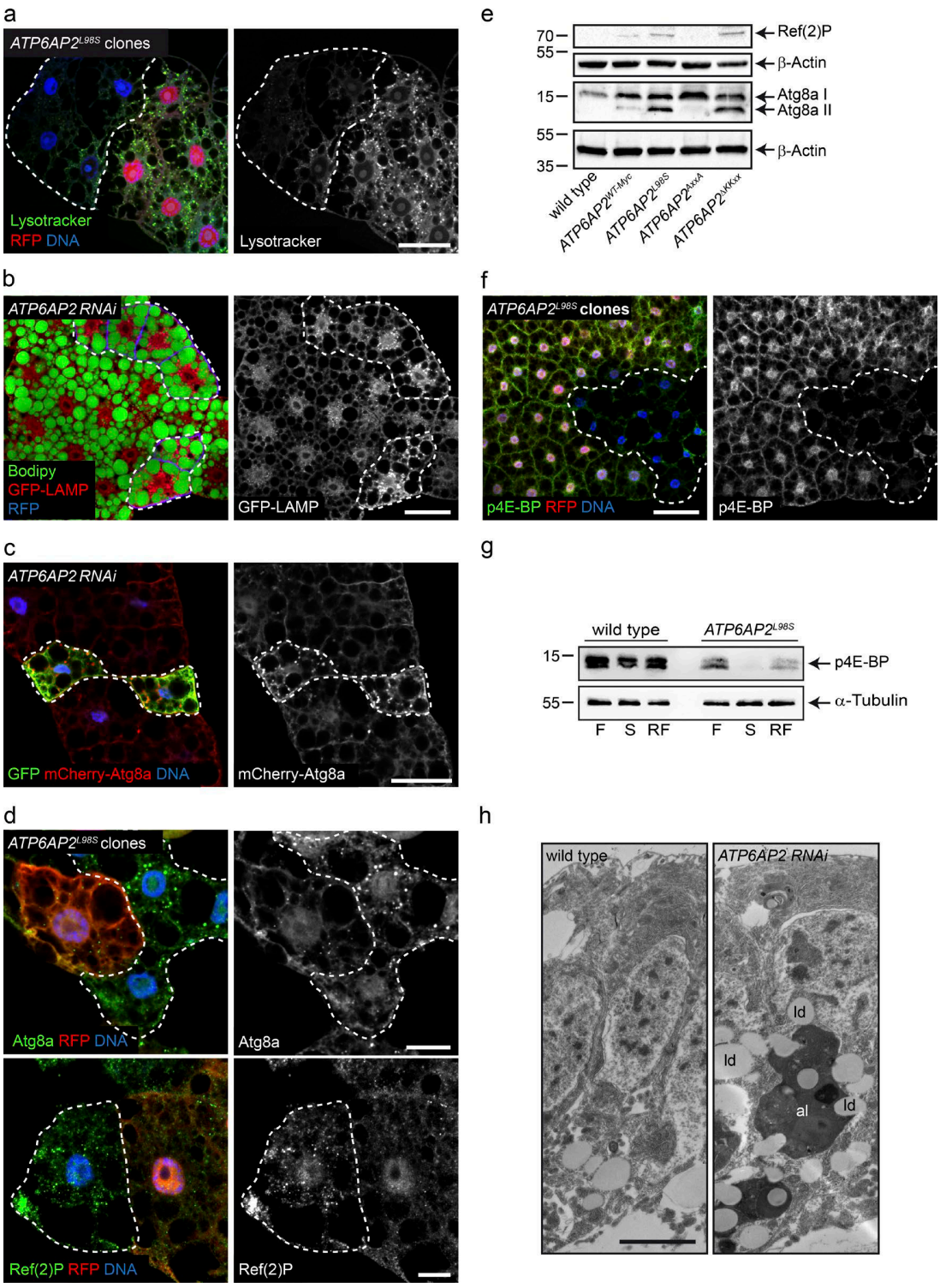

Figure 9. ***ATP6AP2* knockdown and *ATP6AP2*^{L98S} mutation lead to lipid accumulation as a result of autophagic defects.** (a) Lysotracker labeling (green in merged panel) of *ATP6AP2*^{L98S} clonal populations (RFP-negative) of fat body cells surrounded by *ATP6AP2*$^{WT\text{-}Myc}$ cells (RFP-positive). Bar, 50 µm. (b) GFP-LAMP accumulation (red in merged panel) and increased lipid droplet size in *ATP6AP2* knockdown cells (RFP-positive, blue in merged panel). Lipid droplets stained with Bodipy (green in merged panel). Bar, 50 µm. (c) Atg8a-mCherry accumulation (red in merged panel) in *ATP6AP2* knockdown cells (GFP-positive, green in merged panel). Bar, 50 µm. (d) Endogenous Atg8a (upper) and Ref(2)P (lower) staining (green in merged panel) in *ATP6AP2*^{L98S} clonal populations (RFP-negative) of fat body cells surrounded by *ATP6AP2*$^{WT\text{-}Myc}$ cells (RFP-positive). Bars, 20 µm. (e) Western blot of Ref(2)P and Atg8a in whole

2017). Finally, we found an increase of Atg8a–II and Ref(2)p in *ATP6AP2*$^{\Delta KKxx}$, but not in *ATP6AP2*^{AxxA} larval lysates (Fig. 9 e), suggesting that ER retrieval but not cleavage is essential for ATP6AP2 function in autophagy.

The V-ATPase has also been involved in the activation of mammalian target of rapamycin (mTOR) signaling (Zoncu et al., 2011), which conversely triggers autophagy when inhibited (Noda and Ohsumi, 1998). Thus, to analyze whether the *ATP6AP2*^{L98S} mutant could alter mTOR activity, we tested the phosphorylation status of 4E-BP, an important downstream effector of mTOR. Fat body clones expressing *ATP6AP2*^{L98S} showed reduced levels of phospho-4E-BP (p4E-BP) compared with the surrounding *ATP6AP2*$^{WT\text{-}Myc}$ tissue (Fig. 9 f). Likewise, p4E-BP was reduced in Western blotting of fed, starved, and refed *ATP6AP2*^{L98} whole larvae compared with control animals (Fig. 9 g), suggesting that stimulation of autophagy cause by mTOR inactivation in cells where lysosomal degradation is defective could contribute to the pathology. These findings were supported by transmission electron microscopy studies performed in pupal wings, in which knockdown cells showed a strong accumulation of lipid droplets and other organelles in large electron-dense vacuoles (Fig. 9 h). These vacuoles most likely represent autolysosomes with reduced degradative capacity and are reminiscent of the vacuoles found in the liver biopsy of P3 (Fig. 2 d).

Collectively, these results suggest that defects in V-ATPase activity, autophagy, and mTOR signaling are key to the disease caused by *ATP6AP2* missense mutations, particularly with regard to the steatohepatitis.

DISCUSSION

Genetic diseases caused by defective V-ATPase function are clinically diverse. Mutations in the core subunits *ATP6V1B1* and *ATP6V0A4* manifest in cells specialized in proton secretion such as renal intercalated cells and osteoclasts where these subunits are highly expressed (Forgac, 2007). In contrast, mutations in ubiquitously expressed core subunits and V0 assembly factors give rise to more systemic disorders (Kornak et al., 2008; Kortüm et al., 2015; Jansen et al., 2016a,b,c; Van Damme et al., 2017). The clinical similarity of *ATP6AP2* deficiency with mutations in other assembly factors, most notably *ATP6AP1*, strongly argues for a role of ATP6AP2 in the assembly of the V0 sector of the V-ATPase. In support of this hypothesis, we show that ATP6AP2 not only interacts with V0 assembly factors but also requires retrograde delivery to the ER for function as has previously been shown for several yeast assembly factors (Malkus et al., 2004; Ryan et al., 2008; Jansen et al., 2016a). Moreover, the identified missense mutations impair the interaction with ATP6AP1 and can cause reduced proton pump activity.

The acute depletion of ATP6AP2 in the mouse liver was sufficient to recapitulate the glycosylation and autophagy defects of the patients. Mechanistically, both direct and indirect effects on the glycosylation machinery are possible in the absence of V-ATPase activity. Whereas some glycosylation enzymes like sialidases require low pH for optimal activity (al-Awqati et al., 1992), defects in V-ATPase assembly or function could also cause secondary defects in ER and Golgi homeostasis that are responsible for the glycosylation defects. Thus, it remains to be determined how ATP6AP2 deficiency affects glycosylation and how far the glycosylation defect contributes to the clinical symptoms.

The observed defect in autophagic flux can, on the other hand, more easily be linked to V-ATPase dysfunction and to the clinical phenotype. As V-ATPase–mediated acidification is generally indispensable for the final degradation step in autophagy, it can be argued that a ubiquitous small decrease in V-ATPase activity primarily manifests in organs with a high need for autophagy. Whereas plasma cells of the immune system depend on high rates of autophagy to counteract ER expansion when Ig synthesis is high (Pengo et al., 2013), dysfunctional lipophagy can cause steatosis of the liver (Singh et al., 2009; Baiceanu et al., 2016). The latter process was recapitulated in the *Drosophila* mutant, where fat body cells showed lipid accumulation along with reduced organellar acidity and decreased lysosomal degradation. Aggravating the pathology, the decreased mTORC1 activation, observed in these cells, may permit an inappropriate induction of autophagosome formation, autophagosome maturation, and fusion with lysosomes despite the inability to execute degradation in the final step of autophagy (Ramachandran et al., 2013; Mauvezin et al., 2015). Such a block in autophagy flux after its induction is supported by the observed lipidation of LC3/Atg8a and p62/Ref(2)P accumulation and may explain the enlarged autolysosomes seen in the liver biopsies and in the epithelial cells of the fly wings.

Whether the intellectual disability and mild ataxia in patients with *ATP6AP2* missense mutations are also a consequence of reduced autophagy awaits further testing. By

larvae extracts of WT and *ATP6AP2*$^{WT\text{-}Myc}$, *ATP6AP2*^{L98S}, *ATP6AP2*^{AxxA}, and *ATP6AP2*$^{\Delta KKxx}$ flies. β-Actin is used as loading control. Blot is representative of five independent experiments (five animals per genotype per experiment). (f) p-4E-BP staining of *ATP6AP2*^{L98S} clonal populations (RFP-negative) of fat body cells surrounded by *ATP6AP2*$^{WT\text{-}Myc}$ cells (RFP-positive). Bar, 50 µm. (g) Western blot of p4E-BP in fat body extracts of WT and *ATP6AP2*^{L98S} third instar larvae in fed (F), starved (S), and refed (RF) conditions. α-Tubulin is used as loading control. Blot is representative of four independent experiments (20–25 animals per genotype per experiment). (h) EM micrographs of pupal wings in which *ATP6AP2* has been down-regulated in the dorsal compartment using RNAi driven by *apterous-Gal4*. As opposed to WT cells from the ventral epithelium (left), knockdown cells (right) show accumulation of lipid droplets (ld) and other organelles in large autolysosomes (al). Bar, 200 nm. Micrographs of clonal analyses are representative of at least three independent experiments (10–15 animals per genotype per experiment). Molecular mass is indicated in kilodaltons.

removing dysfunctional organelles and macromolecules, autophagy is beyond dispute an important survival mechanism in postmitotic neurons (Hara et al., 2006; Mariño et al., 2011). Accordingly, the neuron-specific down-regulation of ATP6AP2 in *Drosophila* and mouse has been shown to lead to autophagy defects and cognitive impairment (Dubos et al., 2015). However, the premature neuronal differentiation phenotype in the developing *ATP6AP2*^{L98S} fly brains argues for additional defects in signaling pathways involved in neural development. One candidate pathway is Notch signaling that depends on proper V-ATPase function (Yan et al., 2009; Vaccari et al., 2010) and is required to maintain the pool of neural progenitors in the developing fly brain (Bowman et al., 2008; Egger et al., 2010; Wang et al., 2011). Indeed, Notch phenotypes were previously found in *ATP6AP2* mutant wing clones (Hermle et al., 2013), and more importantly, reduction of Notch signaling because of inhibition of the V-ATPase has been shown to deplete neural stem cells in mice by promoting their differentiation (Lange et al., 2011).

Interestingly, late-onset cerebral manifestations such as Parkinsonism and epilepsy are the main problems in patients with exon-skipping mutations in *ATP6AP2* (Ramser et al., 2005; Korvatska et al., 2013). However, these patients do not exhibit any obvious liver, immune, or skin defects. Furthermore, we found almost normal glycosylation in one of these patients as well as no effect on the interaction with ATP6AP1 upon deletion of exon 4 (Fig. S2, a–c). These results suggest that the clinical manifestation of ATP6AP2 deficiency depends on the severity of the mutations. Indeed, whereas the exon-skipping mutations have only partial penetrance reducing the levels of full-size ATP6AP2 transcripts by <50% (Korvatska et al., 2013), the missense mutations described here lead to impaired protein stability and the inability to fully rescue the embryonic lethality of the *Drosophila* null mutation. In particular, we provide evidence that ATP6AP2^{L98S} is misfolded in the ER and targeted for ERAD. Thus, it is very likely that missense mutations have a stronger impact on overall ATP6AP2 function than the exon-skipping mutations.

In summary, we identify three individuals with a new glycosylation and autophagy disorder caused by different point mutations in the luminal domain of ATP6AP2. Our functional studies using cell culture, *Drosophila*, and mouse models suggest that the missense mutations reduce the interaction with V0 assembly factors and, consequently, V-ATPase activity. Interestingly, the lack of the ER retrieval motif caused more cleavage and led to reduced survival, fat accumulation, and autophagy defects in *Drosophila*, suggesting that retrograde Golgi-to-ER transport prevents cleavage in the Golgi and is required for proper ATP6AP2 function. Moreover, we demonstrate that proteolytic processing of ATP6AP2 is tissue-dependent (Fig. 6 e), similar to what has been shown before for ATP6AP1 (Jansen et al., 2016a). Our results thus provide a better understanding of ATP6AP2 functions and pave the way for additional studies on how ATP6AP2 processing and trafficking controls V-ATPase assembly.

MATERIALS AND METHODS

Ethics statement

Research on patients' cells was prospectively reviewed and approved by the Ethical Committee of the University Hospitals of Leuven and Münster.

Exome sequencing

For the p.L98S case, mutation identification was achieved by whole exome sequencing. Genomic DNA was sheared by sonication, platform-specific adaptors were ligated, and the resulting fragments were size selected. The library was captured using the SeqCap EZ Human Exome Library v3.0 (Roche NimbleGen), and paired end (2 × 101 bp) sequenced on a HiSeq2000 (Illumina). Reads were aligned to the human reference genome (hg19) using BWA (v0.6.2), and duplicate reads were removed using Picard MarkDuplicates (v1.78). Local realignment around indels, base quality score recalibration, and variant calling were performed using GATK (v2.4.9) RealignerTargetCreator, IndelRealigner, BaseRecalibrator, and UnifiedGenotyper. Variants were annotated using Annovar (v11-02-2013). Synonymous variants were excluded, whereas variants with a frequency <5% in the 1000 Genomes project, ESP, GoNL, and our in-house database were further considered. Subsequent prioritization was then applied based on recessive inheritance, conservation, and pathogenicity prediction scores.

For the p.R71H cases, whole exome analysis of the patients DNA was done on an Illumina HiSeq2500. Subsequent prioritization in both cases was then applied based on recessive inheritance, conservation, and pathogenicity prediction scores.

Sanger sequencing

Total RNA was isolated from the primary fibroblasts of the patient and control cells using the RNeasy kit (QIAGEN). 2 µg of purified total RNA was subjected to RT with the First-Strand cDNA synthesis kit (GE Healthcare) following the manufacturer's instructions. For PCRs, cDNAs obtained after RT were diluted 1:5.

Genomic DNA was extracted from white blood cells from the patient and controls using the DNeasy Blood & Tissue kit (QIAGEN) according to the manufacturer's protocol. Primers were designed (Primer Blast) to amplify the different exons of the ATP6AP2 gene (available from GenBank under accession no. NM_005765.2), including at least 50 bp of the flanking intronic regions. Sequences of the primers for exon 3 are as follows: ATP6AP2_E03_F: 5′-ACC GCTTTGTGCTTTTCAAT-3′; ATP6AP2_E03_R: 5′-TCACCCACATTGCCTGAATA-3′.

DNA of the patients and family members of family 2 was isolated from EDTA blood using the DNeasy Blood & Tissue kit (QIAGEN) according to the manufacturer's protocol. Primer sequences used for Sanger sequencing of ATP6AP2 (exon 3) were as follows: ATP6AP2 (exon 3) forward: 5′-TTGTCAGTGTCATCTCAGAACCCC-3′; ATP6AP2 (exon 3) reverse: 5′-TGGCTCTCTTTTTCA

AGCCTCTGG-3′. Primers were designed with Primer Blast (Ye et al., 2012).

Glycosylation studies

Capillary zone electrophoresis and isoelectric focusing of serum transferrin were performed as previously described (Zühlsdorf et al., 2015). Glycosylation of serum transferrin was additionally assessed via HPLC using the CDT in serum kit by Chromesystems according to the manufacturer's protocol.

For MALDI-TOF MS analysis, aliquots of 20 µl of mouse sera were mixed with lysis buffer (50 mM phosphate buffer, pH 7.9, containing 0.5% SDS and 1% β-mercaptoethanol) and incubated at 100°C for 20 min. After cooling and the addition of phosphate buffer and 1% Nonidet P-40, three units of PNGase F (Roche Diagnostics) were added, and samples were incubated for 24 h at 37°C. Released glycans were purified on a graphitized carbon column (Alltech). Glycans were permethylated as previously described (Faid et al., 2007) and purified on an SPE C18 column (Alltech). Permethylated glycans were then dissolved in methanol/water (1:1 vol/vol) and mixed with an equal volume of dihydroxyaminobenzoic acid matrix (Aldrich; 20 mg/ml in methanol/water 1:1 vol/vol). Mass spectra were acquired using an Applied Biosystems/MDS Sciex 4800 MALDI-TOF/TOF analyzer at fixed laser intensity for 1000 shots/spectrum. A total of 5000 shots were accumulated in reflectron positive ion mode MS for each sample.

Mouse experiments

Generation of the *ATP6AP2fl/fl* mutant mouse line was described previously (Riediger et al., 2011). For in vivo transduction, 10^9 of adenoviral infectious particles were diluted in 0.9% NaCl and administered retro-orbitally in a total volume of 100 µl per mouse. Mice were sacrificed 10 d after injection. Adenovirus coding for GFP was used as a control in all experiments. GFP and GFP-Cre adenoviral vectors were described previously (Nemazanyy et al., 2013). Animals were fed a standard chow diet (Teklad global protein diet; 20% protein, 75% carbohydrate, 5% fat). All mice were sacrificed at 2–4 pm in a random-fed state. All animal studies were approved by the Direction Départementale des Services Vétérinaires, Préfecture de Police, Paris, France. Liver transaminases ALT and AST and total cholesterol levels in serum were determined with a multiparametric automate Olympus AU 400.

Plasmids

The cDNAs of *Vma21*, *Atp6ap1*, and *Atp6ap2* were generated by gene synthesis (Invitrogen GeneArt Gene Synthesis service) and subcloned using HindIII or NcoI and BamHI sites into pFrog-Myc/HA (a pcDNA3-derivative), resulting in C-terminal tagged versions of the respective proteins as previously described (Blanz et al., 2015). A version of ATP6AP2 lacking exon 4 (101-132aa) was subcloned from the pCS2 vector (Korvatska et al., 2013) into pFrog-Myc. For the AP-MS approach, ATP6AP2 cDNA was subcloned into pDNA4/TO with a triple FLAG-tag. All constructs were verified by sequencing. To obtain all the mutants of ATP6AP2 with single and double amino acid substitutions (ATP6AP2-L98S-HA, ATP6AP2-R71H-HA, and ATP6AP2-QxQxx-HA), the construct pFrog-ATP6AP2-HA was used as a template, and site-direct mutagenesis reactions were performed with the QuickChange II Site-Directed Mutagenesis kit (Agilent) according to the manufacturer's instruction using the following oligos: -ATP6AP2-L98S-HA: forward: 5′-CCCTTCGGA GAATGCAGTTCCTTTTAGTCTAGACAGC-3′, reverse: 5′-CTCCGAAGGGTAGGAGATGACGCTGCCTGC-3′; -ATP6AP2-R71H-HA-forward: 5′-TTCCACATG CCACGGGCTACCATTATGGTGATGG-3′, reverse: 5′-CCCGTGGATGGTGGAATAGGTTACCCACGGCAA GCCC-3′; -ATP6AP2-QxQxx-HA- (sequential mutagenesis): forward: 5′-ATCAGCAGATTCGAATAGATGGAT CCTACCCA-3′, reverse: 5′-AATCTGCTGATTTGTCAT CCTATAGATGATGC-3′; forward: 5′-GATTCAAATAGA TGGATCCTACCCATACGACG-3′, reverse: 5′-CTATTT GAATCTGCTGATTTGTCATCCTATAG-3′.

pcDNA3.1-p97-WT-His and pcDNA3.1-p97-QQ-His were kindly provided by Y. Yihong (National Institute of Diabetes and Digestive and Kidney Diseases, National Institutes of Health, Bethesda, MD).

RNA extraction, RT, and quantitative real-time PCR

Total RNA was isolated from fibroblasts using a QIAGEN RNA extraction kit. cDNA was prepared using reverse transcription iScript cDNA Synthesis kit (Bio-Rad). Relative expression levels of ATP6AP2 were determined using the Power SYBR Green PCR Master Mix (ThermoFisher) and the following primers: ATP6AP2 exon 2 forward, 5′-CTG CATTGTCCATGGGCTTC-3′, and ATP6AP2 exon 3 reverse, 5′-AACAGGTTACCCACTGCGAG-3′. Expression levels were normalized to HPRT.

Cell culture, Western blotting, and immunoprecipitation

Primary fibroblasts from patients and controls were grown from a skin biopsy and cultured in Nutrient Mixture F-12 DMEM/F-12 (ThermoFisher) supplemented with 10% FBS at 37°C under 5% CO_2. Research on patients' cells was prospectively reviewed and approved by the Ethical Committees of the University Hospital of Leuven and Münster. HEK293T cells were routinely grown at 37°C in DMEM (ThermoFisher) containing 10% FBS. HEK293 *STT3A* KO, *STT3B* KO, and the parental HEK293 cells were cultured as described previously (Cherepanova and Gilmore, 2016). Cells were transfected by using Lipofectamine 2000 (Invitrogen) in Opti-MEM (ThermoFisher) according to the manufacturers' instructions.

The expression of ATP6AP2 forms was analyzed by Western blotting 48 h after transfection. For this, cells were harvested in 50 µl of lysis buffer (1% Triton X-100 in PBS) supplemented with protease inhibitor cocktail (Roche). After 30-min incubation in lysis buffer at 4°C, the lysates were then cleared by centrifugation for 10 min at 13,200 rpm at 4°C.

The protein concentration was determined using a Pierce BCA Protein Assay kit (Thermo Scientific). For each experiment, aliquots of the lysate (20 µg total protein per aliquot) were denatured using 1× SDS sample buffer for 25 min at 55°C and analyzed by SDS-PAGE. For immunoblotting, proteins were transferred to nitrocellulose filters by using the iBlot2 Dry Blotting system (ThermoFisher) and then blocked for 1 h in blocking buffer (5% nonfat dry milk, 0.2% Tween-20 in PBS). The membranes were incubated overnight with the specific primaries antibodies, followed by HPR-conjugated secondary antibodies. To assess relative protein levels, band intensity was measured with the ImageJ software.

For the coIP (anti-Myc), HEK293T cells were transfected with 1 µg of ATP6AP2^{WT}-HA, 1 µg of ATP6AP2^{L98S}-HA, and 1 µg of ATP6AP2^{R71H}-HA. For the reciprocal coIP (anti-HA), cells were transfected with 1 µg of ATP6AP2^{WT}-HA, 2 µg of ATP6AP2^{L98S}-HA, and 2 µg of ATP6AP2^{R71H}-HA. Cells were harvested in 100 µl of EBC lysis buffer (120 mM NaCl, 50 mM Tris [pH 8.0], 5 mM EDTA, 50 mM Hepes, and 0,5% NP-40) supplemented with protease inhibitor. After 1 h incubation in lysis buffer at 4°C, the lysates were then centrifuged for 10 min at 13,200 rpm at 4°C, and the protein concentration was determined as before. For each sample, 2 mg of protein was incubated overnight with 1 µg of mouse mAb anti-Myc at 4°C. Next, 50 µl of Dynabeads Protein G (Thermo Scientific) was added 1 h at 4°C and washed according to the manufacturer's instructions. The immunoprecipitated proteins were eluted by addition of 30 µl of 4× SDS sample buffer, followed by 5 min incubation at 95°C. Initial lysates and immunoprecipitated proteins were analyzed by SDS-PAGE and immunoblotted with specific antibodies. For the endogenous immunoprecipitation, 2 mg of lysates were incubated overnight with either rabbit Ig (as control) or with 2 µg of rabbit polyclonal antibody anti-ATP6AP2 at 4°C. 100 µl of Dynabeads Protein G was added, and the proteins were eluted and analyzed by Western blotting as described in the previous paragraph.

The following antibodies were used: rabbit polyclonal anti-Myc antibody (sc-789) and mouse monoclonal anti-Myc antibody (sc-40) both from Santa Cruz Biotechnology, rat monoclonal anti-HA antibody (11867423001; Roche), rabbit polyclonal anti-ATP6AP1 antibody (ab176609; Abcam), and rabbit polyclonal anti-ATP6AP2 antibody (HPA003156), mouse monoclonal anti–β-actin antibody (A1978), and mouse monoclonal antihistidine antibody (H1029), all from Sigma-Aldrich. Secondary antibodies used were antirat, antirabbit, and antimouse Horseradish Peroxidase Conjugated (Thermo Scientific).

Indirect immunofluorescence studies

HeLa cells were grown on glass coverslips in DMEM (ThermoFisher) supplemented with 10% FBS. Cells were transfected with Lipofectamine 2000 (Invitrogen) in Opti-MEM (ThermoFisher) according to the manufacturer's instructions. The localization of ATP6AP2 construct was analyzed 48 h after transfection. For this, cells were fixed with 4% formaldehyde in PBS for 30 min at room temperature. Formaldehyde was quenched with 0.1 M glycine in PBS for 5 min on ice, and cells were made permeable with 0.1% Triton X-100 in PBS 10 min at room temperature. Cells were blocked for 30 min at room temperature in BSA 3% and labeled with the appropriate primary antibodies overnight at 4°C in 0.1% PBS–Tween-20 supplemented with 3% BSA. After washing, cells were incubated 1 h at room temperature with secondary antibodies (dilution 1:200) and Hoechst (0.5 µg ml^{-1}) in PBS. Coverslips were mounted in Moviol. Primary antibodies used were rat anti-HA (11867423001; Roche), mouse anti-Calnexin (ALX-804-014-R100; Enzo Life Science), and rabbit anti-Giantin (Antibody platform Institut Curie). Secondary antibodies used were fluorescent conjugated Alexa Fluor 488 and Alexa Fluor 555 (Invitrogen Molecular Probes).

Analysis of protein stability and glycosidase inhibitor treatments

For the cycloheximide chase assay, 30, 42, 45, and 46 h after transfection, culture medium was changed for the chase medium (DMEM supplemented with 20 mM Hepes), and cycloheximide (Sigma-Aldrich) was added to reach a final concentration of 100 µM. Vehicle controls were treated with DMSO for 18 h.

For the deglycosylation digestion, 20 µg of cell lysates were treated according to the manufacturer's instructions and incubated for 1 h at 37°C with 500 U of Endo H, 500 U of PNGase F, 40,000 U of *O*-glycosidase (New England BioLabs), or 0.005 U Sialidase A (Prozyme).

Proteomics

Transfection of HEK293 cells and AP-MS were performed as previously described (Jäger et al., 2011). In brief, pools of HEK293 cells transiently expressing ATP6AP2-3×FLAG were used to precipitate ATP6AP2 and associated protein complexes using affinity gels followed by MS analysis. Biological triplicates of ATP6AP2-3xFLAG were performed, and only those proteins that were detected in all spectral counts are shown. Data were analyzed with two AP-MS scoring algorithms, MiST (Jäger et al., 2011) and CompPASS (Sowa et al., 2009).

Y2H analysis

The Y2H screen was performed by Hybrigenics Services. The coding sequence of the human ATP6AP2 wt NT$^{17-275}$ was PCR-amplified and cloned into pB27 as a N-terminal fusion to bait fragment (LexA-ATP6AP2 wt NT$^{17-275}$). The constructs were checked by sequencing and used as a bait to screen a random-primed mouse kidney cDNA library constructed into pP6. pB27 and pP6 derive from the original pBTM116 (Vojtek and Hollenberg, 1995) and pGADGH (Bartel et al., 1993) plasmids, respectively. ULTImate Y2H screening was performed against the mouse kidney cDNA library using ATP6AP2 wt NT$^{17-275}$ as a bait. The prey fragments cloned in frame with the Gal4 activation domain into

plasmid pP6, derived from the original pGADGH (Bartel et al., 1993), were checked by sequencing.

For 1-by-1 screening, the prey fragment for the human ATP6AP1 (ATP6AP1-NT$^{30\text{-}254}$, PCR amplified from the coding sequence of the human ATP6AP1-NT$^{30\text{-}254}$), human ATP6AP2^{L98S}NT$^{17\text{-}275}$ (PCR amplified), and human ATP6AP2^{R71H}NT$^{17\text{-}275}$ (fragment synthesized) were cloned in frame with the LexA DNA binding domain into pB27 (LexA-ATP6AP1-NT$^{30\text{-}254}$ and LexA-ATP6AP2^{L98S}NT$^{17\text{-}275}$). The prey fragments for the human ATP6AP2 wt NT$^{17\text{-}275}$, the human ATP6AP2^{L98S}NT$^{17\text{-}275}$, and the ATP6AP2^{R71H}NT$^{17\text{-}275}$ were cloned in frame with the Gal4 AD into plasmid pP7 (AD-ATP6AP2 wt NT$^{17\text{-}275}$, AD-ATP6AP2^{L98S}NT$^{17\text{-}275}$, and AD-ATP6AP2^{R71H}NT$^{17\text{-}275}$). pP7 derives from the original pGADGH (Bartel et al., 1993). The pP7 prey plasmid used in the control assay is derived from the pP6 plasmid. All constructs were checked by sequencing the entire inserts.

Fly strains and husbandry

Drosophila melanogaster stocks were raised on standard cornmeal food at 25°C. The following stocks were used: w^{1118} (used as WT control), FRT82B, *ATP6AP2*$^{\Delta 1}$, ATP6AP2>*ATP6AP2*$^{WT\text{-}Myc}$, ATP6AP2>*ATP6AP2*^{WT}, and ATP6AP2>*ATP6AP2*^{AxxA}, which have all been described in (Hermle et al., 2013), ATP6AP2>*ATP6AP2*^{L98S}, ATP6AP2>*ATP6AP2*$^{\Delta KKxx}$, and UAS>*ATP6AP2*^{L98S} were generated in this study (see next paragraph), *tub*-GFP–LAMP (gift from H. Krämer, UT Southwestern Medical Center, Dallas, TX), *hs-Flp*; tub-FRT-Gal80-FRT-Gal4, UAS–mCD8–mRFP (gift from F. Bosveld, Institut Curie, Paris, France), *hs-Flp;* UAS-Dcr2; R4-mCherry-Atg8, Actin-FRT-CD2-FRT-Gal4,UAS-GFPnls/TM6B (gift from G. Juhasz, Eotvos Lorand University, Budapest, Hungary), UAS-ATP6AP2$^{RNAi,\ GD5830}$, UAS-ATP6V1C1$^{RNAi,\ KK101527}$, UAS-ATP6AP1$^{RNAi,\ GD48017}$ (all from VDRC Stock Center), FRT42D, *ubi*-mRFPnls (Bloomington Stock Center), *hs-Flp*;; Tub-FRT-Gal80-FRT-Gal4, UAS-mCD8-RFP (gift from F. Bosveld), and Gal4 drivers *ptc*-Gal4 and *ap*-Gal4 (Bloomington Stock Center). For the precise genotype used in each figure, see also Table S1.

ATP6AP2>*ATP6AP2*^{L98S}-, ATP6AP2>*ATP6AP2*$^{\Delta KKxx}$-, and UAS>*ATP6AP2*^{L98S}-expressing transgenic flies have been created by site-directed mutagenesis using the QuickChange II Site directed Mutagenesis kit (Agilent) according to the manufacturer's instructions. For ATP6AP2>*ATP6AP2*^{L98S} and ATP6AP2>*ATP6AP2*$^{\Delta KKxx}$, mutagenesis was performed on the pattB plasmid containing the WT extended gene region of ATP6AP2 (Hermle et al., 2013) using the following oligos: -*ATP6AP2*^{L98S}-: forward: 5′-CGTTCCGGAGCC TGTCGACTCGTAGGTCTTGACG-3′, reverse: 5′-CGT TCCGGAGCCTGTCGACTCGTAGGTCTTGACG-3′; -*ATP6AP2*$^{\Delta KKxx}$-: forward: 5′-CCTTAGTTGTCCTTC TAGATGCGGGTAGAGGTC-3′, reverse: 5′-GACCTC TACCCGCATCTAGAAGGACAACTAAGG-3′.

For UAS>*ATP6AP2*^{L98S}, mutagenesis was done on the pUASg-HAattB plasmid containing the coding sequence of ATP6AP2 optimised by GeneArt (Invitrogen) with a final stop codon that impedes the expression of the HA tag, using the following primers: forward: 5′-CGTGAAGACCTACGA GTCGACCGGCAGCGGCACC-3′, reverse: 5′-GGTGCC GCTGCCGGTCGACTCGTAGGTCTTCACG-3′.

All constructs were injected into flies with the attP landing site at 86FB by Bestgene.

Clones were generated using FLP/FRT or flip-out techniques (Xu and Rubin, 1993). Clones in fat bodies were induced in embryos by 2 h heat shock at 37°C (except for clones generated with the *hs-Flp*, UAS-Dcr2;Actin> CD2>Gal4;UAS-GFP,R4-mCherry-Atg8a/TM6B stock, which form spontaneous clones without heat shock) and analyzed 4 d later in wandering third instar larvae.

Percentage of pupariation and eclosion

50–100 third instar larvae of each genotype were collected 90 ± 4 h after egg laying on standard food plates supplemented with dried yeast (2–3 h egg collections) and reared on tubes containing standard food at 25°C. The number of larvae that underwent pupariation was scored twice a day. Pupae were then left to eclose, and the number of surviving adult flies was scored. Five independent experiments were performed with genotypes WT, *ATP6AP2*$^{WT\text{-}Myc}$, *ATP6AP2*^{WT}, and *ATP6AP2*^{L98S}. *ATP6AP2*$^{\Delta KKxx}$ and *ATP6AP2*^{AxxA} were scored in three independent experiments.

Western blotting of *Drosophila* extracts

For whole larval extracts, five wandering third instar larvae per genotype were collected and washed once in PBS, ethanol 70%, and water to remove food, surface bacteria, and other contaminants. Larvae were transferred to an Eppendorf tube containing 100 µl of lysis buffer (50 mM Tris-base, 150 mM NaCl, 1 mM EDTA, 1% Triton X-100) supplemented with protease and phosphatase inhibitors cocktails (Roche) and homogenized three times with a pellet pestle for 10–15 s on ice. For fat body and brain extracts, for preparation of lysates from third instar fat bodies and larval brains, whole fat bodies from 15 larvae per genotype and 50 brains per genotype were dissected in PBS, transferred to Eppendorf tubes containing 50 µl of lysis buffer, incubated for 15 min on ice, and lysed by sonication. Lysates were cleared by centrifugation at maximum speed for 10 min, and the supernatants were transferred to clean Eppendorf tubes. Protein concentration was determined using the Pierce BCA Protein Assay kit (Thermo Scientific) according to the manufacturer's instructions. Samples (20 µg) were analyzed by SDS-PAGE followed by immunoblotting. The following antibodies were used: guinea pig anti-ATP6AP2 (Hermle et al., 2013), mouse anti–β-actin antibody (Sigma-Aldrich, A1978), mouse anti–α-tubulin (Sigma-Aldrich, T6199), rabbit anti-Ref(2)P (gift from T.E. Rusten), rabbit anti–p4E-BP (Cell Signaling, 2855) and rabbit anti-Atg8a (gift from G. Juhasz). Secondary antibodies used were anti–guinea pig, anti–rabbit, and anti–mouse Horseradish Peroxidase Conjugated (Thermo Scientific).

Staging, starvation, and refeeding of larvae

0-2 h egg collections were done at 25°C using egg collection chambers on 60-mm petri dishes containing standard food supplemented with dry yeast. 72 h after larval hatching, 50 larvae (mid third instar) were transferred to vials containing a filter paper soaked in PBS and kept at 25°C for 6 h (starvation). Subsequently, half of the starved larvae were transferred to dishes containing yeast paste and kept at 25°C for 30 min (refeeding). Fat bodies from fed, starved, and refed larvae were dissected and processed as before for Western blotting analyses.

Immunohistochemistry

Brains and fat bodies from third instar larvae were dissected in PBS, fixed for 20 min (30 min in the case of p4E-BP staining) in 4% paraformaldehyde in PBS (+0.1% Triton X-100 for brains), washed three times in PBS-T (PBS + 0.3% Triton X-100 for brains and PBS + 0.1% Triton X-100 for fat bodies), and incubated overnight at 4°C with primary antibodies diluted in PBS-T. After washing, tissues were incubated overnight at 4°C for brains and 2 h at room temperature for fat bodies with secondary antibodies (dilution 1:200) and Hoechst (0.5 µg ml^{-1}) diluted in PBS-T. Tissues were washed twice in PBS-T followed by a wash in PBS. Tissues were mounted in mounting medium (1.25% n-propyl gallate, 75% glycerol, 25% H_2O). Primary antibodies used were rabbit anti-Dpn (1:200, gift from R. Basto), rabbit anti-GFP (1:500, Antibody Platform Institut Curie), rat anti-RFP (1:200, 5F8, ChromoTek), rabbit anti-mCherry (1:100, Clontech), rat anti-ELAV (1:100, 7E8A10, Developmental Studies Hybridoma Bank), guinea-pig anti-ATP6AP2 (Hermle et al., 2013), rabbit anti-Ref(2)P (gift from T.E. Rusten), rabbit anti-Atg8a (gift from G. Juhasz) and rabbit anti–p4E-BP (2855, Cell Signaling). Secondary antibodies used were fluorescent conjugated Alexa Fluor 488, Alexa Fluor 555, Alexa Fluor 633, and Alexa Fluor 647 (Invitrogen Molecular Probes).

Bodipy and LysoTracker staining

For Bodipy labeling, dissected fat bodies were fixed for 30 min in 4% paraformaldehyde in PBS, washed in PBS, and incubated with BODIPY 493/503 (2.5 µg ml^{-1}, Molecular Probes) and Hoechst (0.5 µg ml^{-1}) diluted in PBS for 30 min. Tissues were mounted as described in the Immunohistochemistry section.

For Lysotracker labeling, dissected fat bodies were incubated with LysoTracker Green DND-26 (100 nM, Molecular Probes) and Hoechst (0.5 µg ml^{-1}) diluted in PBS for 3 min, washed in PBS, and fixed in 4% paraformaldehyde in PBS for 10 min. Fat bodies were washed three times in PBS and mounted as before.

Tissue imaging

All images were acquired on a Leica TCS SP8 equipped with a 405-nm laser line and a White Light Laser with a 63x/1.4 DIC Lambda blue PLAN APOCHROMATE objective. Images were processed with Fiji (Schindelin et al., 2012) and Adobe Photoshop.

TAG assay

Five wandering third instar larvae per genotype were collected and washed once in PBS, ethanol 70%, and water to remove food, surface bacteria, and other contaminants. Larvae were transferred to an Eppendorf tube containing 200 µl of PBS-T (PBS+0.05% Triton X-100 supplemented with protease inhibitors, Roche) and homogenized three times with a pellet pestle for 10–15 s on ice. Homogenates were subsequently sonicated. 10 µl of homogenized sample was collected for protein determination, and the rest of the homogenate was incubated at 70°C for 10 min. 20 µl of the sample and also standards were added to tubes containing 20 µl PBS-T + PI (baseline) or 20 µl TAG reagent (Sigma T2449) and incubated for 30 min at 37°C. Samples were centrifuged at maximum speed for 3 min, and 7.5 µl of each sample supernatant was transferred to clear-bottom 96-well plate containing 22.5 µl of PBS-T. 100 µl of free glycerol reagent (Sigma F6428) was added, and the mix was incubated at 37°C for 5 min. Absorbance was measured in a spectrophotometer at 560 nm. TAG concentration for each sample was determined by subtracting the absorbance for the free glycerol in the untreated samples (baseline) from the total glycerol concentration in samples that were incubated in triglyceride reagent. As a final step, samples were normalized to the corresponding protein concentrations.

Electron microscopy

Drosophila prepupal wings (5.5 h APF) were dissected and directly fixed with 4% paraformaldehyde and 1% glutaraldehyde in 0.1 M PB overnight at 4°C. After fixation, wings were washed in PB, treated with 2% OsO_4, stained with uranyl acetate, dehydrated, and embedded in epoxy resin (Durcupan ACM, Fluka, Sigma-Aldrich). 40 nm ultrathin cross sections in the proximal-distal axis were cut using an ultramicrotome (Leica UC6) and analyzed with a Zeiss LEO 906 transmission electron microscope operated at 80 kV and equipped with a 2K CCD camera (Tröndle).

Online supplemental material

Fig. S1 shows the glycosylation diagnostics for patients P2 and P3. Fig. S2 shows the glycosylation diagnostics of the patient with the exon-skipping mutation (P4) and the normal interaction of ATP6AP2 Δexon4 with ATP6AP1. Fig. S3 shows the characterization of *ATP6AP2* cKO mice. Fig. S4 shows the subcellular localization of the different ATP6AP2 constructs in HeLa cells. Fig. S5 shows the interaction between ATP6AP2 and ATP6AP1 using the Y2H method. Table S1 shows the *Drosophila* genotypes used in this study.

ACKNOWLEDGMENTS

We thank Luisa Diogo and Emilia Faria for clinical data on the patient with the p.L98S mutation. We are grateful to Gabor Juhasz, Aurelio Teleman, Frank Perez, Renata Basto, and Tor Erik Rusten and the Developmental Studies Hybridoma Bank for pro-

viding antibodies. We thank Gabor Juhasz, Helmut Krämer, Floris Bosveld, the Bloomington stock center and Vienna Drosophila RNAi Center for providing flies. We also thank Yihong Ye for providing the p97 plasmids, Olga Korvatska for the ATP6AP2 Δ4 plasmid, Reid Gilmore for the *STT3* KO cells, and Geneviève Nguyen/Michael Bader for the *ATP6AP2 KO* mice. We are grateful to Eva Gleixner for preparing fly samples for the electron microscopy experiments. We thank the Imagine Microscopy platform for assistance with microscopy. We are grateful to Jaak Jaeken, Vincent Cantagrel, Floris Bosveld, Massimo D'Agostino, Fred Bernard, Tom Stevens, and Ari Helenius for critically reading the manuscript.

This work has been supported by the ATIP-Avenir program, the Fondation Bettencourt-Schueller (Liliane Bettencourt Chair of Developmental Biology), state funding by the Agence Nationale de la Recherche under the Investissements d'avenir program (grant no. ANR-10-IAHU-01), and a NEPHROFLY grant (no. ANR-14-ACHN-0013) to M. Simons. This research was also supported by an Agence Nationale de la Recherche grant (no. SOLV-CDG) to F. Foulquier and a NUTRISENSPIK grant (no. ANR-16-CE14-0029) to G. Panasyuk. G. Matthijs received support from the European Union's Horizon 2020 research and innovation program under the ERA-NET Cofund action (grant no. 643578); the research was funded by the Research Foundation (FWO, Flanders; EURO-CDG-2 project). F. Folquier, G. Matthijs, and R. Péanne belong to LIA GLYCOLAB4CDG (International Associated Laboratory), funded by CNRS (France) and FWO. R. Péanne is a postdoctoral researcher (Pegasus Marie Curie Fellow) of the FWO. T.D. Bird and W.H. Raskind receive support from the National Institutes of Health (grant no. R01NS069719) and the Department of Veterans Affairs. This work is supported by National Funds through the Fundação para a Ciência e a Tecnologia (Portuguese national funding agency for science, research and technology) in the frameworks of the UID/Multi/00215/2013 project-Unit for Multidisciplinary Research in Biomedicine–UMIB/ICBAS/UP.

The authors declare no competing financial interests.

Author contributions: T. Marquardt, G. Matthijs, E.M. Maier, S. Nobre, P. Garcia, D. Quelhas, P. Freisinger, T.D. Bird, W.H. Raskind, and J.H. Park recruited patients and gathered detailed clinical information and data for the study. J. Reunert, T. Marquardt, R. Péanne, D. Rymen, E. Souche, and G. Matthijs identified mutations in the human *ATP6AP2* gene. S. Duvet, F. Foulquier, G. Matthijs, R. Péanne, D. Rymen, J. Reunert, J.H. Park, T. Marquardt, and Y. Wada performed glycosylation studies. G. Panasyuk designed, performed, and analyzed the mouse experiments. M. Cannata Serio designed, performed, and analyzed the experiments in patient fibroblasts and HEK293 cells. S. Jäger, N.J. Krogan, and M. Schwake. performed proteomics. M.A. Rujano and V. Hauser designed, performed, and analyzed the *Drosophila* experiments. M.C. Guida generated *Drosophila* tools. O. Kretz performed TEM on *Drosophila* samples. M. Simons, T. Marquardt, and G. Matthijs conceived of and supervised the project and analyzed the data. M. Simons wrote the paper with help from M. A. Rujano and M. Cannata Serio. All authors critically reviewed the paper.

Submitted: 10 March 2017

Revised: 1 August 2017

Accepted: 22 September 2017

REFERENCES

al-Awqati, Q., J. Barasch, and D. Landry. 1992. Chloride channels of intracellular organelles and their potential role in cystic fibrosis. *J. Exp. Biol.* 172:245–266.

Baiceanu, A., P. Mesdom, M. Lagouge, and F. Foufelle. 2016. Endoplasmic reticulum proteostasis in hepatic steatosis. *Nat. Rev. Endocrinol.* 12:710–722. https://doi.org/10.1038/nrendo.2016.124

Bartel, P., C.T. Chien, R. Sternglanz, and S. Fields. 1993. Elimination of false positives that arise in using the two-hybrid system. *Biotechniques.* 14:920–924.

Blanz, J., F. Zunke, S. Markmann, M. Damme, T. Braulke, P. Saftig, and M. Schwake. 2015. Mannose 6-phosphate-independent Lysosomal Sorting of LIMP-2. *Traffic.* 16:1127–1136. https://doi.org/10.1111/tra.12313

Bowman, S.K., V. Rolland, J. Betschinger, K.A. Kinsey, G. Emery, and J.A. Knoblich. 2008. The tumor suppressors Brat and Numb regulate transit-amplifying neuroblast lineages in Drosophila. *Dev. Cell.* 14:535–546. https://doi.org/10.1016/j.devcel.2008.03.004

Buechling, T., K. Bartscherer, B. Ohkawara, V. Chaudhary, K. Spirohn, C. Niehrs, and M. Boutros. 2010. Wnt/Frizzled signaling requires dPRR, the Drosophila homolog of the prorenin receptor. *Curr. Biol.* 20:1263–1268. https://doi.org/10.1016/j.cub.2010.05.028

Cherepanova, N.A., and R. Gilmore. 2016. Mammalian cells lacking either the cotranslational or posttranslocational oligosaccharyltransferase complex display substrate-dependent defects in asparagine linked glycosylation. *Sci. Rep.* 6:20946. https://doi.org/10.1038/srep20946

Cherepanova, N., S. Shrimal, and R. Gilmore. 2016. N-linked glycosylation and homeostasis of the endoplasmic reticulum. *Curr. Opin. Cell Biol.* 41:57–65. https://doi.org/10.1016/j.ceb.2016.03.021

Cousin, C., D. Bracquart, A. Contrepas, P. Corvol, L. Muller, and G. Nguyen. 2009. Soluble form of the (pro)renin receptor generated by intracellular cleavage by furin is secreted in plasma. *Hypertension.* 53:1077–1082. https://doi.org/10.1161/HYPERTENSIONAHA.108.127258

Cruciat, C.M., B. Ohkawara, S.P. Acebron, E. Karaulanov, C. Reinhard, D. Ingelfinger, M. Boutros, and C. Niehrs. 2010. Requirement of prorenin receptor and vacuolar H+-ATPase-mediated acidification for Wnt signaling. *Science.* 327:459–463. https://doi.org/10.1126/science.1179802

Dubos, A., A. Castells-Nobau, H. Meziane, M.A. Oortveld, X. Houbaert, G. Iacono, C. Martin, C. Mittelhaeuser, V. Lalanne, J.M. Kramer, et al. 2015. Conditional depletion of intellectual disability and Parkinsonism candidate gene ATP6AP2 in fly and mouse induces cognitive impairment and neurodegeneration. *Hum. Mol. Genet.* 24:6736–6755. https://doi.org/10.1093/hmg/ddv380

Egger, B., K.S. Gold, and A.H. Brand. 2010. Notch regulates the switch from symmetric to asymmetric neural stem cell division in the Drosophila optic lobe. *Development.* 137:2981–2987. https://doi.org/10.1242/dev.051250

Faid, V., F. Chirat, N. Seta, F. Foulquier, and W. Morelle. 2007. A rapid mass spectrometric strategy for the characterization of N- and O-glycan chains in the diagnosis of defects in glycan biosynthesis. *Proteomics.* 7:1800–1813. https://doi.org/10.1002/pmic.200600977

Forgac, M. 2007. Vacuolar ATPases: rotary proton pumps in physiology and pathophysiology. *Nat. Rev. Mol. Cell Biol.* 8:917–929. https://doi.org/10.1038/nrm2272

Freeze, H.H., J.X. Chong, M.J. Bamshad, and B.G. Ng. 2014. Solving glycosylation disorders: fundamental approaches reveal complicated pathways. *Am. J. Hum. Genet.* 94:161–175. https://doi.org/10.1016/j.ajhg.2013.10.024

Hara, T., K. Nakamura, M. Matsui, A. Yamamoto, Y. Nakahara, R. Suzuki-Migishima, M. Yokoyama, K. Mishima, I. Saito, H. Okano, and N. Mizushima. 2006. Suppression of basal autophagy in neural cells causes neurodegenerative disease in mice. *Nature.* 441:885–889. https://doi.org/10.1038/nature04724

Hennet, T., and J. Cabalzar. 2015. Congenital disorders of glycosylation: a concise chart of glycocalyx dysfunction. *Trends Biochem. Sci.* 40:377–384. https://doi.org/10.1016/j.tibs.2015.03.002

Hermle, T., D. Saltukoglu, J. Grünewald, G. Walz, and M. Simons. 2010. Regulation of Frizzled-dependent planar polarity signaling by a V-ATPase subunit. *Curr. Biol.* 20:1269–1276. https://doi.org/10.1016/j.cub.2010.05.057

Hermle, T., M.C. Guida, S. Beck, S. Helmstädter, and M. Simons. 2013. Drosophila ATP6AP2/VhaPRR functions both as a novel planar cell polarity core protein and a regulator of endosomal trafficking. *EMBO J.* 32:245–259. https://doi.org/10.1038/emboj.2012.323

Jäger, S., P. Cimermancic, N. Gulbahce, J.R. Johnson, K.E. McGovern, S.C. Clarke, M. Shales, G. Mercenne, L. Pache, K. Li, et al. 2011. Global landscape of HIV-human protein complexes. *Nature.* 481:365–370.

Jansen, E.J., S. Timal, M. Ryan, A. Ashikov, M. van Scherpenzeel, L.A. Graham, H. Mandel, A. Hoischen, T.C. Iancu, K. Raymond, et al. 2016a. ATP6AP1 deficiency causes an immunodeficiency with hepatopathy, cognitive impairment and abnormal protein glycosylation. *Nat. Commun.* 7:11600. https://doi.org/10.1038/ncomms11600

Jansen, J.C., S. Cirak, M. van Scherpenzeel, S. Timal, J. Reunert, S. Rust, B. Pérez, D.Vicogne, P. Krawitz, Y. Wada, et al. 2016b. CCDC115 Deficiency Causes a Disorder of Golgi Homeostasis with Abnormal Protein Glycosylation. *Am. J. Hum. Genet.* 98:310–321. https://doi.org/10.1016/j.ajhg.2015.12.010

Jansen, J.C., S. Timal, M. van Scherpenzeel, H. Michelakakis, D. Vicogne, A. Ashikov, M. Moraitou, A. Hoischen, K. Huijben, G. Steenbergen, et al. 2016c. TMEM199 Deficiency Is a Disorder of Golgi Homeostasis Characterized by Elevated Aminotransferases, Alkaline Phosphatase, and Cholesterol and Abnormal Glycosylation. *Am. J. Hum. Genet.* 98:322–330. https://doi.org/10.1016/j.ajhg.2015.12.011

Kinouchi, K., A. Ichihara, M. Sano, G.H. Sun-Wada, Y. Wada, A. Kurauchi-Mito, K. Bokuda, T. Narita, Y. Oshima, M. Sakoda, et al. 2010. The (pro) renin receptor/ATP6AP2 is essential for vacuolar H+-ATPase assembly in murine cardiomyocytes. *Circ. Res.* 107:30–34. https://doi.org/10.1161/CIRCRESAHA.110.224667

Kinouchi, K., A. Ichihara, M. Sano, G.H. Sun-Wada, Y. Wada, H. Ochi, T. Fukuda, K. Bokuda, H. Kurosawa, N. Yoshida, et al. 2013. The role of individual domains and the significance of shedding of ATP6AP2/(pro)renin receptor in vacuolar H(+)-ATPase biogenesis. *PLoS One.* 8:e78603. https://doi.org/10.1371/journal.pone.0078603

Kissing, S., S. Rudnik, M. Damme, R. Lullmann-Rauch, A. Ichihara, U. Kornak, E.L. Eskelinen, S. Jabs, J. Heeren, J.K. De Brabander, et al. 2017. Disruption of the vacuolar-type H+-ATPase complex in liver causes MTORC1-independent accumulation of autophagic vacuoles and lysosomes. *Autophagy.* 13:670–685. https://doi.org/10.1080/15548627.2017.1280216

Kornak, U., E. Reynders, A. Dimopoulou, J. van Reeuwijk, B. Fischer, A. Rajab, B. Budde, P. Nürnberg, F. Foulquier, D. Lefeber, et al. ARCL Debré-type Study Group. 2008. Impaired glycosylation and cutis laxa caused by mutations in the vesicular H+-ATPase subunit ATP6V0A2. *Nat. Genet.* 40:32–34. https://doi.org/10.1038/ng.2007.45

Kortüm, F., V. Caputo, C.K. Bauer, L. Stella, A. Ciolfi, M. Alawi, G. Bocchinfuso, E. Flex, S. Paolacci, M.L. Dentici, et al. 2015. Mutations in KCNH1 and ATP6V1B2 cause Zimmermann-Laband syndrome. *Nat. Genet.* 47:661–667. https://doi.org/10.1038/ng.3282

Korvatska, O., N.S. Strand, J.D. Berndt, T. Strovas, D.H. Chen, J.B. Leverenz, K. Kiianitsa, I.F. Mata, E. Karakoc, J.L. Greenup, et al. 2013. Altered splicing of ATP6AP2 causes X-linked parkinsonism with spasticity (XPDS). *Hum. Mol. Genet.* 22:3259–3268. https://doi.org/10.1093/hmg/ddt180

Lange, C., S. Prenninger, P. Knuckles, V. Taylor, M. Levin, and F. Calegari. 2011. The H(+) vacuolar ATPase maintains neural stem cells in the developing mouse cortex. *Stem Cells Dev.* 20:843–850. https://doi.org/10.1089/scd.2010.0484

Malkus, P., L.A. Graham, T.H. Stevens, and R. Schekman. 2004. Role of Vma21p in assembly and transport of the yeast vacuolar ATPase. *Mol. Biol. Cell.* 15:5075–5091. https://doi.org/10.1091/mbc.E04-06-0514

Mariño, G., F. Madeo, and G. Kroemer. 2011. Autophagy for tissue homeostasis and neuroprotection. *Curr. Opin. Cell Biol.* 23:198–206. https://doi.org/10.1016/j.ceb.2010.10.001

Mauvezin, C., P. Nagy, G. Juhász, and T.P. Neufeld. 2015. Autophagosome-lysosome fusion is independent of V-ATPase-mediated acidification. *Nat. Commun.* 6:7007. https://doi.org/10.1038/ncomms8007

Nakagawa, T., C. Suzuki-Nakagawa, A. Watanabe, E. Asami, M. Matsumoto, M. Nakano, A. Ebihara, M.N. Uddin, and F. Suzuki. 2017. Site-1 protease is required for the generation of soluble (pro)renin receptor. *J. Biochem.* 161:369–379. https://doi.org/10.1093/jb/mvw080

Nemazanyy, I., B. Blaauw, C. Paolini, C. Caillaud, F. Protasi, A. Mueller, T. Proikas-Cezanne, R.C. Russell, K.L. Guan, I. Nishino, et al. 2013. Defects of Vps15 in skeletal muscles lead to autophagic vacuolar myopathy and lysosomal disease. *EMBO Mol. Med.* 5:870–890. https://doi.org/10.1002/emmm.201202057

Nguyen, G., F. Delarue, C. Burcklé, L. Bouzhir, T. Giller, and J.D. Sraer. 2002. Pivotal role of the renin/prorenin receptor in angiotensin II production and cellular responses to renin. *J. Clin. Invest.* 109:1417–1427. https://doi.org/10.1172/JCI0214276

Nilsson, T., M. Jackson, and P.A. Peterson. 1989. Short cytoplasmic sequences serve as retention signals for transmembrane proteins in the endoplasmic reticulum. *Cell.* 58:707–718. https://doi.org/10.1016/0092-8674(89)90105-0

Noda, T., and Y. Ohsumi. 1998. Tor, a phosphatidylinositol kinase homologue, controls autophagy in yeast. *J. Biol. Chem.* 273:3963–3966. https://doi.org/10.1074/jbc.273.7.3963

Pengo, N., M. Scolari, L. Oliva, E. Milan, F. Mainoldi, A. Raimondi, C. Fagioli, A. Merlini, E. Mariani, E. Pasqualetto, et al. 2013. Plasma cells require autophagy for sustainable immunoglobulin production. *Nat. Immunol.* 14:298–305. https://doi.org/10.1038/ni.2524

Pulipparacharuvil, S., M.A. Akbar, S. Ray, E.A. Sevrioukov, A.S. Haberman, J. Rohrer, and H. Krämer. 2005. Drosophila Vps16A is required for trafficking to lysosomes and biogenesis of pigment granules. *J. Cell Sci.* 118:3663–3673. https://doi.org/10.1242/jcs.02502

Ramachandran, N., I. Munteanu, P. Wang, A. Ruggieri, J.J. Rilstone, N. Israelian, T. Naranian, P. Paroutis, R. Guo, Z.P. Ren, et al. 2013. VMA21 deficiency prevents vacuolar ATPase assembly and causes autophagic vacuolar myopathy. *Acta Neuropathol.* 125:439–457. https://doi.org/10.1007/s00401-012-1073-6

Ramser, J., F.E. Abidi, C.A. Burckle, C. Lenski, H. Toriello, G. Wen, H.A. Lubs, S. Engert, R.E. Stevenson, A. Meindl, et al. 2005. A unique exonic splice enhancer mutation in a family with X-linked mental retardation and epilepsy points to a novel role of the renin receptor. *Hum. Mol. Genet.* 14:1019–1027. https://doi.org/10.1093/hmg/ddi094

Riediger, F., I. Quack, F. Qadri, B. Hartleben, J.K. Park, S.A. Potthoff, D. Sohn, G. Sihn, A. Rousselle, V. Fokuhl, et al. 2011. Prorenin receptor is essential for podocyte autophagy and survival. *J. Am. Soc. Nephrol.* 22:2193–2202. https://doi.org/10.1681/ASN.2011020200

Ryan, M., L.A. Graham, and T.H. Stevens. 2008. Voa1p functions in V-ATPase assembly in the yeast endoplasmic reticulum. *Mol. Biol. Cell.* 19:5131–5142. https://doi.org/10.1091/mbc.E08-06-0629

Sato, T., Y. Sako, M. Sho, M. Momohara, M.A. Suico, T. Shuto, H. Nishitoh, T. Okiyoneda, K. Kokame, M. Kaneko, et al. 2012. STT3B-dependent posttranslational N-glycosylation as a surveillance system for secretory protein. *Mol. Cell.* 47:99–110. https://doi.org/10.1016/j.molcel.2012.04.015

Schafer, S.T., J. Han, M. Pena, O. von Bohlen Und Halbach, J. Peters, and F.H. Gage. 2015. The Wnt adaptor protein ATP6AP2 regulates multiple stages of adult hippocampal neurogenesis. *J. Neurosci.* 35:4983–4998. https://doi.org/10.1523/JNEUROSCI.4130-14.2015

Schefe, J.H., M. Menk, J. Reinemund, K. Effertz, R.M. Hobbs, P.P. Pandolfi, P. Ruiz, T. Unger, and H. Funke-Kaiser. 2006. A novel signal transduction cascade involving direct physical interaction of the renin/prorenin receptor with the transcription factor promyelocytic zinc finger protein. *Circ. Res.* 99:1355–1366. https://doi.org/10.1161/01.RES.0000251700.00994.0d

Schindelin, J., I. Arganda-Carreras, E. Frise, V. Kaynig, M. Longair, T. Pietzsch, S. Preibisch, C. Rueden, S. Saalfeld, B. Schmid, et al. 2012. Fiji: an open-source platform for biological-image analysis. *Nat. Methods.* 9:676–682. https://doi.org/10.1038/nmeth.2019

Scott, K., T. Gadomski, T. Kozicz, and E. Morava. 2014. Congenital disorders of glycosylation: new defects and still counting. *J. Inherit. Metab. Dis.* 37:609–617. https://doi.org/10.1007/s10545-014-9720-9

Sihn, G., C. Burckle, A. Rousselle, T. Reimer, and M. Bader. 2013. (Pro)renin receptor: subcellular localizations and functions. *Front. Biosci. (Elite Ed.).* 5:500–508. https://doi.org/10.2741/E631

Singh, R., S. Kaushik, Y. Wang, Y. Xiang, I. Novak, M. Komatsu, K. Tanaka, A.M. Cuervo, and M.J. Czaja. 2009. Autophagy regulates lipid metabolism. *Nature.* 458:1131–1135. https://doi.org/10.1038/nature07976

Sowa, M.E., E.J. Bennett, S.P. Gygi, and J.W. Harper. 2009. Defining the human deubiquitinating enzyme interaction landscape. *Cell.* 138:389–403. https://doi.org/10.1016/j.cell.2009.04.042

Trepiccione, F., S.D. Gerber, F. Grahammer, K.I. López-Cayuqueo, V. Baudrie, T.G. Păunescu, D.E. Capen, N. Picard, R.T. Alexander, T.B. Huber, et al. 2016. Renal Atp6ap2/(Pro)renin Receptor Is Required for Normal Vacuolar H+-ATPase Function but Not for the Renin-Angiotensin System. *J. Am. Soc. Nephrol.* 27:3320–3330. https://doi.org/10.1681/ASN.2015080915

Ugur, B., K. Chen, and H.J. Bellen. 2016. Drosophila tools and assays for the study of human diseases. *Dis. Model. Mech.* 9:235–244. https://doi.org/10.1242/dmm.023762

Vaccari, T., S. Duchi, K. Cortese, C. Tacchetti, and D. Bilder. 2010. The vacuolar ATPase is required for physiological as well as pathological activation of the Notch receptor. *Development*. 137:1825–1832. https://doi.org/10.1242/dev.045484

Van Damme, T., T. Gardeitchik, M. Mohamed, S. Guerrero-Castillo, P. Freisinger, B. Guillemyn, A. Kariminejad, D. Dalloyaux, S. van Kraaij, D.J. Lefeber, et al. 2017. Mutations in ATP6V1E1 or ATP6V1A Cause Autosomal-Recessive Cutis Laxa. *Am. J. Hum. Genet.* 100:216–227. https://doi.org/10.1016/j.ajhg.2016.12.010

Vojtek, A.B., and S.M. Hollenberg. 1995. Ras-Raf interaction: two-hybrid analysis. *Methods Enzymol.* 255:331–342. https://doi.org/10.1016/S0076-6879(95)55036-4

Wang, W., W. Liu, Y. Wang, L. Zhou, X. Tang, and H. Luo. 2011. Notch signaling regulates neuroepithelial stem cell maintenance and neuroblast formation in Drosophila optic lobe development. *Dev. Biol.* 350:414–428. https://doi.org/10.1016/j.ydbio.2010.12.002

Xu, T., and G.M. Rubin. 1993. Analysis of genetic mosaics in developing and adult Drosophila tissues. *Development*. 117:1223–1237.

Yan, Y., N. Denef, and T. Schüpbach. 2009. The vacuolar proton pump, V-ATPase, is required for notch signaling and endosomal trafficking in Drosophila. *Dev. Cell.* 17:387–402. https://doi.org/10.1016/j.devcel.2009.07.001

Yasugi, T., D. Umetsu, S. Murakami, M. Sato, and T. Tabata. 2008. Drosophila optic lobe neuroblasts triggered by a wave of proneural gene expression that is negatively regulated by JAK/STAT. *Development*. 135:1471–1480. https://doi.org/10.1242/dev.019117

Ye, J., G. Coulouris, I. Zaretskaya, I. Cutcutache, S. Rozen, and T.L. Madden. 2012. Primer-BLAST: a tool to design target-specific primers for polymerase chain reaction. *BMC Bioinformatics.* 13:134. https://doi.org/10.1186/1471-2105-13-134

Ye, Y., H.H. Meyer, and T.A. Rapoport. 2001. The AAA ATPase Cdc48/p97 and its partners transport proteins from the ER into the cytosol. *Nature.* 414:652–656. https://doi.org/10.1038/414652a

Zoncu, R., L. Bar-Peled, A. Efeyan, S. Wang, Y. Sancak, and D.M. Sabatini. 2011. mTORC1 senses lysosomal amino acids through an inside-out mechanism that requires the vacuolar H(+)-ATPase. *Science.* 334:678–683. https://doi.org/10.1126/science.1207056

Zühlsdorf, A., J.H. Park, Y. Wada, S. Rust, J. Reunert, I. DuChesne, M. Grüneberg, and T. Marquardt. 2015. Transferrin variants: pitfalls in the diagnostics of Congenital disorders of glycosylation. *Clin. Biochem.* 48:11–13. https://doi.org/10.1016/j.clinbiochem.2014.09.022

SUPPLEMENTAL MATERIAL

Rujano et al., https://doi.org/10.1084/jem.20170453

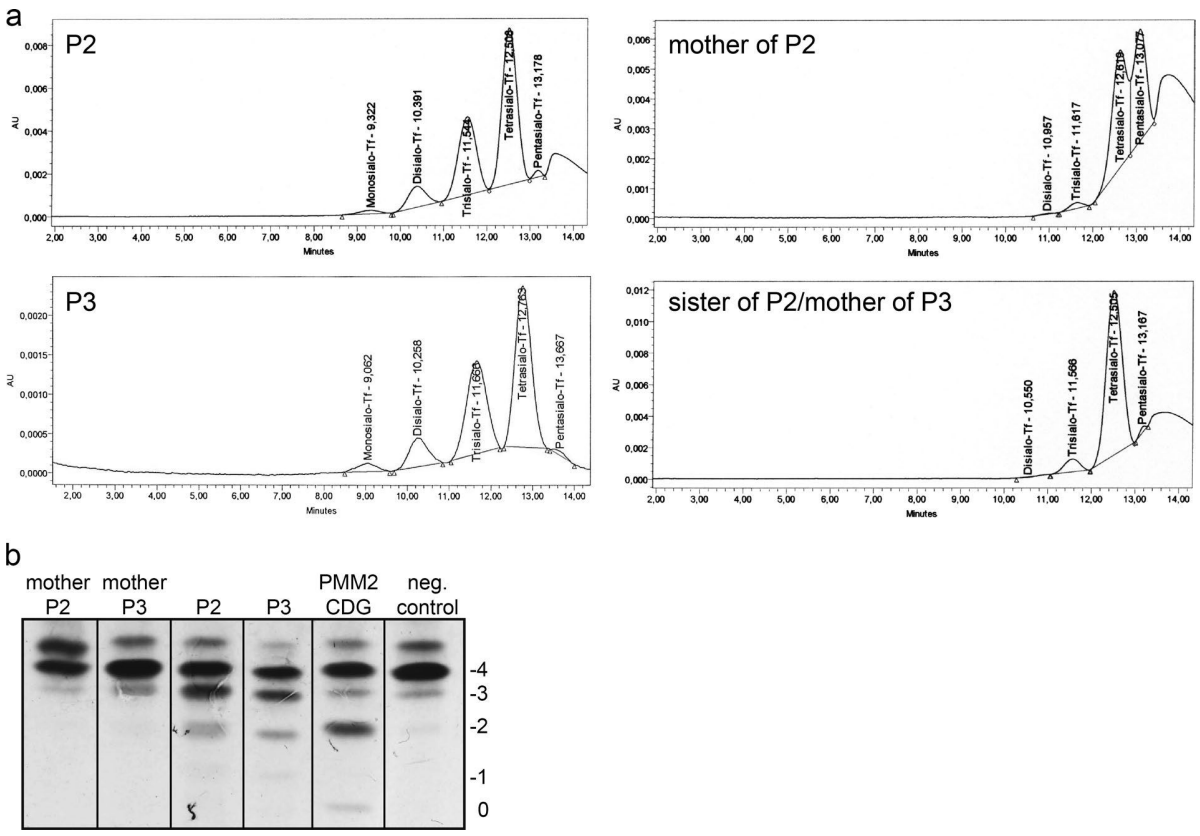

Figure S1. **Glycosylation diagnostics for patient P2 and P3 with missense mutations.** (a) HPLC of serum transferrin in a sample from P2 revealed elevated mono- (1.7%), di- (10.0%), and trisialo-transferrin (34.9%), whereas tetrasialo-transferrin was found to be reduced (53.3%). P3 shows a similar dysglycosylation pattern with elevated mono- (3.14%), di- (10.27%), and trisialo-transferrin (35.41%) as well as diminished tetrasialo-transferrin (50.28%). The samples of both unaffected relatives show a grossly normal transferrin glycosylation with a slight increase of tri- and pentasialo-transferrin, respectively (b). HPLC reference ranges are as followed: asialo-transferrin 0%, monosialo-transferrin 0%, disialo-transferrin 0.38–1.82%, trisialo-transferrin 1.16–6.36%, tetrasialo-transferrin 85.7–94.0%, and pentasialo-transferrin 2.6–10.2%. (b) Isoelectric focusing of serum transferrin samples from family F2. Analysis of samples from P2 and P3 revealed a type II congenital disorder of glycosylation (CDG) pattern with increased tri- (-3), di- (-2), and monosialo-transferrin (-1), whereas tetrasialo-transferrin is diminished. Serum samples of P2's mother (mother P2) and sister (sister P2/mother P3) show grossly normal transferrin glycosylation except for a slightly increase in trisialo-transferrin in the sister's sample as well as an increase of pentasialo-transferrin in the mother's sample. AU, arbitrary units; neg., negative.

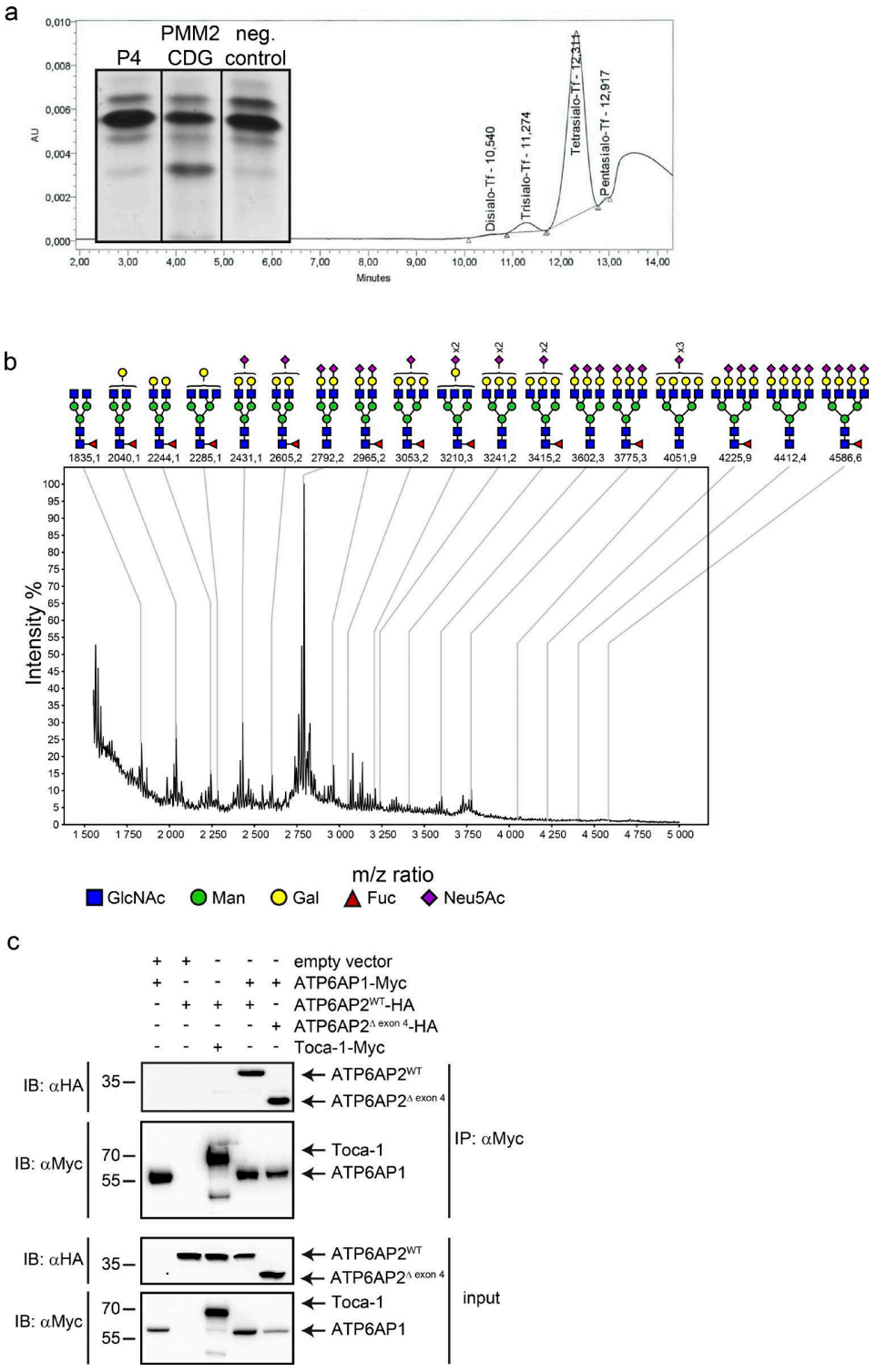

Figure S2. **Characteristics of a patient with exon-skipping mutation (P4).** (a) Isoelectric focusing (IEF) and HPLC of serum transferrin samples from P4 revealed a normal glycosylation pattern. (b) Representative MALDI-TOF MS spectra of permethylated N-glycans derived from the serum of patient P4 (Korvatska et al., 2013). P4 N-glycoproteins show only a very mild undersialylation compared with the L98S patient. (c) CoIP in HEK293T cells using the indicated constructs. Proteins were immunoprecipitated with anti-Myc antibody and cell lysates were subjected to immunoblotting with anti-HA and anti-Myc antibodies. Data in (c) are representative of two independent experiments. AU, arbitrary units; neg., negative. Molecular mass is indicated in kilodaltons.

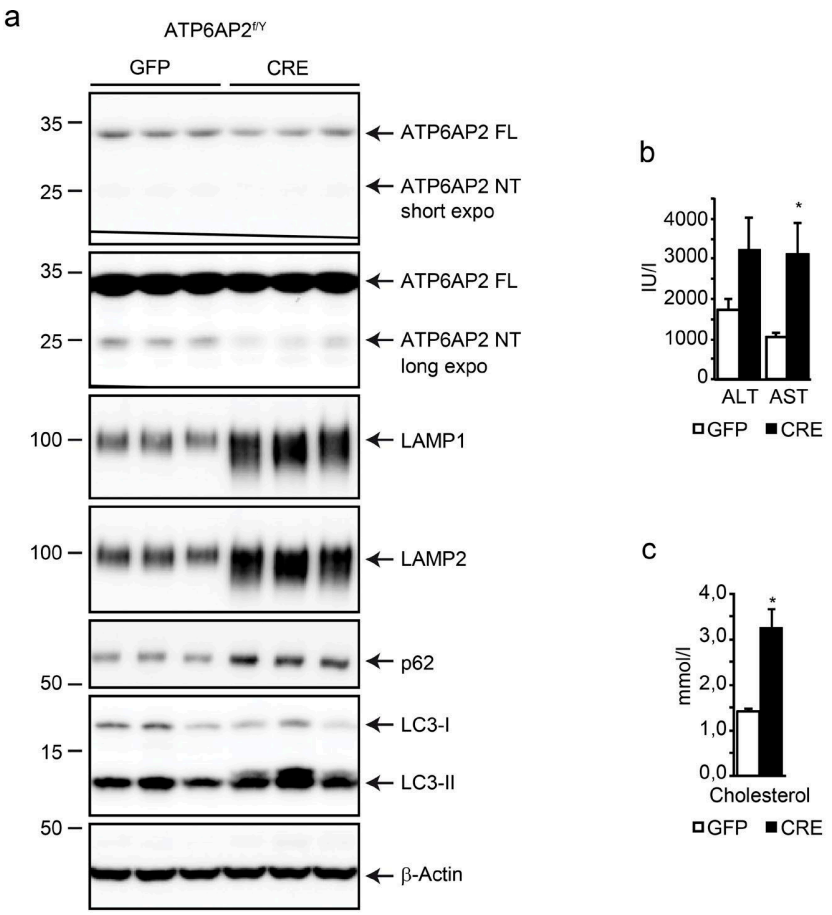

d

mass m/z																	
1578.7		1660.7		1834.7		2039.7		2256.6		2460.6		2606.8		2634.5		2851	
GFP	CRE	GFP	CRE	GFP	CRE	GFP	CRE	GFP	CRE	GFP	CRE	GFP	CRE	GFP	CRE	GFP	CRE
3,30	0,00	0	30,9	10,35	22,7	11,8	24,9	7	40,8	14,7	32,2	16,9	28	13,3	25,6	100	100
3,50	7,50	0	0	9,12	18,9	12,6	25	6,9	12,3	14,9	22,7	18,3	0	15,1	19,3	100	100
0,00	24,4	0	53,9	18,2	42	22,7	43,1	8,7	75,5	18,3	36,5	0	0	16,4	21,3	100	100
6,60	0,00	0	25,7	10,2	21	15,4	21,5	9,2	33	15,7	28,8	0	0	13,6	17,8	100	100
6,80	20,1	0	54,4	11,6	24,6	15,9	30,2	10,9	58	20,4	28,6	0	0	13,4	16,3	100	100
0,00		0		0		5,2		4,9		9,9		0		9,9		100	
7,90		0		17,2		18,7		12,3		22,1		13		13,3		100	

Figure S3. **Characterization of ATP6AP2 conditional knockout (cKO) mice.** (a) Immunoblot analysis of liver tissue extracts with indicated antibodies. Male mice carrying a floxed allele of the X-linked *ATP6AP2* mice were transduced with adeno-GFP or adeno-CRE viral vectors and tissue collected 10 d after injection in a random-fed state. The protein bands on the respective immunoblot panels are indicated by arrows. β-Actin served as a loading control. Molecular mass is indicated in kilodaltons. (b) Plasmatic ALT and AST. (c) Total serum cholesterol levels. Samples are derived from random fed male mice treated as in a. Data are mean ± SEM of six to eight independent experiments. Significance was determined by a two-tailed unpaired Student's *t* test. *, $P < 0.05$. (d) Permethylation and MALDI-TOF MS analysis of *N*-glycans from controls (GFP, $n = 7$) and *ATP6AP2* cKO mice (CRE, $n = 5$) were performed as described in Materials and methods. Relative intensities of significantly altered *N*-glycan structures (mass m/z: 1660, 1835, 2040, 2256, 2460) were determined taking into account peak 2851(m/z) as 100%. Red boxes indicate underglycosylated side chains with the corresponding values in gray for adeno-CRE.

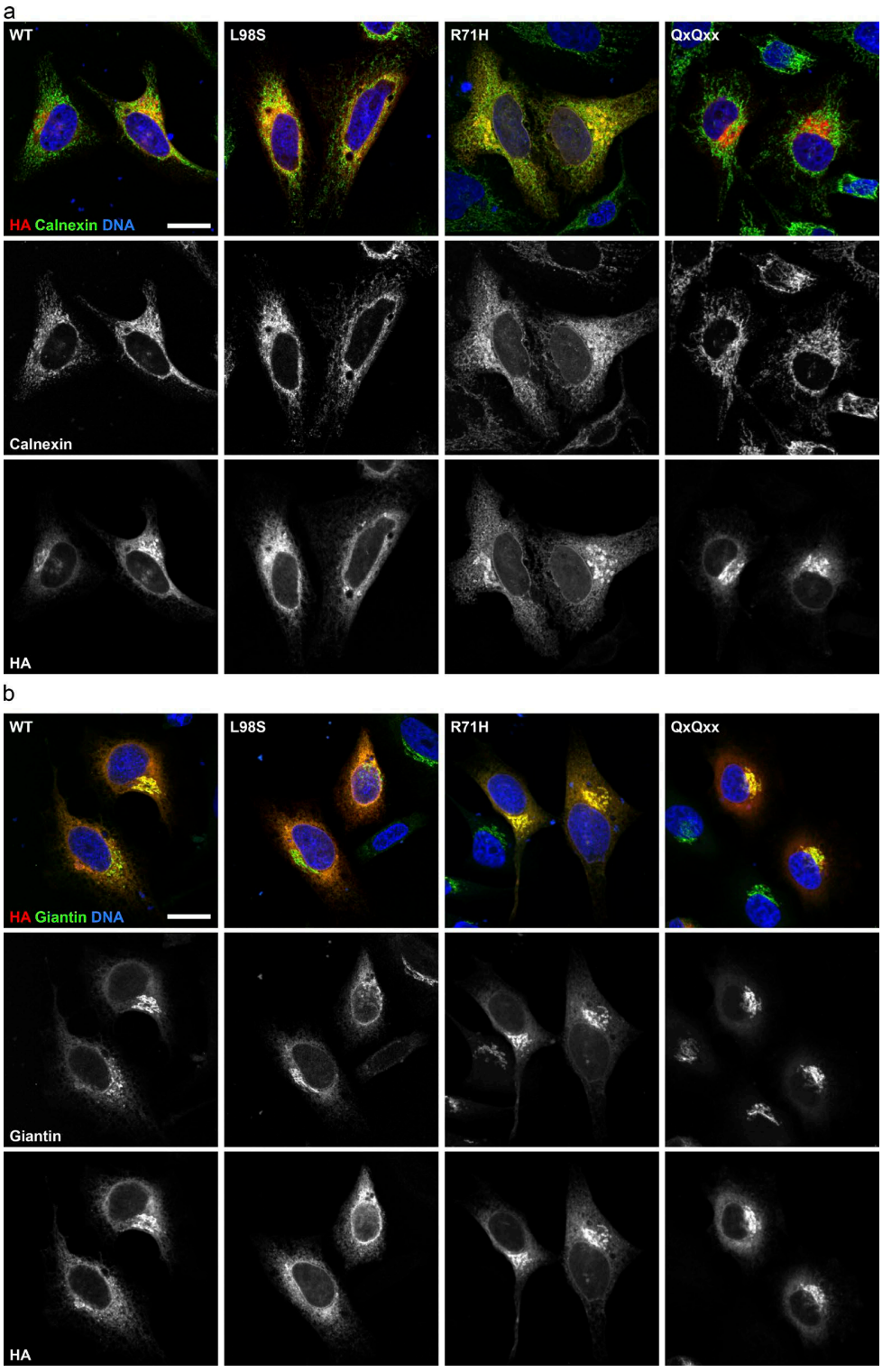

Figure S4. **Localization studies of ATP6AP2 constructs in HeLa cells.** (a) Colocalization studies of ATP6AP2^{WT}, ATP6AP2^{L98S}, ATP6AP2^{R71H}, and ATP6AP2^{QxQxx} in overexpression. ATP6AP2 constructs are stained with anti-HA antibody (red), ER with anti-Calnexin (green), and DNA stained with Hoechst (blue). (b) Colocalization studies with ATP6AP2 constructs stained with anti-HA antibody (red), Golgi with anti-Giantin (green), and DNA stained with Hoechst (blue). Images in a and b are representative of two independent experiments. Bars, 20 µm.

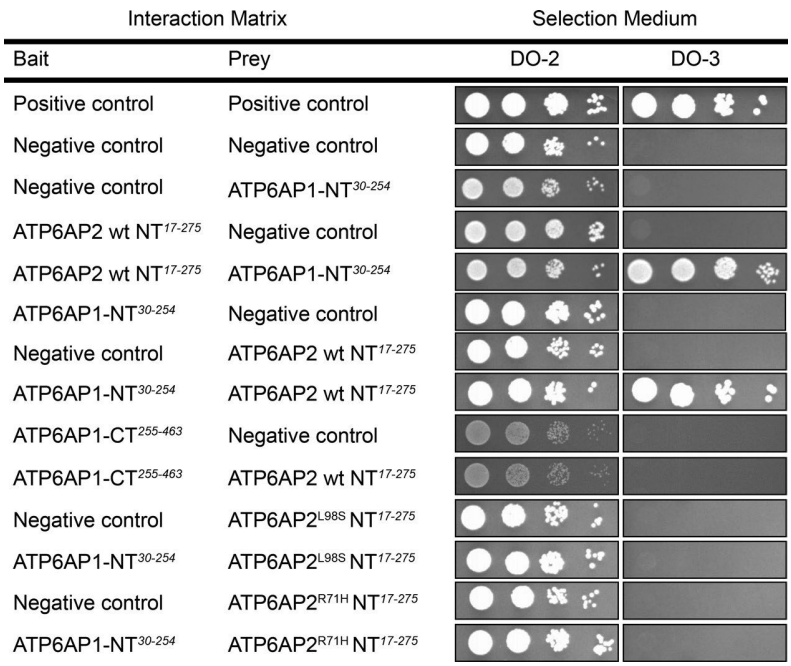

Figure S5. **The interaction of ATP6AP2 with ATP6AP1 is lost in the missense mutants.** Direct 1-by-1 Y2H assay for protein–protein interactions. Different fragments of mouse ATP6AP1, ATP6AP2^{WT}, ATP6AP2^{L98S}, and ATP6AP2^{R71H} proteins were expressed in yeast as bait and prey as indicated. Cells were grown in DO-2 selective medium without tryptophan and leucine or in DO-3 selective medium without tryptophan, leucine, and histidine. Growth in DO-3 medium indicates a positive protein–protein interaction.

Table S1. ***Drosophila*** **genotypes used in this study**

Genotype	Figure
w^{1118}	Fig. 6, a–e and g
	Fig. 7, a–d
	Fig. 9, e and g
w; ATP6AP2>*ATP6AP2*^{L98S}; FRT82B, *ATP6AP2*$^{\Delta 1}$	Fig. 6, a–e and g
	Fig. 7, a–d
	Fig. 9, e and g
w; ATP6AP2>*ATP6AP2*$^{WT\text{-}myc}$; FRT82B, *ATP6AP2*$^{\Delta 1}$	Fig. 6, c and d
	Fig. 7 d
	Fig. 9 e
w; ATP6AP2>*ATP6AP2*$^{\Delta KKxx}$; FRT82B, *ATP6AP2*$^{\Delta 1}$	Fig. 6, a–d
	Fig. 7 d
	Fig. 9 e
w; ATP6AP2>*ATP6AP2*^{AxxA}; FRT82B, *ATP6AP2*$^{\Delta 1}$	Fig. 6, a–d
	Fig. 7 d
	Fig. 9 e
w; ATP6AP2>*ATP6AP2*^{WT}; FRT82B, *ATP6AP2*$^{\Delta 1}$	Fig. 6, a, b, and e
hs-Flp; FRT42D, ATP6AP2>*ATP6AP2*^{WT}, ubi-mRFP.nls/FRT42D, ATP6AP2>*ATP6AP2*^{L98S}; *ATP6AP2*$^{\Delta 1}$	Fig. 7 e
	Fig. 9, a, d, and f
hs-Flp; tub-FRT-Gal80-FRT-Gal4, UAS–mCD8–mRFP/+; UAS-ATP6AP2 RNAi (Vienna, GD5830)/+	Fig. 7, f and g
hs-Flp; tub-FRT-Gal80-FRT-Gal4, UAS–mCD8–mRFP/+; UAS-ATP6V1C1 RNAi (Vienna, KK101527)/+	Fig. 7, f and g
hs-Flp; tub-FRT-Gal80-FRT-Gal4, UAS–mCD8–mRFP/+; UAS-ATP6AP1 RNAi (Vienna, GD48017)/+	Fig. 7, f and g
hs-Flp; Tub>GFP-Lamp/+; Tub-FRT-Gal80-FRT-Gal4, UAS-mCD8-RFP/UAS-ATP6AP2 RNAi (Vienna, GD5830)	Fig. 9 b
hs-Flp; UAS-Dcr2; R4-mCherry-Atg8, Actin-FRT-CD2-FRT-Gal4, UAS-GFPnls/UAS-ATP6AP2 RNAi (Vienna, GD5830)	Fig. 9 c
ptc-GAL4; UAS-*ATP6AP2*^{WT}/+	Fig. 5 c
ptc-GAL4; UAS-*ATP6AP2*^{L98S}/+	Fig. 5 c
ap-GAL4; UAS-ATP6AP2 RNAi (Vienna, GD5830)/+	Fig. 9 h

REFERENCE

Korvatska, O., N.S. Strand, J.D. Berndt, T. Strovas, D.H. Chen, J.B. Leverenz, K. Kiianitsa, I.F. Mata, E. Karakoc, J.L. Greenup, et al. 2013. Altered splicing of ATP6AP2 causes X-linked parkinsonism with spasticity (XPDS). *Hum. Mol. Genet.* 22:3259–3268. https://doi.org/10.1093/hmg/ddt180

PART II

Mutations in the V-ATPase assembly factor VMA21 cause a glycosylation disorder with autophagic liver disease

Article

Mutations in the XMEA gene *VMA21* cause a congenital disorder of glycosylation with autophagic liver disease

Magda Cannata Serio[*], Laurie A. Graham[*], Angel Ashikov[*], Sharita Timal, Kimiyo Raymond, Margret Ryan, Jos Jansen, Elzbieta Czarnowska, Miao He, Can Ficicioglu, Linda Hasadsri, Christian Gilissen, Richard Rodenburg, Eva Morava, Joris A. Veltman, Piotr Socha, Tom H. Stevens[#], Matias Simons[#] & Dirk J. Lefeber[#]

In preparation

Autorship note:
[*]Magda Cannata Serio, [*]Laurie A. Graham and [*]Angel Ashikov contributed equally to this work.

Mutations in the V-ATPase assembly factor VMA21 cause a congenital disorder of glycosylation with autophagic liver disease.

Magda Cannata Serio[1,2*], Laurie A. Graham[3*], Angel Ashikov[4,5*], Sharita Timal[4,5], Kimiyo Raymond[6], Margret Ryan[7], Jos Jansen[8], Elzbieta Czarnowska[9], Miao He[10,11], Can Ficicioglu[12], Linda Hasadsri[13], Christian Gilissen[14], Richard Rodenburg[15,16], Eva Morava[17,18,19], Joris A. Veltman[20,21], Piotr Socha[22], Tom H. Stevens[7#], Matias Simons[1,2#] & Dirk J. Lefeber[4,5#]

1 - Laboratory of Epithelial Biology and Disease, Imagine Institute, Paris, France.
2 - Université Paris Descartes-Sorbonne Paris Cité, Imagine Institute, Paris, France.
3 - Department of Chemistry and Biochemistry, Institute of Molecular Biology, University of Oregon, Eugene, OR, USA.
4 - Department of Neurology, Donders Institute for Brain, Cognition and Behaviour, Radboud University Medical Center, Nijmegen, The Netherlands.
5 - Department of Laboratory Medicine, Translational Metabolic Laboratory, Radboud Institute for Molecular Life Sciences, Radboud University Medical Center, Nijmegen, The Netherlands.
6 - Department of Laboratory Medicine and Pathology, Mayo College of Medicine, Rochester, MN, USA.
7 - Department of Chemistry and Biochemistry, Institute of Molecular Biology, University of Oregon, Eugene, OR, USA.
8 - Department of Gastroenterology and Hepatology, Translational Metabolic Laboratory, Radboud Institute for Molecular Life Sciences, Radboud University Medical Center, Nijmegen, The Netherlands.
9 - Department of Pathology, The Children's Memorial Health Institute, Warsaw, Poland.
10 - Department of Pathology and Laboratory Medicine, University of Pennsylvania, Perelman School of Medicine, Philadelphia, PA, USA.
11 - Division of Laboratory Medicine, The Children's Hospital of Philadelphia, Philadelphia, PA, USA.
12 - Division of Human Genetics, Department of Pediatrics, The Children's Hospital of Philadelphia, Philadelphia, PA, USA.
13 - Division of Laboratory Genetics, Department of Laboratory Medicine and Pathology, Mayo Clinic, Rochester, MN, USA.
14 - Department of Human Genetics, Donders Centre for Neuroscience, Radboud University Medical Center, Nijmegen, The Netherlands.
15 - Department of Laboratory Medicine, Translational Metabolic Laboratory, Radboud Institute for Molecular Life Sciences, Radboud University Medical Center, Nijmegen, The

Netherlands.
16 - Department of Pediatrics, Nijmegen Centre for Mitochondrial Disorders (NCMD), Radboud University Medical Center, Nijmegen, The Netherlands.
17 - Department of Pediatrics, Tulane University Medical School, New Orleans, Los Angeles, CA, USA.
18 - Department of Pediatrics, University Medical School of Leuven, Leuven, Belgium.
19 - Department of Pediatrics, Radboud University Medical Center, Nijmegen, The Netherlands.
20 - Department of Human Genetics, Donders Centre for Neuroscience, Radboud University Medical Center, Nijmegen, The Netherlands.
21 - Institute of Genetic Medicine, International Centre for Life, Newcastle University, Newcastle upon Tyne, UK.
22 - Department of Gastroenterology, Hepatology, Feeding Disorders and Pediatrics, Children's Memorial Health Institute, Warsaw, Poland.

* shared first authors
# shared last authors

Contact Information
Dr. Matias Simons, Laboratory of Epithelial biology and disease, Institute Imagine - Inserm UMR 1163, 24 Boulevard du Montparnasse - 75015 Paris France, Tel: +33(0)1 42 75 44 55, Email: matias.simons@institutimagine.org

Dr. Dirk J. Lefeber, Translational Metabolic Laboratory, Department of Neurology, Donders Center for Brain, Cognition and Behavior, Radboud university medical center, Box 9101, 6500 HB Nijmegen, The Netherlands. Tel: +31(0)2 43 61 45 67, Email: Dirk.Lefeber@radboudumc.nl

Abstract

The V-ATPase is a multi-subunit protein complex required for acidification of intracellular compartments. At least five different assembly factors are known to be essential for its assembly. Genetic defects in four of these V-ATPase assembly factors have overlapping clinical features, including steatotic liver disease and mild hypercholesterolemia. An exception is the assembly factor VMA21, whose X-linked mutations lead to autophagic myopathy. Here, we report pathogenic mutations in *VMA21* in male patients with abnormal protein glycosylation, chronic elevations of liver enzymes, hypercholesterolemia and steatosis in hepatocytes. By using patient fibroblasts, hepatocytes and yeast, we show that *VMA21* mutations are loss-of-function mutations that lead to V-ATPase misassembly and dysfunction. As a consequence, lysosomal acidification and degradation is impaired causing lipid droplet (LD) accumulation in autolysosomes. Moreover, VMA21 deficiency triggers ER stress and sequestration of unesterified cholesterol in lysosomes, causing activation of the sterol response element-binding protein (SREBP)-mediated cholesterol synthesis pathways. Our data therefore suggest that the impaired lipophagy, the ER stress-dependent LD formation and the increased cholesterol synthesis collectively promote defects in hepatocyte lipid metabolism. Together with the deficiencies in the other V-ATPase assembly factors, the identified *VMA21* mutations highlight the importance of proton pump assembly and function in the pathogenesis of liver disease.

Keywords

Congenital Disorders of Glycosylation, NAFLD, cholesterol impairment, V-ATPase assembly, vacuolar myopathy, VMA21, ER stress.

Introduction

The vacuolar H^+-ATPase complex, or V-ATPases, are large multisubunit protein complexes that are involved in pH homeostasis of intracellular organelles [1]. They are organized into two domains, a membrane-integral V_0 domain, responsible for proton translocation, and a cytosolic V_1 domain, that carries out ATP hydrolysis [1]. For the biogenesis of the proton pump, studies in *S. cerevisiae* have shown that V_0 and V_1 domains are assembled separately in the endoplasmic reticulum (ER) and cytosol, respectively. The assembly of the V_0 domain was shown to depend on a set of ER-resident chaperones [2, 3]: Vma12p, Vma21p, Voa1p, Pkr1p and Vma22p [3–7]. In the first step of the assembly, Vma21p comes into contact with subunit *c'*, and this interaction promotes the assembly of the proteolipid subunits into a ring [3, 4]. In a second parallel step, a complex of Vma12p and Vma22p interacts transiently with subunit *a* of the V_0 domain and mediates its assembly with the proteolipid ring [2]. Once the V_0 is fully assembled, Vma21p escort the V_0 domain to the *cis*-Golgi, where it will bind the V_1 domain to form the functional V-ATPase [3]. Owing to its ER retention motif KK*XX*, Vma21p is transported back to the ER in order to assist in additional rounds of V_0 assembly [3].

Vma12p, Vma21p and Vma22p correspond to TMEM199, VMA21 and CCDC115, respectively, in mammals. Voa1p has been replaced by ATP6AP1 and ATP6AP2 [8, 9] while Pkr1p does not have a mammalian ortholog. Whether the assembly of the mammalian V_0 is mechanistically similar to yeast V_0 assembly is currently unclear. But what the mammalian assembly factors have in common is that their mutations lead to overlapping phenotypes in humans. Patients with mutations in four of these assembly factors *ATP6AP1*, *ATP6AP2*, *TMEM199* and *CCDC115* show overlapping clinical features including hypercholesterolemia, low ceruloplasmin and hepatic phenotypes that range from chronic elevations of liver enzymes to end-stage liver disease necessitating liver transplantation. All patients were found to have abnormal serum protein glycosylation, associated with impaired Golgi homeostasis [8, 10–12].

In contrast, *VMA21* mutations have been associated with a X-linked myopathy with excessive autophagy (XMEA), a disorder characterized by progressive vacuolation and atrophy of the skeletal muscle [13]. Most of the XMEA mutations are intronic variants that reduce splicing efficiency. They are hypomorphic and reduce, but do not eliminate, VMA21 expression [13–17]. The severity of XMEA has often been correlated with the expression of VMA21. XMEA has an adult onset [13, 16, 18], but there are also more severe cases with prenatal/neonatal onset, usually associated with death in infancy, where the mutations result in greater reduction of the VMA21 expression compared to the other mutation [16, 19, 20].

Here, we identified a novel clinical presentation of VMA21 deficiency, causing a chronic liver disease with abnormal glycosylation and defective autophagy. Using patient fibroblasts, hepatocytes and yeast models, we show that deficiency of VMA21 impairs V-ATPase activity, leading to defective autophagy and, ultimately, compromised lipid homeostasis by defective LD degradation and ER stress. Our results indicate that a loss of VMA21 can result in a more widespread disease spectrum, ranging from a autophagic hepatopathy to a pure muscle disease.

Results

Clinical phenotype of VMA21 deficiency

Three male patients, aged 9, 28 and 35 years, from three independent families, presented with a heterogeneous hepatopathy with overlapping symptoms of chronically elevated liver enzymes and variable abnormalities in cholesterol and ceruloplasmin. Neurocognitive examination was age appropriate. Below and in the Supplementary case reports, additional clinical and laboratory details are reported.

Patient 1 is a 9-year old boy with a clinical history of hepatosplenomegaly that regressed with age, chronic elevation of liver enzymes (ALT, AST, ALP and GGT), hypoglycemia, hyperinsulinemia, neutropenia and an abnormal coagulation cascade. Mild hypotonia was noticed with recurrent slightly elevated CK that had normalized on his last visit. Serum ceruloplasmin, cholesterol and lipid profile were low normal.

Patient 2 is 35-year old with a family history of hearing loss and kidney disease. DNA of the family members was unavailable for further genetic testing. At the age of 3 years, he was diagnosed with bilateral sensorineural hearing loss. At age 28, he underwent surgical removal of a non-functioning, hydronephrotic left kidney. The patient's past medical history was also significant for severe myopia, bilateral ocular keratitis, severe *pectus excavatum* and idiopathic polycythemia. He had hyperlipidemia and abnormal liver function tests since childhood. Laboratory investigations revealed mildly elevated cholesterol, elevated LDL, total bilirubin, AST and ALP and low serum copper and ceruloplasmin.

Patient 3 is a 21-year old man and was found to have elevated transaminases during routine blood tests at the age of 3 years. At 6y, chronic hepatitis had developed with elevated transaminases and high cholesterol. Laboratory investigations showed low serum ceruloplasmin and copper. A diagnosis of Wilson's disease was excluded by sequence analysis of ATP7B.

VMA21 mutations lead to hepatosteatosis

Liver biopsy was performed on P3 at age 12y and revealed a normal liver architecture without features of inflammation or fibrosis. However, hepatocytes were irregularly shaped and PAS staining showed positive areas of glycogen (**Suppl. Fig. 1 A-D**). Microvesicular steatosis was found in 10-20% of hepatocytes (**Suppl. Fig. 1 E**). Ultrastructural investigations in hepatocytes revealed the presence of lipid droplets (LDs) inside autolysosomes or lysosome-like structures, abundant glycogen, autophagic vacuoles and multilamellar structures similar as in Niemann-Pick disease type C (**Fig. 1**). The mitochondria were often enlarged with normal *cristae* but in matrix crystalloid-like inclusions (**Fig. 1 A, B**) and matrical granules were often found. In the majority of the cells, the Golgi apparatus exhibited dilatation and occasionally fragmentation, with accumulation of electron-dense material within both cisterns and vesicles (**Fig. 1 C-F**). Moreover, similar electron-dense

material was found in lysosome-like structures located in proximity to the Golgi (**Fig. 1 E**). Kupffer cells contained numerous lysosomes filled with electron-dense material and single apparently pit cells with expanded Golgi apparatus and large multivesicular bodies in the cytoplasm (**Fig. 1 G-J**).

VMA21 deficiency causes a combined disorder of N- and O-glycosylation of serum proteins

The three patients as described above were part of our cohort of patients with unsolved congenital disorder of glycosylation (CDG). Abnormal CDG screening results were identified during metabolic diagnostics. Analysis of N-glycosylation by isofocusing of plasma transferrin was indicative of a Golgi glycosylation disorder with increased di- and trisialotransferrin (**Table S1**). In addition, isofocusing of apolipoprotein CIII (ApoCIII) showed increased ApoCIII-1 and decreased ApoCIII-2 (**Table S1**), indicating abnormal mucin O-glycosylation with reduced sialic acid incorporation. As it is known that hepatopathy can result in false-positive CDG screening test results, total serum N-glycan profiling by MALDI-LTQ mass spectrometry was performed on CDG-P3, showing an increase of undersialylated glycans at m/z 2434 (**Suppl. Fig. 2**) without an increase of N-glycan fucosylation. In contrast, hepatopathy is characterized by increased fucosylation (m/z 2607) (**Suppl. Fig. 2**).

Identification of causative mutations in X-linked VMA21

To identify genetic variants underlying the hepatopathy with abnormal glycosylation, whole exome sequencing was performed of patient 3. Genetic variants were ordered using a previously described prioritization scheme [21], which identified *VMA21* as a candidate gene. *VMA21* is located on ChrXq28 and comprises three exons. Sanger sequencing of *VMA21* in a cohort of male patients with abnormal glycosylation resulted in the identification of genetic variants in VMA21 in patients 1 and 2. Patient 1 showed a hemizygous mutation in the 5' UTR of *VMA21* (c.-10C>T), which was detected as heterozygous in the mother and was absent in the father, in agreement with X-linked recessive inheritance (**Fig. 2 A**). The c.-10C>T mutation results in a new ATG initiation codon, 11 basepairs upstream of the first exon, that could lead to a frameshift and a premature stop codon at position c.26-28 in the protein. Patient 2 showed a hemizygous mutation resulting in a predicted missense substitution of arginine for glycine (p.Arg18Gly). Analysis of cDNA showed the formation of a predominant alternative transcript, generated by disruption of the 5' and use of a cryptic splice site, which resulted in the inclusion of 93 base pairs of intronic sequence. On the protein level, the new splice variant results in premature stop codon after the arginine to glycine substitution (p.Arg18Gly*) (**Suppl Fig. 3 A, B**). In patient 3, c.188A>G in VMA21 was prioritized as the most likely candidate mutation (**Table S2**), which is present in heterozygous form in the mother and absent in the father. The mutation results in a substitution of asparagine at position 63 for glycine

(p.Asn63Gly). Both amino acid substitutions (p.Arg18Gly and p.Asn63Gly) are highly conserved down to *Drosophila melanogaster* (**Fig. 2 B, C, Table S3**). p.Asn63Gly is localized in the luminal loop region of the protein just prior to the second predicted transmembrane region (**Fig. 2 B, C**), while p.Arg18Gly is localized in the N-terminal cytoplasmic domain.

Comparison of VMA21 CDG versus XMEA mutations

Thus far, VMA21 deficiency has only been reported as a cause for XMEA myopathy [13]. Nevertheless, increased transaminases have been reported as incidental finding in some patients [15, 19] and recently a previous described mutation has been reported as causative of a fatal hepatic failure [22]. For XMEA patient 1 (XMEA-P1), previously reported as vacuolar myopathy with p.G91A missense substitution in *VMA21* [13], we found normal transaminases [ALT 54 (10–70 U/L), AST 35 (15–45 U/L)], increased GGT [181 (15–115 U/L)], high cholesterol 5.8 (<6 mmol/L) with increased LDL 4.1 (<3.0 mmol/L) and low normal ceruloplasmin [206 (160–450 mg/L)]. CK was elevated as reported [593 (40–280 U/L)]. Together with the finding of hypercholesterolemia and increased transaminases in our patients, this indicates elevated serum cholesterol and elevations of transaminases as more frequent features of VMA21 deficiency and of V-ATPase assembly defects in general [10-12]. In addition, we compared transferrin N-glycosylation in available plasma samples of CDG patients 1 and 3 and of three XMEA patients by QTOF mass spectrometry. For CDG patients 1 and 3, a clear reduction in sialic acid was identified and an additional minor loss of galactose (**Fig. 3 A**). For XMEA-P1, a reduction in sialic acid was also identified, while transferrin glycosylation was completely normal for XMEA-P2 and XMEA-P3. These combined results indicate that VMA21 deficiency covers a broad and overlapping disease spectrum, ranging from nonsyndromic liver disease with abnormal glycosylation to vacuolar myopathy with increased transaminases and cholesterol as more common/subclinical features.

VMA21 mutations are hypomorphic and reduce protein expression

To functionally validate the *VMA21* mutations found in the CDG patients, we employed patient fibroblasts and compared them to control fibroblasts and fibroblasts from XMEA patient 1 (XMEA-P1). A strongly reduced VMA21 expression was found for CDG-P1 (c.10C>T) and CDG-P2 (p.Arg18Gly), while CDG-P3 (p.Asp63Gly) and XMEA showed a milder protein reduction (**Fig. 4 A, B**). To discriminate if the protein levels were reduced because of mRNA instability, we tested the mRNA expression in patient fibroblasts by qPCR. Interestingly, the mRNA transcript levels were strongly reduced in all CDG patients suggesting mRNA instability as a cause for the reduced protein levels (**Fig. 4 C**). In contrast, although the p.Gly91Ala (XMEA-P1) mutation was reported to abolish a predicted splice enhancer site, it only slightly reduced mRNA expression in fibroblasts (**Fig. 4 C**).

VMA21 mutations impair V-ATPase assembly

In order to study the impact of VMA21 mutations on the assembly of the V_0 and V_1 domains of the V-ATPase, fibroblasts from control and patients were subjected to western blot analysis. As expected, steady state levels of the V_1 subunits ATP6V1D1 and ATP6V1B1/2 revealed that the expression of subunits in total cell extracts remained unaffected, confirming that the assembly of the V_1 domain, which occurs in the cytosol [1], is not impaired by mutation of the ER assembly factor VMA21 (**Fig. 4 D-F**). By contrast, the expression of the V_0 subunits ATP6V0D1 and ATP6V0C was reduced in fibroblasts from CDG and XMEA patients compared to control, indicating an impairment of the V_0 assembly in the ER, thus leading to an overall defect in V-ATPase assembly (**Fig. 4 G-I**).

Although any reduction in expression levels is sufficient to explain reduced assembly, we tested by overexpression whether the mutated proteins could have decreased interactions with V-ATPase components. Upon transient transfection of Myc-tagged VMA21^{R18G}, VMA21^{D63G} and VMA21^{G91A} in HEK293T cells, the levels of the three overexpressed proteins were comparable to VMA21^{WT} (**Suppl. Fig. 4 A, B**). Yet, they showed reduced interaction with the assembly factor ATP6AP2 and V_0 subunit ATP6V0C (**Suppl. Fig. 4 C, D**). This suggests that in addition to the lower expression levels, the missense mutations might also impair protein interactions of VMA21, interfering with the proper assembly of the V-ATPase.

VMA21 mutations cause reduced proton pump function

Vma21p is the yeast ortholog of human VMA21. The two proteins show 30% similarity but VMA21 lacks the C-terminal dilysine motif necessary for the steady state localization of Vma21p in the ER [23] (**Fig. 3 B, C**). Normally, yeast vacuoles utilize the proton gradient generated by the V-ATPase to maintain cellular ion homeostasis, allowing growth even in presence of elevated divalent cations, such as zinc [2, 24-26] (**Fig. 5 A**). Strains lacking a functional Vma21p are unable to grow in these non-permissive conditions. To test the effect of the *VMA21* missense mutations on V-ATPase function by using the high zinc yeast model, the human sequences carrying the appropriate amino acid changes were introduced by homologous recombination into the yeast genomic locus. While the expression of VMA21^{WT} rescued the yeast growth under elevated zinc conditions (**Fig. 5 A**), both CDG missense mutations and the XMEA mutation impaired the rescue (**Fig. 5 A**).

To test whether such proton pump dysfunction could also be detected in patient fibroblasts, we used Lysotracker, a dye that labels acidic cellular compartment. Live fibroblasts from both CDG-P1 and XMEA showed a strong reduction in number and intensity of Lysotracker-positive *punctae* compared with the control fibroblasts (**Fig. 5 B, C**). Taken together, these results indicate that *VMA21* mutations reduce V-ATPase function.

VMA21 deficiency leads to autophagic defects

In order to understand if the impaired organellar acidification could lead to decreased lysosomal degradation, we next tested the activity of the lysosomal Cathepsin B (CTSB) enzyme [27, 28] by using a cresyl violet fluorophore fused to a peptide sequence that can be cleaved by CTSB. By live cell imaging, we could demonstrate a strong reduction of CTSB activity in patient fibroblasts compared to controls (**Fig. 5 D, E**). As a positive control, we used the V-ATPase inhibitor Bafilomycin A1, which also led to a reduced intensity of the fluorophore (**Fig. 5 D, E**).

Next, we tested whether reduced lysosomal acidification and degradation also affected autophagy [12, 13]. For this, we performed immunofluorescence staining and western blot analysis of control and patients fibroblasts. The staining of the lysosomal marker LAMP1 revealed a strong increase in VMA21-deficient fibroblasts compared to the respective control cells (**Fig. 6 A, B**), and the LAMP1-positive vesicles appeared to be enlarged suggesting an impairment in the turnover of these organelles (**Fig. 6 A**). Moreover, we observed an accumulation of the protein by western blot in patients fibroblasts compared to a healthy control (**Fig. 6 C, E**).

Consistent with an increased activation of the autophagy pathway, we found an accumulation of the autophagosome-associated lipidated form of LC3 (LC3-II) by western blotting in patients fibroblasts compared to control cells (**Fig. 6 D, G**). To assess if the LAMP1 and LC3 accumulations were due to a block in the autophagic flux, we tested protein levels of the autophagosomal substrate p62. We found an accumulation of p62 in western blotting, suggesting a decreased autophagic degradation (**Fig. 6 C, F**). Importantly, siRNA-mediated downregulation of VMA21 in human Huh7 hepatocytes was able to recapitulate the LAMP1, p62 and LC3 accumulation, confirming the loss-of-function effects of the *VMA21* mutations on the lysosomal-autophagic pathway (**Suppl. Fig. 5 A-D**).

VMA21 mutations lead to ER stress and lipid abnormalities in patient fibroblasts

Given the steatotic liver phenotypes and LDs observed in the patient hepatocytes, we next tested whether impaired lysosomal degradation could be the cause of LD accumulation. LDs are cytoplasmic organelles that have a core of triglycerides and cholesterol surrounded by a single layer of phospholipids [30]. LDs are formed in the ER, where triglycerides are synthesized with the help of esterification enzymes, such as the ER-resident diacylglycerol acyltransferases 1 and 2 (DGAT1 and DGAT2) [31]. LD degradation can either occur via cytoplasmic lipases [32] or in the context of autophagy (lipophagy) [33].

The number of LDs was assessed by BODIPY staining in patients and control fibroblasts. CDG-P1 and XMEA-P1 cells showed a clear accumulation of LDs compared to the control cells (**Fig. 6 H-J**). Importantly, treatment with Bafilomycin A1 increased LD formation

in control and XMEA fibroblasts (**Fig. 6 H-J**), but not in CDG-P1 cells, suggesting that the cause of LD accumulation in the latter cells is decreased lipophagy, confirming a block in the last steps of the lysosomal degradation as consequence of impaired acidification.
In the lysosomal storage disease Niemann-Pick C, cholesterol accumulates inside the lysosomes due to defective extraction via the NPC1 and NPC2 proteins [34]. As the lysosomal cholesterol extraction occurs in a pH-dependent manner [35], we tested whether the hypercholesterolemia observed in the CDG patients could also be linked to decreased lysosomal acidification. For this, we labelled unesterified cholesterol with the Filipin dye. As expected, the staining revealed an accumulation of cholesterol in vesicular structures of CDG-P1 fibroblasts compared to control cells, while the XMEA fibroblasts show a tendency, but not significant, accumulation of cholesterol (**Fig. 6 K, L**). Similar to the LDs, pre-treatment of the cells with the autophagy inhibitor Bafilomycin A1 led to an accumulation of cholesterol in both control and XMEA fibroblasts but not in CDG-P1 cells (**Fig. 6 K, L**). The sequestration of cholesterol in lysosomes can lower cholesterol content in the ER, triggering lipogenic pathways mediated by the sterol response element-binding protein-1 (SREBP1) [34, 36] that finally lead to an overproduction of lipoprotein particles and elevated serum lipid levels. To test whether such *de novo* lipogenic pathways are increased in the patient cells, SREBP1 activation and cleavage was analyzed by western blotting of patient and control fibroblasts. This revealed an increase of the amount of mature SREBP1 in CDG-P1 compared to the healthy control and the XMEA mutation (**Fig. 7 A, B**). Taken together, this suggests that VMA21 deficiency leads to LD and cholesterol accumulation, which may be related to the defects in lysosome/autophagy pathway.

CDG-P1 mutation causes PERK-mediated ER stress

As defective V_0 assembly has been associated with ER stress [9], we next examined whether CDG-P1 cells display any ER stress. We tested all the three unfolded protein response (UPR) stress branches, but found only a strong activation of the PKR-like ER kinase (PERK) branch in the CDG-P1 but not in control or XMEA fibroblasts (**Suppl. Fig. 6 A-E**). This was demonstrated by the autophosphorylation of PERK on Thr980 (**Fig. 7 C**). PERK activation led to the upregulation of several UPR target genes including the activating transcription factor 4 (ATF4), C/EBP homologous protein (CHOP) and the Glucose Regulated Protein 94 (GRP94) as demonstrated by qPCR and immunostaining (**Fig. 7 D-G**). Finally, since ER stress can also cause enhanced LD formation and SREBP1 activation [37] , we tested whether PERK-induced ER stress may also contribute to enhanced LD biogenesis. For this, we simultaneously inhibited the ER-resident esterification enzymes DGAT1 and DGAT2 before performing BODIPY staining. DGAT inhibition led to a suppression of LD number and size in control and XMEA fibroblasts, suggesting that ER stress may enhance the steatotic phenotype (**Fig. 6 H-J**).

Discussion

Here, we identified three mutations in the ER assembly factor VMA21 that lead to a novel CDG featured by a mild form of chronic liver disease with mild hyperlipidemia and increased LDL. Our functional studies demonstrated that both *VMA21* CDG and XMEA mutations are hypomorphic mutations lowering mRNA and protein levels. As a consequence of VMA21 reduction, there was an impairment of V-ATPase assembly, marked by reduced V_0 subunit expression and reduced interaction with the ER assembly factor ATP6AP2, that led to reduced proton pump activity. This in turn caused reduced lysosomal acidification and protease activation, as well as the inability to execute the final steps of the (auto)-lysosomal degradation. In fibroblasts, the impaired lysosomal acidification led to defective lipophagy, consistent with the presence of enlarged LD-containing autolysosomes in the hepatocytes of the liver biopsy of CDG-P3.

Moreover, since the extraction of endocytosed cholesterol from lysosomes is usually performed in a pH-dependent manner [34], the observed cholesterol accumulation in the fibroblasts may also have been caused by the reduced lysosomal acidification. Interestingly, it has been demonstrated that in the lysosomal storage disorder NPC the activity of the lysosomal protease CTSB can be impaired by both the altered lysosomal pH and the accumulation of lipid material inside lysosomes [38]. Thus, also in VMA21-deficient cells the accumulated cholesterol could impair lysosomal function. As we additionally observed an increased cleavage of SREBP1, it can be hypothesized that the failure to properly extract cholesterol from the lysosomes leads to an overall decline of cellular cholesterol, which in turn triggers SREBP1 cleavage and the *de novo* production of cholesterol [34]. As newly synthesized cholesterol can directly be secreted into the serum together with lipoprotein particles, the hypercholesterolemia observed in the patients further may be a result of SREBP1 activation and *de novo* cholesterol synthesis.

While reduced proton pump function is at the heart of this pathogenic cascade, it should be pointed out that hypercholesterolemia and liver steatosis have not yet been observed in patients with mutations in V-ATPase core subunits. Interestingly, the PERK branch which was shown to be activated in the CDG-P1 cells is also able to activate SREBP1-mediated *de novo* lipogenesis [39, 40], suggesting that the ER stress responses might further contribute to cholesterol accumulation. This could also be the case for the LD accumulation, as increased LD formation has been linked to ER stress in many instances, particularly in hepatocytes. Accordingly, the inhibition of fatty acid esterification into triglycerides obtained through the inhibition of the DGAT1 and 2 enzymes led to a partial rescue of LD number and size in VMA21 patients fibroblasts.

What causes the ER stress in the VMA21-deficient cells is unclear. Interestingly, in plants it has been shown that VMA21 interacts and helps Erv41p/Erv46p [41], an early secretory-localized complex involved in the protein loading into COPII vesicles for transport to the Golgi. Lack of Vma21p in ΔVma21p strains resulted in a complete absence of the v-SNARE Bos1 in the COPII vesicles [41], suggesting an impaired ER-to-Golgi transport

also in CDG patients fibroblasts. Likewise, given the involvement of VMA21 in retrograde transport back to the ER, disturbance of ER and Golgi homeostasis might also stem from defects in this trafficking pathway. Moreover, lack of another ER assembly factor has previously also been associated with ER stress [9], suggesting that it may be directly related to the defective V_0 assembly [23, 42]. This is supported by the phenotypic similarities between the different assembly factor deficiencies, particularly with regard to the liver [8,10–12].

The phenotypic difference between XMEA and the VMA21 deficiencies described here also motivated us to explore functional differences between the underlying mutations [13, 14]. Overall, we found that these differences are mild and that both mutations have overlapping pathomechanisms. Given that liver involvement has already been described in XMEA patients, ranging from increased liver transaminases to fatal hepatic failure [15, 19, 22], while CK elevation could be observed in one of the CDG patients, it seems clear that more patients are needed to fully appreciate the phenotypic spectrum of VMA21 deficiency. Nevertheless, we did find that XMEA patient sera lacked glycosylation abnormalities and that CDG mutations had a stronger impact on VMA21 expression and PERK phosphorylation than the XMEA mutation. Therefore, we conclude that a stronger reduction of VMA21 might correlate with a stronger effect on ER stress and glycosylation and that these processes seem to be more sensitive to VMA21 protein dosage compared to the lysosomal acidification.

In summary, we identify three individuals with a CDG featured by autophagic defects and ER stress caused by different mutations in *VMA21*. Our data suggest that X-linked VMA21 deficiency is a novel cause for mild chronic liver disease that can be identified by glycosylation screening of patient blood samples and/or genetic testing. As the liver phenotype observed in our patients can be compared to the steatosis observed in patients with non-alcoholic fatty liver disease (NAFLD), a better understanding of how ER stress and autophagic defects contribute to liver disease in VMA21 patients may also help in the development of new therapeutic strategies in NAFLD.

Materials and Methods

Patient materials. Blood and fibroblasts of affected individuals were obtained for diagnostics of inborn errors of metabolism and were used, together with parental DNA, after written informed consent from parents and treating physicians, according to the declaration of Helsinki.

Whole exome sequencing. Genomic DNA was extracted from fibroblast pellets of patient 3 according to the manufacturer's protocol using a Qiagen Mini kit (Qiagen), and was checked for DNA degradation on agarose gels. Total RNA was extracted from skin fibroblast from patient 2 using TRIzol Reagent (Invitrogen) following the manufacturer instructions. High-quality cDNA was obtained by the RevertAid First Strand cDNA Synthesis Kit (Thermo Fisher) using the oligo-dT primer. PCR was performed on cDNA with primers AA092 and AA093 (See **Table S4**), products were separated in 2% Agarose gel electrophoresis, excised fragments from the gel were purified by QIAquick gel extraction kit (Qiagen) and used as a template for Sanger sequencing.

Next generation sequencing (NGS) and analysis was performed as described [10]. In brief, exome enrichment was performed using the SureSelect Human All Exon 50 Mb Kit (Agilent), covering 21,000 genes. The exome library was sequenced on a SOLiD 5500xl sequencer (Life Technologies). Color space reads were iteratively mapped to the hg19 reference genome with the SOLiD LifeScope software version 2.1. Called variants and indels were annotated using an in-house annotation pipeline (14, 36) and common variants were filtered out based on a frequency of >0.5% in dbSNP (137) and a frequency of >0.3% in our in-house database of >5000 exomes. Quality criteria were applied to filter out variants with less than 5 variant reads and less than 20% variation. Furthermore, synonymous variants, deep intronic, intergenic and UTR variants were excluded.

Sanger sequencing. Genomic DNA was extracted from fibroblast pellets or white blood cells from the affected individuals and available family members. The primers, extended with an M13 tail to the 5'- and 3'-ends were designed to amplify the different exons of the *VMA21* gene (GenBank accession number NM_001017980.3), including at least 50 bp of the flanking intronic regions (see **Table S4** for primers list). Standard PCR reactions were based on 1 μL of 100 ng/μL DNA and 7.5 μL AmpliTaq Gold® 360 DNA Polymerase (Applied Biosystems) in a total volume of 15 μL. The reaction conditions were 10 min at 95°C, then 35 cycles of 30 sec at 94°C, 30 sec at 60 °C and 1 min at 72°C. The reaction was completed with a final elongation of 10 min at 72°C. After purification of the PCR product, sequence reactions were performed with primers annealing to the M13 tails and using the BigDye® Terminator v3.1 Cycle Sequencing Kit (Applied Biosystems) according to the manufacturer's protocol. The resulting fragments were analysed on an 3130xl Genetic Analyzer (Applied Biosystems).

Glycosylation studies. Isoelectric focusing of serum transferrin (TIEF) for analysis of protein N-glycosylation defects and of serum apolipoprotein CIII for analysis of mucin type O-glycosylation defects were carried out as described before [11]. A transferrin polymorphism was excluded by neuraminidase digestion of the sample prior to TIEF and the presence of neuraminidase was excluded by measuring enzyme activity in plasma. Plasma N-glycan profiling was performed by MALDI linear ion trap mass spectrometry (MS) as described before [43], using 10 μL of plasma. High resolution mass spectrometry of intact transferrin was performed on a 6540 nanochip QTOF (Agilent) operated with C8 nanochip, according to published protocols [44].

Liver biopsy. At age 6 years, a liver biopsy was performed of patient 3. For ultrastructural investigations, the liver biopsy was fixed in 2,5% glutaraldehyde in 0,1M phosphate buffer. After fixation in 1% OsO4 in phosphate buffer, tissue specimens were dehydrated in ascendant ethanol and embedded in Epon 812. Thin sections stained with uranyl acetate and lead citrate were examined on a Jem 1011 (Jeol) EM.

Yeast functional assays. PCR fragment containing human *VMA21* ORF was generated from cDNA clone MGC:125515 with primers that also possessed sequence homologous to yeast *VMA21* 5' and 3' UTR sequence. Plasmid borne HA and GFP epitope tagged versions of human *VMA21* under control of the yeast *VMA21* promoter were generated using previously described protocols [45]. Point mutations were introduced using PCR based mutagenesis with complementary primers both containing the single nucleotide change. Growth tests of serial dilutions of yeast cells carrying human VMA21 and points mutants were prepared as previously described [7].

Plasmids. The cDNA of *VMA21* and *ATP6AP2* was generated by gene synthesis (Invitrogen™ GeneArt™ Gene Synthesis service) and subcloned, using HindIII or NcoI and BamHI sites into pcDNA3.1-Myc and pcDNA3.1-HA respectively, resulting in C-terminal tagged versions of the protein as previously described 23. To obtain all the mutants of VMA21 with single amino acid substitutions (VMA21^{R18G}Myc, VMA21^{D63G}Myc and VMA21^{G91A}Myc), the construct pcDNA3.1-VMA21-Myc was used as a template and site direct mutagenesis reactions were performed with the QuickChange II Site-Directed Mutagenesis Kit (Agilent) according to the manufacturer instruction (see **Table S4** for primers list). All constructs were verified by sequencing. pCS2-ATP6V0C-FLAG was kindly provided from Cristina Maria Cruciat (Heidelberg, Germany).

RNA extraction, reverse transcription PCR (RT-PCR) and quantitative real time PCR (qRT-PCR). Total RNA was isolated from fibroblasts using a Qiagen RNA extraction kit (Qiagen). cDNA was prepared using reverse transcriptase iScript

cDNA Synthesis Kit (Bio-Rad). RT-PCR was performed on cDNA. Relative expression levels of *VMA21*, *BiP*, *XBP1* total, *XBP1* unspliced, *XBP1* spliced, *ATF4*, *CHOP* were determined using the Power SYBR Green PCR Master Mix (Thermo Fisher). Expression levels were normalized to HPRT (see **Table S4** for primers list).

Cell culture, siRNA oligonucleotides and transfection. Primary fibroblasts from patients and controls were grown from a skin biopsy and cultured in Dulbecco's modified Eagle Medium DMEM (Thermo Fisher) supplemented with 10% fetal bovine serum (FBS), 1% L-glutamine and 1% Penicillin/Streptomycin at 37°C under 5% CO2. Research on patients' cells was prospectively reviewed and approved by the Ethical Committees of the University Hospital of Nijmegen. HEK293T and Huh7 cells were routinely grown at 37°C in Dulbecco's Modified Eagle Medium DMEM (Thermo Fisher) containing 10% FBS, 1% L-glutamine and 1% Penicilline/Streptomycin. HEK293T were transfected by using Lipofectamine 2000 (Invitrogen) in Opti-MEM (Thermo Fisher) according to the manufacturer's instructions. The expression of VMA21, ATP6AP2 and ATP6V0C forms was analysed by western blotting 48 h post transfection. siRNA oligonucleotides against the *VMA21*, as well as non-targeting siRNA as a vehicle treated control, were purchased from Dharmacon: ON-TARGETplus Human *VMA21* (203547) J-031593-17, J-031593-18, J-031593-20 and ON-TARGETplus Non-targeting Control Pool D001810-10. Transfection of these siRNA oligonucleotides was achieved using Lipofectamine^{TM} 2000 reagent (Invitrogen) and the Huh7 KD for VMA21 were analysed by western blotting or immunostaining 72 h post transfection.

Western Blotting. Western blot was performed as previously described [11]. The following antibodies were used: rabbit polyclonal anti-VMA21 (sc-102008), rabbit polyclonal anti-ATP6V1D (sc-20945), mouse monoclonal anti-ATP6V1B1/2 (sc-55544), mouse monoclonal anti-Myc (sc-40), rabbit polyclonal anti-GRP78 antibody (sc-376768), all antibodies from Santa Cruz Biotechnology; rabbit polyclonal anti-ATP6V0D1 antibody (Abcam ab56441); mouse monoclonal anti-β-Actin antibody (A1978), mouse monoclonal anti-FLAG antibody (F3165) and mouse monoclonal anti- α-Tubulin (T6199), all antibodies from Sigma; rat monoclonal anti-HA antibody (Roche, 11867423001); rabbit polyclonal anti-ATP6V0C, gift from P. Saftig; mouse monoclonal anti-LAMP1 (DSHB, 1D4B); rabbit polyclonal anti-LC3 (MBL International, PM036); rabbit polyclonal anti-SQSTM1 (Enzo Life Sciences, BML-PW-9860); rabbit polyclonal anti-PERK antibody (3192), rabbit polyclonal anti-phospho PERK antibody (3179), all antibodies from Cell Signalling Technologies; mouse monoclonal anti- SREBP1 antibody (Novus Biologicals, NB600-582). Secondary antibodies used were: anti-rabbit, anti-mouse and anti-rat Horseradish Peroxidase Conjugated (Thermo Scientific). For the co-IP, HEK293T cells were transfected with 1 μg of total DNA for each lane with the following constructs, alone or in co-expression: VMA21^{WT}Myc, VMA21^{R18G}Myc, VMA21^{D63G}Myc, VMA21^{G91A}Myc,

ATP6AP2-HA, Toca-1-Myc and ATP6V0C-FLAG. The samples were prepared as previously described in [12]. Initial lysates and immunoprecipitated proteins were analyzed by SDS-PAGE and immunoblotted with specific antibodies.

Modulation of Lipid Droplet formation. Fibroblasts were grown on glass coverslips and when confluent were incubated overnight at 37°C with DGAT 1 and 2 inhibitors 10 μM (Sigma) diluted in pre-warmed complete DMEM medium. After the overnight, control fibroblasts were incubated for 1 h in Bafilomycin A1 100 nM (Calbiochem, 196000) diluted in pre-warmed complete DMEM. Then the cells were washed in PBS and subjected to indirect immunofluorescence, as indicated below.

Indirect immunofluorescence studies. Primary fibroblasts and Huh7 were grown on glass coverslips. Cells were fixed with 4% paraformaldehyde in PBS for 10 min at room temperature. Paraformaldehyde was quenched with 0,1 M Glycine in PBS for 5 min on ice and cells were made permeable with PBS-0,1% Saponin (for lysosomal staining) or PBS-Triton 0,1% (for ER staining) 15 min RT. Cells were blocked for 30 min at RT in BSA 3% and labeled with the appropriate primaries antibodies overnight at 4°C in blocking solution. After washing, cells were incubated 2 h at room temperature with secondary antibodies (dilution 1:200) and Hoechst (0.5 μg ml^{-1}) in PBS. Coverslips were mounted in Mowiol. Primary antibodies used were: mouse monoclonal anti-LAMP1 (DSHB, 1D4B), rabbit polyclonal anti-GRP94 antibody (Abcam, ab3674). Secondary antibodies used were: fluorescent conjugated Alexa Fluor 488 and Alexa Fluor 555 (Molecular probes, Invitrogen).

BODIPY, Filipin, Cathepsin B and Lysotracker staining. For BODIPY and Filipin labelling, fibroblasts or Huh7 cells were fixed for 10 min in 4% paraformaldehyde in PBS, washed in PBS and incubated with BODIPY® 493/503 (2.5 μg ml^{-1}, Molecular Probes) and Hoechst (0.5 μg ml^{-1}) diluted in PBS-Triton 0,1% for 2 h, or with Filipin (F9765, Sigma) diluted in PBS for 1 h at RT. Fibroblasts and cells were mounted as described above.

For Cathepsin B and Lysotracker labelling, fibroblasts were grown on MatTek glass bottom dishes and were incubated for 20 min at 37°C with Magic Red Cathepsin assay (ImmunoChemistry Technologies, LLC) or 5 min at 37°C with LysoTracker® Red DND-99 (50 nM, Molecular Probes), diluted in pre-warmed complete DMEM medium. Then the cells were washed in PBS and the probe-containing medium was replaced with fresh medium. The cells observed live using a confocal microscope.

Cells imaging. All images were acquired on a Leica TCS SP8 or Leica TCS SP8 STED equipped with a 405 nm laser line and a White Light Laser with a 63x/1.4 DIC Lambda blue PLAN APOCHROMATE objective. Images were processed with Fiji, Adobe Pho-

toshop and Imaris.

Statistical analysis. All data are mean ± SEM, statistical significance was determined by an ordinary one-way ANOVA followed by a Bonferroni multiple comparisons test.

References

1. Forgac M. Vacuolar ATPases: rotary proton pumps in physiology and pathophysiology. Nat Rev Mol Cell Biol. 2007;8(11):917-929. doi:10.1038/nrm2272

2. Graham LA, Flannery AR, Stevens TH. Structure and assembly of the yeast V-ATPase. J Bioenerg Biomembr. 2003;35(4):301-312.

3. Malkus P, Graham LA, Stevens TH, Schekman R. Role of Vma21p in assembly and transport of the yeast vacuolar ATPase. Mol Biol Cell. 2004;15(11):5075-5091. doi:10.1091/mbc.e04-06-0514

4. Davis-Kaplan SR, Compton MA, Flannery AR, et al. PKR1 encodes an assembly factor for the yeast V-type ATPase. J Biol Chem. 2006;281(42):32025-32035. doi:10.1074/jbc.M606451200

5. Hill KJ, Stevens TH. Vma22p is a novel endoplasmic reticulum-associated protein required for assembly of the yeast vacuolar H(+)-ATPase complex. J Biol Chem. 1995;270(38):22329-22336.

6. Hirata R, Umemoto N, Ho MN, Ohya Y, Stevens TH, Anraku Y. VMA12 is essential for assembly of the vacuolar H(+)-ATPase subunits onto the vacuolar membrane in Saccharomyces cerevisiae. J Biol Chem. 1993;268(2):961-967.

7. Ryan M, Graham LA, Stevens TH. Voa1p functions in V-ATPase assembly in the yeast endoplasmic reticulum. Mol Biol Cell. 2008;19(12):5131-5142. doi:10.1091/mbc.e08-06-0629

8. Jansen EJR, Timal S, Ryan M, et al. ATP6AP1 deficiency causes an immunodeficiency with hepatopathy, cognitive impairment and abnormal protein glycosylation. Nat Commun. 2016;7:11600. doi:10.1038/ncomms11600

9. Guida MC, Hermle T, Graham LA, et al. ATP6AP2 functions as a V-ATPase assembly factor in the endoplasmic reticulum. Riezman H, ed. Mol Biol Cell. 2018;29(18):2156-2164. doi:10.1091/mbc.E18-04-0234

10. Jansen JC, Timal S, van Scherpenzeel M, et al. TMEM199 Deficiency Is a Disorder of Golgi Homeostasis Characterized by Elevated Aminotransferases, Alkaline Phosphatase, and Cholesterol and Abnormal Glycosylation. Am J Hum Genet. 2016;98(2):322-330. doi:10.1016/j.ajhg.2015.12.011

11. Jansen JC, Cirak S, van Scherpenzeel M, et al. CCDC115 Deficiency Causes a Disorder of Golgi Homeostasis with Abnormal Protein Glycosylation. Am J Hum Genet. 2016;98(2):310-321. doi:10.1016/j.ajhg.2015.12.010

12. Rujano MA, Cannata Serio M, Panasyuk G, et al. Mutations in the X-linked ATP6AP2 cause a glycosylation disorder with autophagic defects. J Exp Med. 2017;214(12):3707-

3729. doi:10.1084/jem.20170453

13. Ramachandran N, Munteanu I, Wang P, et al. VMA21 deficiency prevents vacuolar ATPase assembly and causes autophagic vacuolar myopathy. Acta Neuropathol (Berl). 2013;125(3):439-457. doi:10.1007/s00401-012-1073-6

14. Crockett CD, Ruggieri A, Gujrati M, et al. Late adult-onset of X-linked myopathy with excessive autophagy. Muscle Nerve. 2014;50(1):138-144. doi:10.1002/mus.24197

15. Saraste A, Koskenvuo JW, Airaksinen J, et al. No cardiomyopathy in X-linked myopathy with excessive autophagy. Neuromuscul Disord NMD. 2015;25(6):485-487. doi:10.1016/j.nmd.2015.03.003

16. Munteanu I, Ramachandran N, Ruggieri A, Awaya T, Nishino I, Minassian BA. Congenital autophagic vacuolar myopathy is allelic to X-linked myopathy with excessive autophagy. Neurology. 2015;84(16):1714-1716. doi:10.1212/WNL.0000000000001499

17. Munteanu I, Kalimo H, Saraste A, Nishino I, Minassian BA. Cardiac autophagic vacuolation in severe X-linked myopathy with excessive autophagy. Neuromuscul Disord NMD. 2017;27(2):185-187. doi:10.1016/j.nmd.2016.10.007

18. Mercier S, Magot A, Caillon F, et al. Muscle magnetic resonance imaging abnormalities in X-linked myopathy with excessive autophagy. Muscle Nerve. 2015;52(4):673-680. doi:10.1002/mus.24664

19. Ruggieri A, Ramachandran N, Wang P, et al. Non-coding VMA21 deletions cause X-linked myopathy with excessive autophagy. Neuromuscul Disord NMD. 2015;25(3):207-211. doi:10.1016/j.nmd.2014.11.014

20. Konialis C, Assimakopoulos E, Hagnefelt B, Karapanou S, Sotiriadis A, Pangalos C. Prenatal diagnosis of X-linked myopathy associated with a VMA21 gene mutation afforded through a novel targeted exome sequencing strategy applied in fetuses with abnormal ultrasound findings. Clin Case Rep. 2017;5(3):308-311. doi:10.1002/ccr3.822

21. Timal S, Hoischen A, Lehle L, et al. Gene identification in the congenital disorders of glycosylation type I by whole-exome sequencing. Hum Mol Genet. 2012;21(19):4151-4161. doi:10.1093/hmg/dds123

22. Ackerley CA, Cooper MA, Munoz DG, Minassian BA. Fatal hepatic failure and pontine and extrapontine myelinolysis in XMEA. Neurology. 2016;87(13):1417-1419. doi:10.1212/WNL.0000000000003155

23. Hill KJ, Stevens TH. Vma21p is a yeast membrane protein retained in the endoplasmic reticulum by a di-lysine motif and is required for the assembly of the vacuolar H(+)-ATPase complex. Mol Biol Cell. 1994;5(9):1039-1050.

24. Klionsky DJ, Herman PK, Emr SD. The fungal vacuole: composition, function, and biogenesis. Microbiol Rev. 1990;54(3):266-292. 25. Eide DJ, Clark S, Nair TM, et al. Characterization of the yeast ionome: a genome-wide analysis of nutrient mineral and trace element homeostasis in Saccharomyces cerevisiae. Genome Biol. 2005;6(9):R77. doi:10.1186/gb-2005-6-9-r77

26. Kane PM. The where, when, and how of organelle acidification by the yeast vacuolar

H+-ATPase. Microbiol Mol Biol Rev MMBR. 2006;70(1):177-191. doi:10.1128/MMBR.70.1.177-191.2006

27. Sloane BF. Cathepsin B and cystatins: evidence for a role in cancer progression. Semin Cancer Biol. 1990;1(2):137-152.

28. Reiser J, Adair B, Reinheckel T. Specialized roles for cysteine cathepsins in health and disease. J Clin Invest. 2010;120(10):3421-3431. doi:10.1172/JCI42918

29. Leung-Toung R, Li W, Tam TF, Karimian K. Thiol-dependent enzymes and their inhibitors: a review. Curr Med Chem. 2002;9(9):979-1002.

30. Olzmann JA, Carvalho P. Dynamics and functions of lipid droplets. Nat Rev Mol Cell Biol. 2019;20(3):137-155. doi:10.1038/s41580-018-0085-z

31. Yen C-LE, Stone SJ, Koliwad S, Harris C, Farese RV. Thematic review series: glycerolipids. DGAT enzymes and triacylglycerol biosynthesis. J Lipid Res. 2008;49(11):2283-2301. doi:10.1194/jlr.R800018-JLR200

32. Greenberg AS, Coleman RA, Kraemer FB, et al. The role of lipid droplets in metabolic disease in rodents and humans. J Clin Invest. 2011;121(6):2102-2110. doi:10.1172/JCI46069

33. Singh R, Kaushik S, Wang Y, et al. Autophagy regulates lipid metabolism. Nature. 2009;458(7242):1131-1135. doi:10.1038/nature07976

34. Vance JE, Karten B. Niemann-Pick C disease and mobilization of lysosomal cholesterol by cyclodextrin. J Lipid Res. 2014;55(8):1609-1621. doi:10.1194/jlr.R047837

35. Deffieu MS, Pfeffer SR. Niemann-Pick type C 1 function requires lumenal domain residues that mediate cholesterol-dependent NPC2 binding. Proc Natl Acad Sci U S A. 2011;108(47):18932-18936. doi:10.1073/pnas.1110439108

36. Brown MS, Goldstein JL. The SREBP Pathway: Regulation of Cholesterol Metabolism by Proteolysis of a Membrane-Bound Transcription Factor. Cell. 1997;89(3):331-340. doi:10.1016/S0092-8674(00)80213-5

37. Zhang X, Zhang K. Endoplasmic Reticulum Stress-Associated Lipid Droplet Formation and Type II Diabetes. Biochem Res Int. 2012;2012:247275. doi:10.1155/2012/247275

38. Elrick MJ, Lieberman AP. Autophagic dysfunction in a lysosomal storage disorder due to impaired proteolysis. Autophagy. 2013;9(2):234-235. doi:10.4161/auto.22501

39. Harding HP, Zhang Y, Khersonsky S, et al. Bioactive small molecules reveal antagonism between the integrated stress response and sterol-regulated gene expression. Cell Metab. 2005;2(6):361-371. doi:10.1016/j.cmet.2005.11.005

40. Bobrovnikova-Marjon E, Hatzivassiliou G, Grigoriadou C, et al. PERK-dependent regulation of lipogenesis during mouse mammary gland development and adipocyte differentiation. Proc Natl Acad Sci U S A. 2008;105(42):16314-16319. doi:10.1073/pnas.0808517105

41. Welsh LM, Tong AHY, Boone C, Jensen ON, Otte S. Genetic and molecular interactions of the Erv41p-Erv46p complex involved in transport between the endoplasmic reticulum and Golgi complex. J Cell Sci. 2006;119(Pt 22):4730-4740. doi:10.1242/jcs.03250

42. Esmail S, Kartner N, Yao Y, Kim JW, Reithmeier RAF, Manolson MF. N-linked glycosylation of a subunit isoforms is critical for vertebrate vacuolar H+ -ATPase (V-

ATPase) biosynthesis. J Cell Biochem. 2018;119(1):861-875. doi:10.1002/jcb.26250
43. Guillard M, Gloerich J, Wessels HJCT, Morava E, Wevers RA, Lefeber DJ. Automated measurement of permethylated serum N-glycans by MALDI-linear ion trap mass spectrometry. Carbohydr Res. 2009;344(12):1550-1557. doi:10.1016/j.carres.2009.06.010
44. van Scherpenzeel M, Steenbergen G, Morava E, Wevers RA, Lefeber DJ. High-resolution mass spectrometry glycoprofiling of intact transferrin for diagnosis and subtype identification in the congenital disorders of glycosylation. Transl Res J Lab Clin Med. 2015;166(6):639-649.e1. doi:10.1016/j.trsl.2015.07.005
45. Neubert C, Graham LA, Black-Maier EW, et al. Arabidopsis has two functional orthologs of the yeast V-ATPase assembly factor Vma21p. Traffic Cph Den. 2008;9(10):1618-1628. doi:10.1111/j.1600-0854.2008.00799.x
46. Blanz J, Zunke F, Markmann S, et al. Mannose 6-phosphate-independent Lysosomal Sorting of LIMP-2. Traffic Cph Den. 2015;16(10):1127-1136. doi:10.1111/tra.12313

Case report descriptions

Patient 1 (-10C>T) is a 9-year old boy, born from healthy African-American parents. The clinical history revealed hepatosplenomegaly that regressed with age, a chronic elevation of liver enzymes (ALT, AST, ALP and GGT), hypoglycemia, hyperinsulinemia, neutropenia and an abnormal coagulation cascade. Hypotonia was noticed with recurrent slightly elevated CK (322 U/L; ref: <305 U/L) that normalised on his last visit. Serum ceruloplasmin was low normal (19 mg/dL; ref: 18–37 mg/dL). Cholesterol levels and a lipid profile were normal. He had significant macrocephaly at 15 months, OFC was 52 cm and height 76.3 cm (3rd percentile). Dysmorphic appearance included macrocephaly, hypotonic facies, depressed nasal bridge and a short upturned nose. The neurocognitive exam was age appropriate.

Patient 2 (R18G)): 35-year old male was referred for evaluation of multiple congenital anomalies, congenital bilateral sensorineural hearing loss, hereditary nephritis. He is the third child of two unrelated parents of Hispanic descent, born at 38 weeks gestational age and required hospitalization due to feeding difficulties for one month after delivery. The patient cannot recall his developmental history, but he was clumsy and continues to be clumsy. He was born deaf (mother noticed that he could not hear in the first year of life) but diagnosed only at the age of 3 years with bilateral sensorineural hearing loss for which he received hearing aids. He had no speech until 3 years of age. After receiving the hearing aids at that time he had speech therapy from 3 years to the seventh grade and his speech improved. He has a history of repeating the fifth grade. He required special education due to the speech and slow processing and learning until high school and then he was in full stream regular classes. He had completed four years of college in finance and now works in property management and finance. The patient was born with a left ureteropelvic joint junction obstruction. He had left flank pain for over 30 years. He underwent left simple laparoscopic nephrectomy for non-functioning, hydronephrotic kidney secondary to congenital UPJ obstruction in 2006. Past medical history is also significant for bilateral ocular keratitis, severe *pectus excavatum*, idiopathic polycythemia with history of periodic phlebotomies, hyperlipidemia and abnormal liver function tests. He reports polycythemia, hyperlipidemia and unexplained abnormal liver tests since childhood. The patient is physically active, he is a runner and preparing for half marathon. He has dysmorphic features of microcephaly, long face, high arched palate, retrognatia and epicanthal folds. His neurologic findings are normal. Laboratory investigations revealed mildly elevated cholesterol (206 mg/dL; ref: 0–200 mg/dL) and LDL (134 mg/dL; ref: 0–100 mg/dL). A routine metabolic panel was significant for elevated total bilirubin (2.6 mg/dL; ref: 0.3–1.5 mg/dL), AST (51 U/L, ref: 15–41 U/L), and alkaline phosphatase (128 U/L; ref: 31-107 U/L). The patient was also found to have low serum copper (67 μg/dL; ref: 72–166 μg/dL) and low ceruloplasmin (13 mg/dL; ref: 15-30

mg/dL). Pathology was remarkable for chronic tubulointerstitial injury, glomerulosclerosis, arteriosclerosis and mesangial electron dense material in one glomerular segment on electron microscopy but no features of a basement membrane nephropathy.

Patient 3 (D63G): a 21-year old male patient was born as second child to healthy unrelated parents. After an uneventful newborn period, he was found to have elevated transaminases during routine blood tests at the age of 3 years. At 6y, chronic hepatitis had developed with elevated transaminases and high cholesterol (295–321 mg/dL; ref: 0–200 mg/dL). Laboratory investigations showed low serum ceruloplasmin (8 mg/dL; ref: 15–60 mg/dL) and copper (24 g/dL; ref: 70–140 g/dL), suggesting a diagnosis of Wilson's disease (WD). 24h urine Cu excretion (115 g/24h; 100 g/24h in WD) and 24h urine Cu in a penicillamine test (844 g/24h; 1000 g/24h in WD) showed border-line values for WD diagnosis. In liver biopsy, unspecific features of inflammation and fibrosis were visible, with slightly elevated liver copper (131 g/g dry weight, WD>250 g/g dry weight). Patient's response to routine zinc treatment was abnormal, resulting in borderline or normal ALT, elevated and subsequently normal cholesterol, very low ceruloplasmin and extremely low urine copper. After two years of treatment, the boy was hospitalized because of pallor, anemia, leukopenia and pains in lower limbs. Leukopenia with severe neutropenia was reported. Bone marrow biopsy revealed abnormal erythroid to lymphoid ratio (1.5:1; normal 1:3), characteristic for maturation arrest of erythrocyte precursors. 6 months after cessation of treatment, elevated values for transaminases and cholesterol were found as before Zn treatment. As no mutation could be found in the copper transporter ATP7B, a diagnosis of WD was questioned and further research to explain the chronic hepatitis was initiated, finally resulting in a diagnosis of VMA21-CDG. Currently, the patient is an intelligent 21-yr old man with elevated cholesterol and transaminases and diminished serum copper and ceruloplasmin. His main clinical problem concerns his hip joints which require surgery. X-Ray of his hip joints showed thickening of acetabular roofs with irregular areas of calcification and irregular sclerotic-osteolytic remodeling of femoral heads.

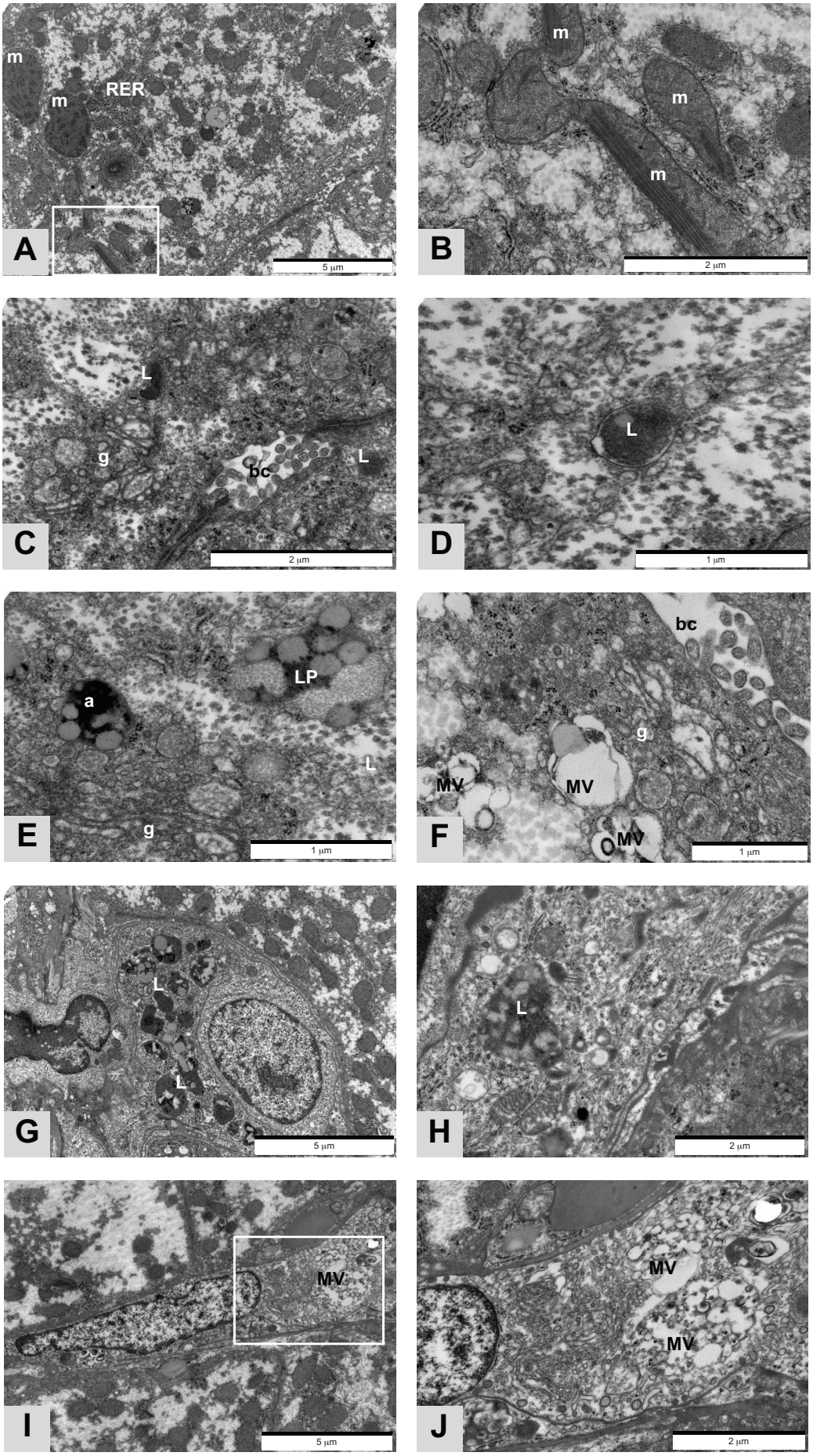
m
m
RER
A
5 µm
m
m
m
B
2 µm
L
g
bc
L
C
2 µm
L
D
1 µm
LP
a
L
g
E
1 µm
bc
g
MV
MV
MV
F
1 µm
L
L
G
5 µm
L
H
2 µm
MV
I
5 µm
MV
MV
J
2 µm

Figure 1: Ultrastructure of hepatocytes and Kupffer cells of a liver biopsy of CDG-P3
(A-B) Hepatocytes with normal RER and giant mitochondria (m) containing crystalloid inclusions (A and box, zoomed-in in B);
(C-F) Hepatocytes showing bile canaliculi (bc) with microvilli filling its lumen (C), dilated Golgi (g), autolysosomes (a), lysosome-like structures (L) or multilamellar bodies (MV) and lipolysosomes (LP) with incorporated bubbles containing fibro-granular material in the bile canalicular zone;
(G-J) Kupffer cells with numerous deposits in form of lysosomes-like (L) or multilamellar bodies (MV).

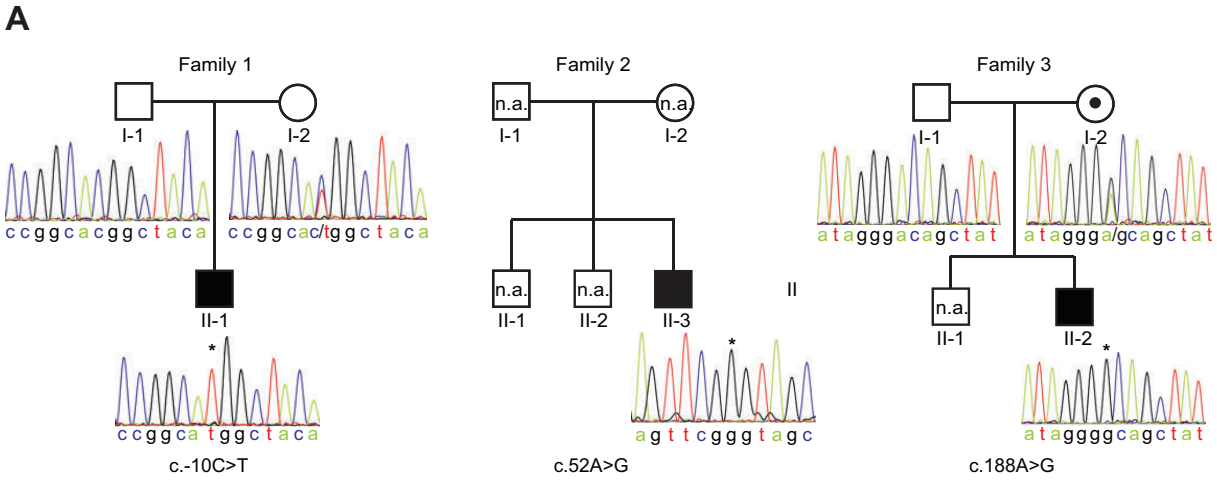
A
Family 1
I-1
I-2
II-1
c.-10C>T
Family 2
n.a.
I-1
n.a.
I-2
n.a.
II-1
n.a.
II-2
II-3
c.52A>G
Family 3
I-1
I-2
n.a.
II-1
II-2
c.188A>G

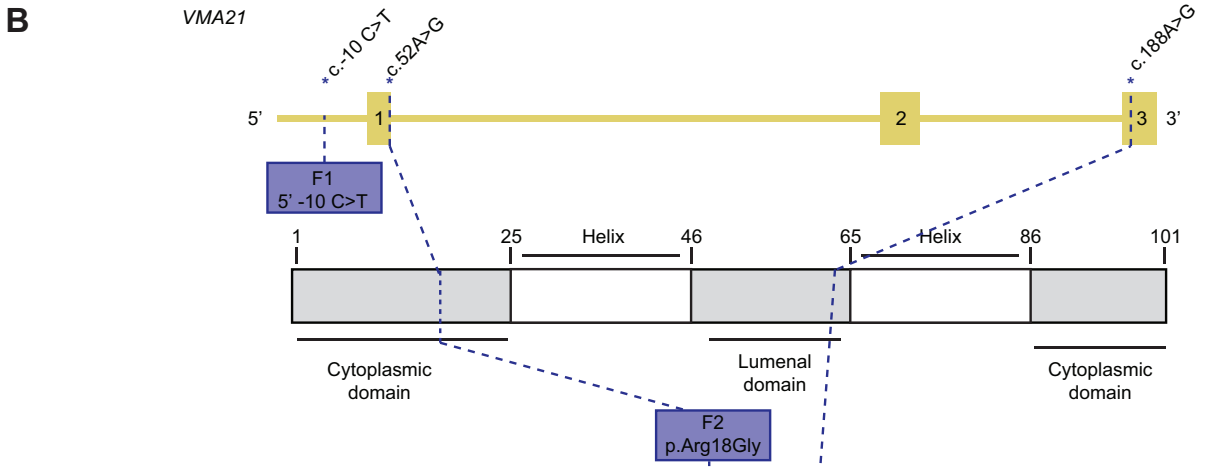
B
VMA21
c.-10 C>T
c.52A>G
c.188A>G
5'
1
2
3
3'
F1
5' -10 C>T
1
25
Helix
46
65
Helix
86
101
Cytoplasmic domain
Lumenal domain
Cytoplasmic domain
F2
p.Arg18Gly

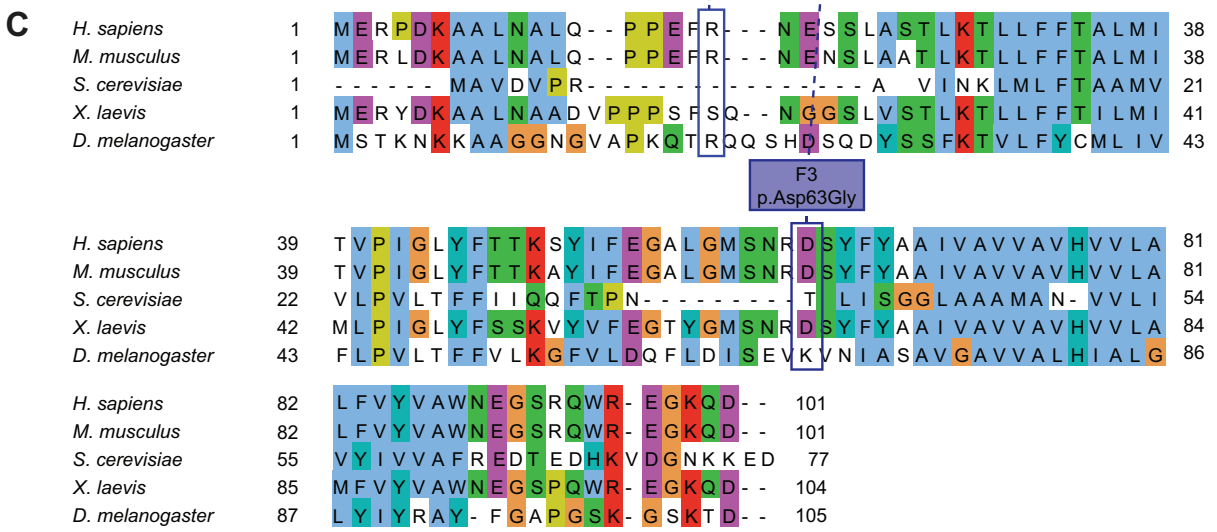
C
F3
p.Asp63Gly
H. sapiens
M. musculus
S. cerevisiae
X. laevis
D. melanogaster

Figure 2: Figure 2: VMA21 mutations cause a congenital disorder of glycosylation

(A) Pedigree and segregation status of VMA21 mutations in families F1, F2 and F3. Partial chromatograms show X-linked segregation for all patients. On the left side, family F1 shows the segregation of the pathogenic mutation in the 5' UTR of VMA21 (c.-10C>T) identified in patient P1 (F1-II-2). In the middle, the pedigree for family F2 shows the segregation of the missense mutation (c.52A>G) to patient P2 (F2-II-3). On the right side, the pedigree for family F3 shows the segregation of the missense mutation (c.188A>G) (F3-II-2). Black-filled squares indicate affected males, black dots in white-filled circles indicate healthy carrier females. The asterisk indicates the nucleotide changes.
(B) Exon structure of human *VMA21* (in yellow) and the domain structure of the encoded protein (in white and grey boxes), the numbers delimiting the different domains refer to amino acids positions. The blue dotted lines indicate the positions of the missense mutations within the families, both at the nucleotide and the protein level (blue boxes).
(C) The sequence alignment shows the conservation of the affected amino acids of VMA21 in *Homo sapiens*, *Mus musculus*, *Xenopus laevis*, *S. cerevisiae* and *D. melanogaster*, respectively. The ER retrieval motif KK*XX* is present only in *S. cerevisiae*.

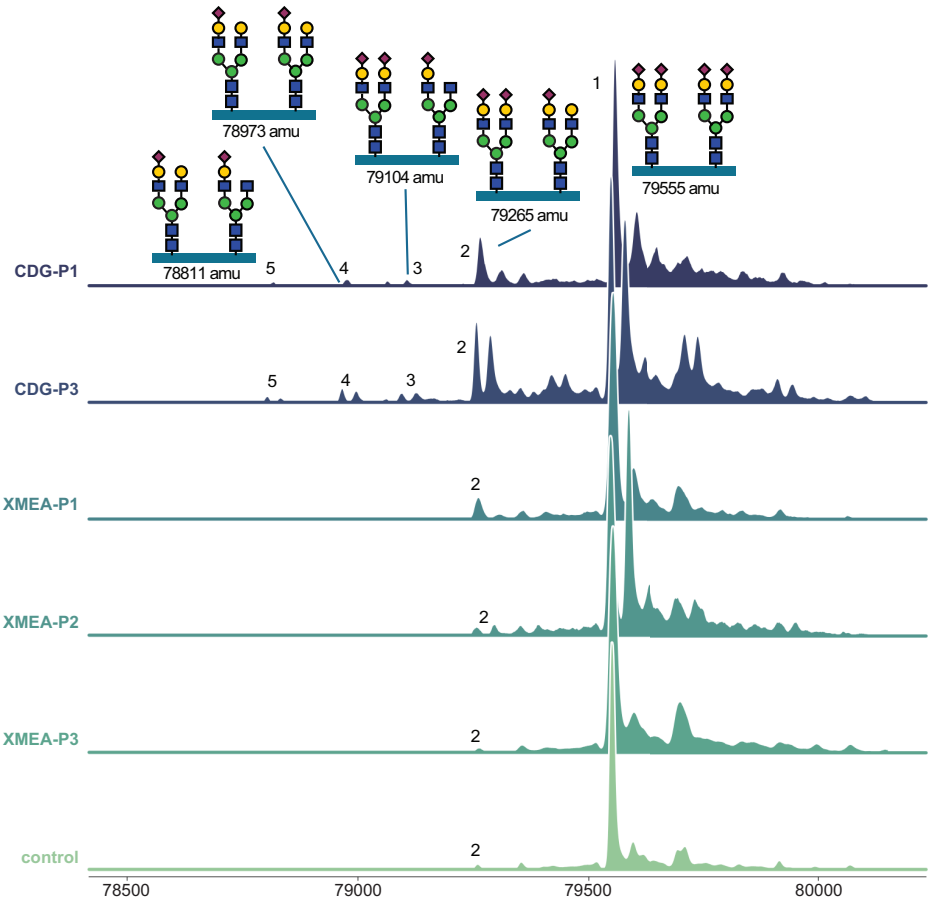

Figure 3: High resolution glycosylation analysis of intact plasma transferrin

N-linked glycans of plasma transferrin were analysed from a healthy individual (control) and patients. Patients included CDG-P1, CDG-P3, XMEA-P1 (c.272C>G), XMEA-P2 (c.*6A>G), and XMEA-P3 (c.164-7T>G). The level of sialic acid loss (peak at 79265 amu) was slightly increased for XMEA-P1 (9%, control <6%).

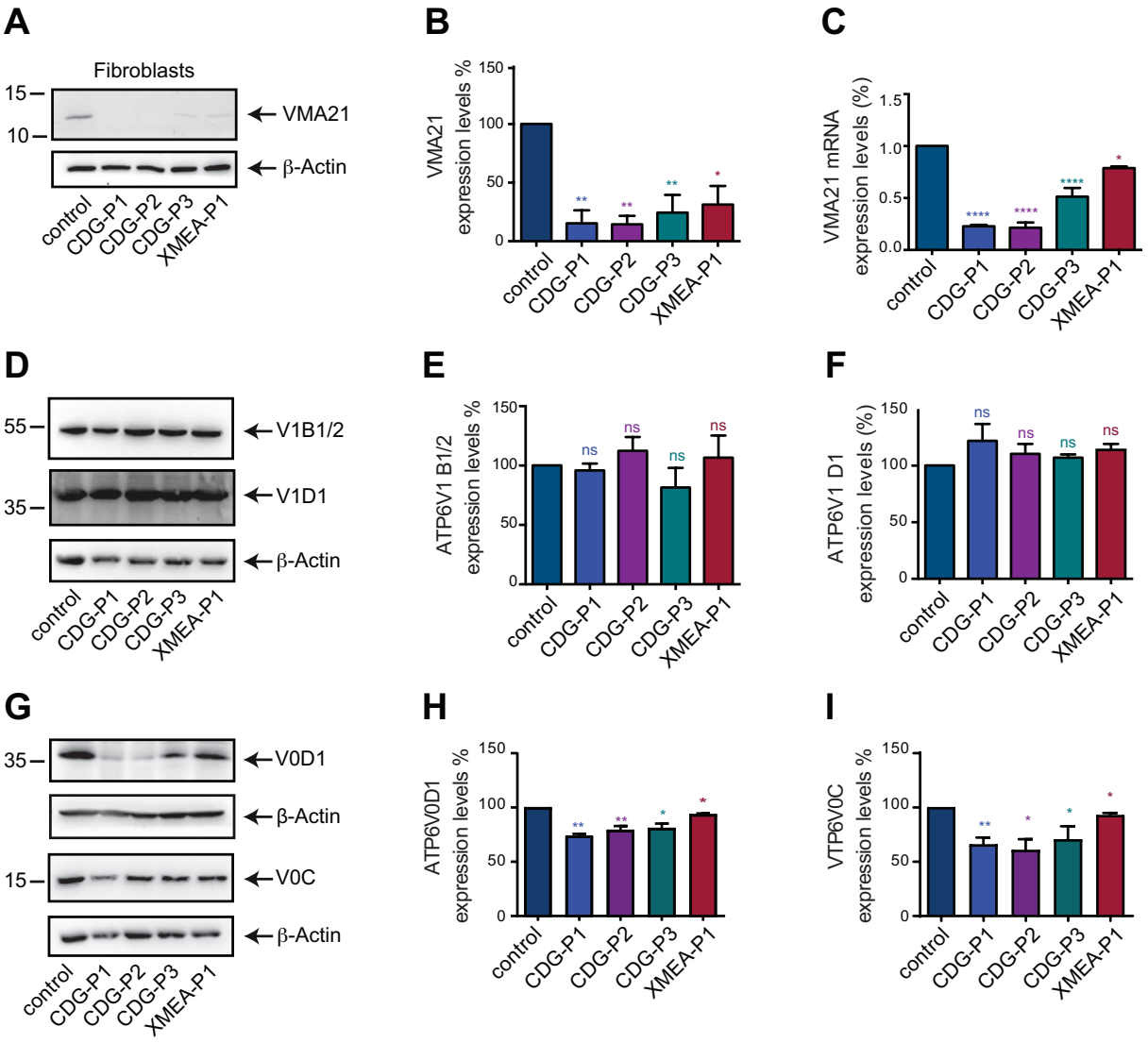

Figure 4: Characterization of the VMA21 mutations

(A, B) Western blot showing the endogenous level of VMA21 in control and patients fibroblasts using anti-VMA21 antibody. Results were normalized to the loading control β-Actin, (n=3).
(C) VMA21 mRNA quantification in control and patients fibroblasts (n=3).
(D-F) Western blot showing the steady state levels of the V1 subunits in control and patients fibroblasts using anti-ATP6V1B1/2 and anti-ATP6V1D1 antibodies. Results were normalized to the loading control β-Actin (n=5 and 4 respectively).
(G-I) Western blot showing the steady state levels of the V-ATPase V_0 subunits in patients fibroblasts compared to control fibroblasts using anti-ATP6V0D1 and anti-ATP6V0C antibodies. β-Actin is used as loading control.
(H, I) Western blot showing the steady state levels of the V_0 subunits in control and patients fibroblasts using anti-ATP6V0D1 and anti-ATP6V0C antibodies. Results were normalized to the loading control β-Actin (n=5 and 3 respectively).
ns, not significant, *, $P < 0.05$, **$P < 0.01$, ****, $P < 0.0001$.

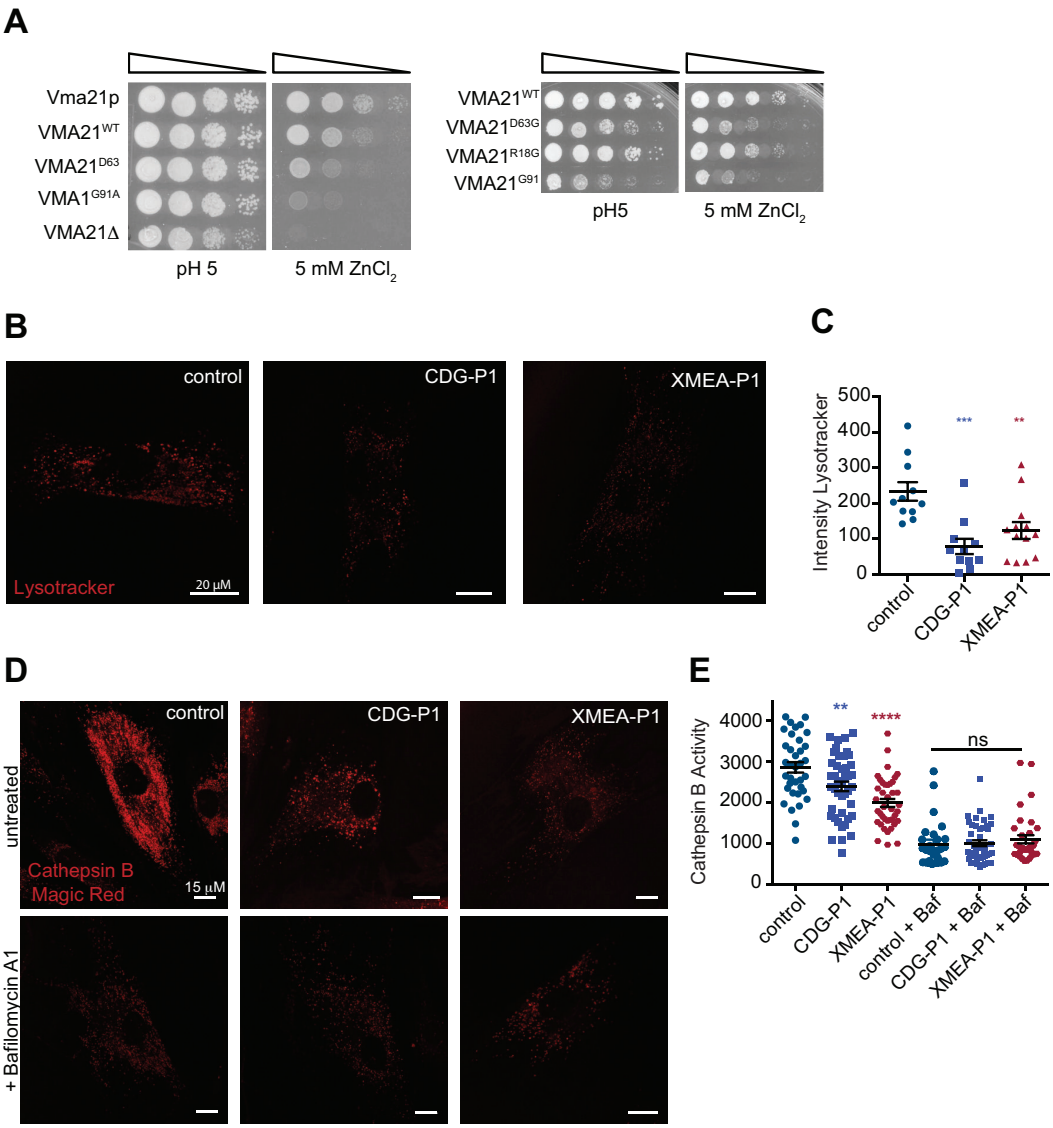

Figure 5: VMA21 mutations cause reduced proton pump function

(A) V-ATPase dependent growth tests on permissive (pH 5) or non-permissive (5 mM ZnCl2) conditions of strains expressing $VMA21^{WT}$, $VMA21^{R18G}$,$VMA21^{D63G}$ and $VMA21^{G91A}$. compared to Vma21p and ΔVma21p.
(B, C) Lysotracker staining of patients fibroblasts CDG-P1 and XMEA-P1 compared to control fibroblasts (n=2, >10 cells/genotype). Scale bars: 20 µm.
(D, E) Magic Red staining for Cathepsin B activity of control and patient fibroblasts, in untreated conditions or upon BafilomycinA1 100 nM treatment (1h) (n=3, >30 cells/genotype). Scale bars: 15 µm.
ns, not significant, **P < 0.01, ***, P < 0.001, ****, P < 0.0001.

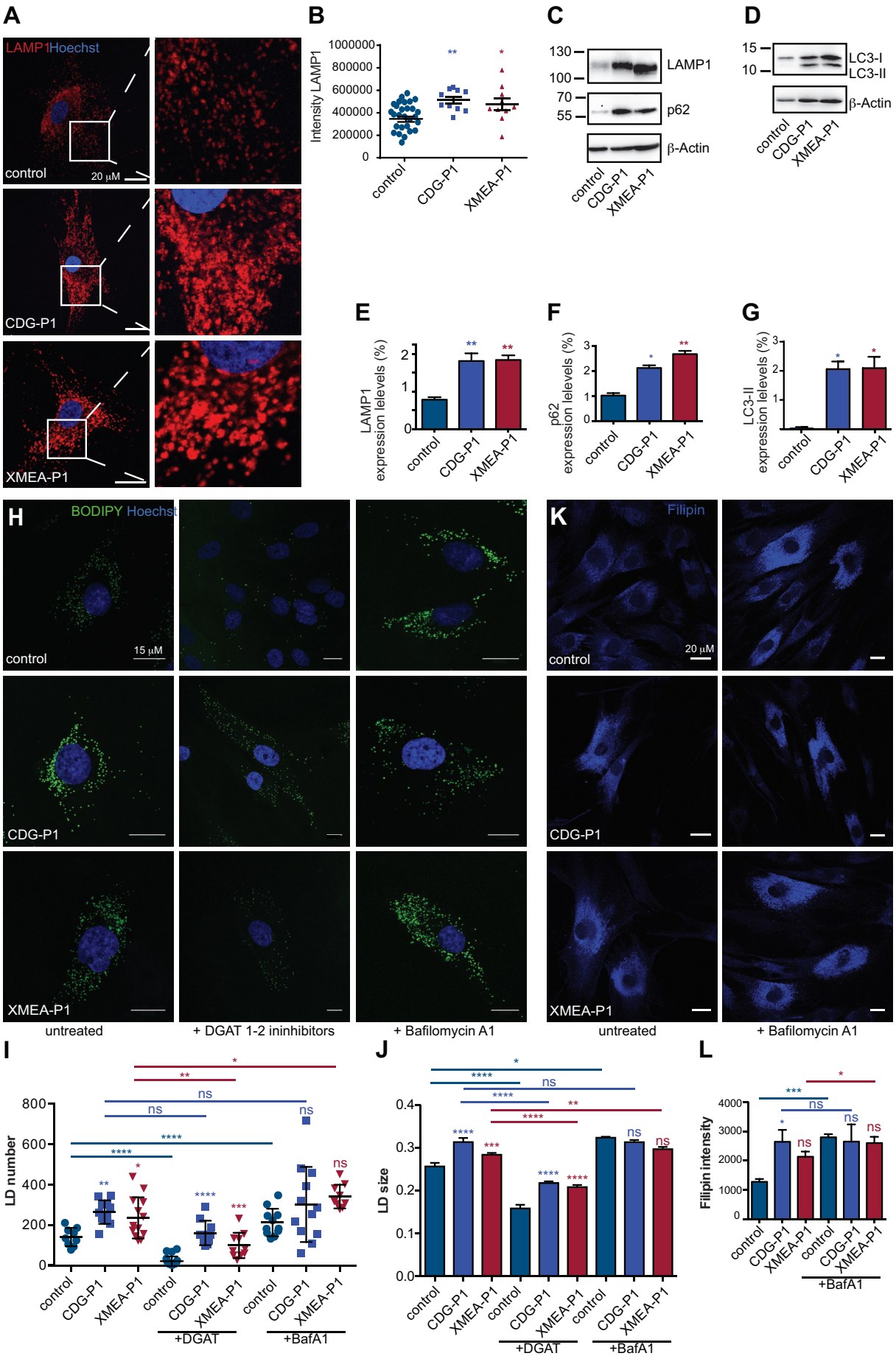
A
LAMP1Hoechst
control
20 µM
CDG-P1
XMEA-P1
B
Intensity LAMP1
1000000
800000
600000
400000
200000
0
control
CDG-P1
XMEA-P1
C
130
100
70
55
LAMP1
p62
β-Actin
control
CDG-P1
XMEA-P1
D
15
10
LC3-I
LC3-II
β-Actin
control
CDG-P1
XMEA-P1
E
LAMP1 expression lelevels (%)
F
p62 expression lelevels (%)
G
LC3-II expression lelevels (%)
H
BODIPY Hoechst
control
15 µM
CDG-P1
XMEA-P1
K
Filipin
control
20 µM
CDG-P1
XMEA-P1
untreated
+ DGAT 1-2 ininhibitors
+ Bafilomycin A1
untreated
+ Bafilomycin A1
I
LD number
+DGAT
+BafA1
J
LD size
+DGAT
+BafA1
L
Filipin intensity
+BafA1

Figure 6: VMA21 deficiency leads to autophagic defects

(A, B) Immunofluorescence analyses of control and patient fibroblasts showing LAMP1-positive vesicles. Scale bars: 20 μm. Right panels are magnifications of the insets demarked in left panels.
(C-G) Western blot of LAMP1, p62 and LC3 in control and patients fibroblasts. Results were normalized to the loading control β-Actin (n= 3, 2, 2).
(H-J) BODIPY staining of LDs in control and patients fibroblasts. The staining was performed in untreated samples, upon treatment with 10 M DGAT 1-2 inhibitors (overnight) or 100 nM Bafilomycin A1 (1h). Scale bars: 15 μm.
(K, L) Immunolabelling of unesterified cholesterol by Filipin staining in control and patient fibroblasts, in untreated samples or upon or 1h 100 nM Bafilomycin A1 treatment (n=3, >10 cells/genotype). Scale bars: 20 μm.
ns, not significant, *, $P < 0.05$, **$P < 0.01$, ***, $P < 0.001$, ****, $P < 0.0001$.

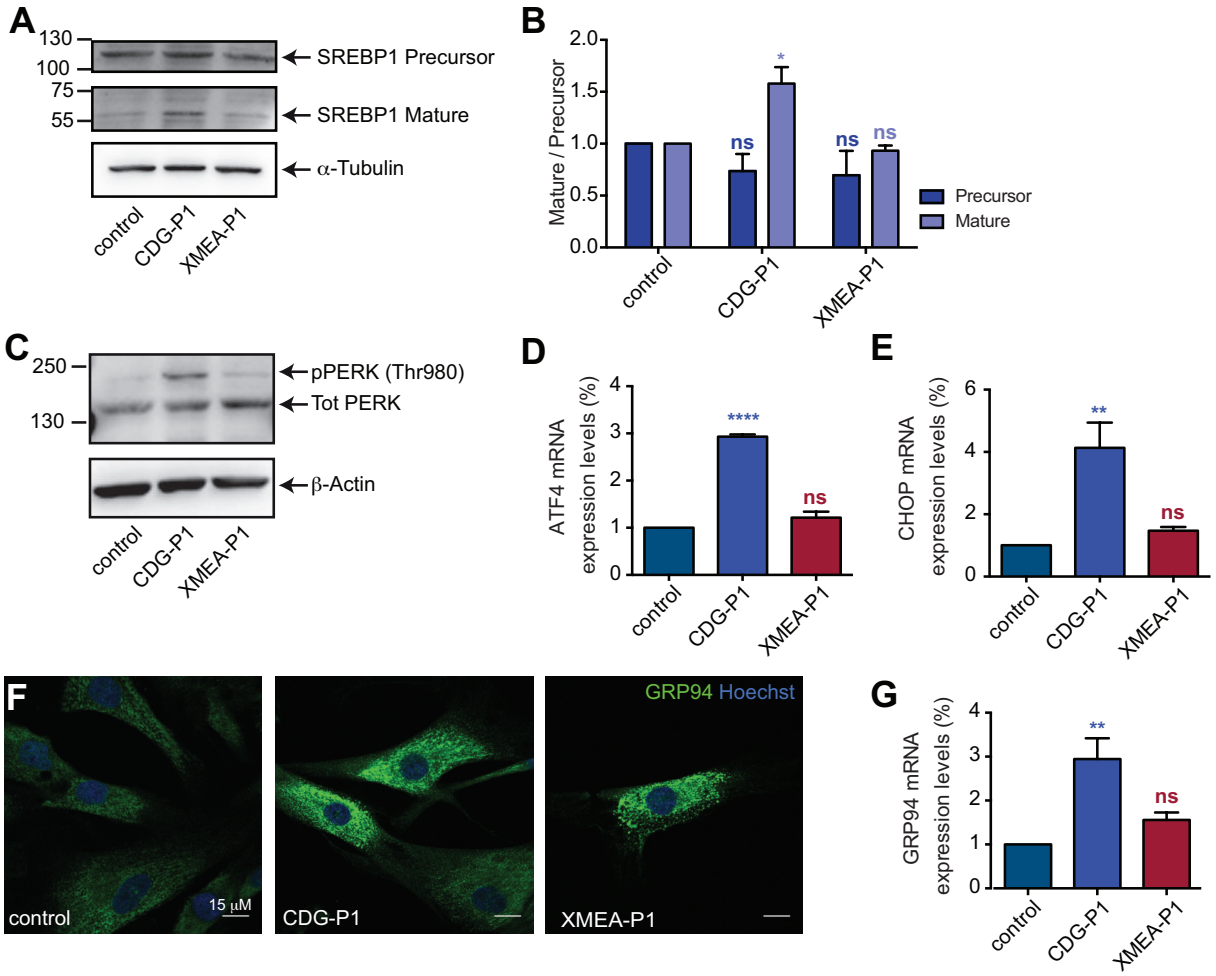

Figure 7: Characterization of the lipid abnormalities in patient fibroblasts

(A, B) Western blot on control and patient fibroblasts showing the full-length (precursor) and the cleaved form (mature) of SREBP1. Results were normalized to the loading control α-Tubulin, (n=3).
(C) Western blot of total and phosphorylated (Thr980) PERK in control and patients fibroblasts. Results were normalized to the loading control β-Actin, (n=3).
(D-E) ATF4 and CHOP mRNA quantification in control and patient fibroblasts (n=3).
(F) GRP94 immunofluorescence analyses in patients fibroblasts compared to control fibroblasts. Scale bars: 15 μm.
(G) GRP94 mRNA quantification in control and patient fibroblasts, (n=3).
ns, not significant, *, $P < 0.05$, **$P < 0.01$, ****, $P < 0.0001$.

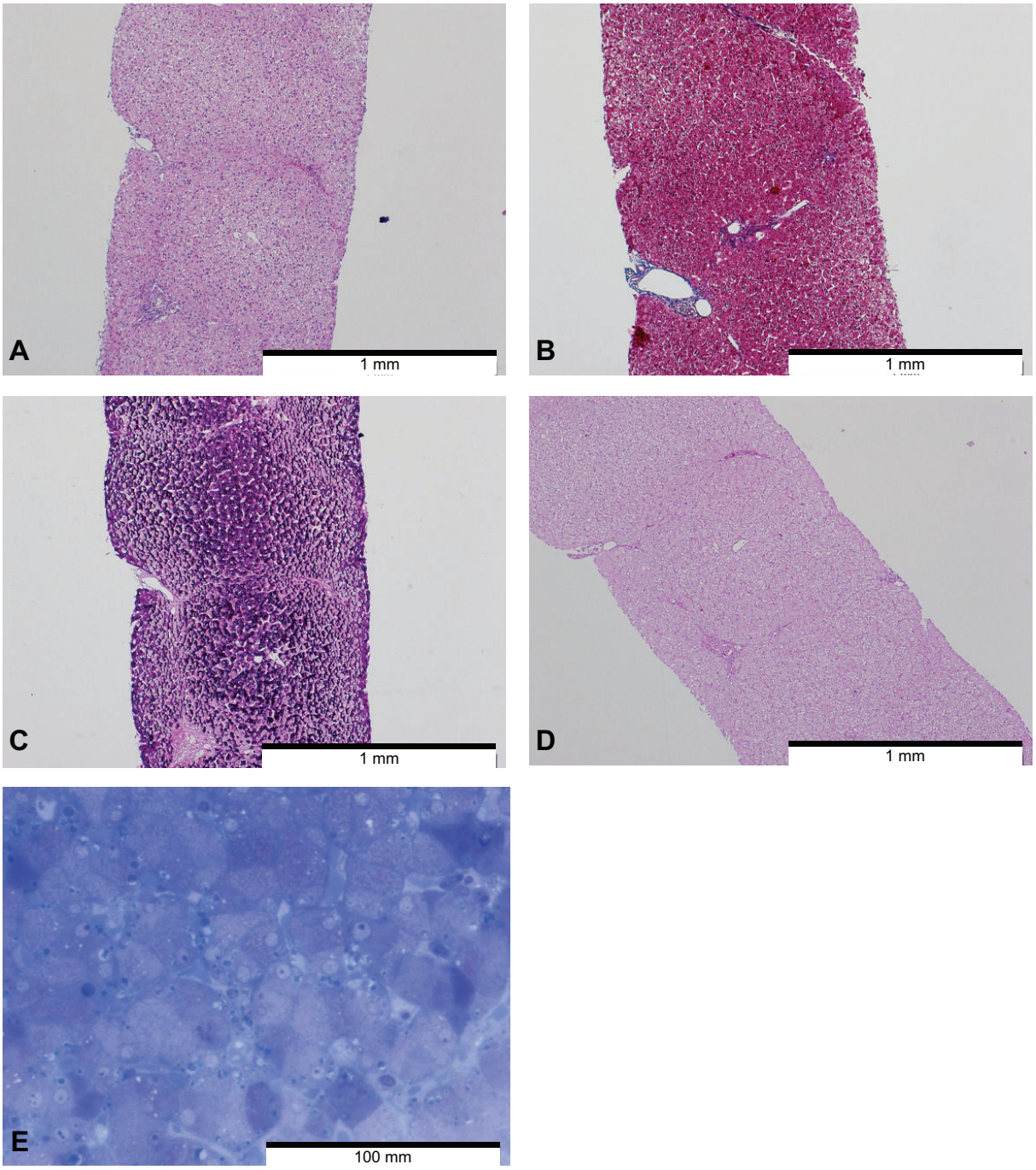

Figure S1: Histology of a liver biopsy of CDG-P3

(A, B) Normal liver architecture without fibrosis (tissue sections stained HE and Masson Trichrome, respectively).
(C, D) Glycogen accumulation in hepatocytes (stained PAS and PAS with diastase, respectively).
(E) Microvesicular steatosis in some hepatocytes (semithin section stained with methylene blue.

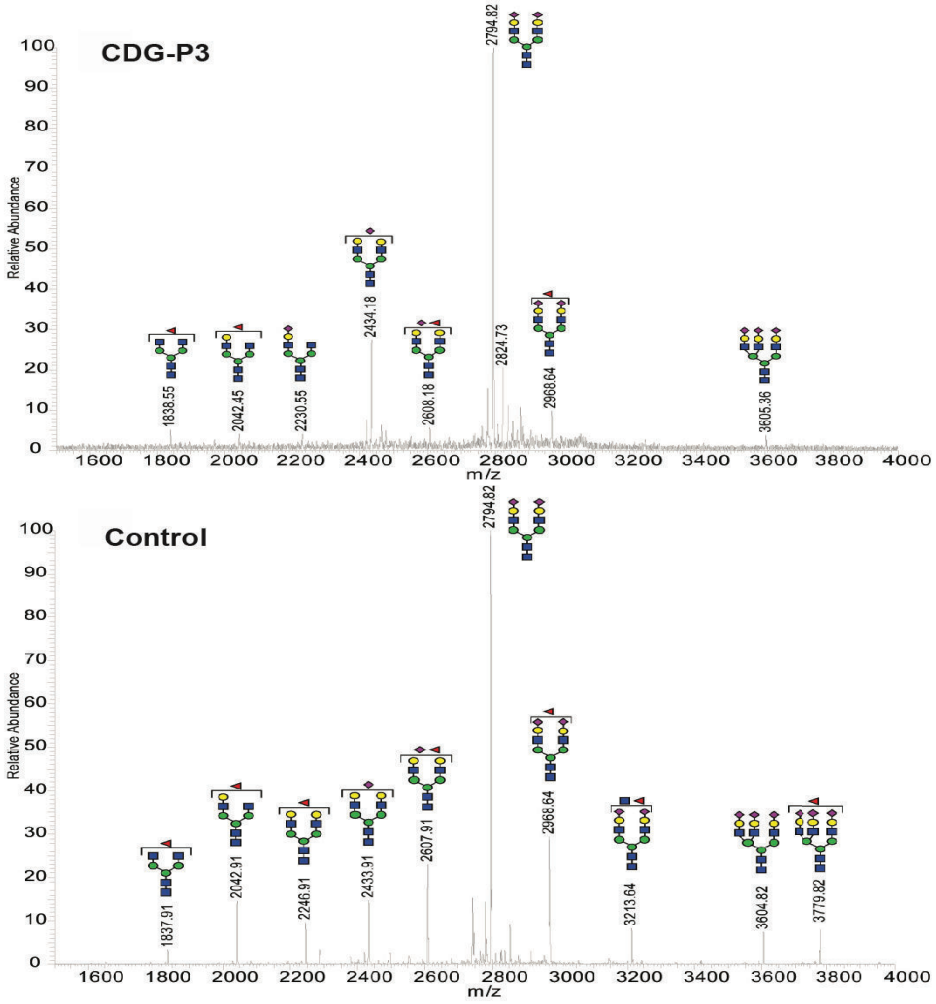

Figure S2: Hypoglycosylation of serum proteins in samples from CDG-P3 compared to hepatopathy

Total serum N-glycan profiling by MALDI-LTQ mass spectrometry show an increase of m/z 2434 of the monosialylated biantennary N-glycan and a minor peak at m/z 2230 of a truncated glycan lacking a galactose-sialic acid disaccharide on one antenna in CDG-P3 (upper panel). In contrast, increased fucosylation (m/z 2607) and bisecting GlcNAc (m/z 3213) is observed in liver disease (control) (lower panel)

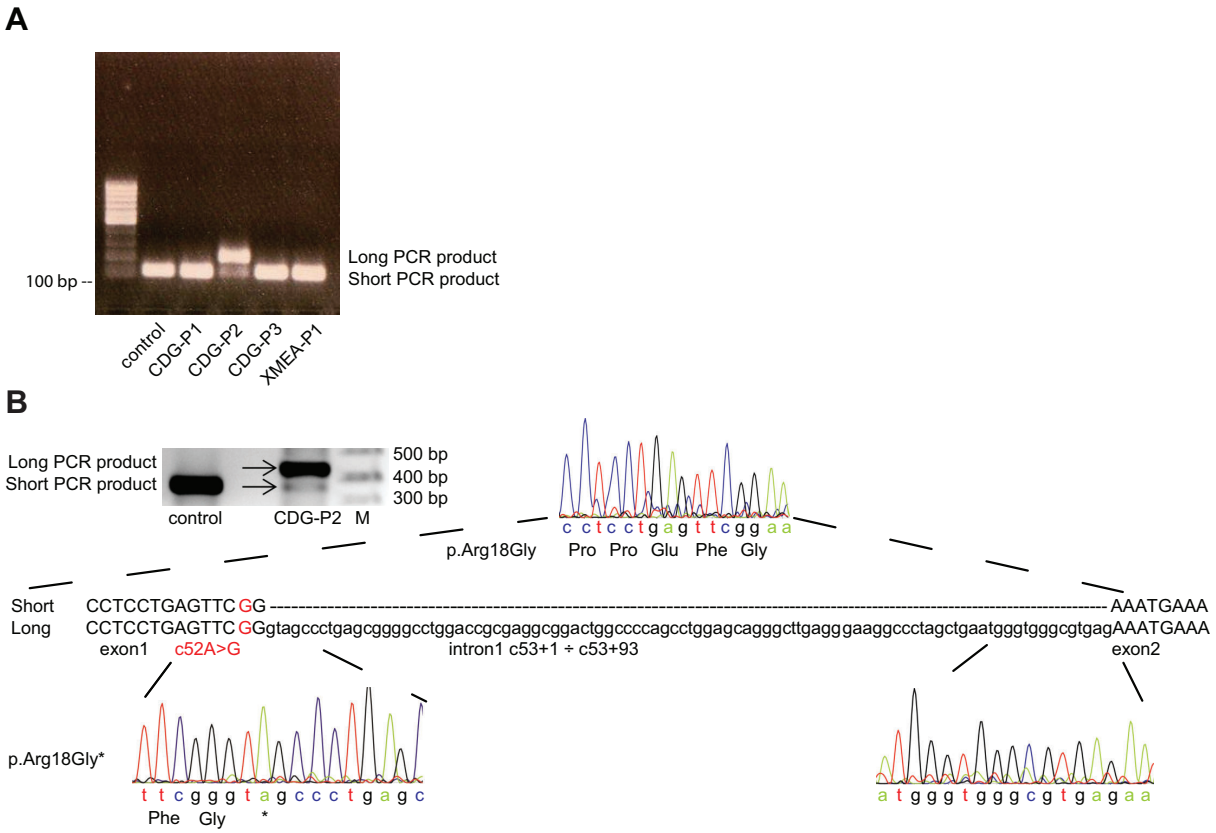

Figure S3: Effects of *VMA21* mutations on the mRNA

(A) RT-PCR on cDNA from control and mutant fibroblasts showing the normal transcript (short PCR product) and a long PCR product in the VMA21 gene for the CDG-P2 (p.Arg18Gly) compared to the control and the other patients.
(B) RT-PCR on cDNA from CDG-P2 compared to control showing that the long PCR product is the consequence of an intronic inclusion in the *VMA21* gene for the CDG-P2 due to a splicing defect (p.Arg18Gly).

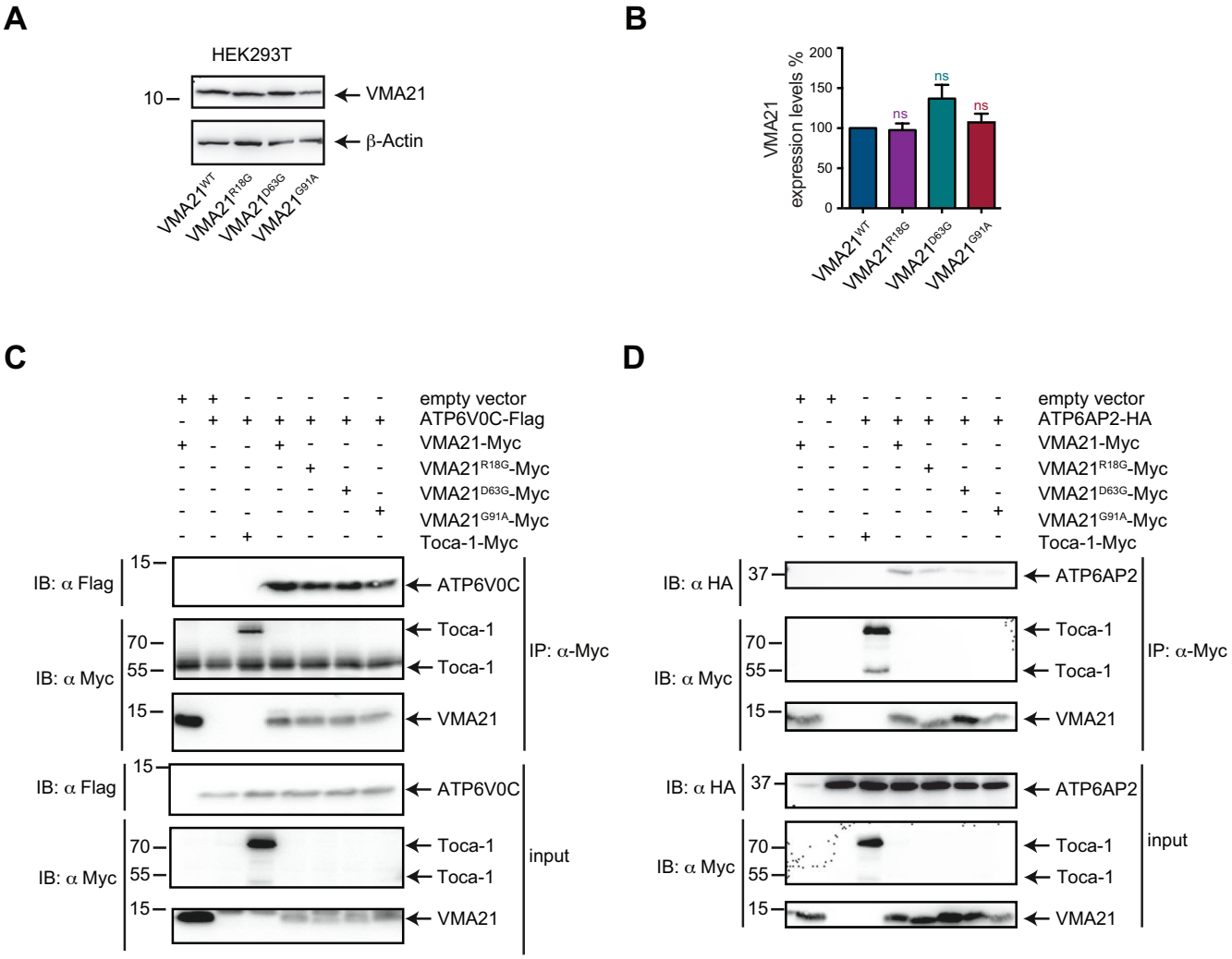

Figure S4: VMA21 mutations impairs V-ATPase assembly in overexpression

(A, B) Western blot showing the expression of Myc-tagged VMA21$^{\mathrm{WT}}$, VMA21$^{\mathrm{R18G}}$, VMA21$^{\mathrm{D63G}}$ and VMA21$^{\mathrm{G91A}}$ in HEK293T cells using anti-Myc antibody. Results were normalized to the loading control β-Actin (n=3).
(C, D) Co-immunoprecipitations in HEK293T cells using the indicated constructs. Proteins were immunoprecipitated with anti-Myc antibody and cell lysates were subjected to immunoblotting with anti-HA, anti-Myc and anti-FLAG antibodies. Lysate inputs of proteins are indicated in the lower panel. Toca-1-Myc is a negative control (n=3).
All data are mean ± SEM, statistical significance was determined by an ordinary one-way ANOVA followed by a Bonferroni multiple comparisons test. ns, not significant.

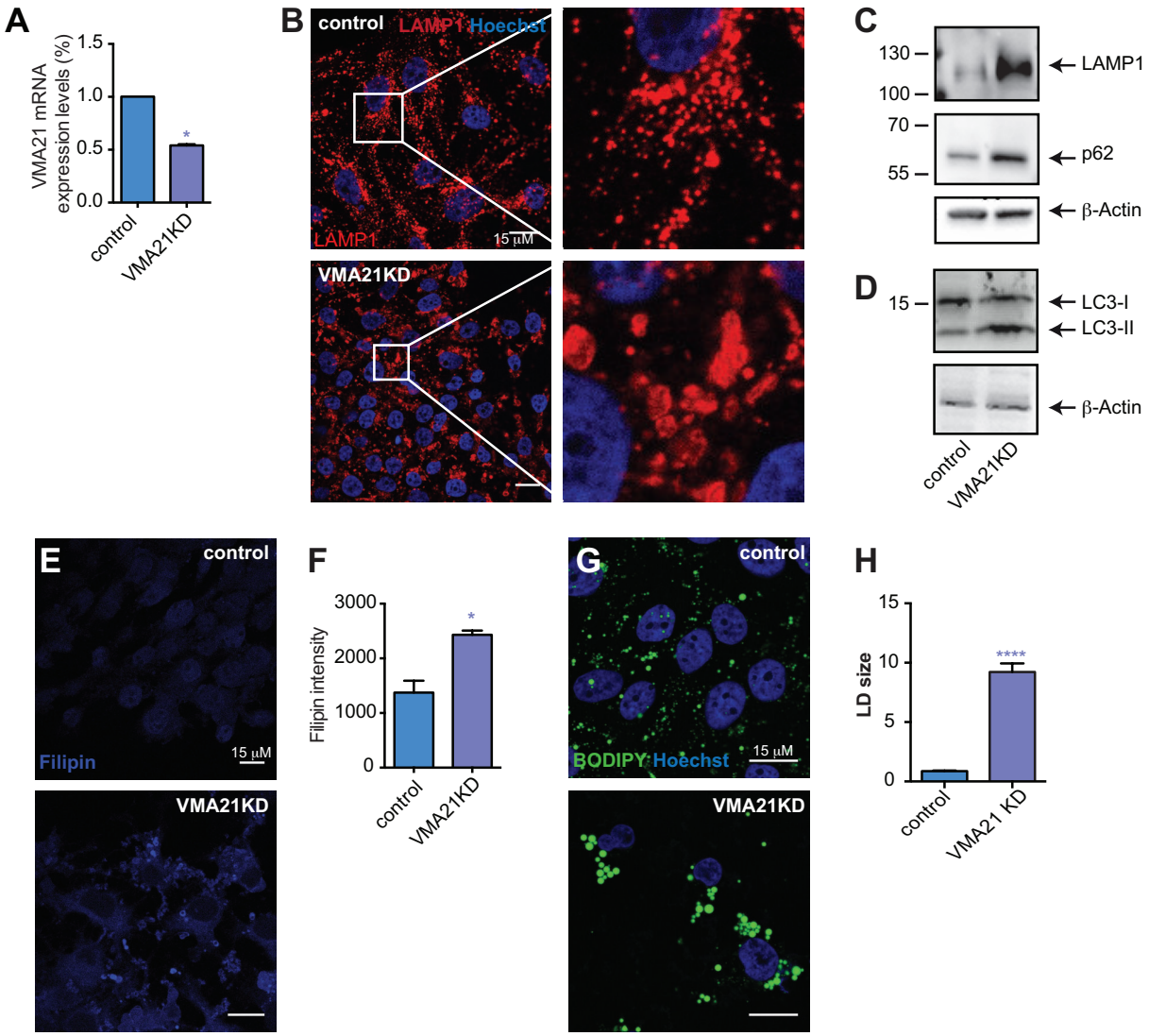

Figure S5: VMA21 KD in hepatocytes Huh7 recapitulates lysosomal/autophagic dysfunction observed in patients fibroblasts

(A) VMA21 mRNA quantification in control siRNA and VMA21 siRNA Huh7 cells. Data are mean ± SEM of three independent experiments.
(B) Immunofluorescence analyses of control siRNA and VMA21KD Huh7 cells showing LAMP1-positive vesicles. Scale bars: 15 µm. Right panels are magnifications of the insets demarked in left panels.
(C, D) Western blot of LAMP1, p62 and LC3 in control siRNA and VMA21KD Huh7 cells. β-Actin is used as loading control.
(E, F) Filipin staining in control and VMA21KD Huh7 cells (n=3, >15 cells/genotype). Scale bars: 15 µm.
(G, H) BODIPY staining in control siRNA and VMA21 siRNA Huh7 (n=3, >6 cells/genotype). Scale bars: 15 µm.
All data are mean ± SEM, statistical significance was determined by Unpaired t test with Mann-Whitney correction. *, $P < 0.05$, ****, $P < 0.0001$.

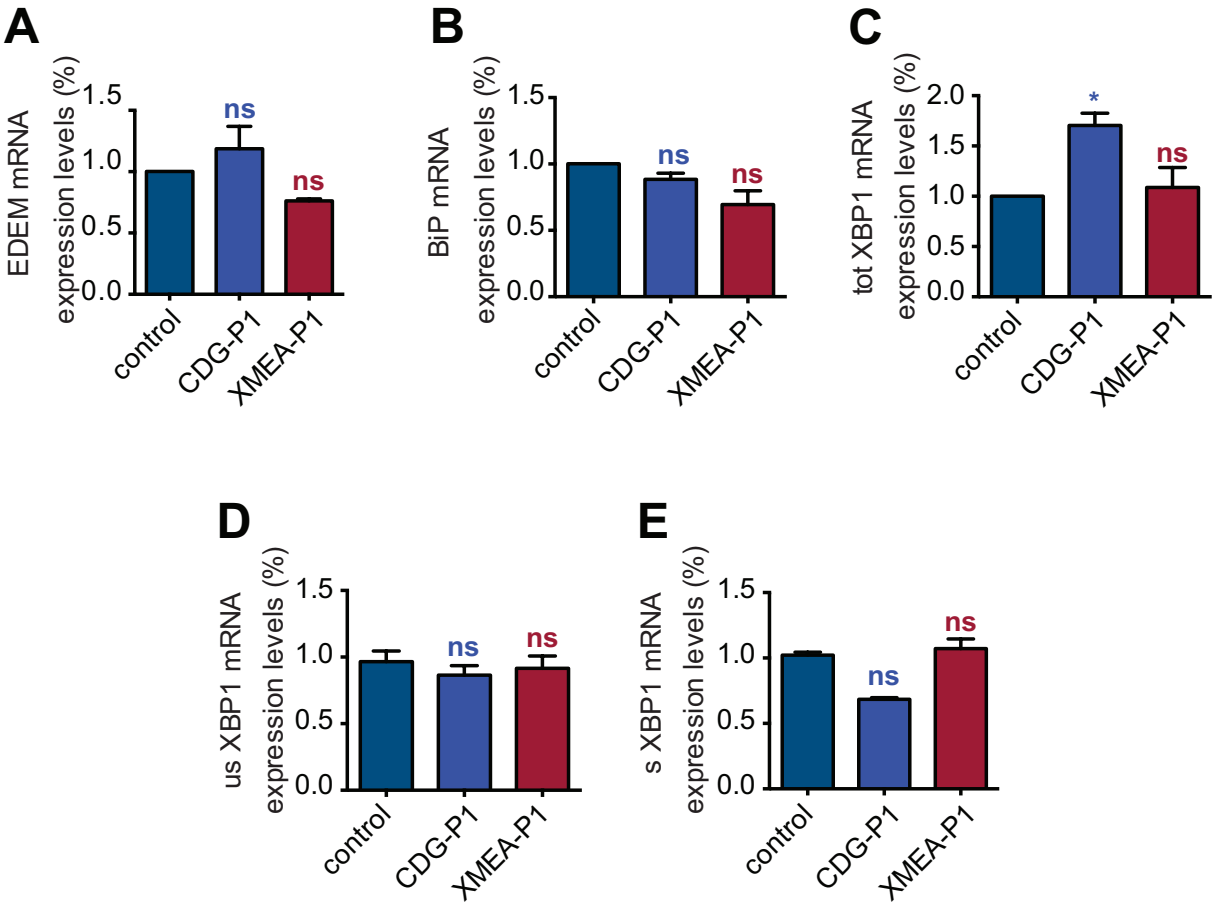

Figure S6: VMA21 mutations selectively activate PERK branch of UPR **(A–E)** mRNA quantification in control, CDG-P1 and XMEA-P1 fibroblasts of EDEM, BiP, totXBP1, unspliced XBP1 (usXBP1) and spliced XBP1 (sXBP1) respectively. All data are mean ± SEM of three independent experiments. ns, not significant, *, $P < 0.05$. The statistical significance was determined by Unpaired t test with Mann-Whitney correction.

	Age of sampling	N-glycosylation by isofocusing of Transferrin									Mucin O-glycosylation by isofocusing of ApoCIII		
		Trf-0	Trf-1	Trf-2	Trf-3	Trf-4	Trf-5	Trf-6			ApoCII I-0	ApoCII I-1	ApoCIII-2
CDG-P1	4 months	4.4	10.7	20.1	27.9	274	8.6	1			8	73.3	18.7
	8 months	1.1	2.5	7.7	20.6	51.3	14.7	2.1			4.6	75.7	19.7
	4 yr. 3 months	0.8	1.7	10.2	25.3	45.9	13.5	2.5			7.0	78.6	14.4
CDG-P3	11 yr. 3 months	1.5	2.3	8.8	25.2	45.2	14.3	2.6			3.8	76.4	19.8
	11 yr. 5 months	1.8	2.6	9.2	24.1	45.2	14.3	2.7			2.9	78.6	18.5
XMEA-P1	**c.272C>G**	0.3	0.5	3.3	12.8	63.6	16	3.5			4.3	66.1	29.6
XMEA-P2	**c.164-7T>G**	0.9	2.1	2.9	7.3	65.5	17.6	3.9			n/a	n/a	n/a
Control range		0-3	0-5.8	2.5-9.8	3.4-13.7	43.7-68.1	14.5-27	3.2-11.6	0-1 yr		0.2-4.5	42.7-69.8	26.2-56.7
		0-3.2	0-5	3.3-7.6	4.9-10.6	47.3-62.7	18.7-31.5	3.2-7.8	1-18 yr		1.4-9.5	48.5-75.2	21-45.8

Table S1: Screening results for CDG-P1 and CDG-P3

Chr.	Genomic position [hg19]	Reference nucleotide	Variant nucleotide	Coverage	Variant reads	% Variant reads	SNP ID	SNP Frequency [%]	In-house db	Gene	Isoform ID	Strand	cDNA position	Protein position	PhyloP	Grantham Score
Homozygous variants:																
chr7	95434097	C	A	6	5	83.3			7	DYNC1I1	NM_004411	+	56C>A	A19E	5.787	107
chrX	14869050	G	A	45	4	95.6	rs1416	0.0297	0	TMEM185	NM_032508	-	230G>A	T77M	5.582	81
chr4	10047936	C	T	7	6	85.7			0	TRMT10A	NM_152292	-	194C>T	R65Q	4.474	43
chrX	15057341	A	G	14	1	100			0	VMA21	NM_001017	+	188A>G	D63G	4.387	94
chrX	54161277	C	G	10	8	80			3	FAM120C	NM_017848	-	1603C>G	G535R	2.71	125
chrX	44107568	T	C	5	5	100			0	EFHC2	NM_025184	-	1061T>C	Y354C	2.377	194
chr9	13186649	G	C	7	7	100	rs1482	0.04	8	CRAT	NM_000755	-	384G>C	D128E	1.65	45
chrX	63488716	C	T	19	1	100	rs1423	0.0149	3	MTMR8	NM_017677	-	1816C>T	A606T	0.097	58
chr10	46143736	G	A	31	2	83.9	rs2017	0.1163	2	ZFAND4	NM_001282	-			-0.171	0
chr11	60689464	C	G	5	5	100			1	TMEM109	NM_024092	+	559C>G	L187V	-1.839	32
chrX	10185820	C	G	32	3	100	rs2001	NA	0	ARMCX5	NM_001168	+	1134C>G	D378E	-2.17	45
Possible compound heterozygous variants																
chr4	85598550	C	A	24	7	29.2			0	WDFY3	NM_014991	-			5.593	0
chr4	85758147	C	T	37	1	43.2			0	WDFY3	NM_014991	-	511C>T	G171R	3.974	125
chr12	53225280	C	T	81	2	30.9	rs1448	0.09	12	KRT79	NM_175834	-	608C>T	R203Q	3.026	43
chr12	53225365	C	A	20	5	25			0	KRT79	NM_175834	-	523C>A	A175S	2.434	99
chr10	12990990	G	A	98	4	41.8	rs3707	0.0116	0	MKI67	NM_002417	-			0.466	0
chr10	12989753	A	G	13	6	46.2			2	MKI67	NM_002417	-			-1.272	0
chr20	58476737	A	C	60	1	21.7			7	SYCP2	NM_014258	-	1162A>C	F388V	3.007	50
chr20	58443989	C	T	88	3	34.1	rs2012	0.0465	2	SYCP2	NM_014258	-			-0.696	0

Chr. = Chromosome; SNP ID = dbSNP137 identifier; NA= No frequency information available; In-house db = In-house database count in >5000 exomes; PhyloP = 46 vertebrate PhyloP score

Table S2: Prioritized variants from whole exome sequencing (WES) of CDG-P3

	Patient	CDG-P1	CDG-P2	CDG-P3
Mutation	genomic	ChrX(GRCh37):g.150565771C>T	ChrX(GRCh37):g.150565832A>G	ChrX(GRCh37):g.150573412A>G
	cDNA or mRNA	NM_001017980.3(VMA21):c.-10C>T	NM_001017980.3(VMA21):c.52A>G; r.[52A>Gins 53+1_53+93]	NM_001017980.3(VMA21):c.188A>G
	protein	N/A	p.(Arg18Gly); (Arg18Gly*)	p.(Asp63Gly)
	Missense pathogenicity prediction			
Algorithm	AlignGVGD	N/A	Class C0* (GV: 242.22 - GD: 3.24)	Class C65* (GV: 0.00 - GD: 93.77)
	SIFT	N/A	Deleterious (score: 0.03)	Deleterious (score: 0)
	MutationTaster	N/A	Disease causing (p-value: 0.913)	Disease causing (p-value: 1)
	PolyPhen-2	N/A	BENIGN with a score of 0.295	PROBABLY DAMAGING with a score of 0.997
	Prediction of effect on splicing			
Algorithm	SpliceSiteFinder	-	Loss of 5' splicing site	-
	MaxEntScan	-	Loss of 5' splicing site	-
	NNSPLICE	-	Loss of 5' splicing site	-
	GeneSplicer	-	-	-
	Human Splicing Finder	-	New 5' splicing site at position c.47-48	-
	EX-SKIP	-	Exon skipping	-

***** GVGD: Grantham Variation Grantham Deviation; classified from most likely to interfere with function (C65) to least likely (C0).

Table S3: Pathogenicity predictions of the *VMA21* missense mutations

Table S4: List of primers

AA092	Fw	TTCCCTCGCGGAGCTTACTG
AA093	Rev	CAAATCAGATGGCCCCCTCC
VMA21 exon 1	Fw	tgtaaaacgacggccagtATGCACTTGGTCCAATTACCTGCG
VMA21 exon 1	Rev	caggaaacagctatgaccAGCTGCAAGTCGCTGGTGATGTGGC
VMA21 exon 2	Fw	tgtaaaacgacggccagtTCCTCCTGCATAGCATCTCA
VMA21 exon 2	Rev	caggaaacagctatgaccGGAAAACTGTCAAGCTGAAACA
VMA21 exon 3	Fw	tgtaaaacgacggccagtACTTTGCTGGCCCTGAGAAT
VMA21 exon 3	Rev	aggaaacagctatgaccAGCATTCCAGCGTAAAGTGG
M13 tail	Fw	TGTAAAACGACGGCCAGT
M13 tail	Rev	CAGGAAACAGCTATGACC
VMA21^{R18G}Myc	Fw	GAGTTCggaAATGAAAGCTCATTAGCATCTACAC
VMA21^{R18G}Myc	Rev	CATTTCCGAACTCAGGAGGCTGCAGTGCGTTCAGC
VMA21^{D63G}Myc	Fw	ATAGGggcAGCTATTTTTACGCTGCTATTGTTGC
VMA21^{D63G}Myc	Rev	TAGCTGCCCCTATTGGACATCCCAAGGGCGCC
VMA21^{G91A}Myc	Fw	ATGAAgccTCACGACAGTGGCGTGAAGGCAAACAGG
VMA21^{G91A}Myc	Rev	CGTGAGGCTTCATTCCAGGCCACATACACAAAGAGG
VMA21 RT-PCR exon 1	Fw	TGGAGCGCCCGGATAAGG
VMA21 RT-PCR exon 2	Rev	GAAGAACAGGAGCGTCTTCAG
sXBP1	Fw	CTGAGTCCGAATCAGGTGCAG
sXBP1	Rev	ATCCATGGGGAGATGTTCTGG
usXBP1	Fw	CAGCACTCAGACTACGTGCA
usXBP1	Rev	ATCCATGGGGAGATGTTCTGG

Total XBP1	Fw	TGGCCGGGTCTGCTGAGTCCG
Total XBP1	Rev	ATCCATGGGGAGATGTTCTGG
ATF4	Fw	GTTCTCCAGCGACAAGGCTA
ATF4	Rev	ATCCTGCTTGCTGTTGTTGG
CHOP	Fw	AGAACCAGGAAACGGAAACAGA
CHOP	Rev	TCTCCTTCATGCGCTGCTTT
BiP	Fw	TGTTCAACCAATTATCAGCAAACTC
BiP	Rev	TTCTGCTGTATCCTCTTCACCAGT
GRP94	Fw	GAAACGGATGCCTGGTGG
GRP94	Rev	GCCCCTTCTTCCTGGGTC
EDEM	Fw	CAAGTGTGGGTACGCCACG
EDEM	Rev	AAAGAAGCTCTCCATCCGGTC

Discussion

Summary of the Findings and Discussion

Mutations in the ER assembly factors form a new subgroup of metabolic diseases with autophagic defects, impaired glycosylation and liver steatosis: solving the function of the enigmatic ATP6AP2 protein

In this project, whole exome sequencing (WES) was performed on a small cohort of unsolved CDG patients presenting *N*- and *O*-glycosylation defects. This analysis allowed us and our collaborators to identify two missense mutations in the *ATP6AP2* gene.

The mutations. So far, mutations in *ATP6AP2* have not been implicated in any glycosylation disorder. Previously, exon-skipping variants have been described in X-linked mental retardation and epilepsy (XMRE) and X-linked parkinsonism with spasticity (XPDS) (**Ramser *et al.*, 2005; Korvatska *et al.*, 2013**). Both mutations are caused by silent mutations in the exon 4 of ATP6AP2, in a putative exonic splice enhancer (ESE) site and lead to partial skipping of the exon 4, with up to 50% of wild type protein expression (**Ramser *et al.*, 2005; Korvatska *et al.*, 2013**). ATP6AP2 is a type I transmembrane protein synthesized as a full-length protein in the ER. It is formed by a large extracellular domain harboring a cleavage site, a transmembrane domain and short C-terminal tail, harboring a R*x*K*xx* ER retrieval motif that mediates the retrograde transport of ATP6AP2 to the ER (**Nilsson *et al.*, 1989; Schefe *et al.*, 2006; Sihn *et al.*, 2013**). ATP6AP2 molecules that are not transported back to the ER undergo a double cleavage, mediated by S1P and furin. The cleavage allows to the formation of two different fragments, the extracellular NTF and the short CTF, containing the transmembrane domain (**Nakagawa *et al.*, 2017**). In collaboration with the groups of G. Mathijs (Leuven) and T. Marquardt (Münster), we identified two novel hemizygous mutations in *ATP6AP2*. Both mutations are localized in the same functional domain, the cleavable extracellular domain. While the previous described mutations lead to a partial exon-skipping of exon 4, the missense mutations are both localized in the coding region of third exon of the gene. Although a crystallographic structure of the protein is not available, the two residues

are only 27 amino acids apart, suggesting that both positions could be involved in the interaction with the same protein.

The phenotype. The predominant symptoms of the patients carrying the new missense mutations in *ATP6AP2* are hepatopathy and immunodeficiency. P1 suffered from hepatosplenomegaly with increased liver transaminases AST and ALT, recurrent infections with low levels of Igs, decreased level of CD4+ and increased levels of CD8+ lymphocytes. Also P2 presented with hepatosplenomegaly with elevated serum cholesterol and mildly elevated transaminases AST and ALT, recurrent pulmonary and upper respiratory tract infections with reduced IgG1 and IgG3. P3 showed liver failure at 5 months. Although he has repeatedly suffered from infections, his immunological status appears to be normal. Additional clinical features for the ATP6AP2 patients are *cutis laxa* (P1, P2 and P3), dysmorphic features (P1 and P2), mild intellectual disability (P1 and P2), and mild ataxia (P2).

The glycosylation defects. Based on the transferrin IEF and on HPLC analysis, all the ATP6AP2 patients show a CDG type II with decreased tetrasialotransferrin and increased tri-, di- and monosialotransferrin. Moreover, MALDI-TOF mass spectrometry confirmed the increase of undersialylated glycans in P1. Interestingly, the analysis of one boy carrying the exon skipping mutation revealed a normal transferrin glycosylation profile and only a slight undersialylation of total serum proteins. The last observation suggested that both missense mutations are stronger than the partial exon-skipping mutation or are acting through a different molecular mechanism.

Pathomechanisms of *ATP6AP2* mutations

Over the years, numerous functions have been associated with ATP6AP2: (i) prorenin receptor in the RAS system (**Nguyen *et al.*, 2002**), (ii) interactor in the canonical and non-canonical Wnt pathways (**Amsterdam *et al.*, 2004; Buechling *et al.*, 2010; Cruciat *et al.*, 2010; Hermle *et al.*, 2010, 2013**), (iii) accessory subunit of the V-ATPase (**Ludwig *et al.*, 1998; Amsterdam *et al.*, 2004; Cruciat *et al.*, 2010; Kinouchi *et al.*, 2010, 2013**), (iv) non-autonomous effects of the cleaved ECD s(P)RR) (**Bader, 2007**). Our analysis carried out *in vitro*, in patients fibroblasts and in HEK293T cells, and *in vivo*, in *Drosophila* (only for the mutation p.L98S, because the p.Arg71 is not conserved), not only confirmed the pathogenicity of the mutations but also suggested an important function in V_0 assembly, which may even explain many of the abovementioned functions.

(i) In *Drosophila*, the complete knockout of *ATP6AP2* (*ATP6AP2Δ1* null allele) leads to embryonic lethality (**Hermle *et al.*, 2013**), similar to the constitutive mouse *ATP6AP2* knockout (**Kaneshiro *et al.*, 2006**). The expression of $ATP6AP2^{L98S}$ in the background of the *ATP6AP2Δ1* null allele was not able to rescue the viability: $ATP6AP2^{L98S}$ impaired the transition from *larva* to *pupa* and significantly reduced the

percentage of adults eclosing from the pupal case.

(ii) In patients fibroblasts, ATP6AP2^{L98S} is an hypomorphic mutation, with reduced protein and mRNA expression, while ATP6AP2^{R71H} is normally expressed. In overexpression in HEK293T, both mutations reduced the protein expression because of instability of the proteins. Indeed, chase assays performed by using cycloheximide, a eukaryote protein synthesis inhibitor, showed that both mutant proteins have a shorter half-life. Previous studies in *Saccharomyces cerevisiae* have shown that lack of the ER assembly factors (e. g. Vma21p or the complex Vma12p/Vma22p) leads to misassembly of the V_0 subunits, that are rapidly degraded via the ERAD pathway, by which misfolded transmembrane proteins are targeted for proteasomal degradation via retro-translocation into the cytoplasm. Accordingly, inhibition of ERAD, through the expression of a dominant-negative version of the crucial protein p97 (**Ye *et al.*, 2001**), caused a significant accumulation of ATP6AP2^{L98S}, while it did not affect the levels of ATP6AP2^{R71H}. ATP6AP2^{L98S} also showed reduced levels of the cleavage products, suggesting a defective export out of the ER, while ATP6AP2^{R71H} had a normal cleavage.

(iv) In patient fibroblasts and upon overexpression in HEK293T cells, ATP6AP2^{L98S} exhibited an additional slower migrating band, sensitive to treatment with the *N*-glycosidases endoglycosidase H (Endo H) and peptide-*N*-glycosidase F (PNGase F) revealing that a fraction of ATP6AP2^{L98S} is *N*-glycosylated (PNGase F sensitivity) and localized in the ER (Endo H sensitivity). It has been shown that misfolded proteins can be post-translationally *N*-glycosylated by oligosaccharyltransferase (OST) complexes STT3B-containing (**Sato *et al.*, 2012; Cherepanova *et al.*, 2016**). We found that the glycosylation of the slower band of ATP6AP2^{L98S} is mediated by the STT3B complex, suggesting that ATP6AP2^{L98S} is misfolded and undergoes to post-translational *N*-glycosylation in the ER.

(v) Localization studies confirmed ER and Golgi localization for ATP6AP2^{WT} and ATP6AP2^{R71H}, while ATP6AP2^{L98S} is localized primarily to the ER.

Altogether these results suggest the following scenario: the p.L98S mutation is a hypomorphic mutation with reduced mRNA and protein expression. The remaining expressed protein is misfolded and accumulates in the ER. Here, the protein is rapidly post-translationally *N*-glycosylated by the OST complex STT3B and undergoes to retro-translocation and degradation via proteasome. Accordingly, in whole *Drosophila* animal the expression of *ATP6AP2^{L98S}* is not able to rescue the viability of *ATP6AP2Δ1* null alleles. In addition, our results pinpoint, for the first time, a new function in V_0 assembly, mediated by the ER retrieval motif (KIRMD in humans and KKDN in *Drosophila*) and carried by the uncleaved full-length protein.

(i) We generated a construct harboring a mutation in the ER retrieval signal, ATP6AP2^{QxQxx}. In overexpression in HEK293T, ATP6AP2^{QxQxx} was mostly localized to the Golgi, was highly cleaved and showed the higher half-life in cycloheximide pulse assays, confirming that the ER retrieval motif is well recognized by the COPI machinery

in mammalian cells.

(ii) In *Drosophila*, flies harboring a mutation in the cleavage site, the *ATP6AP2*^{AxxA} in the background of the *ATP6AP2Δ1* null allele were able to completely restore the viability of the flies.

(iii) In *Drosophila*, flies lacking the ER retrieval motif, the *ATP6AP2*$^{\Delta KKNN}$ in the background of the *ATP6AP2Δ1* null allele drastically reduced the percentage of adults eclosing from the pupal case and the few adult survivors demonstrated poor mobility, decreased or absent climbing capabilities and died within few days after the eclosion. Interestingly, the lack of the ER retrieval motif caused also in *Drosophila* more ATP6AP2 cleavage, leading to a reduced amount of full-length protein available.

From these observations it can be concluded that the full-length ATP6AP2 should have an important function in the ER and that the correct cycling from the Golgi to the ER is crucial for this function. By contrast, at least in *Drosophila*, the cleavage and the cleavage products (NTF and CTF) are dispensable, arguing against the non-autonomous role of s(P)RR. We therefore concluded that uncleaved ATP6AP2 should rather be associated with V-ATPase assembly in the ER. Moreover, a recent analysis in *Drosophila* wing cells led our group to observe that lack of ATP6AP2 causes ER stress and that the induction of ER stress is sufficient to cause PCP phenotypes, highlighting to the role of the full-length ATP6AP2 in the assembly of the V-ATPase V_0 proton pore (**Guida *et al.*, 2018**).

This conclusion was supported by our affinity purification coupled to mass spectrometry (AP-MS) approach in HEK293 cells, where we found interactions with several assembly factors for the V_0 domain (ATP6AP1, VMA21 and TMEM199) and V_0 subunits themselves (ATP6V0A2 and ATP6V0D1), three of which have been implicated in CDG (ATP6AP1, TMEM199 and ATP6V0A2) (**Kornak *et al.*, 2008; Jansen *et al.*, 2016b, c**). We confirmed the interaction between ATP6AP2 and VMA21 in overexpression and the interaction between ATP6AP1 and ATP6AP2 in overexpression, in endogenous conditions and in a Y2H screen. Mapping experiments with different truncated constructs in yeast suggested that the interaction required the N-terminal luminal domains of both proteins. Interestingly, both missense N-terminal mutations in ATP6AP2 reduced the interaction with ATP6AP1 in both Y2H and reciprocal co-IP experiments. By contrast, a construct depleted for the exon 4 and mimicking the effect of the exon skipping mutation previously reported did not show defects in the interaction with ATP6AP1.

The relationship with ATP6AP1, the other "accessory subunit", is a special one. Both proteins are type I transmembrane with an extracellular domain, that can be cleaved off. As already described for ATP6AP2, only the C-terminal of ATP6AP1 is highly conserved through vertebrates and invertebrates (**Schoonderwoert *et al.*, 2002; Jansen and Martens, 2012**). Moreover, the proteolytic processing of ATP6AP2 is tissue-dependent, similarly to what has been shown before for ATP6AP1 (**Jansen *et al.*, 2016c**). Indeed, both proteins undergo to proteolytic cleavage upon their passage in the *cis*-Golgi. Recently, ATP6AP1 turned out to be more than a simple accessory subunit for the V-

ATPase, being indeed an ER assembly factor (**Jansen *et al.*, 2016c**). Patients with deficiency of the V-ATPase due to mutations in the ER assembly factors show a similar phenotype to our patients, especially regarding the liver involvement (**Jansen *et al.*, 2016a, b**). But more interestingly, patients with ATP6AP1 mutations show not only a similar liver involvement, but also immune system abnormalities, strongly arguing for a role of ATP6AP2 in the assembly of the V_0 domain of the V-ATPase, probably together with ATP6AP1.

More recently, our group revealed that in yeast strains depleted for Voa1p (the yeast ortholog of ATP6AP1) the co-expression of the human ATP6AP1 together with the human ATP6AP2 fulfil Voa1p functions and rescue the yeast growth more efficiently than ATP6AP1 or ATP6AP2 alone (**Guida *et al.*, 2018**). It is interesting to note that in yeast ATP6AP2 does not exist, while Voa1p possesses an ER retrieval motif KKNN. In humans, is ATP6AP2 to harbor the ER retrieval motif KIRMD, while ATP6AP1 lacks the ER retrieval motif in its C-tail, but harbors an autonomous internalization signal that drives the V-ATPase to vacuolar structures (**Jansen *et al.*, 1998; Schoonderwoert and Martens, 2002; Feng *et al.*, 2008**). Altogether, these results have different implications: (i) in higher organisms, the two proteins ATP6AP1 and ATP6AP2 interact together, (ii) the interaction occurs through the N-terminal domains, (iii) the ATP6AP1/ATP6AP2 complex is important for the V-ATPase assembly and trafficking. We therefore speculate that the two proteins are evolutionarily derived from the same ancestral protein Voa1p and that during evolution, ATP6AP2 has kept the ER retrieval motif.

Once in the Golgi, escaped proteins harboring ER retrieval motif are incorporated into COPI vesicles allowing the travel back to the ER. Interestingly, is well known that the interaction between one of the ER retrieval motif (KDEL) and its specific receptor (KDELR) is pH-sensitive (**Wilson *et al.*, 1993; Bräuer *et al.*, 2019**). We could therefore speculate that increased Golgi pH, due to impaired V-ATPase activity, could lead to accumulation of escaped proteins inside the Golgi as result of impaired recruitment of the COPI machinery. This enrichment in the Golgi could, on one side, impair the retrograde trafficking and, on the other side, affect overall Golgi homeostasis. In this manner, the correct cleavage of both ATP6AP1 and ATP6AP2 could be considered as a quality control step for the cell to inactivate proteins escaped from the retrieval mechanism, or the cleavage of the ER assembly factors may expose binding sites for the V_1 complex on the V_0 subunits, allowing the formation of a full holoenzyme only under appropriate folding conditions. The failure to form the final proton pump could exacerbate the acidification defects, creating a negative loop of increased pH and reduced traffic between Golgi and ER.

Thus, it appears that the molecular mechanism by which ATP6AP2 acts on the V-ATPase is the contribution to the assembly and stability of the V_0 domain and not any function associated with the peripheral V-ATPase holoenzyme, as has been suggested in

many publications (**Kinouchi *et al.*, 2010; Oshima *et al.*, 2011; Riediger *et al.*, 2011; Kurauchi-Mito *et al.*, 2014**). However, how the assembly of the V_0 domain occurs in humans still remains to be deciphered. Recently, new findings have confirmed the interaction of ATP6AP2 with ATP6V0D1 (**Jung *et al.*, 2018**), as we had already noticed in our AP-MS. This may suggest a very coordinated assembly, with each chaperone interacting with a specific subunit: VMA21 and ATP6AP1 with the proteolipid ring, ATP6AP2 with the *d* subunit on a side and ATP6AP1 on the other side. It would be interesting to confirm these theories with different techniques, for example by following the anterograde trafficking of the V_0 domain/assembly factors from the ER to the Golgi and the retrograde transport of the chaperones to the ER in immunostaining or live imaging experiments. However, the lack of good specific antibodies directed against endogenous ER assembly factors makes the first possibility difficult to achieve. On the one hand, the need to position the tag away from specific signals contained at the C-terminal of the assembly factors (e. g. ER retrieval motif and autonomous internalization signal) and the need to express the assembly factors in a correct stoichiometric ratio pose problems for the live imaging experiments. Indeed, we and other groups observed that overexpression might lead to escape from ER retrieval mechanism and localize the proteins to endo/lysosomal structures (**Pellicano *et al.*, 2006, 2010**), or ERGIC (**Jansen *et al.*, 2016b**). Thus, endogenous tagging with CRISPR/Cas9 would have to be the next step in additional mechanistic studies.

A major downstream effect of decreased V-ATPase assembly is an impairment in the autophagy pathway. To understand the consequences of the decreased interactions with V-ATPase assembly factors, we compared knockdown cells and ATP6AP2 mutant cells in *Drosophila*. Of note, for all the studies on autophagy and the mTOR pathway, patients fibroblasts turned out to be without phenotype. In fact, we found that fibroblasts had the ability to compensate for the defects after several rounds of passaging. Therefore, the use of the *Drosophila* model was crucial for the mechanistic studies. We found that both knockdown and $ATP6AP2^{L98S}$ decreased V-ATPase activity, as demonstrated by reduced Lysotracker staining, suggesting that the p.L98S is a loss-of-function mutation. In accordance with the importance of V-ATPase-mediated acidification for autophagic degradation (**Mauvezin *et al.*, 2015**), we found an accumulation of lipid droplets (LDs) in both knockdown and mutant cells. Moreover, we observed an accumulation of the lipidated form of the autophagosomal markers LC3-II and p62, suggesting a decreased autophagic degradation. As result of the reduced degradation, we found an increased LD size, suggesting that the clearance cannot take place inside the autolysosomes, leading to the accumulation of enlarged autolysosomes with undegraded material. These findings were obtained in the fat body of the flies, a liver-like organ, and confirmed by transmission electron microscopy studies performed also in different tissues, such as the pupal wing. In both tissues, the knockdown cells showed a strong accumulation of LDs and other organelles in large autolysosomes with reduced degradative capacity, suggesting that these

defects are the result of the block in the last autophagic steps.

Another potential consequence of the autophagic block is the failure of hydrolytic proteases to degrade proteins in autolysosomes, leading to a reduction in the pool of free amino acids, condition that could inhibit the mTORC1 pathway. Moreover, it has been suggested that the V-ATPase plays a more direct role in the mTORC1 signalling acting as a scaffold complex (**Zoncu *et al.*, 2011**), thus reduction of V-ATPase on the lysosomes membrane could direct affect the mTORC1 pathway. Indeed, we found reduced levels of phospho-4EBP1 (p4EBP1) in cells with the $ATP6AP2^{L98S}$ mutations compared to the surrounding $ATP6AP2^{WT}$ tissue. Interestingly, the fusion between lysosomes and autophagosomes appears to not be impaired, as already suggested (**Mauvezin *et al.*, 2015**). Indeed, in transmission electron microscopy studies performed in pupal wings, we found the accumulation of large autolysosomes, suggesting a continuous growth of these organelles due to normal fusion of autophagosome with lysososmes. Altogether, these results suggest a pathogenic feedback loop: the autophagic block due to V-ATPase defective activity/assembly leads to inactivation of mTOR, while the stimulation of autophagy due to mTOR inactivation in cells where lysosomal degradation is defective leads to the accumulation of autophagolysosomes with incompletely digested contents that could contribute to the pathology, particularly regarding the steatohepatitis.

In summary, our data show that missense mutations in ATP6AP2 reduce protein expression and stability and reduce the interaction with ATP6AP1, one of the ER assembly factors of the V_0 domain of the V-ATPase. We further demonstrate that the deficiency of ATP6AP2 leads to autophagic dysregulation, with impaired lysosomal acidification and mTOR signalling. We unravel the function of ATP6AP2 as full-length protein involved in the ER assembly of the V-ATPase and not anymore as simple accessory subunit. Altogether, our data suggest that the missense mutations in *ATP6AP2* lead to impaired V-ATPase assembly and subsequent defects in glycosylation and autophagy.

Mutations in the ER assembly factors form a new subgroup of metabolic diseases with autophagic defects, impaired glycosylation and liver steatosis: insights from VMA21

In this project, we identified three males from three unrelated families from a cohort of unsolved CDG carrying three different mutations in *VMA21*. In addition to the defective glycosylation of serum proteins, the patients displayed hepatopathy, elevated serum transaminases and hypercholesterolemia.

VMA21 encodes a small protein of 11 kDa ubiquitously expressed. VMA21 is formed by two hydrophobic transmembrane domains, with the N- and C-terminal domain cytoplasmically exposed and a short luminal loop. VMA21 is the master chaperone of the V_0 domain of the V-ATPase in the ER: it drives the coordinated assembly of the various V_0 subunits, interacting with the proteolipid ring and allowing the association and stabilizationion of the other subunit to the V_0 domain. Once the V_0 is fully assembled, VMA21 can finally escort it inside COPII vesicles from the ER to the Golgi (**Malkus *et al.*, 2004; Ramachandran *et al.*, 2013**). Previously, mutations in *VMA21* have been associated with XMEA, a rare X-linked autosomal recessive disorder, characterized by myopathy with excessive autophagy (**Ramachandran *et al.*, 2013**). Despite the ubiquitous expression of the V-ATPase, XMEA is exclusively a skeletal muscle disease. The XMEA mutations are mostly rare intronic variants, with the single exception of a missense mutation in the C-terminal of the protein. All the mutations reduce the splicing efficiency and thus have hypomorphic effects.

In this study, we embarked on the comparison of the *VMA21* mutations leading to a CDG phenotype with the previous described missense mutation that give a XMEA manifestation with the aim to identify the cause for the two distinct clinical manifestations.

The mutations. In this work, we identified three hemizygous *VMA21* mutations with different distribution along the short gene: the first one is localized upstream of the gene (in the 5' UTR), the second is in the first exon, corresponding to the N-terminal of VMA21 exposed in the cytoplasm, and the third is in the third exon, corresponding to the luminal loop between the two transmembrane domains.

The phenotype. The predominant symptoms of the patients carrying mutations in *VMA21* are hepatopathy with elevated liver enzymes and variable abnormalities in cholesterol. P1 suffered from hepatosplenomegaly regressing with age and chronic elevation of liver enzymes (AST, ALT and ALP) but normal cholesterol. Also P2 suffered from hepatomegaly with mildly elevated serum cholesterol, elevated LDL, elevated total bilirubin and elevated liver enzymes (AST, ALT and ALP). P3 shows chronic hepatitis at 6 years, with elevated cholesterol and elevated liver transaminases (AST and ALT). Additional clinical features for the *VMA21* patients include for P1 mild hypotonia, hypoglycemia, hy-

perinsulinemia, neutropenia, abnormal coagulation cascade and slightly elevated CK; for P2: bilateral sensorineual hearing loss, kidney disease, myopia, bilateral ocular keratitis, severe *pectus excavatum* and idiopathic polycythemia; for P2 and P3: low ceruloplasmin and copper.

The glycosylation defects. Based on the transferrin IEF, all the *VMA21* patients show a CDG type II with defective *N*-glycosylation, as demonstrated by increased di- and trisialotransferrin. In addition, all the patients show defective mucin-type *O*-glycosylation with reduced sialic acid incorporation based on isofocusing of apolipoprotein CIII (ApoCIII), showing increased ApoCIII-1 and decreased ApoCIII-2. MALDI-LTQ mass spectrometry confirmed the increase of undersialylated glycans in all the patients. Interestingly, analysis of two boys carrying the XMEA missense mutation revealed a normal transferrin glycosylation profile.

Pathomechanisms of *VMA21* mutations

Through functional studies, we have shown that all the analyzed mutations are hypomorphic mutations that reduce both mRNA and protein expression in patient fibroblasts. Moreover, the mutations led to the reduction of V_0 subunits with consequent decreased V_0 assembly and V-ATPase holoenzyme activity. Reduced VMA21 expression was not found upon overexpression of the missense mutation-containing cDNAs in HEK293T cells, suggesting that the amino acid changes do not impair the stability of the protein. However, the missense mutations reduced the capacity of VMA21 to interact with the ER assembly factor ATP6AP2. Using the yeast model, our collaborator Tom Stevens showed that although the human VMA21 is able to rescue the yeast growth in strains depleted of Vma21p, the ortholog of *VMA21*, this is not the case for the proteins harboring the missense mutations when they are subjected to selective growth media. Moreover, these mutants also show reduced V-ATPase activity on vacuoles purified from yeast cells. These findings suggest on the one hand that the phenotype could be caused simply by the lack of the protein, in fact, as we already demonstrated for ATP6AP2, the mutations reduce the amount of the protein expressed in the cells and thus reduce the coordinated assembly of the V_0 domain at the level of the ER. On the other hand, our findings also highlight the importance of amino acid changes themselves at the level of protein function. Indeed, the point mutations reduce the ability of VMA21 to interact with both V_0 subunits and ER assembly factors, indicating that mutations may interfere with the proper assembly of the V-ATPase. It would therefore be interesting to perform further experiments to test the interaction of the different point mutations of VMA21 with other ER assembly factors.

In agreement with the proposed role of VMA21 for the V-ATPase and in a similar fashion to what we have before observed for the deficiency of ATP6AP2, we found that mutations in VMA21 lead to a cascade of events: (i) defects in V-ATPase assembly with

a consequent reduction in activity, (ii) increase of lysosomal pH and impairment of the activity of the lysosomal hydrolases, (iii) partial block in late steps of autophagic flux, (iv) accumulation of lipids inside the lysosomes/autolysosomes.

In detail, we found that the VMA21 mutations lead to defective degradation of autophagosomes, as demonstrated by the accumulation of p62 and the lipidated form of LC3-II. Moreover, we could observe accumulation of enlarged and abundant lysosomes decorated by the marker LAMP1. We hypothesized that these enlarged lysosomes could be the result of a defective degradation activity. As expected, the organellar acidity measured through the Lysotracker probes results to be increased while the lysosomal degradation was reduced, as demonstrated by the decreased CTSB hydrolytic activity. Because of the reduced degradative activity of the autolysosomes, we proposed that the clearance of LDs cannot take place, giving rise to the steatotic phenotype observed by electron microscopy in the hepatocytes of the patients. As we already demonstrated in the ATP6AP2 deficiency, also here our data suggest that the lack of V-ATPase activity does not disturb the membrane fusion between lysosomes with autolysosomes, but rather creates a block in the degradation of autophagic cargos inside the lysosomes, leading in a block of the autophagic flux (**Mauvezin *et al.*, 2015**). It has been demonstrated that lysosomal acid hydrolases need of an acidic environment to be activated. Analysis of the CTSB in the patients fibroblasts revealed a strong reduction of CTSB activity suggesting from a side an impaired organellar acidification and on the other confirmed the decreased lysosomal degradation. Interestingly, it has been reported that in the lysosomal storage disorder Niemann-Pick disease type C (NPC) the activity of the lysosomal CTSB is strongly reduced. This defect appears to be caused by inhibition of CTSB activity by lipid storage material inside the lysosomes, more than by altered processing/trafficking of CTSB or by altered lysosomal pH (**Elrick and Lieberman, 2013**). Further studies could elucidate if VMA21 mutations lead to reduced CTSB activity because of the altered lysosomal pH rather than accumulation of lipids inside the lysosomes, or by the sum of the two effects. Unfortunately, we were unable to observe any effects on mTOR in the patient fibroblasts. Indeed, both in fed conditions and upon starvation, we could not detect any difference in the levels of phosphorylation of S6K between control and patients fibroblasts. Similar to the ATP6AP2 fibroblasts, we therefore assume that these fibroblasts have adapted to any mTOR defect. It would therefore be more appropriate to carry out these studies directly on primary hepatocytes, e.g. from biopsies, or on fibroblasts reprogrammed into hepatocytes (**Nakamori *et al.*, 2017**). The reprogramming could also eliminate the problem of choosing an appropriate control, obtaining personalized controls for each patient through correction of the pathological mutation with CRISPR/Cas9 technology. Also in this case, the *Drosophila* model could be a useful tool for the mechanistic studies.

With the help of the Filipin dye, we further found an accumulation of unesterified cholesterol inside the lysosomes. As already proposed for NPC, the reduced lysosomal

acidification may lead to the accumulation of cholesterol inside the lysosomes. Indeed, the NPC1 and NPC2 proteins are required for the extraction of endocytosed cholesterol from lysosomes, which occurs in a pH-dependent manner (**Vance and Karten, 2014**). We hypothesized that the failure to extract cholesterol from the lysosomes through the NPC proteins could reduce the total amount of cellular cholesterol, driving the cell to produce new cholesterol and triggering *de novo* lipogenetic pathways mediated by the sterol regulatory element-binding protein 1 (SREBP1) cleavage. Thereby, the hypercholesterolemia observed in the patients could be the manifestation of the increased synthesis of cholesterol and consequent secretion from the hepatocytes into the serum. It could therefore be interesting to determine exactly which metabolic enzymes are implicated in the cholesterol synthesis increase, downstream of SREBP1 activation. Finally, we could observe that VMA21 mutations lead to the activation of the protein kinase R (PKR)-like endoplasmic reticulum kinase (PERK) branch of the unfolded protein response (UPR). Previously, our group already demonstrated that the lack the ER assembly factor ATP6AP2 could be associated with ER stress (**Guida *et al.*, 2018**). It may seem plausible that ER stress occurs as a consequence of defective V_0 assembly and increased degradation of ER assembly factors and V_0 subunits through the ERAD pathway (**Hill *et al.*, 1994; Esmail *et al.*, 2018a**). ER stress may also be responsible for increased LD formation, thereby contributing to LD accumulation in addition to the abovementioned autophagic degradation of LDs. Recent studies have indeed suggested that, under metabolic stress signals, proteins localized in the ER, and responsive to ER stress, can regulate lipogenic programs promoting LD formation (**Zhang *et al.*, 2012**). Moreover, ER stress responses may directly lead to LD synthesis in the attempt to protect the ER against toxic lipids (**Lee *et al.*, 2012; Zhang and Zhang, 2012**). Accordingly, the inhibition of esterification of fatty acids into triglycerides obtained with the treatment with diacylglycerol acyltransferase (DGAT) inhibitors led to a partial reduction of LD number and size in the VMA21-CDG patient. Interestingly, the PERK branch itself is also known to activate *de novo* lipogenesis SREBP1-mediated, suggesting that the ER stress might trigger both triglyceride and cholesterol accumulation. In summary, our data show that similar to ATP6AP2 deficiency missense mutations in *VMA21* reduce V_0 subunit expression and impair the V-ATPase assembly. We further demonstrate that the deficiency of VMA21 leads to dysfunction of the V-ATPase, with autophagic defects, impaired lysosomal acidification and accumulation of LDs. We show that reduced V-ATPase activity causes accumulation of cholesterol as a consequence of either autophagic defects and activated UPR responses. We suggest that this situation triggers SREBP-dependent *de novo* lipogenesis and hypercholesterolemia in the patients. Overall, we found that the differences between CDG and XMEA fibroblasts were rather mild and both mutations almost phenocopy all the defects, suggesting that CDG and XMEA may be rather similar disease entities with a similar underlying pathomechanisms. We therefore concluded that more patients are needed to fully appreciate the disease spectrum in this ultrarare disease.

Mutations in the ER assembly factors ATP6AP2 and VMA21 are associated with impaired glycosylation

Why do mutations in the V-ATPase assembly factors induce alterations in glycosylation? There are several theories that can be postulated. First, it should be emphasized that most of the mutations described, both in the assembly factors and in V-ATPase core subunits, induce a type 2 CDG that is featured by both *N*- and *O*-glycosylation deficits. This means that the glycosylation defects should be the result of a disturbance in the Golgi. Many evidences show that the activity of the V-ATPase begins at the *cis*-Golgi, where the assembly of the final V-ATPase holoenzyme occurs (**Forgac, 2007**). Thus, it can be assumed that an altered Golgi pH may contribute to the glycosylation defect. This can be due to three different reasons: (i) the increase of the pH causes incorrect distribution of divalent cations, such as Ca^{2+}, Mg^{2+} and/or Mn^{2+}, that are required for the catalytic activity of most of the glycosyltransferases (**Petrová *et al.*, 2001**); (ii) some glycosylation enzymes, like the sialidases, require a low pH for optimal activity (**al-Awqati *et al.*, 1992**); (iii) the increase of the pH causes incorrect localization of glycosyltransferases in the Golgi (**Rivinoja *et al.*, 2009a, b; Maeda and Kinoshita, 2010**). Indeed, some glycosyltransferases need an acidic pH to form aggregates that enable their rapid movement through the Golgi stack (**Opat *et al.*, 2001a, b**). Moreover, impaired acidification also causes impaired cholesterol trafficking. This could indirectly affect the distribution of the Golgi glycosyltransferases, which are preferably retained in thinner membranes instead of the cholesterol-rich post-Golgi membranes (**Munro, 1995; Axelsson *et al.*, 2001**). Interestingly, the increase of 0.2 unit in the Golgi pH leads to mislocalization of some sialyltransferases, inhibiting the terminal sialylation of *N*-glycans (**Rivinoja *et al.*, 2009a, b**). It would therefore be interesting to confirm any pH alteration in the Golgi apparatus in the fibroblasts of our cohort of CDG patients. The measurement could be performed by using different systems, among which the use of proteins tagged with a ratiometric variant of the pH-sensitive intrinsically fluorescent protein pHluorin (**Ma *et al.*, 2017**).

Another hypothesis that could explain for the glycosylation defects is that the deficiency of some ER assembly factors and V_0 subunits could may lead to specific defects in vesicle fusion and Golgi trafficking. As outlined above, it has been shown that the V_0 subunits *a* and *c* can interact directly with SNAREs on synaptic vesicles later on in the secretory pathway (**Bennet *et al.*, 1992; O'Connor *et al.*, 1993; Galli *et al.*, 1996; Shiff *et al.*, 1996; Di Giovanni *et al.*, 2010**) and are involved in the formation of trans-complexes of V_0 domains after the docking and pairing of the SNAREs, helping the fusion of vacuoles (**Bayer *et al.*, 2003**). Even if a specific role in fusion of COPII vesicles could not be proven for VMA21, we cannot exclude this role for the V_0 subunits. Indeed, mutations in the V0A2 subunit, that is specifically expressed in the Golgi, lead to protein trafficking defects and glycosylation impairment, suggesting a function of this subunit

in vesicles fusion (**Kornak *et al.*, 2008**). Moreover, in plants it has been shown that VMA21 interacts with the complex Erv41p/Erv46p. This complex is localized in the early secretory pathway and is involved in the protein loading into COPII vesicles for transport to the Golgi. It has been shown that VMA21 helps the complex Erv41p/Erv46p in this function, since in yeast strains lacking for Vma21p the v-SNARE Bos1 is not efficiently loaded in COPII vesicles, also if these vesicles are fully fusion competent (**Welsh *et al.*, 2006**). Further analysis could shed light on the role of the ER assembly factors and V_0 subunits in the traffic of the V_0 domain from the ER to the Golgi.

Based on these reasons, it can be asked why some mutations in V-ATPase subunits/assembly factors do not cause CDG and impaired Golgi glycosylation. This is the case for three V-ATPase subunits and one assembly factor: (i) ATP6V0A3, (ii) ATP6V0A4, (iii) ATP6V1B1 and (iv) VMA21-XMEA. The first three cases may be explained by the specific tissue expression and cellular localization patterns. Indeed, mutations of the ATP6V0A3 subunit, expressed only on the plasma membrane of osteoclasts, are associated with osteopetrosis (**Frattini *et al.*, 2000; Kornak *et al.*, 2000; Bhargava *et al.*, 2012**); mutations of the ATP6V0A4 subunit, expressed only on the plasma membrane of renal intercalated cells and inner ear, are associated with distal renal tubular acidosis with deafness (**Karet *et al.*, 1999; Vargas-Poussou *et al.*, 2006; Guillard *et al.*, 2009; Guillard, 2012**), while mutations in ATP6V1B1, a subunit expressed on the intercalated cells in the collecting duct, are associated with recessive distal renal tubular acidosis (dRTA) (**Guillard *et al.*, 2009; Guillard, 2012**). By contrast, glycosylation and Golgi defects are seen for the more ubiquitously expressed core subunits (ATP6V0A2, ATP6V1A and ATP6V1E1) and V_0 assembly factors (ATP6AP1, ATP6AP2, CCDC115, TMEM199 and VMA21). While these disorders are more systemic in nature than the abovementioned V-ATPase diseases (**Kornak *et al.*, 2008; Jansen *et al.*, 2016a, b, c; Van Damme *et al.*, 2016**), they nevertheless seem to affect some tissues in particular. The *cutis laxa* phenotype can be explained by inadequate glycosylation of extracellular matrix proteins. The liver involvement, however, may only in part be a result of impaired glycosylation. In addition, it is the defect in autophagic flux that strongly contributes to the steatotic phenotype. Indeed, the V-ATPase-mediated acidification is required for the final degradation step in autophagy, it can be argued that a ubiquitous small decrease in V-ATPase activity primarily manifests in organs with a high need for autophagy, thus impairment in the lipophagy can cause steatosis of the liver (**Singh*et al.*, 2009; Baiceanu *et al.*, 2016**).

Are mutations in the ER assembly factors ATP6AP2 and VMA21 a novel form of non-alcoholic fatty liver disease (NAFLD)?

NAFLD is the most common hepatic disease in Western countries with an overall prevalence expected of 20-30% (**Chalasani *et al.*, 2012**). While alcohol consumption as a cause is always ruled out, NAFLD can be associated with hepatic insulin resistance and type 2 diabetes (**Birkenfeld and Shulman, 2014**). It usually begins with benign steatosis that then progresses to steatohepatitis, cirrhosis and even hepatocellular carcinoma (HCC) (**Mao *et al.*, 2016**). NAFLD-related liver disease is predicted to become the most important indication for liver transplantation in the United States of America in the next five years (**Kwanten *et al.*, 2014**). The mechanisms that trigger NAFLD still remains poorly understood. While lipophagy has been shown to be important in preventing steatosis (**Singh *et al.*, 2009; Ueno and Komatsu, 2017**), other studies have also shown that lipotoxicity induced by free fatty acid (FFA) can increase the protein misfolding, leading to a consequent ER stress, which can exacerbate NAFLD (**Greenberg *et al.*, 2011**). As autophagy can be induced to dispose of misfolded proteins unable to undergo ERAD (**Kroeger *et al.*, 2009**), it is conceivable that the interplay between autophagy and ER stress leads to a vicious circle. In addition, prolonged ER stress by itself is known to impose detrimental pathological outcome, involving fat deposition, inflammation and dysregulated autophagy, all being processes capable of provoking the development of NAFLD (**Wang *et al.*, 2018**). The phenotype in our CDG patients can be regarded as a new type of NAFLD, in which both autophagic defects and ER stress contribute to the development of hepatosteatosis. However, while the contribution of autophagy was investigated rather thoroughly, further analysis is needed to understand the contribution of ER stress.

The precise understanding of the liver disease pathogenesis in our patients could also be important for identifying new therapeutic strategies in NAFLD. One possibility might be the treatment with cyclodextrins (CD), already used in treatment for NPC (NIH Phase 2b/3 clinical trials). Beneficial effects of the monomeric cyclodextrin 2HPβCD have been already demonstrated, with reduction of lipid storage in endolysosomes (**Liu *et al.*, 2008, 2009; Davidson *et al.*, 2009; Vance and Karten, 2014; Puglisi and Yagci, 2019**). However, the treatment with 2HPβCD can be difficult, mainly due to its poor pharmacokineticy and high citotoxicity (**Puglisi and Yagci, 2019**). Another possible treatment to overcome the hypercholesterolemia associated with the hepatopathy is the use of statins, which are lipid-lowering drugs already in use in the treatment of NAFLD (**Nascimbeni *et al.*, 2019**). Studies on NAFLD patients demonstrated that statins are effective not only in improving the lipid profile by reducing total cholesterol, LDL cholesterol and triglycerides, but are also able to increase HDL cholesterol and de-

crease free fatty acids (**Nascimbeni *et al.*, 2019**). Moreover, treatment with statins have shown beneficial effects on the liver-related complications, including cirrhosis, portal hypertension and HCC. The treatment with statins may also exert systemic effects, that collectively may improve steatosis, sterile inflammation, fibrosis and tumorigenesis (**Nascimbeni *et al.*, 2019**). Thus, our work could stimulate additional studies on how ER stress and autophagic defects lead to NAFLD in the context of V-ATPase defective activity.

Conclusion

In summary, we have identified individuals with a new glycosylation disorder, characterized by autophagic impairment and NAFLD, caused by different mutations in the ER assembly factors ATP6AP2 and VMA21. Our work and previous studies demonstrate that genetic diseases caused by impairment of V-ATPase assembly and activity, due to mutations in all the ER assembly factors, should be grouped in a specific subgroup of CDG and that these genes should be considered in the screening of novel cases of CDG type II, hypercholesterolemia and NAFLD. Our functional studies suggest the following model: (1) missense mutations reduce the protein expression and the interaction with V_0 assembly factors; (2) consequently, the V-ATPase assembly is reduced and the V-ATPase activity impaired; (3) the ineffective V-ATPase assembly leads to increased Golgi pH with altered glycosylation of proteins; (4) in a similar fashion, insufficient V-ATPase activity raises the lysosomal pH; (5) the increased lysosomal pH reduces the activity of lysosomal hydrolases; (6) the reduced hydrolase activity leads to a partial block of the terminal steps of autophagy; (7) impaired V-ATPase activity and hydrolase function also potently induce autophagy, via inhibition of the mTORC1 pathway; (8) induction of autophagic flux in the context of impaired autophagy causes a pathogenic loop, resulting in the accumulation of enlarged autophagolysosomes and LDs.

The formation of the latter is additionally enhanced as a consequence of ER stress. Another consequence of the increased lysosomal pH is an impairment in the extraction of cholesterol from the endo/lysosomal structures. The cholesterol then is blocked in these organelles, leading to a reduction of intracellular cholesterol and the induction of *de novo* lipogenesis through SREBP. These events give rise to the hypercholesterolemia observed in several of our patients on a side, and together with the accumulation of LDs, to the NAFLD phenotype (**Figure 20**).

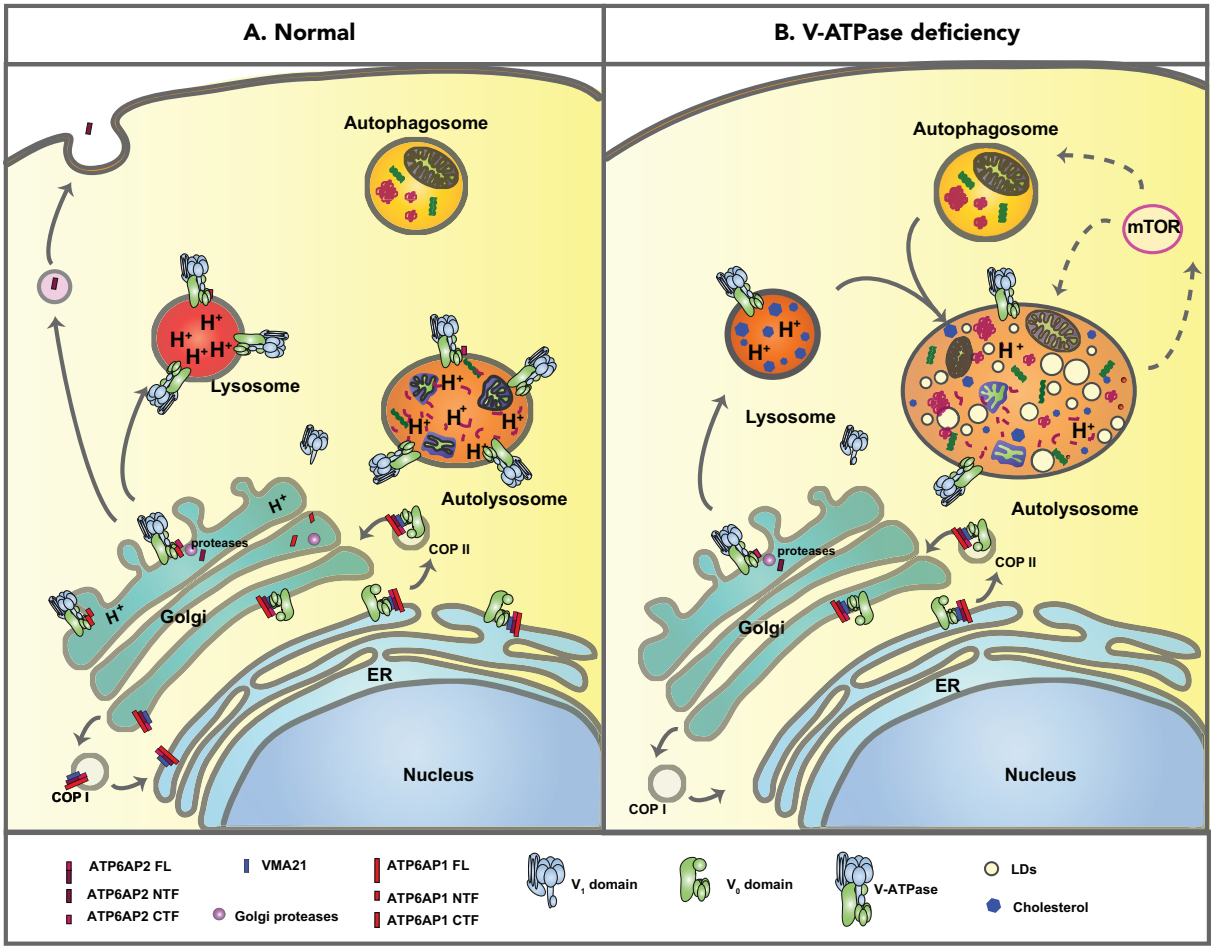

Figure 20: V-ATPase and autophagy in health and disease

(A) The ER assembly factors ATP6AP2 (colored purple), ATP6AP1 (colored red) and VMA21 (colored blue) bind to the *c'* subunit of the V-ATPase in the ER and initiate the assembly of the V_0 domain (colored green). The ER assembly factors ATP6AP1, ATP6AP2 and VMA21 escort the V_0 domain in COPII vesicles to the Golgi, where they partially dissociate from the V_0 domain. In the Golgi, the V-ATPase assembly is completed by addition of the ATP-hydrolytic domain (V_1; colored turquoise). Proton pumping by the V-ATPase is critical for regulating the pH of the Golgi and the lysosomes. Fusion of lysosomes with autophagosomes generates autolysosomes that degrade target proteins and organelles.
(B) In the V-ATPase deficiency, lack of VMA21 or ATP6AP2 leads to failure of V_0 assembly, reduced levels of V-ATPase and a decrease in Golgi and lysosomal pH, that impairs lysosomal and autophagic degradation of cellular proteins, organelles, cholesterol and LDs. Reduced interaction with V-ATPase and decreased protein degradation may also modulate the mTOR signalling pathway, which, in turn, upregulates autophagy. This leads to accumulation of engulfed autophagosomes, autolysosomes and autophagic vacuoles in the hepatocytes of the patients. Inspired from Hirano and Di Mauro, 2009.

Bibliography

Bibliography

al-Awqati, Q., Barasch, J., Landry, D. (1992) Chloride channels of intracellular organelles and their potential role in cystic fibrosis. *J Exp Biol*, 172: 245–66.

Ackerley, C. A., Cooper, M. A., Munoz, D. G., Minassian, B. A. (2016) Fatal hepatic failure and pontine and extrapontine myelinolysis in XMEA. *Neurology*, 87(13): 1417–9.

Advani, A., Kelly, D. J., Cox, A. J., White, K. E., Advani, S. L., Thai, K., Connelly, K. A., Yuen, D., Trogadis, J., Herzenberg, A. M., Kuliszewski, M. A., Leong-Poi, H., Gilbert, R. E. (2009) The (Pro)renin receptor: site-specific and functional linkage to the vacuolar H^+-ATPase in the kidney. *Hypertension*, 54(2): 261–9.

Aebi, M., Helenius, A., Schenk, B., Barone, R., Fiumara, A., Berger, E. G., Hennet, T., Imbach, T., Stutz, A., Bjursell, C., Uller, A., Wahlström, J. G., Briones, P., Cardo, E., Clayton, P., Winchester, B., Cormier-Dalre, V., de Lonlay P., Cuer, M., Dupré, T., Seta, N., de Koning, T., Dorland, L., de Loos, F., Kupers, L., et al. (1999) Carbohydrate-deficient glycoprotein syndromes become congenital disorders of glycosylation: an updated nomenclature for CDG. First International Workshop on CDGS. *Glycoconj J*, 16(11): 669–71.

Amsterdam, A., Nissen, R. M., Sun, Z., Swindell, E. C., Farrington, S., Hopkins, N. (2004) Identification of 315 genes essential for early zebrafish development. *Proc Natl Acad Sci U S A*, 101: 1279–12797.

Anderson, R. G., Pathak, R. K. (1985) Vesicles and cisternae in the trans Golgi apparatus of human fibroblasts are acidic compartments. *Cell*, 40(3): 635–43.

Auranen, M., Villanova, M., Muntoni, F., Fardeau, M., Scherer, S. W., Kalino, H., Minassian, B. A. (2000) X-linked vacuolar myopathies: two separate loci and refined genetic mapping. *Ann Neurol*, 47(5): 666–9.

Axe, E. L., Walker, S. A., Manifava, M., Chandra, P., Roderick, H. L., Habermann, A., Griffiths, G., Ktistakis, N. T. (2008) Autophagosome formation from membrane compartments enriched in phosphatidylinositol 3-phosphate and dynamically connected to the endoplasmic reticulum. *J Cell Biol*, 182(4): 685–701.

Axelsson, M. A., Karlsson, N. G., Steel, D. M., Ouwendijk, J., Nilsson, T., Hansson, G. C. (2001) Neutralization of pH in the Golgi apparatus causes redistribution of glycosyltransferases and changes in the O-glycosylation of mucins. *Glycobiology*, 11(8): 633–44.

Bachhawat, A. K., Manolson, M. F., Murdock, D. G., Garman, J. D., Jones, E. W. (1993) The VPH2 gene encodes a 25 kDa protein required for activity of the yeast vacuolar H(+)-ATPase. *Yeast*, 9(2): 175–84.

Bader, M., Bohnemeier, H., Zollmann, F. S., Lockley-Jones, O. E., Ganten, D. (2000) Transgenic animals in cardiovascular disease research. *Exp Physiol*, 85: 713–31.

Bader, M. (2005) Mouse knockout models of hypertension. *Methods Mol Med*, 108: 17–32.

Bader, M. (2007) The second life of the (pro)renin receptor. *J Renin Angiotensin Aldosterone Syst*, 8(4): 205–8.

Baiceanu, A., Mesdom, P., Lagouge, M., Foufelle, F. (2016) Endoplasmic reticulum proteostasis in hepatic steatosis. *Nat Rev Endocrinol*, 12(12): 710–722.

Balakrishna, A. M., Basak, S., Manimekalai, M. S., Grüber, G. (2015) Crystal structure of subunits D and F in complex gives insight into energy transmission of the eukaryotic V-ATPase from Saccharomyces cerevisiae. *J Biol Chem*, 290(6): 3183–96.

Balemans, W., Van Wesenbeeck, L., Van Hul, W. (2005) A clinical and molecular overview of the human osteopetroses. *Calcif Tissue Int*, 77(5): 263–74.

Barth, S., Glick, D., Macleod, K. F. (2010) Autophagy: assays and artifacts. *J Pathol*, 221(2): 117–24.

Batenburg, W. W., Krop, M., Garrelds, I. M., de Vries, R., de Bruin, R. J. A., Burckle, C., Müller, D. N., Bader, M., Nguyen, G., Danser, A. H. J. (2007) Prorenin is the endogenous agonist of the (pro)renin receptor. Binding kinetics of renin and prorenin in rat vascular smooth muscle cells overexpressing the human (pro)renin receptor. *J Hypertens*, 25: 2441–2453.

Bayer, M. J., Reese, C., Buhler, S., Peters, C., Mayer, A. (2003) Vacuole membrane fusion: V_0 functions after trans-SNARE pairing and is coupled to the Ca^{2+}-releasing channel. *J Cell Biol*, 162(2): 211–22.

Benlekbir, S., Bueler, S. A., Rubinstein, J. L. (2012) Structure of the vacuolar-type ATPase from Saccharomyces cerevisiae at 11-Å resolution. *Nat Struct Mol Biol*, 19(12): 1356–62.

Bhargava, A., Voronov, I., Wang, Y., Glogauer, M., Kartner, N., Manolson, M. F. (2012) Osteopetrosis mutation R444L causes endoplasmic reticulum retention and misprocessing of vacuolar H^+-ATPase a3 subunit. *J Biol Chem*, 287(32): 26829–39.

Bilic, J., Huang, Y. L., Davidson, G., Zimmermann, T., Cruciat, C. M., Bienz, M., Niehrs, C. (2007) Wnt induces LRP6 signalosomes and promotes dishevelled-dependent LRP6 phosphorylation. *Science*, 316(5831): 1619–22.

Birkenfeld, A. L., Shulman, G. I. (2014) Nonalcoholic fatty liver disease, hepatic insulin resistance, and type 2 diabetes. *Hepatology*, 59(2): 713–23.

Blair, H. C., Teitelbaum, S. L., Ghiselli, R., Gluck, S. (1989) Osteoclastic bone resorption by a polarized vacuolar proton pump. *Science*, 245(4920): 855–7.

Blitzer, J. T., Nusse, R. (2006) A critical role for endocytosis in Wnt signaling. *BMC Cell Biol*, 7: 28.

Blomme, B., Van Steenkiste, C., Callewaert, N., Van Vlierberghe, H. (2009) Alteration of protein glycosylation in liver diseases. *J Hepatol*, 50(3): 592–603.

Bond, S., Forgac, M. (2008) The Ras/cAMP/protein kinase A pathway regulates glucose-dependent assembly of the vacuolar (H^+)-ATPase in yeast. *J Biol Chem*, 283(52): 36513–21.

Bonifacino, J. S., Traub, L. M. (2003) Signals for sorting of transmembrane proteins to endosomes and lysosomes. *Annu Rev Biochem*, 72: 395–447.

Bowman, B. J., Bowman, E. J. (2002) Mutations in subunit C of the vacuolar ATPase confer resistance to bafilomycin and identify a conserved antibiotic binding site. *J Biol Chem*, 277(6): 3965–72.

Bracke, A., von Bohlen Und Halbach, O. (2018) Roles and functions of Atp6ap2 in the brain. *Neural Regen Res*, 13(12): 2038–2043.

Bräuer, P., Parker, J. L., Gerondopoulos, A., Zimmermann, I., Seeger, M. A., Barr, F. A., Newstead, S. (2019) Structural basis for pH-dependent retrieval of ER proteins from the Golgi by the KDEL receptor. *Science*, 363(6431): 1103–1107.

Breton, S., Brown, D. (2013) Regulation of lumenal acidification by the V-ATPase. *Physiology (Bethesda)*, 28(5): 318–29.

Brown, D., Breton, S. (2000) H(+)V-ATPase-dependent luminal acidification in the kidney collecting duct and the epididymis/vas deferens: vesicle recycling and transcytotic pathways. *J Exp Biol*, 203(Pt 1): 137–45.

Buechling, T., Bartscherer, K., Ohkawara, B., Chaudhary, V., Spirohn, K., Niehrs, C., Boutros, M. (2010) Wnt/Frizzled signaling requires dPRR, the Drosophila homolog of the prorenin

receptor. *Curr Biol*, 20(14): 1263–8.

Burcklé, C., Bader, M. (2006) Prorenin and its ancient receptor. *Hypertension*, 48: 549–51.

Burcklé, C. A., Danser, A. H. J., Müller, D. N., Garrelds, I. M., Gasc, J. M., Popova, E., Plehm, R., Peters, J., Bader, M., Nguyen, G. (2006) Elevated blood pressure and heart rate in human renin receptor transgenic rats. *Hypertension*, 47: 552–556.

Campbell, D. J. (2008) Critical review of prorenin and (pro)renin receptor research. *Hypertension* 51(5): 1259–64.

Campbell, B. J., Yu, L. G., Rhodes, J. M. (2001) Altered glycosylation in inflammatory bowel disease: a possible role in cancer development. *Glycoconj J*, 18(11–12): 851–8.

Cang, C., Aranda, K., Seo, Y. J., Gasnier, B., Ren, D. (2015) TMEM175 Is an Organelle K(+) Channel Regulating Lysosomal Function. *Cell*, 162(5): 1101–12.

Capecci, J., Forgac, M. (2013) The function of vacuolar ATPase (V-ATPase) a subunit isoforms in invasiveness of MCF10a and MCF10CA1a human breast cancer cells. *J Biol Chem*, 288(45): 32731–41.

Caplan, M. J., Stow, J. L., Newman, A. P., Madri, J., Anderson, H. C., Farquhar, M. G., Palade, G. E., Jamieson, J. D. (1987) Dependence on pH of polarized sorting of secreted proteins. *Nature*, 329(6140): 632–5.

Carr, G., Williams, D. E., Diaz-Marrero, A. R., Patrick, B. O., Bottriell, H., Balgi, A. D., Donohue, E., Roberge, M., Andersen, R. J. (2010) Bafilomycins produced in culture by Streptomyces spp. isolated from marine habitats are potent inhibitors of autophagy. *J Nat Prod*, 73(3): 422–427.

Casey, J. R., Grinstein, S., Orlowski, J. (2010) Sensors and regulators of intracellular pH. *Nat Rev Mol Cell Biol*, 11(1): 50–61.

Chabrol, B., Figarella-Branger, D., Coquet, M., Mancini, J., Fontan, D., Pedespan, J. M., Francannet, C., Pouget, J., Beaufrère, A. M., Pellissier, J. F. (2001) X-linked myopathy with excessive autophagy: a clinicopathological study of five new families. *Neuromuscul Disord*, 11(4): 376–88.

Chalasani, N., Younossi, Z., Lavine, J. E., Diehl, A. M., Brunt, E. M., Cusi, K., Charlton, M., Sanyal, A. J.; American Gastroenterological Association; American Association for the Study of Liver Diseases; American College of Gastroenterologyh. (2018) The diagnosis and management of non-alcoholic fatty liver disease: practice guideline by the American Gastroenterological Association, American Association for the Study of Liver Diseases, and American College of Gastroenterology. *Gastroenterology*, 142(7): 1592–609.

Chan, C. Y., Parra, K. J. (2014) Yeast phosphofructokinase-1 subunit Pfk2p is necessary for pH homeostasis and glucose-dependent vacuolar ATPase reassembly. *J Biol Chem*, 289(28): 19448–57.

Clark, S. L. (1957) Cellular differentiation in the kidneys of newborn mice studies with the electron microscope. *J Biophys Biochem Cytol*, 3(3): 349–362.

Clevers, H. (2006) Wnt/beta-catenin signaling in development and disease. *Cell*, 127(3): 469–80.

Collins, M. P., Forgac, M. (2018) Regulation of V-ATPase Assembly in Nutrient Sensing and Function of V-ATPases in Breast Cancer Metastasis. *Front Physiol*, 9: 902.

Connelly, K. A., Advani, A., Kim, S., Advani, S. L., Zhang, M., White, K. E., Kim, Y. M., Parker, C., Thai, K., Krum, H., Kelly, D. J., Gilbert, R. E. (2011) The cardiac (pro)renin receptor is primarily expressed in myocyte transverse tubules and is increased in experimental diabetic cardiomyopathy. *J Hypertens*, 29(6): 1175–84.

Coonrod, E. M., Graham, L. A., Carpp, L. N., Carr, T. M., Stirrat, L., Bowers, K., Bryant, N. J., Stevens, T. H. (2013) Homotypic vacuole fusion in yeast requires organelle acidification and not the V-ATPase membrane domain. *Dev Cell*, 27(4): 462–8.

Contrepas, A., Walker, J., Koulakoff, A., Franek, K. J., Qadri, F., Giaume, C., Corvol, P., Schwartz, C. E., Nguyen, G. (2009) A role of the (pro)renin receptor in neuronal cell

differentiation. *Am J Physiol Regul Integr Comp Physiol*, 297(2): 250–7.

Cotter, K., Capecci, J., Sennoune, S., Huss, M., Maier, M., Martinez-Zaguilan, R., Forgac, M. (2015) Activity of plasma membrane V-ATPases is critical for the invasion of MDA-MB231 breast cancer cells. *J Biol Chem*, 290(6): 3680–92.

Cotter, K., Stransky, L., McGuire, C., Forgac, M. (2015) Recent Insights into the Structure, Regulation, and Function of the V-ATPases. *Trends Biochem Sci*, 40(10): 611–622.

Cousin, C., Bracquart, D., Contrepas, A., Corvol, P., Muller, L., Nguyen, G. (2009) Soluble form of the (pro)renin receptor generated by intracellular cleavage by furin is secreted in plasma. *Hypertension*, 53(6): 1077–82.

Crockett, C. D., Ruggieri, A., Gujrati, M., Zallek, C. M., Ramachandran, N., Minassian, B. A., Moore, S. A. (2014) Late adult-onset of X-linked myopathy with excessive autophagy. *Muscle Nerve*, 50(1): 138–44.

Cruciat, C. M., Ohkawara, B., Acebron, S. P., Karaulanov, E., Reinhard, C., Ingelfinger, D., Boutros, M., Niehrs C. (2010) Requirement of prorenin receptor and vacuolar H^+-ATPase mediated acidification for Wnt signaling. *Science*, 327(5964): 459–63.

Davidson, C. D., Ali, N. F., Micsenyi, M. C., Stephney, G., Renault, S., Dobrenis, K., Ory, D. S., Vanier, M. T., Walkley, S. U. (2009) Chronic cyclodextrin treatment of murine Niemann-Pick C disease ameliorates neuronal cholesterol and glycosphingolipid storage and disease progression. *PLoS One*, 4(9): e6951.

Davis-Kaplan, S. R., Compton, M. A., Flannery, A. R., Ward, D. M., Kaplan, J., Stevens, T. H., Graham, L. A. (2006) PKR1 encodes an assembly factor for the yeast V-type ATPase. *J Biol Chem*, 281(42): 32025–35.

Davis-Kaplan, S. R., Ward, D. M., Shiflett, S. L., Kaplan, J. (2004) Genome-wide analysis of iron-dependent growth reveals a novel yeast gene required for vacuolar acidification. *J Biol Chem*, 279(6): 4322–9.

Dechant, R., Binda, M., Lee, S. S., Pelet, S., Winderickx, J., Peter, M. (2010) Cytosolic pH is a second messenger for glucose and regulates the PKA pathway through V-ATPase. *EMBO J*, 29(15): 2515–26.

De Duve, C., Wattiaux, R. (1966) Functions of lysosomes. *Annu Rev Physiol*, 28: 435–492.

Demaurex, N., Furuya, W., D'Souza, S., Bonifacino, J. S., Grinstein, S. (1998) Mechanism of acidification of the trans-Golgi network (TGN). In situ measurements of pH using retrieval of TGN38 and furin from the cell surface. *J Biol Chem*, 273(4): 2044–51.

Diab, H., Ohira, M., Liu, M., Cobb, E., Kane, P. M. (2009) Subunit interactions and requirements for inhibition of the yeast V1-ATPase. *J Biol Chem*, 284(20): 13316–25.

Díaz-Troya, S., Pérez-Pérez, M. E., Florencio, F. J., Crespo, J. L. (2008) The role of TOR in autophagy regulation from yeast to plants and mammals. *Autophagy*, 4(7): 851–65.

Dibble, C. C., Manning, B. D. (2013) Signal integration by mTORC1 coordinates nutrient input with biosynthetic output. *Nat Cell Biol*, 15(6): 555–64.

Di Giovanni, J., Boudkkazi, S., Mochida, S., Bialowas, A., Samari, N., Lévêque, C., Youssouf, F., Brechet, A., Iborra, C., Maulet, Y., Moutot, N., Debanne, D., Seagar, M., El Far, O. (2010) V-ATPase membrane sector associates with synaptobrevin to modulate neurotransmitter release. *Neuron*, 67(2): 268–79.

Dimitrov, B., Himmelreich, N., Hipgrave Ederveen, A. L., Lüchtenborg, C., Okun, J. G., Breuer, M., Hutter, A. M., Carl, M., Guglielmi, L., Hellwig, A., Thiemann, K. C., Jost, M., Peters, V., Staufner, C., Hoffmann, G. F., Hackenberg, A., Paramasivam, N., Wiemann, S., Eils, R., Schlesner, M., Strahl, S., Brügger, B., Wuhrer, M., Christoph Korenke, G., Thiel, C. (2018) Cutis laxa, exocrine pancreatic insufficiency and altered cellular metabolomics as additional symptoms in a new patient with ATP6AP1-CDG. *Mol Genet Metab*, 123(3): 364–374.

Dowling, J. J., Moore, S. A., Kalimo, H., Minassian, B. A. (2015) X-linked myopathy with excessive autophagy: a failure of self-eating. *Acta Neuropathol*, 129(3): 383–90.

Du, D., Kato, T., Nabi, A. H., Suzuki, F., Park, E. Y. (2008) Expression of functional human (pro)renin receptor in silkworm (Bombyx mori) larvae using BmMNPV bacmid. *Biotechnol Appl Biochem*, 49: 195–202.

Eide, D. J., Clarke, S., Nair, T. M., Gehl, M., Gribskov, M., Guerinot M. L., Harper, J. F. (2005) Characterization of the yeast ionome: a genome-wide analysis of nutrient mineral and trace element homeostasis in Saccharomyces cerevisiae. *Genome Biol*, 6(9): R77.

Elrick, M. J., Lieberman, A. P. (2013) Autophagic dysfunction in a lysosomal storage disorder due to impaired proteolysis. *Autophagy*, 9(2): 234–5.

Ellis, M. A., Weisz, O. A. (2006) In vitro assays differentially recapitulate protein export from the trans-Golgi network. *Anal Biochem*, 354(2): 314–6.

English, L., Chemali, M., Duron, J., Rondeau, C., Laplante, A., Gingras, D., Alexander, D., Leib, D., Norbury, C., Lippé, R., Desjardins, M. (2009) Autophagy enhances the presentation of endogenous viral antigens on MHC class I molecules during HSV-1 infection. *Nat Immunol*, 10(5): 480–7.

Eskelinen, E. L. (2005) Maturation of autophagic vacuoles in mammalian cells. *Autophagy*, 1: 1–10.

Eskelinen, E. L. (2008) To be or not to be? Examples of incorrect identification of autophagic compartments in conventional transmission electron microscopy of mammalian cells. *Autophagy*, 4: 257–260.

Esmail, S., Kartner, N., Yao, Y., Kim, J. W., Reithmeier, R. A. F., Manolson, M. F. (2018a) N-linked glycosylation of a subunit isoforms is critical for vertebrate vacuolar H^+-ATPase (V-ATPase) biosynthesis. *J Cell Biochem*, 119(1): 861–875.

Esmail, S., Kartner, N., Yao, Y., Kim, J. W., Reithmeier, R. A. F., Manolson, M. F. (2018b) Molecular mechanisms of cutis laxa- and distal renal tubular acidosis-causing mutations in V-ATPase a subunits, ATP6V0A2 and ATP6V0A4. *J Biol Chem*, 293(8): 2787–2800.

Farinas, J., Verkman, A. S. (1999) Receptor-mediated targeting of fluorescent probes in living cells. *J Biol Chem*, 274(12): 7603–6.

Feldt, S., Batenburg, W. W., Mazak, I., Maschke, U., Wellner, M., Kvakan, H., Dechend, R., Fiebeler, A., Burcklé, C., Contrepas, A., Jan Danser, A. H., Bader, M., Nguyen, G., Luft, F. C., Muller, D. N. (2008a) Prorenin and renin-induced extracellular signal-regulated kinase 1/2 activation in monocytes is not blocked by aliskiren or the handle-region peptide. *Hypertension*, 51: 682–8.

Feldt, S., Maschke, U., Dechend, R., Luft, F. C., Muller, D. N. (2008b) The putative (pro)renin receptor blocker HRP fails to prevent (pro)renin signaling. *J Am Soc Nephrol*, 19(4): 743–8.

Feng, H., Cheng, T., Pavlos, N. J., Yip, K. H., Carrello, A., Seeber, R., Eidne, K., Zheng, M. H., Xu, J. (2008) Cytoplasmic terminus of vacuolar type proton pump accessory subunit Ac45 is required for proper interaction with V(0) domain subunits and efficient osteoclastic bone resorption. *J Biol Chem*, 283(19): 13194–204.

Fimia, G. M., Stoykova, A., Romagnoli, A., Giunta, L., Di Bartolomeo, S., Nardacci, R., Corazzari, M., Fuoco, C., Ucar, A., Schwartz, P., Gruss, P., Piacentini, M., Chowdhury, K., Cecconi, F. (2007) Ambra1 regulates autophagy and development of the nervous system. *Nature*, 447(7148): 1121–5.

Flannery, A. R., Graham, L. A., Stevens, T. H. (2004) Topological characterization of the c, c', and c" subunits of the vacuolar ATPase from the yeast Saccharomyces cerevisiae. *J Biol Chem*, 279(38): 39856–62.

Forgac, M. (2007) Vacuolar ATPases: rotary proton pumps in physiology and pathophysiology. *Nat Rev Mol Cell Biol*, 8(11): 917–29.

Frattini, A., Orchard, P. J., Sobacchi, C., Giliani, S., Abinun, M., Mattsson, J. P., Keeling, D. J., Andersson, A. K., Wallbrandt, P., Zecca, L., Notarangelo, L. D., Vezzoni, P., Villa, A. (2000) Defects in TCIRG1 subunit of the vacuolar proton pump are responsible for a subset of human autosomal recessive osteopetrosis. *Nat Genet*, 25(3): 343–6.

Freeze, H. H., Chong, J. X., Bamshad, M. J., Ng, B. G. (2014) Solving glycosylation disorders: fundamental approaches reveal complicated pathways. *Am J Hum Genet*, 94(2): 161–175.

Fukushima, A., Kinugawa, S., Homma, T., Masaki, Y., Furihata, T., Abe, T., Suga, T., Takada, S., Kadoguchi, T., Okita, K., Matsushima, S., Tsutsui, H. (2013) Increased plasma soluble (pro)renin receptor levels are correlated with renal dysfunction in patients with heart failure. *Int J Cardiol*, 168(4): 4313–4.

Funke-Kaiser, H., Zollmann, F. S., Schefe, J. H., Unger, T. (2010) Signal transduction of the (pro)renin receptor as a novel therapeutic target for preventing end-organ damage. *Hypertens Res*, 33(2): 98–104.

Fyhrquist, F., Saijonmaa, O. (2008) Renin-angiotensin system revisited. *J Intern Med*, 264: 224–36.

Galli, T., McPherson, P. S., De Camilli, P. (1996) The V_0 sector of the V-ATPase, synaptobrevin, and synaptophysin are associated on synaptic vesicles in a Triton X-100-resistant, freeze-thawing sensitive, complex. *J Biol Chem*, 271(4): 2193–8.

Gálvez-Prieto, B., Bolbrinker, J., Stucchi, P., de Las Heras, A. I., Merino, B., Arribas, S., Ruiz-Gayo, M., Huber, M., Wehland, M., Kreutz, R., Fernandez-Alfonso, M. S. (2008) Comparative expression analysis of the renin-angiotensin system components between white and brown perivascular adipose tissue. *J Endocrinol*, 197(1): 55–64.

Gawlitzek, M., Ryll, T., Lofgren, J., Sliwkowski, M. B. (2000) Ammonium alters N-glycan structures of recombinant TNFR-IgG: degradative versus biosynthetic mechanisms. *Biotechnol Bioeng*, 68(6): 637–46.

Getlawi, F., Laslop, A., Schägger, H., Ludwig, J., Haywood, J., Apps, D. (1996) Chromaffin granule membrane glycoprotein IV is identical with Ac45, a membrane-integral subunit of the granule's H(+)-ATPase. *Neurosci Lett*, 219(1): 13–6.

Girard, M., Poujois, A., Fabre, M., Lacaille, F., Debray, D., Rio, M., Fenaille, F., Cholet, S., Ruel, C., Caussé, E., Selves, J., Bridoux-Henno, L., Woimant, F., Dupré, T., Vuillaumier-Barrot, S., Seta, N., Alric, L., de Lonlay, P., Bruneel, A. (2018) CCDC115-CDG: A new rare and misleading inherited cause of liver disease. *Mol Genet Metab*, 124(3): 228–235.

Gleixner, E. M., Canaud, G., Hermle, T., Guida, M. C., Kretz, O., Helmstädter, M., Huber, T. B., Eimer, S., Terzi, F., Simons, M. (2014) V-ATPase/mTOR signaling regulates megalin-mediated apical endocytosis. *Cell Rep*, 8(1): 10–9.

Glick, D., Barth, S., Macleod, K. F. (2010) Autophagy: cellular and molecular mechanisms. *J Pathol*, 221(1): 3–12.

Goldstein, B., Speth, R. C., Trivedi, M. (2016) Renin-angiotensin system gene expression and neurodegenerative diseases. *J Renin Angiotensin Aldosterone Syst*, 17(3). pii: 1470320316666750.

Gomez-Navarro, N., Miller, E. (2016) Protein sorting at the ER-Golgi interface. *J Cell Biol*, 215(6): 769–778.

Grabe, M., Oster, G. (2001) Regulation of organelle acidity. *J Gen Physiol*, 117(4): 329–44.

Graham, L. A., Hill, K. J., Stevens, T. H. (1998) Assembly of the yeast vacuolar H^+-ATPase occurs in the endoplasmic reticulum and requires a Vma12p/Vma22p assembly complex. *J Cell Biol*, 142(1): 39–49.

Graham, L. A., Stevens, T. H. (1999) Assembly of the yeast vacuolar proton-translocating ATPase. *J Bioenerg Biomembr*, 31(1): 39–47.

Graham, L. A., Powell, B., Stevens, T. H. (2000) Composition and assembly of the yeast

vacuolar H(+)-ATPase complex. *J Exp Biol*, 203(Pt 1): 61–70.

Graham, L. A., Flannery, A. R., Stevens, T. H. (2003) Structure and assembly of the yeast V-ATPase. *J Bioenerg Biomembr*, 35(4): 301–12.

Greenberg, A. S., Coleman, R. A., Kraemer, F. B., McManaman, J. L., Obin, M. S., Puri, V., Yan, Q. W., Miyoshi, H., Mashek, D. G. (2011) The role of lipid droplets in metabolic disease in rodents and humans. *J Clin Invest*, 121(6): 2102–10.

Griffiths, G., Quinn, P., Warren, G. (1983) Dissection of the Golgi complex. I. Monensin inhibits the transport of viral membrane proteins from medial to trans Golgi cisternae in baby hamster kidney cells infected with Semliki Forest virus. *J Cell Biol*, 96(3): 835–50.

Gross, J. M., Perkins, B. D., Amsterdam, A., Egaña, A., Darland, T., Matsui, J. I., Sciascia, S., Hopkins, N., Dowling, J. E. (2005) Identification of zebrafish insertional mutants with defects in visual system development and function. *Genetics*, 170(1): 245–61.

Guida, M. C., Hermle, T., Graham, L. A., Hauser, V., Ryan, M., Stevens, T. H., Simons, M. (2018) ATP6AP2 functions as a V-ATPase assembly factor in the endoplasmic reticulum. *Mol Biol Cell*, 29(18): 2156–2164.

Guillard, M. (2012) Biochemical and clinical investigations for the diagnosis of Congenital Disorders of Glycosylation. Thesis Radboud University Nijmegen, 2012.

Guillard, M., Dimopoulou, A., Fischer, B., Morava, E., Lefeber, D. J., Kornak, U., Wevers, R. A. (2009) Vacuolar H^+-ATPase meets glycosylation in patients with cutis laxa. *Biochim Biophys Acta*, 1792(9): 903–14.

Gupta, H. V., Vengoechea, J., Sahaya, K., Virmani, T. (2015) A splice site mutation in ATP6AP2 causes X-linked intellectual disability, epilepsy, and parkinsonism. *Parkinsonism Relat Disord*, 21(12): 1473–5.

Gutierrez, M. G., Munafo, D. B., Beron, W., Colombo, M. I. (2004) Rab7 is required for the normal progression of the autophagic pathway in mammalian cells. *J Cell Sci*, 117: 2687–2697.

Hamada, K., Taniguchi, Y., Shimamura, Y., Inoue, K., Ogata, K., Ishihara, M., Horino, T., Fujimoto, S., Ohguro, T., Yoshimoto, Y., Ikebe, M., Yuasa, K., Hoshino, E., Iiyama, T., Ichihara, A., Terada, Y. (2013) Serum level of soluble (pro)renin receptor is modulated in chronic kidney disease. *Clin Exp Nephrol*, 17(6): 848–56.

Hardie, D. G. (2014) AMPK sensing energy while talking to other signaling pathways. *Cell Metab*, 20(6): 939–52.

Hardie, D. G. (2015) AMPK: positive and negative regulation, and its role in whole-body energy homeostasis. *Curr Opin Cell Biol*, 33: 1–7.

Hayashi-Nishino, M., Fujita, N., Noda, T., Yamaguchi, A., Yoshimori, T., Yamamoto, A. (2009) A subdomain of the endoplasmic reticulum forms a cradle for autophagosome formation. *Nat Cell Biol*, 11(12): 1433–1437.

Hermle, T., Saltukoglu, D., Grünewald, J., Walz, G., Simons, M. (2010) Regulation of Frizzled-dependent planar polarity signaling by a V-ATPase subunit. *Curr Biol*, 20(14): 1269–76.

Hermle, T., Petzoldt, A. G., Simons, M. (2011) The role of proton transporters in epithelial Wnt signaling pathways. *Pediatr Nephrol*, 26(9): 1523–7.

Hermle, T., Guida, M. C., Beck, S., Helmstädter, S., Simons, M. (2013) Drosophila ATP6AP2/VhaPRR functions both as a novel planar cell polarity core protein and a regulator of endosomal trafficking. *EMBO J*, 32(2): 245–59.

Hiesinger, P. R., Fayyazuddin, A., Mehta, S. Q., Rosenmund, T., Schulze, K. L., Zhai, R. G., Verstreken, P., Cao, Y., Zhou, Y., Kunz, J., Bellen, H. J. (2005) The v-ATPase V_0 subunit a1 is required for a late step in synaptic vesicle exocytosis in Drosophila. *Cell*, 121(4): 607–620.

Hill, K., Cooper, A. A. (2000) Degradation of unassembled Vph1p reveals novel aspects of the yeast ER quality control system. *EMBO J*, 19(4): 550–61.

Hill, K. J., Stevens, T. H. (1994) Vma21p is a yeast membrane protein retained in the endoplasmic reticulum by a di-lysine motif and is required for the assembly of the vacuolar H(+)-ATPase complex. *Mol Biol Cell*, 5(9): 1039–50.

Hill, K. J., Stevens, T. H. (1995) Vma22p is a novel endoplasmic reticulum-associated protein required for assembly of the yeast vacuolar H(+)-ATPase complex. *J Biol Chem*, 270(38): 22329–36.

Hinton, A., Sennoune, S. R., Bond, S., Fang, M., Reuveni, M., Sahagian, G. G., Jay, D., Martinez-Zaguilan, R., Forgac, M. (2009) Function of a subunit isoforms of the V-ATPase in pH homeostasis and in vitro invasion of MDA-MB231 human breast cancer cells. *J Biol Chem*, 284(24): 16400–8.

Hirano, M., DiMauro, S. (2009) VMA21 deficiency: a case of myocyte indigestion. *Cell*, 37(2): 213–5.

Hirata, R., Graham, L. A., Takatsuki, A., Stevens, T. H, Anraku Y. (1997) VMA11 and VMA16 encode second and third proteolipid subunits of the *Saccharomyces cerevisiae* vacuolar membrane H^+-ATPase. *J Biol Chem*, 272: 4795–4803.

Hirata, T., Iwamoto-Kihara, A., Sun-Wada, G. H., Okajima, T., Wada, Y., Futai, M. (2003) Subunit rotation of vacuolar-type proton pumping ATPase: relative rotation of the G and C subunits. *J Biol Chem*, 278(26): 23714–9.

Hirata, R., Umemoto, N., Ho, M. N., Ohya, Y., Stevens, T. H., Anraku, Y. (1993) VMA12 is essential for assembly of the vacuolar H(+)-ATPase subunits onto the vacuolar membrane in *Saccharomyces cerevisiae*. *J Biol Chem*, 268(2): 961–7.

Hirose, T., Hashimoto, M., Totsune, K., Metoki, H., Hara, A., Satoh, M., Kikuya, M., Ohkubo, T., Asayama, K., Kondo, T., Kamide, K., Katsuya, T., Ogihara, T., Izumi, S., Rakugi, H., Takahashi, K., Imai, Y. (2011) Association of (pro)renin receptor gene polymorphisms with lacunar infarction and left ventricular hypertrophy in Japanese women: the Ohasama study. *Hypertens Res*, 34: 530–535.

Ho, M. N., Hill, K. J., Lindorfer, M. A., Stevens, T. H. (1993) Isolation of vacuolar membrane H(+)-ATPase-deficient yeast mutants; the VMA5 and VMA4 genes are essential for assembly and activity of the vacuolar H(+)-ATPase. *J Biol Chem*, 268(1): 221–7.

Holliday, L. S., Lu, M., Lee, B. S., Nelson, R. D., Solivan, S., Zhang, L., Gluck, S. L. (2000) The amino-terminal domain of the B subunit of vacuolar H^+-ATPase contains a filamentous actin binding site. *J Biol Chem*, 275(41): 32331–7.

Holthuis, J. C., Jansen, E. J., Schoonderwoert, V. T., Burbach, J. P., Martens, G. J. (1999) Biosynthesis of the vacuolar H^+-ATPase accessory subunit Ac45 in Xenopus pituitary. *Eur J Biochem*, 262(2): 484–91.

Huang, Y., Wongamorntham, S., Kasting, J., McQuillan, D., Owens, R. T., Yu, L., Noble, N. A., Border, W. (2006) Renin increases mesangial cell transforming growth factor-beta1 and matrix proteins through receptor-mediated, angiotensin II-independent mechanisms. *Kidney Int*, 69: 105–13.

Huang, Y., Border, W. A., Noble, N. A. (2007a) Functional renin receptors in renal mesangial cells. *Curr Hypertens Rep*, 9 (2): 133–139.

Huang, Y., Noble, N. A., Zhang, J., Xu, C., Border, W. A. (2007b) Renin-stimulated TGF-β1 expression is regulated by a mitogen-activated protein kinase in mesangial cells. *Kidney Int*, 72: 45–52.

Hucthagowder, V., Morava, E., Kornak, U., Lefeber, D. J., Fischer, B., Dimopoulou, A., Aldinger, A., Choi, J., Davis, E. C., Abuelo, D. N., Adamowicz, M., Al-Aama, J., Basel-Vanagaite, L., Fernandez, B., Greally, M. T., Gillessen-Kaesbach, G., Kayserili, H., Lemyre, E., Tekin, M., Türkmen, S., Tuysuz, B., Yüksel-Konuk, B., Mundlos, S., Van Maldergem, L., Wevers, R. A., Urban. Z. (2009) Loss-of-function mutations in ATP6V0A2 impair

vesicular trafficking, tropoelastin secretion and cell survival. *Hum Mol Genet*, 18(12): 2149–65.

Hurtado-Lorenzo, A., Skinner, M., El Annan, J., Futai, M., Sun-Wada, G. H., Bourgoin, S., Casanova, J., Wildeman, A., Bechoua, S., Ausiello, D. A., Brown, D., Marshansky, V. (2006) V-ATPase interacts with ARNO and Arf6 in early endosomes and regulates the protein degradative pathway. *Nat Cell Biol*, 8(2): 124–36.

Huss, M., Ingenhorst, G., König, S., Gassel, M., Dröse, S., Zeeck, A., Altendorf, K., Wieczorek, H. (2002) Concanamycin A, the specific inhibitor of V-ATPases, binds to the V_0 subunit c. *J Biol Chem*, 277(43): 40544–8.

Ichihara, A. (2012) (Pro)renin receptor and vacuolar H(+)-ATPase. *Keio J Med*, 61(3): 73–8.

Ichihara, A., Hayashi, M., Kaneshiro, Y., Suzuki, F., Nakagawa, T., Tada, Y., Koura, Y., Nishiyama, A., Okada, H., Uddin, M. N., Nabi, A. H., Ishida, Y., Inagami, T., Saruta, T. (2004) Inhibition of diabetic nephropathy by a decoy peptide corresponding to the "handle" region for nonproteolytic activation of prorenin. *J Clin Invest*, 114: 1128–35.

Ichihara, A., Kaneshiro, Y., Takemitsu, T., Sakoda, M., Suzuki, F., Nakagawa, T., Nishiyama, A., Inagami, T., Hayashi, M. (2006a) Nonproteolytic activation of prorenin contributes to development of cardiac fibrosis in genetic hypertension. *Hypertension*, 47: 894–900.

Ichihara, A., Kaneshiro, Y., Takemitsu, T., Sakoda, M., Itoh, H. (2007) The (pro)renin receptor and the kidney. *Semin Nephrol*, 27(5): 524–8.

Ichihara, A., Kinouchi, K. (2011) Current knowledge of (pro)renin receptor as an accessory protein of vacuolar H^+-ATPase. *J Renin Angiotensin Aldosterone Syst*, 12(4): 638–40.

Ichihara, A., Suzuki, F., Nakagawa, T., Kaneshiro, Y., Takemitsu, T., Sakoda, M., Nabi, A. H., Nishiyama, A., Sugaya, T., Hayashi, M., Inagami, T. (2006b) Prorenin receptor blockade inhibits development of glomerulosclerosis in diabetic angiotensin II type 1a receptor-deficient mice. *J Am Soc Nephrol*, 17: 1950–1961.

Ichihara, A., Sakoda, M., Kurauchi-Mito, A., Narita, T., Kinouchi, K., Murohashi-Bokuda, K., Itoh, H. (2010) Possible roles of human (pro)renin receptor suggested by recent clinical and experimental findings. *Hypertens Res*, 33(3): 177–80.

Imamura, H., Nakano, M., Noji, H., Muneyuki, E., Ohkuma, S., Yoshida, M., Yokoyama, K. (2003) Evidence for rotation of V_0-ATPase. *Proc Natl Acad Sci U S A*, 100(5): 2312–5.

Jääskeläinen, S. K., Juel, V. C., Udd, B., Villanova, M., Liguori, R., Minassian, B. A., Falck, B., Niemi, P., Kalimo, H. (2002) Electrophysiological findings in X-linked myopathy with excessive autophagy. *Ann Neurol*, 51(5): 648–52.

Jackson, D. D., Stevens, T. H. (1997) VMA12 encodes a yeast endoplasmic reticulum protein required for vacuolar H^+-ATPase assembly. *J Biol Chem*, 272(41): 25928–34.

Jaeken, J., Hennet, T., Matthijs, G., Freeze, H. H. (2009) CDG nomenclature: time for a change! *Biochim Biophys Acta*, 1792(9): 825–6.

Jaeken, J., Péanne, R. (2017) What is new in CDG? *J Inherit Metab Dis*, 40(4): 569–586.

Jäger, S., Bucci, C., Tanida, I., Ueno, T., Kominami, E., Saftig, P., Eskelinen, E. L. (2004) Role for Rab7 in maturation of late autophagic vacuoles. *J Cell Sci*, 117(Pt 20): 4837–48.

Jansen, E. J., Holthuis, J. C., McGrouther, C., Burbach, J. P., Martens, G. J. (1998) Intracellular trafficking of the vacuolar H^+-ATPase accessory subunit Ac45. *J Cell Sci*, 111 (Pt 20): 2999–3006.

Jansen, E. J., Martens, G. J. (2012) Novel insights into V-ATPase functioning: distinct roles for its accessory subunits ATP6AP1/Ac45 and ATP6AP2/(pro) renin receptor. *Curr Protein Pept Sci*, 13(2): 124–33.

Jansen, E. J., Scheenen, W. J., Hafmans, T. G., Martens, G. J. (2008) Accessory subunit Ac45 controls the V-ATPase in the regulated secretory pathway. *Biochim Biophys Acta*, 1783(12): 2301–10.

Jansen, J. C., Timal, S., van Scherpenzeel, M., Michelakakis, H., Vicogne, D., Ashikov, A., Moraitou, M., Hoischen, A., Huijben, K., Steenbergen, G., van den Boogert, M. A., Porta, F., Calvo, P. L., Mavrikou, M., Cenacchi, G., van den Bogaart, G., Salomon, J., Holleboom, A. G., Rodenburg,, R. J., Drenth, J. P., Huynen, M. A., Wevers, R. A., Morava, E., Foulquier, F., Veltman, J. A., Lefeber, D. J. (2016a) TMEM199 Deficiency Is a Disorder of Golgi Homeostasis Characterized by Elevated Aminotransferases, Alkaline Phosphatase, and Cholesterol and Abnormal Glycosylation. *Am J Hum Genet*, 98(2): 322–30.

Jansen, J. C., Cirak, S., van Scherpenzeel, M., Timal, S., Reunert, J., Rust, S., Pérez, B., Vicogne, D., Krawitz, P., Wada, Y., Ashikov, A., Pérez-Cerdá, C., Medrano, C., Arnoldy, A., Hoischen, A., Huijben, K., Steenbergen, G., Quelhas, D., Diogo, L., Rymen, D., Jaeken, J., Guffon, N., Cheillan, D., van den Heuvel, L. P., Maeda, Y., Kaiser, O., Schara, U., Gerner, P., van den Boogert, M. A., Holleboom, A. G., Nassogne, M. C., Sokal, E., Salomon, J., van den Bogaart, G., Drenth, J. P., Huynen, M. A., Veltman, J. A., Wevers, R. A., Morava, E., Matthijs, G., Foulquier, F., Marquardt, T., Lefeber, D. J. (2016b) CCDC115 Deficiency Causes a Disorder of Golgi Homeostasis with Abnormal Protein Glycosylation. *Am J Hum Genet*, 98(2): 310–21.

Jansen, E. J., Timal, S., Ryan, M., Ashikov, A., van Scherpenzeel, M., Graham, L. A., Mandel, H., Hoischen, A., Iancu, T. C., Raymond, K., Steenbergen, G., Gilissen, C., Huijben, K., van Bakel, N. H., Maeda, Y., Rodenburg, R. J., Adamowicz, M., Crushell, E., Koenen, H., Adams, D., Vodopiutz, J., Greber-Platzer, S., Müller, T., Dueckers, G., Morava, E., Sykut-Cegielska, J., Martens, G. J., Wevers, R. A., Niehues, T., Huynen, M. A., Veltman, J. A., Stevens, T. H., Lefeber, D. J. (2016c) ATP6AP1 deficiency causes an immunodeficiency with hepatopathy, cognitive impairment and abnormal protein glycosylation. *Nat Commun*, 7: 11600.

Jefferies, K. C., Forgac, M. (2008) Subunit H of the vacuolar (H+) ATPase inhibits ATP hydrolysis by the free V1 domain by interaction with the rotary subunit F. *J Biol Chem*, 283(8): 4512–9.

Jung, Y. S., Jun, S., Kim, M. J., Lee, S. H., Suh, H. N., Lien, E. M., Jung, H. Y., Lee, S., Zhang, J., Yang, J. I., Ji, H., Wu, J. Y., Wang, W., Miller, R. K., Chen, J., McCrea, P. D., Kopetz, S., Park, J. I. (2018) TMEM9 promotes intestinal tumorigenesis through vacuolar-ATPase-activated Wnt/β-catenin signalling. *Nat Cell Biol*, 20(12): 1421–1433.

Kalimo, H., Savontaus, M. L., lang, H., Paljarvi, L., Sonninen, V., Dean, P. B., Katevuo, K., Salminen, A. (1988) X-linked myopathy with excessive autophagy: a new hereditary muscle disease. *Ann Neurol*, 23, 258–65.

Kanda, A., Noda, K., Yuki, K., Ozawa, Y., Furukawa, T., Ichihara, A., Ishida, S. (2013) Atp6ap2/(pro)renin receptor interacts with Par3 as a cell polarity determinant required for laminar formation during retinal development in mice. *J Neurosci*, 33(49): 19341–51.

Kane, P. M. (1995) Disassembly and reassembly of the yeast vacuolar H(+)-ATPase in vivo. *J Biol Chem*, 270(28): 17025–32.

Kane, P. M. (2006) The where, when, and how of organelle acidification by the yeast vacuolar H^+-ATPase. *Microbiol Mol Biol Rev*, 70(1): 177–91.

Kane, P. M. (2007) The long physiological reach of the yeast vacuolar H^+-ATPase. *J Bioenerg Biomembr*, 39: 415–21.

Kane, P. M. (2012) Targeting reversible disassembly as a mechanism of controlling V-ATPase activity. *Curr Protein Pept Sci*, 13(2): 117–23.

Kaneshiro, Y., Ichihara, A., Sakoda, M., Takemitsu, T., Nabi, A. H., Uddin M. N., Nakagawa, T., Nishiyama, A., Suzuki, F., Inagami, T., Itoh, H. (2007) Slowly progressive, angiotensin II-independent glomerulosclerosis in human (pro)renin receptor-transgenic rats. *J Am Soc Nephrol*, 18(6): 1789–95.

Kaneshiro, Y., Ichihara, A., Takemitsu, T., Sakoda, M., Suzuki, F., Nakagawa, T., Hayashi, M., Inagami, T. (2006) Increased expression of cyclooxygenase-2 in the renal cortex of human prorenin receptor gene-transgenic rats. *Kidney Int*, 70(4): 641–6.

Karet, F. E., Finberg, K. E., Nelson, R. D., Nayir, A., Mocan, H., Sanjad, S. A., Rodriguez-Soriano, J., Santos, F., Cremers, C. W., Di Pietro, A., Hoffbrand, B. I., Winiarski, J., Bakkaloglu, A., Ozen, S., Dusunsel, R., Goodyer, P., Hulton, S. A., Wu, D. K., Skvorak, A. B., Morton, C. C., Cunningham, M. J., Jha, V., Lifton, R. P. (1999) Mutations in the gene encoding B1 subunit of H^+-ATPase cause renal tubular acidosis with sensorineural deafness. *Nat Genet*, 21(1): 84–90.

Kasper, D., Planells-Cases, R., Fuhrmann, J. C., Scheel, O., Zeitz, O., Ruether, K., Schmitt, A., Poët, M., Steinfeld, R., Schweizer, M., Kornak, U., Jentsch, T. J. (2005) Loss of the chloride channel ClC-7 leads to lysosomal storage disease and neurodegeneration. *EMBO*, 24(5): 1079–91.

Kawasaki-Nishi, S., Nishi, T., Forgac, M. (2001) Yeast V-ATPase complexes containing different isoforms of the 100-kDa a-subunit differ in coupling efficiency and in vivo dissociation. *J Biol Chem*, 276(21): 17941–8.

Kawasaki-Nishi, S., Nishi, T., Forgac, M. (2003) Interacting helical surfaces of the transmembrane segments of subunits a and c' of the yeast V-ATPase defined by disulfide-mediated cross-linking. *J Biol Chem*, 278(43): 41908–13.

Kelley, L. A., Mezulis, S., Yates, C. M., Wass, M. N., Sternberg, M. J. (2015) The Phyre2 web portal for protein modeling, prediction and analysis. *Nat Protoc*, 10(6): 845–58.

Kellokumpu, S., Sormunen, R., Kellokumpu, I. (2002) Abnormal glycosylation and altered Golgi structure in colorectal cancer: dependence on intra-Golgi pH. *FEBS*, 516(1-3): 217–24.

Kettner, C., Bertl, A., Obermeyer, G., Slayman, C., Bihler, H. (2003) Electrophysiological analysis of the yeast V-type proton pump: variable coupling ratio and proton shunt. *Biophys J*, 85(6): 3730–8.

Kim, J. H., Lingwood, C. A., Williams, D. B., Furuya, W., Manolson, M. F., Grinstein, S. (1996) Dynamic measurement of the pH of the Golgi complex in living cells using retrograde transport of the verotoxin receptor. *J Cell Biol*, 134(6): 1387–99.

Kim, Y. C., Guan, K. L. (2015) mTOR: a pharmacologic target for autophagy regulation. *J Clin Invest*, 125(1): 25–32.

Kim, Y. C., Park, H. W., Sciarretta, S., Mo, J. S., Jewell, J. L., Russell, R. C., Wu, X., Sadoshima, J., Guan, K. L. (2014) Rag GTPases are cardioprotective by regulating lysosomal function. *Nat Commun*, 5: 4241.

Kinouchi, K., Ichihara, A., Sano, M., Sun-Wada, G. H., Wada, Y., Kurauchi-Mito, A., Bokuda, K., Narita, T., Oshima, Y., Sakoda, M., Tamai, Y., Sato, H., Fukuda, K., Itoh, H. (2010) The (pro)renin receptor/ATP6AP2 is essential for vacuolar H^+-ATPase assembly in murine cardiomyocytes. *Circ Res*, 107(1): 30–34.

Kinouchi, K., Ichihara, A., Sano, M., Sun-Wada, G. H., Wada, Y., Ochi, H., Fukuda, T., Bokuda, K., Kurosawa, H., Yoshida, N., Takeda, S., Fukuda, K., Itoh, H. (2013) The role of individual domains and the significance of shedding of ATP6AP2/(pro)renin receptor in vacuolar H(+)-ATPase biogenesis. *PLoS One*, 8(11): e78603.

Kirkin, V., McEwan, D. G., Novak, I., Dikic, I. (2009) A role for ubiquitin in selective autophagy. *Mol Cell*, 34(3): 259–69.

Klionsky, D. J. (2007) Autophagy: from phenomenology to molecular understanding in less than a decade. *Nat Rev Mol Cell Biol*, 8: 931–937.

Klionsky, D. J., Herman, P. K., Emr, S. D. (1990) The fungal vacuole: composition, function, and biogenesis. *Microbiol Rev*, 54(3): 266–292.

Koike, M., Shibata, M., Waguri, S., Yoshimura, K., Tanida, I., Kominami, E., Gotow, T., Peters, C., von Figura, K., Mizushima, N., Saftig, P., Uchiyama, Y. (2005) Participation of autophagy in storage of lysosomes in neurons from mouse models of neuronal ceroid-lipofuscinoses (Batten disease). *Am J Pathol*, 167(6): 1713–1728.

Konialis, C., Assimakopoulos, E., Hagnefelt, B., Karapanou, S., Sotiriadis, A., Pangalos, C. (2017) Prenatal diagnosis of X-linked myopathy associated with a VMA21 gene mutation afforded through a novel targeted exome sequencing strategy applied in fetuses with abnormal ultrasound findings. *Clin Case Rep*, 5(3): 308–311.

Kornak, U., Reynders, E., Dimopoulou, A., van Reeuwijk, J., Fischer, B., Rajab, A., Budde, B., Nürnberg, P., Foulquier, F., ARCL Debré-type Study Group, Lefeber, D., Urban, Z., Gruenewald, S., Annaert, W., Brunner, H. G., van Bokhoven, H., Wevers, R., Morava, E., Matthijs, G., Van Maldergem, L., Mundlos, S. (2008) Impaired glycosylation and cutis laxa caused by mutations in the vesicular H^+-ATPase subunit ATP6V0A2. *Nat Genet*, 40(1): 32–4.

Kornak, U., Schulz, A., Friedrich, W., Uhlhaas, S., Kremens, B., Voit, T., Hasan, C., Bode, U., Jentsch, T. J., Kubisch, C. (2000) Mutations in the a3 subunit of the vacuolar H(+)-ATPase cause infantile malignant osteopetrosis. *Hum Mol Genet*, 9(13): 2059–63.

Korvatska, O., Strand, N. S., Berndt, J. D., Strovas, T., Chen, D. H., Leverenz, J. B., Kiianitsa, K., Mata, I. F., Karakoc, E., Greenup, J. L., Bonkowski, E., Chuang, J., Moon, R. T., Eichler, E. E., Nickerson, D. A., Zabetian, C. P., Kraemer, B. C., Bird, T. D., Raskind, W. H. (2013) Altered splicing of ATP6AP2 causes X-linked parkinsonism with spasticity (XPDS). *Hum Mol Genet*, 22(16): 3259–68.

Krebs, C., Hamming, I., Sadaghiani, S., Steinmetz, O. M., Meyer-Schwesinger, C., Fehr, S., Stahl, R. A., Garrelds, I. M., Danser, A. H., van Goor, H., Contrepas, A., Nguyen, G., Wenzel, U. (2007) Antihypertensive therapy upregulates renin and (pro)renin receptor in the clipped kidney of Goldblatt hypertensive rats. *Kidney Int*, 72(6): 725–30.

Kroeger, H., Miranda, E., MacLeod, I., Pérez, J., Crowther, D. C., Marciniak, S. J., Lomas, D. A. (2009) Endoplasmic reticulum-associated degradation (ERAD) and autophagy cooperate to degrade polymerogenic mutant serpins. *J Biol Chem*, 284(34): 22793–802.

Krop, M., Lu, X., Danser, A. H., Meima, M. E. (2013) The (pro)renin receptor. A decade of research: what have we learned? *Pflugers Arch*, 465(1): 87–97.

Kuismanen, E., Saraste, J., Pettersson, R. F. (1985) Effect of monensin on the assembly of Uukuniemi virus in the Golgi complex. *J Virol*, 55(3): 813–22.

Kundu, M., Thompson, C. B. (2005) Macroautophagy versus mitochondrial autophagy: a question of fate? *Cell Death Diff*, 12: 1484–1489.

Kurashige, T., Takahashi, T., Yamazaki, Y., Nagano, Y., Kondo, K., Nakamura, T., Yamawaki, T., Tsuburaya, R., Hayashi, Y. K., Nonaka, I., Nishino, I., Matsumoto, M. (2013) Elevated urinary β2 microglobulin in the first identified Japanese family afflicted by X-linked myopathy with excessive autophagy. *Neuromuscul Disord*, 23(11): 911–6.

Kurauchi-Mito, A., Ichihara, A., Bokuda, K., Sakoda, M., Kinouchi, K., Yaguchi, T., Yamada, T., Sun-Wada, G. H., Wada, Y., Itoh, H. (2014) Significant roles of the (pro)renin receptor in integrity of vascular smooth muscle cells. *Hypertens Res*, 37(9): 830–5.

Kwanten, W. J., Martinet, W., Michielsen, P. P., Francque, S. M. (2014) Role of autophagy in the pathophysiology of nonalcoholic fatty liver disease: a controversial issue. *World J Gastroenterol*, 20(23): 7325–38.

Lee, B. S., Gluck, S. L., Holliday, L. S. (1999) Interaction between vacuolar H(+)-ATPase and microfilaments during osteoclast activation. *J. Biol. Chem*, 274(41): 29164–29171.

Lee, J. S., Mendez, R., Heng, H. H., Yang, Z. Q., Zhang, K. (2012) Pharmacological ER stress promotes hepatic lipogenesis and lipid droplet formation. *Am J Transl Res*, 4(1): 102–13.

Lemmon, M. A, Schlessinger, J. (2010) Cell signaling by receptor tyrosine kinases. *Cell*, 141(7): 1117–34.

Li, S. C., Diakov, T. T., Xu, T., Tarsio, M., Zhu, W., Couoh-Cardel, S., Weisman, L. S., Kane, P. M. (2014) The signaling lipid PI(3,5)P_2 stabilizes V_1-V_0 sector interactions and activates the V-ATPase. *Mol Biol Cell*, 25(8): 1251–62.

Li, W., Peng, H., Seth, D. M., Feng, Y. (2012) The Prorenin and (Pro)renin Receptor: New Players in the Brain Renin-Angiotensin System? *Int J Hypertens*, 2012: 290635.

Liang, C., Feng, P., Ku, B., Dotan, I., Canaani, D., Oh, B. H., Jung, J. U. (2006) Autophagic and tumour suppressor activity of a novel Beclin1-binding protein UVRAG. *Nat Cell Biol*, 8(7): 688–99.

Liégeois, S., Benedetto, A., Garnier, J. M., Schwab, Y., Labouesse, M. (2006) The V0-ATPase mediates apical secretion of exosomes containing Hedgehog-related proteins in Caenorhabditis elegans. *J Cell Biol* 173(6): 949–61.

Lindau, M., Almers, W. (1995) Structure and function of fusion pores in exocytosis and ectoplasmic membrane fusion. *Curr Opin Cell Biol*, 7(4): 509–17.

Liu, B., Li, H., Repa, J. J., Turley, S. D., Dietschy, J. M. (2008) Genetic variations and treatments that affect the lifespan of the NPC1 mouse. *J Lipid Res*, 49(3): 663–9.

Liu, B., Turley, S. D., Burns, D. K., Miller, A. M., Repa, J. J., Dietschy, J. M. (2009) Reversal of defective lysosomal transport in NPC disease ameliorates liver dysfunction and neurodegeneration in the npc1-/- mouse. *Proc Natl Acad Sci U S A*, 106(7): 2377–82.

Louagie, E., Taylor, N. A., Flamez, D., Roebroek, A. J., Bright, N. A., Meulemans, S., Quintens, R., Herrera, P. L., Schuit, F., Van de Ven, W. J., Creemers, J. W. (2008) Role of furin in granular acidification in the endocrine pancreas: identification of the V-ATPase subunit Ac45 as a candidate substrate. *Proc Natl Acad Sci U S A*, 105(34): 12319–24.

Louboutin, J. P., Villanova, M., Ulrich, G., De Clerck, L. S., Fardeau, M., Sagniez, M. (1996) Elevated levels of complement components C5 and C9 and decreased antitrypsin activity in the serum of patients with X-linked vacuolated myopathy. *Muscle Nerve*, 19(9): 1144–7.

Lu, M., Sautin, Y. Y., Holliday, L. S., Gluck, S. L. (2004) The glycolytic enzyme aldolase mediates assembly, expression, and activity of vacuolar H^+-ATPase. *J Biol Chem*, 279(10): 8732–9.

Ludwig, J., Kerscher, S., Brandt, U., Pfeiffer, K., Getlawi, F., Apps, D. K., Schagger, H. (1998) Identification and characterization of a novel 9.2-kDa membrane sector-associated protein of vacuolar proton-ATPase from chromaffin granules. *J Biol Chem*, 273(18): 10939–47.

Ma, L., Ouyang, Q., Werthmann, G. C., Thompson, H. M., Morrow, E. M. (2017) Live-cell Microscopy and Fluorescence-based Measurement of Luminal pH in Intracellular Organelles. *Front Cell Dev Biol*, 5: 71.

MacDonald, B. T., Tamai, K., He, X. (2009) Wnt/beta-catenin signaling: components, mechanisms, and diseases. *Dev Cell*, 17(1): 9–26.

MacLeod, K. J., Vasilyeva, E., Merdek, K., Vogel, P. D., Forgac, M. (1999) Photoaffinity labeling of wild-type and mutant forms of the yeast V-ATPase A subunit by 2-azido-[(32)P]ADP. *J Biol Chem*, 274(46): 32869–74.

Maeda, Y., Ide, T., Koike, M., Uchiyama, Y., Kinoshita, T. (2008) GPHR is a novel anion channel critical for acidification and functions of the Golgi apparatus. *Nat Cell Biol*, 10(10): 1135–45.

Maeda, Y., Kinoshita, T. (2010) The acidic environment of the Golgi is critical for glycosylation and transport. *Methods Enzymol*, 480: 495–510.

Maher, M. J., Akimoto, S., Iwata, M., Nagata, K., Hori, Y., Yoshida, M., Yokoyama, S., Iwata, S., Yokoyama, K. (2009) Crystal structure of A3B3 complex of V-ATPase from Thermus thermophilus. *EMBO J*, 28(23): 3771–9.

Maiuri, M. C., Le Toumelin, G., Criollo, A., Rain, J. C., Gautier, F., Juin, P., Tasdemir,

E., Pierron, G., Troulinaki, K., Tavernarakis, N., Hickman, J. A., Geneste, O., Kroemer, G. (2007) Functional and physical interaction between Bcl-X(L) and a BH3-like domain in Beclin-1. *EMBO J*, 26(10): 2527–39.

Majoul, I., Straub, M., Hell, S. W., Duden, R., Söling, H. D. (2001) KDEL-cargo regulates interactions between proteins involved in COPI vesicle traffic: measurements in living cells using FRET. *Dev Cell*, 1(1): 139–53.

Malkus, P., Graham L. A., Stevens, T. H., Schekman, R. (2004) Role of Vma21p in assembly and transport of the yeast vacuolar ATPase. *Mol Biol Cell*, 15(11): 5075–91.

Manolson, M. F., Wu, B., Proteau, D., Taillon, B. E., Roberts, B. T., Hoyt, M. A., Jones, E. W. (1994) STV1 gene encodes functional homologue of 95-kDa yeast vacuolar H(+)-ATPase subunit Vph1p. *J Biol Chem*, 269(19): 14064–74.

Mao, Y., Yu, F., Wang, J., Guo, C., Fan, X. (2016) Autophagy: a new target for nonalcoholic fatty liver disease therapy. *Hepat Med*, 8: 27–37.

Marques-da-Silva, D., Dos Reis Ferreira, V., Monticelli, M., Janeiro, P., Videira, P. A., Witters, P., Jaeken, J., Cassiman, D. (2017) Liver involvement in congenital disorders of glycosylation (CDG). A systematic review of the literature. *J Inherit Metab Dis*, 40(2): 195–207.

Marshansky, V., Rubinstein, J. L., Grüber, G. (2014) Eukaryotic V-ATPase: novel structural findings and functional insights. *Biochim Biophys Acta*, 1837(6): 857–79.

Martina, J. A., Chen, Y., Gucek, M., Puertollano, R. (2012) MTORC1 functions as a transcriptional regulator of autophagy by preventing nuclear transport of TFEB. *Autophagy*, 8(6): 903–14.

Martina, J. A., Puertollano, R. (2013) Rag GTPases mediate amino acid-dependent recruitment of TFEB and MITF to lysosomes. *J Cell Biol*, 200(4): 475–91.

Maruyama, N., Segawa, T., Kinoshita, N., Ichihara, A. (2013) Novel sandwich ELISA for detecting the human soluble (pro)renin receptor. *Front Biosci (Elite Ed)*, 5: 583–90.

Matlin, K. S. (1986) The sorting of proteins to the plasma membrane in epithelial cells. *J Cell Biol*, 103(6 Pt 2): 2565c8.

Matsunaga, K., Saitoh, T., Tabata, K., Omori, H., Satoh, T., Kurotori, N., Maejima, I., Shirahama-Noda, K., Ichimura, T., Isobe, T., Akira, S., Noda, T., Yoshimori, T. (2009) Two Beclin 1-binding proteins, Atg14L and Rubicon, reciprocally regulate autophagy at different stages. *Nat Cell Biol*, 11(4): 385–96.

Mauvezin, C., Nagy, P., Juhasz, G., Neufeld, T. P. (2015) Autophagosome-lysosome fusion is independent of V-ATPase-mediated acidification. *Nat Commun*, 6: 7007.

Maxson, M. E., Grinstein, S. (2014) The vacuolar-type H^+-ATPase at a glance - more than a proton pump. *J Cell Sci*, 127(Pt 23): 4987–93.

McGuire, C., Stransky, L., Cotter, K., Forgac, M. (2017) Regulation of V-ATPase activity. *Front Biosci (Landmark Ed)*, 22: 609–622.

McGuire, C. M., Forgac, M. (2018) Glucose starvation increases V-ATPase assembly and activity in mammalian cells through AMP kinase and phosphatidylinositide 3-kinase/Akt signaling. *J Biol Chem*, 293(23): 9113–9123.

Mercier, S., Magot, A., Caillon, F., Isidor, B., David, A., Ferrer, X., Vital, A., Coquet, M., Penttilä, S., Udd, B., Mussini, J. M., Pereon, Y. (2015) Muscle magnetic resonance imaging abnormalities in X-linked myopathy with excessive autophagy. *Muscle Nerve*, 52(4): 673–80.

Mijaljica, D., Prescott, M., Devenish, R. J. (2011) V-ATPase engagement in autophagic processes. *Autophagy*, 7(6): 666–668.

Miles, A. L., Burr, S. P., Grice, G. L., Nathan, J. A. (2017) The vacuolar-ATPase complex and assembly factors, TMEM199 and CCDC115, control HIF1 αprolyl hydroxylation by regulating cellular iron levels. *Elife*, 6. pii: e22693.

Minassian, B. A., Aiyar, R., Alic, S., Banwell, B., Villanova, M., Fardeau, M., Mandell,

J. W., Juel, V. C., Rafii, M., Auranen, M., Kalimo, H. (2002) Narrowing in on the causative defect of an intriguing X-linked myopathy with excessive autophagy. *Neurology*, 59(4): 596–601.

Miranda, K. C., Karet, F. E., Brown, D. (2010) An extended nomenclature for mammalian V-ATPase subunit genes and splice variants. *PLoS One*, 5(3): e9531.

Mitchener, J. S., Shelburne, J. D., Bradford, W. D., Hawkins, H. K. (1976) Cellular autophagocytosis induced by deprivation of serum and amino acids in HeLa cells. *Am J Pathol*, 83(3): 485–492.

Mizushima, N. (2007) Autophagy: process and function. *Genes Dev*, 21: 2861–2873.

Mizushima, N., Yoshimori, T., Levine, B. (2010) Methods in mammalian autophagy research. *Cell*, 140(3): 313–26.

Mizushima, N., Komatsu, M. (2011) Autophagy: renovation of cells and tissues. *Cell*, 147(4): 728–741.

Mizushima, N., Klionsky, D. J. (2007) Protein turnover via autophagy: implications for metabolism. *Ann Rev Nutr*, 27: 19–40.

Morano, K. A., Klionsky, D. J. (1994) Differential effects of compartment deacidification on the targeting of membrane and soluble proteins to the vacuole in yeast. *J. Cell Sci*, 107, 2813–2824.

Morava, E., Lefeber, D. J., Urban, Z., de Meirleir, L., Meinecke, P., Gillessen Kaesbach, G., Sykut-Cegielska, J., Adamowicz, M., Salafsky, I., Ranells, J., Lemyre, E., van Reeuwijk, J., Brunner, H. G., Wevers, R. A. (2008) Defining the phenotype in an autosomal recessive cutis laxa syndrome with a combined congenital defect of glycosylation. *Eur J Hum Genet*, 16(1): 28–35.

Morimoto, S., Ando, T., Niiyama, M., Seki, Y., Yoshida, N., Watanabe, D., Kawakami-Mori, F., Kobori, H., Nishiyama, A., Ichihara, A. (2014) Serum soluble (pro)renin receptor levels in patients with essential hypertension. *Hypertens Res*, 37(7): 642–8.

Morisawa, Y., Fujieda, M., Murakami, N., Naruse, K., Okada, T., Morita, H., Sawada, K., Miyazaki, J., Kurashige, T., Nonaka, I. (1998) Lysosomal glycogen storage disease with normal acid maltase with early fatal outcome. *J Neurol Sci*, 160(2): 175–9.

Mortimore, G. E., Schworer, C. M. (1977) Induction of autophagy by amino-acid deprivation in perfused rat liver. *Nature*, 270(5633): 174–176.

Muench, S. P., Huss, M., Song, C. F., Phillips, C., Wieczorek, H., Trinick, J., Harrison, M. A. (2009) Cryo-electron microscopy of the vacuolar ATPase motor reveals its mechanical and regulatory complexity. *J Mol Biol*, 386(4): 989–99.

Müller, D. N., Klanke, B., Feldt, S., Cordasic, N., Hartner, A., Schmieder, R. E., Luft, F. C., Hilgers, K. F. (2008) (Pro)renin receptor peptide inhibitor "handle-region" peptide does not affect hypertensive nephrosclerosis in Goldblatt rats. *Hypertension*, 51: 676–681.

Munteanu, I., Ackerley, C. A., Mnatzakanian, G. N., Kissel, J. T., Minassian, B. A. (2005) Electrophysiology extends the phenotypic spectrum of X-linked myopathy with excessive autophagy. *Neurology*, 64(5): 927–8.

Munteanu, I., Ramachandran, N., Ruggieri, A., Awaya, T., Nishino, I., Minassian, B. A. (2015) Congenital autophagic vacuolar myopathy is allelic to X-linked myopathy with excessive autophagy. *Neurology*, 84(16): 1714–6.

Munteanu, I., Kalimo, H., Saraste, A., Nishino, I., Minassian, B. A. (2017) Cardiac autophagic vacuolation in severe X-linked myopathy with excessive autophagy. *Neuromuscul Disord*, 27(2): 185–187.

Nabi, A. H. M. N., Kageshima, A., Uddin, M. N., Nakagawa, T., Park, E. Y., Suzuki, F. (2006) Binding properties of rat prorenin and renin to the recombinant rat renin/prorenin receptor prepared by a baculovirus expression system. *Int J Mol Med*, 18: 483–488.

Nakagawa, T., Suzuki-Nakagawa, C., Watanabe, A., Asami, E., Matsumoto, M., Nakano, M., Ebihara, A., Uddin, M. N., Suzuki, F. (2017) Site-1 protease is required for the generation of

soluble (pro)renin receptor. *J Biochem*, 161(4): 369–379.

Nakamori, D., Akamine, H., Takayama, K., Sakurai, F., Mizuguchi, H. (2017) Direct conversion of human fibroblasts into hepatocyte-like cells by ATF5, PROX1, FOXA2, FOXA3, and HNF4A transduction. *Sci Rep*, 7(1): 16675.

Nakamura, I., Takahashi, N., Udagawa, N., Moriyama, Y., Kurokawa, T., Jimi, E., Sasaki, T., Suda, T. (1997) Lack of vacuolar proton ATPase association with the cytoskeleton in osteoclasts of osteosclerotic (oc/oc) mice. *FEBS Lett*, 401(2-3): 207–12.

Nakatogawa, H., Suzuki, K., Kamada, Y., Ohsumi, Y. (2009) Dynamics and diversity in autophagy mechanisms: lessons from yeast. *Nat Rev Mol Cell Biol*, 10: 458–467.

Nascimbeni, F., Pellegrini, E., Lugari, S., Mondelli, A., Bursi, S., Onfiani, G., Carubbi, F., Lonardo, A. (2019) Statins and nonalcoholic fatty liver disease in the era of precision medicine: More friends than foes. *Atherosclerosis*, 284: 66–74.

Nelson, N. (2003) A journey from mammals to yeast with vacuolar H^+-ATPase (V-ATPase). *J Bioenerg Biomembr*, 35(4): 281–9.

Nelson, N., Harvey, W. R. (1999) Vacuolar and plasma membrane proton-adenosinetriphosphatases. *Physiol Rev*, 79(2): 361–85.

Nguyen, G., Blanchard, A., Curis, E., Bergerot, D., Chambon, Y., Hirose, T., Caumont-Prim, A., Tabard, S. B., Baron, S., Frank, M., Totsune, K., Azizi, M. (2014) Plasma soluble (pro)renin receptor is independent of plasma renin, prorenin, and aldosterone concentrations but is affected by ethnicity. *Hypertension*, 63(2): 297–302.

Nguyen, G., Delarue, F., Burcklé, C. A., Bouzhir, L., Giller, T., Sraer, J. D. (2002) Pivotal role of the renin/prorenin receptor in angiotensin II production and cellular responses to renin. *J Clin Invest*, 109(11): 1417–27.

Nguyen, G., Jan Danser, A. H. (2006) The (pro)renin receptor: therapeutic consequences. *Expert Opinion on Investigational Drugs*, 15: 1131–1135.

Niehrs, C. (2012) The complex world of WNT receptor signalling. *Nat Rev Mol Cell Biol*, 13(12): 767–79.

Nishi, T., Forgac, M. (2002) The vacuolar (H+)-ATPases: nature's most versatile proton pumps. *Nat Rev Mol Cell Biol*, 3(2): 94–103.

Nishino, I. (2006). Autophagic vacuolar myopathy. *Semin Pediatr Neurol*, 13(2): 90–5.

Nuckels, R. J., Ng, A., Darland, T., Gross, J. M. (2009) The vacuolar-ATPase complex regulates retinoblast proliferation and survival, photoreceptor morphogenesis, and pigmentation in the zebrafish eye. *Invest Ophthalmol Vis Sci*, 50(2): 893–905.

O'Callaghan, K. M., Ayllon, V., O'Keeffe, J., Wang, Y., Cox, O. T., Loughran, G., Forgac, M., O'Connor, R. (2010) Heme-binding protein HRG-1 is induced by insulin-like growth factor I and associates with the vacuolar H^+-ATPase to control endosomal pH and receptor trafficking. *J Biol Chem*, 285(1): 381–91.

Ohya, Y., Miyamoto, S., Ohsumi, Y., Anraku, Y. (1986a) Calcium-sensitive cls4 mutant of Saccharomyces cerevisiae with a defect in bud formation. *J Bacteriol*, 165(1): 28–33.

Ohya, Y., Ohsumi, Y., Anraku, Y. (1986b) Isolation and characterization of Ca^{2+}-sensitive mutants of Saccharomyces cerevisiae. *J Gen Microbiol*, 132(4): 979–88.

Ohya, Y., Umemoto, N., Tanida, I., Ohta, A., Iida, H., Anraku, Y. (1991) Calcium-sensitive cls mutants of Saccharomyces cerevisiae showing a Pet- phenotype are ascribable to defects of vacuolar membrane H(+)-ATPase activity. *J Biol Chem*, 266(21): 13971–7.

Oot, R. A., Couoh-Cardel, S., Sharma, S., Stam, N. J., Wilkens, S. (2017) Breaking up and making up: The secret life of the vacuolar H^+-ATPase. *Protein Sci*, 26(5): 896–909.

Opat, A. S., Houghton, F., Gleeson, P. A. (2001a) Steady-state localization of a medial-Golgi glycosyltransferase involves transit through the trans-Golgi network. *Biochem J*, 358(Pt 1): 33–40.

Opat, A. S., van Vliet, C., Gleeson, P. A. (2001b) Trafficking and localisation of resident Golgi glycosylation enzymes. *Biochimie*, 83(8): 763–73.

Oshima, Y., Kinouchi, K., Ichihara, A., Sakoda, M., Kurauchi-Mito, A., Bokuda, K., Narita, T., Kurosawa, H., Sun-Wada, G. H., Wada, Y., Yamada, T., Takemoto, M., Saleem, M. A., Quaggin, S. E., Itoh, H. (2011) Prorenin receptor is essential for normal podocyte structure and function. *J Am Soc Nephrol*, 22(12): 2203–12.

Palokangas, H., Ying, M., Väänänen, K., Saraste, J. (1998) Retrograde transport from the pre-Golgi intermediate compartment and the Golgi complex is affected by the vacuolar H^+-ATPase inhibitor bafilomycin A1. *Mol Biol Cell*, 9(12): 3561–78.

Pamarthy, S., Kulshrestha, A., Katara, G. K., Beaman, K. D. (2018) The curious case of vacuolar ATPase: regulation of signaling pathways. *Mol Cancer*, 17(1): 41.

Paroutis, P., Touret, N., Grinstein, S. (2004) The pH of the secretory pathway: measurement, determinants, and regulation. *Physiology (Bethesda)*, 19: 207–15.

Parra, K. J., Kane, P. M. (1998) Reversible association between the V1 and V0 domains of yeast vacuolar H^+-ATPase is an unconventional glucose-induced effect. *Mol Cell Biol*, 18(12): 7064–74.

Pattingre, S., Tassa, A., Qu, X., Garuti, R., Liang, X. H., Mizushima, N., Packer, M., Schneider, M. D., Levine, B. (2005) Bcl-2 antiapoptotic proteins inhibit Beclin 1-dependent autophagy. *Cell*, 122(6): 927–39.

Pellicano, F., Inglis-Broadgate, S. L., Pante, G., Ansorge, W., Iwata, T. (2006) Expression of coiled-coil protein 1, a novel gene downstream of FGF2, in the developing brain. *Gene Expr Patterns*, 6(3): 285–93.

Pellicano, F., Thomson, R. E., Inman, G. J., Iwata, T. (2010) Regulation of cell proliferation and apoptosis in neuroblastoma cells by ccp1, a FGF2 downstream gene. *BMC Cancer*, 10: 657.

Peri, F., Nüsslein-Volhard, C. (2008) Live imaging of neuronal degradation by microglia reveals a role for v0-ATPase a1 in phagosomal fusion in vivo. *Cell* 133(5): 916–27.

Peters, J. (2017) The (pro)renin receptor and its interaction partners. *Pflugers Arch*, 469(10): 1245–1256.

Petrová, P., Koca, J., Imberty, A. (2001) Molecular dynamics simulations of solvated UDP-glucose in interaction with Mg^{2+} cations. *Eur J Biochem*, 268(20): 5365–74.

Pfeffer, S. R. (2007) Unsolved mysteries in membrane traffic. *Annu Rev Biochem*, 76: 629–45.

Poëa-Guyon, S., Ammar, M. R., Erard, M., Amar, M., Moreau, A. W., Fossier, P., Gleize, V., Vitale, N., Morel, N. (2013) The V-ATPase membrane domain is a sensor of granular pH that controls the exocytotic machinery. *J Cell Biol*, 203(2): 283–98.

Puglisi, A., Yagci, Y. (2019) Cyclodextrin-Based Macromolecular Systems as Cholesterol-Mopping Therapeutic Agents in Niemann-Pick Disease Type C. *Macromol Rapid Commun*, 40(1): e1800557.

Qin, A., Cheng, T. S., Pavlos, N. J., Lin, Z., Dai, K. R., Zheng, M. H. (2012) V-ATPases in osteoclasts: structure, function and potential inhibitors of bone resorption. *Int J Biochem Cell Biol*, 44(9): 1422–35.

Rabinowitz, J. D., White, E. (2010) Autophagy and metabolism. *Science*, 330(6009): 1344–8.

Rama, S., Boumedine-Guignon, N., Sangiardi, M., Youssouf, F., Maulet, Y., Lévêque, C., Belghazi, M., Seagar, M., Debanne, D., El Far, O. (2018) Chromophore-Assisted Light Inactivation of the V-ATPase V0c Subunit Inhibits Neurotransmitter Release Downstream of Synaptic Vesicle Acidification. *Mol Neurobiol*, 2018 Aug 28.

Ramachandran, N., Munteanu, I., Wang, P., Ruggieri, A., Rilstone, J. J., Israelian, N., Naranian, T., Paroutis, P., Guo, R., Ren, Z. P., Nishino, I., Chabrol, B., Pellissier, J. F., Minetti, C., Udd, B., Fardeau, M., Tailor, C. S., Mahuran, D. J., Kissel, J. T., Kalimo, H., Levy, N., Manolson, M. F., Ackerley, C. A., Minassian, B. A. (2013) VMA21 deficiency prevents vacuolar ATPase assembly and causes autophagic vacuolar myopathy. *Acta Neuropathol*, 125(3): 439–57.

Ramser, J., Abidi, F. E., Burcklé, C. A., Lenski, C., Toriello, H., Wen, G., Lubs, H. A., Engert, S., Stevenson, R. E., Meindl, A., Schwartz, C. E., Nguyen, G. (2005) A unique exonic splice enhancer mutation in a family with X-linked mental retardation and epilepsy points to a novel role of the renin receptor. *Hum Mol Genet*, 14: 1019–27.

Recchi, C., Chavrier, P. (2006) V-ATPase: a potential pH sensor. *Nat Cell Biol*, 8(2): 107–9.

Riediger, F., Quack, I., Qadri, F., Hartleben, B., Park, J. K., Potthoff, S. A., Sohn, D., Sihn, G., Rousselle, A., Fokuhl, V., Maschke, U., Purfürst, B., Schneider, W., Rump, L. C., Luft. F. C., Dechend, R., Bader, M., Huber, T. B., Nguyen, G., Muller, D. N. (2011) Prorenin receptor is essential for podocyte autophagy and survival. *J Am Soc Nephrol*, 22(12): 2193–202.

Rivinoja, A. (2009a) Golgi pH and glycosylation. *Acta Universitatis Ouluensis. A scientiae rerum naturalium*. University of Oulu, 2009.

Rivinoja, A., Hassinen, A., Kokkonen, N., Kauppila, A., Kellokumpu, S. (2009b) Elevated Golgi pH impairs terminal N-glycosylation by inducing mislocalization of Golgi glycosyltransferases. *J Cell Physiol*, 220(1): 144–54.

Roh, S. H., Stam, N. J., Hryc, C. F., Couoh-Cardel, S., Pintilie, G., Chiu, W., Wilkens, S. (2018) The 3.5-Å CryoEM Structure of Nanodisc-Reconstituted Yeast Vacuolar ATPase V_0 Proton Channel. *Mol Cell*, 69(6): 993–1004.

Rousselle, A., Sihn, G., Rotteveel, M., Bader, M. (2014) (Pro)renin receptor and V-ATPase: from Drosophila to humans. *Clin Sci (Lond)*, 126(8): 529–36.

Ruggieri, A., Ramachandran, N., Wang, P., Haan, E., Kneebone, C., Manavis, J., Morandi, L., Moroni, I., Blumbergs, P., Mora, M., Minassian, B. A. (2015) Non-coding VMA21 deletions cause X-linked myopathy with excessive autophagy. *Neuromuscul Disord*, 25(3): 207–11.

Ryan, M., Graham, L. A., Stevens, T. H. (2008) Voa1p functions in V-ATPase assembly in the yeast endoplasmic reticulum. *Mol Biol Cell*, 19(12): 5131–42.

Saftig, P., Beertsen, W., Eskelinen, E. L. (2008) LAMP-2. *Autophagy*, 4: 510–512.

Sakoda, M., Ichihara, A., Kurauchi-Mito, A., Narita, T., Kinouchi, K., Murohashi-Bokuda, K., Saleem, M. A., Nishiyama, A., Suzuki, F., Itoh, H. (2010) Aliskiren inhibits intracellular angiotensin II levels without affecting (pro)renin receptor signals in human podocytes. *Am J Hypertens*, 23(5): 575–80.

Salzet, M., Deloffre, L., Breton, C., Vieau, D., Schoofs, L. (2001) The angiotensin system elements in invertebrates. *Brain Res Brain Res Rev*, 36(1): 35–45.

Saraste, A., Koskenvuo, J. W., Airaksinen, J., Ramachandran, N., Munteanu, I., Udd, B., Huovinen, S., Kalimo, H., Minassian, B. A. (2015) No cardiomyopathy in X-linked myopathy with excessive autophagy. *Neuromuscul Disord*, 25(6): 485–7.

Saraste, A., Villard, L., des Portes, V., Levy, N., Louboutin, J. P., Recan, D., Coquet, M., Chabrol, B., Figarella-Branger, D., Chelly, J., Pellissier, J. F., Fontes, M. (2000) Linkage of X-linked myopathy with excessive autophagy (XMEA) to Xq28. *Eur J Hum Genet*, 8(2): 125–9.

Saris, J. J., 't Hoen, P. A., Garrelds, I. M., Dekkers, D. H., den Dunnen, J. T., Lamers, J. M., Jan Danser, A. H. (2006) Prorenin induces intracellular signaling in cardiomyocytes independently of angiotensin II. *Hypertension*, 48: 564–71.

Satofuka, S., Ichihara, A., Nagai, N., Koto, T., Shinoda, H., Noda, K., Ozawa, Y., Inoue, M., Tsubota, K., Itoh, H., Oike, Y., Ishida, S. (2007) Role of nonproteolytically activated prorenin in pathologic, but not physiologic, retinal neovascularization. *Invest Ophthalmol Vis Sci*, 48: 422–429.

Satofuka, S., Ichihara, A., Nagai, N., Tsubota, K., Itoh, H., Ishida, S. (2008) Pathologic roles of prorenin and (pro)renin receptor in the eye. *Front Biosci*, 13: 3884–95.

Satofuka, S., Ichihara, A., Nagai, N., Yamashiro, K., Koto, T., Shinoda, H., Noda, K., Ozawa, Y., Inoue, M., Tsubota, K., Suzuki, F., Oike, Y., Ishida, S. (2006) Suppression

of ocular inflammation in endotoxin-induced uveitis by inhibiting nonproteolytic activation of prorenin. *Invest Ophthalmol Vis Sci* , 47: 2686–2692.

Sautin, Y. Y., Lu, M., Gaugler, A., Zhang, L., Gluck, S. L. (2005) Phosphatidylinositol 3-kinase-mediated effects of glucose on vacuolar H^+-ATPase assembly, translocation, and acidification of intracellular compartments in renal epithelial cells. *Mol Cell Biol*, 25(2): 575–89.

Saviranta, P., Lindlof, M., Lehesjoki, A. E. Kalimo H, Lang H, Sonninen V, Savontaus ML, de la Chapelle A. (1988) Linkage studies in a new X-linked myopathy, suggesting exclusion of DMD locus and tentative assignment to distal Xq. *Am J Hum Genet*, 42(1): 84–88.

Schapiro, F. B., Grinstein, S. (2000) Determinants of the pH of the Golgi complex. *J Biol Chem*, 275(28): 21025–32.

Schoonderwoert, V. T., Jansen, E. J., Martens, G. J. (2002) The fate of newly synthesized V-ATPase accessory subunit Ac45 in the secretory pathway. *Eur J Biochem*, 269(7): 1844–53.

Schoonderwoert, V. T., Martens, G. J. (2002) Targeted disruption of the mouse gene encoding the V-ATPase accessory subunit Ac45. *Mol Membr Biol*, 19(1): 67–71.

Schefe, J. H., Menk, M., Reinemund, J., Effertz, K., Hobbs, R. M., Pandolfi, P. P., Ruiz, P., Unger, T., Funke-Kaiser, H. (2006) A novel signal transduction cascade involving direct physical interaction of the renin/prorenin receptor with the transcription factor promyelocytic zinc finger protein. *Circ Res*, 99: 1355–66.

Schefe, J. H., Neumann, C., Goebel, M., Danser, J., Kirsch, S., Gust, R., Kintscher, U., Unger, T., Funke-Kaiser, H. (2008a) Prorenin engages the (pro)renin receptor like renin and both ligand activities are unopposed by aliskiren. *J Hypertens*, 26(9): 1787–94.

Schefe, J. H., Unger, T., Funke-Kaiser, H. (2008b) PLZF and the (pro)renin receptor. *J Mol Med (Berl)*, 86(6): 623–7.

Schwarten, M., Mohrlüder, J., Ma, P., Stoldt, M., Thielmann, Y., Stangler, T., Hersch, N., Hoffmann, B., Merkel, R., Willbold, D. (2009) Nix directly binds to GABARAP: a possible crosstalk between apoptosis and autophagy. *Autophagy*, 5(5): 690–8.

Semenza, G. L. (2010) HIF-1: upstream and downstream of cancer metabolism. *Curr Opin Genet Dev*, 20(1): 51–6.

Settembre, C., Ballabio, A. (2014) Lysosome: regulator of lipid degradation pathways. *Trends Cell Biol*, 24(12): 743–50.

Settembre, C., Di Malta, C., Polito, V. A., Garcia Arencibia, M., Vetrini, F., Erdin, S., Erdin, S. U., Huynh, T., Medina, D., Colella, P., Sardiello, M., Rubinsztein, D. C., Ballabio, A. (2011) TFEB links autophagy to lysosomal biogenesis. *Science*, 332(6036): 1429–33.

Settembre, C., Fraldi, A., Medina, D. L., Ballabio, A. (2013) Signals from the lysosome: a control centre for cellular clearance and energy metabolism. *Nat Rev Mol Cell Biol*, 14(5): 283–96.

Settembre, C., Zoncu, R., Medina, D. L., Vetrini, F., Erdin, S., Erdin, S., Huynh, T., Ferron, M., Karsenty, G., Vellard, M. C., Facchinetti, V., Sabatini, D. M., Ballabio, A. (2012) A lysosome-to-nucleus signalling mechanism senses and regulates the lysosome via mTOR and TFEB. *EMBO J*, 31(5): 1095–108.

Shibayama, Y., Fujimori, T., Nguyen, G., Hirose, T., Totsune, K., Ichihara, A., Kitada, K., Nakano, D., Kobori, H., Kohno, M., Masaki, T., Suzuki, Y., Yachida, S., Nishiyama, A. (2015) (Pro)renin receptor is crucial for Wnt/β-catenin-dependent genesis of pancreatic ductal adenocarcinoma. *Sci Rep*, 5: 8854.

Shimobayashi, M., Hall, M. N. (2014) Making new contacts: the mTOR network in metabolism and signalling crosstalk. *Nat Rev Mol Cell Biol*, 15(3): 155–62.

Shum, W. W. C., Ruan, Y. C., Da Silva, N., Breton, S. (2011) Establishment of cell-cell cross talk in the epididymis: control of luminal acidification. *J. Androl*, 32, 576–586.

Sihn, G., Burckle, C., Rousselle, A., Reimer, T., Bader, M. (2013) (Pro)renin receptor:

subcellular localizations and functions. *Front Biosci*, 5: 500–508.

Simonsen, A., Tooze, S. A. (2009) Coordination of membrane events during autophagy by multiple class III PI3–kinase complexes. *J Cell Biol*, 186: 773–782.

Singh, R., Kaushik, S., Wang, Y., Xiang, Y., Novak, I., Komatsu, M., Tanaka, K., Cuervo, A. M., Czaja, M. J. (2009) Autophagy regulates lipid metabolism. *Nature*, 458(7242): 1131–5.

Smardon, A. M., Diab, H. I., Tarsio, M., Diakov, T. T., Nasab, N. D., West, R. W., Kane, P. M. (2014) The RAVE complex is an isoform-specific V-ATPase assembly factor in yeast. *Mol Biol Cell*, 25(3): 356–67.

Smardon, A. M., Tarsio, M., Kane, P. M. (2002) The RAVE complex is essential for stable assembly of the yeast V-ATPase. *J Biol Chem*, 277(16): 13831–9.

Smith, A. N., Lovering, R. C., Futai, M., Takeda, J., Brown, D., Karet, F. E. (2003) Revised nomenclature for mammalian vacuolar-type H^+-ATPase subunit genes. *Mol Cell*, 12(4): 801–3.

Smith, A. N., Skaug, J., Choate, K. A., Nayir, A., Bakkaloglu, A., Ozen, S., Hulton, S. A., Sanjad, S. A., Al-Sabban, E. A., Lifton, R. P., Scherer, S. W., Karet, F. E. (2000) Mutations in ATP6N1B, encoding a new kidney vacuolar proton pump 116-kD subunit, cause recessive distal renal tubular acidosis with preserved hearing. *Nat Genet*, 26(1): 71–5.

Steinberg, B. E., Huynh, K. K., Brodovitch, A., Jabs, S., Stauber, T., Jentsch, T. J., Grinstein, S. (2010) A cation counterflux supports lysosomal acidification. *J Cell Biol* 189(7): 1171–86.

Stevens, T. H., Forgac, M. (1997) Structure, function and regulation of the vacuolar ATPase. *Annu Rev Cell Dev Biol*, 13, 779–808.

Stover, E. H., Borthwick, K. J., Bavalia, C., Eady, N., Fritz, D. M., Rungroj, N., Giersch, A. B., Morton, C. C., Axon, P. R., Akil, I., Al-Sabban, E. A., Baguley, D. M., Bianca, S., Bakkaloglu, A., Bircan, Z., Chauveau, D., Clermont, M. J., Guala, A., Hulton, S. A., Kroes, H., Li Volti, G., Mir, S., Mocan, H., Nayir, A., Ozen, S., Rodriguez Soriano, J., Sanjad, S. A., Tasic, V., Taylor, C. M., Topaloglu, R., Smith, A. N., Karet, F. E. (2002) Novel ATP6V1B1 and ATP6V0A4 mutations in autosomal recessive distal renal tubular acidosis with new evidence for hearing loss. *J Med Genet*, 39(11): 796–803.

Stransky, L. A., Forgac, M. (2015) Amino Acid Availability Modulates Vacuolar H^+-ATPase Assembly. *J Biol Chem*, 290(45): 27360–9.

Strasser, B., Iwaszkiewicz, J., Michielin, O., Mayer, A. (2011) The V-ATPase proteolipid cylinder promotes the lipid-mixing stage of SNARE-dependent fusion of yeast vacuoles. *EMBO J*, 30(20): 4126–41.

Su, A. I., Wiltshire, T., Batalov, S., Lapp, H., Ching, K. A., Block, D., Zhang, J., Soden, R., Hayakawa, M., Kreiman, G., Cooke, M. P., Walker, J. R., Hogenesch, J. B. (2004) A gene atlas of the mouse and human protein-encoding transcriptomes. *Proc Natl Acad Sci USA*, 101 (16): 6062–6067.

Sumner, J. P., Dow, J. A., Earley, F. G., Klein, U., Jäger, D., Wieczorek, H. (1995) Regulation of plasma membrane V-ATPase activity by dissociation of peripheral subunits. *J Biol Chem*, 270(10): 5649–53.

Sun-Wada, G. H., Wada, Y. (2013) Vacuolar-type proton pump ATPases: acidification and pathological relationships. *Histol Histopathol*, 28: 805–815.

Sun-Wada, G. H., Toyomura, T., Murata, Y., Yamamoto, A., Futai, M., Wada, Y. (2006) The a3 isoform of V-ATPase regulates insulin secretion from pancreatic beta-cells. *J Cell Sci*, 119(Pt 21): 4531–40.

Supek, F., Supekova, L., Mandiyan, S., Pan, Y. C., Nelson, H., Nelson, N. (1994) A novel accessory subunit for vacuolar H(+)-ATPase from chromaffin granules. *J Biol Chem*, 269(39): 24102–6.

Suzuki, F., Hayakawa, M., Nakagawa, T., Nasir, U. M., Ebihara, A., Iwasawa, A., Ishida,

Y., Nakamura, Y., Murakami, K. (2003) Human prorenin has "gate and handle" regions for its non-proteolytic activation. *J Biol Chem*, 278(25): 22217–22.

Suzuki-Nakagawa, C., Nishimura, M., Noda, M., Iwata, H., Hattori, M., Ebihara, A., Suzuki, F., Nakagawa, T. (2014a) Intracellular retention of the extracellular domain of the (pro)renin receptor in mammalian cells. *Biosci Biotechnol Biochem*, 78(7): 1187–90.

Suzuki-Nakagawa, C., Nishimura, M., Tsukamoto, T., Aoyama, S., Ebihara, A., Suzuki, F., Nakagawa, T. (2014b) Participation of the extracellular domain in (pro)renin receptor dimerization. *Biochem Biophys Res Commun*, 444(4): 461–6.

Takahashi, Y., Coppola, D., Matsushita, N., Cualing, H. D., Sun, M., Sato, Y., Liang, C., Jung, J. U., Cheng, J. Q., Mulé, J. J., Pledger, W. J., Wang, H. G. (2007) Bif-1 interacts with Beclin 1 through UVRAG and regulates autophagy and tumorigenesis. *Nat Cell Biol*, 9(10): 1142–51.

Takahashi, K., Ohba, K., Tajima, K., Nishijima, T., Sakurai, S. (2017) Soluble (Pro)renin Receptor and Obstructive Sleep Apnea Syndrome: Oxidative Stress in Brain? *Int J Mol Sci*, 18(6). pii: E1313.

Takahashi, K., Yamamoto, H., Hirose, T., Hiraishi, K., Shoji, I., Shibasaki, A., Kato, I., Kaneko, K., Sasano, H., Satoh, F., Totsune, K. (2010) Expression of (pro)renin receptor in human kidneys with end-stage kidney disease due to diabetic nephropathy. *Peptides*, 31(7): 1405–8.

Tanaka, Y., Guhde, G., Suter, A., Eskelinen, E. L., Hartmann, D., Lüllmann-Rauch, R., Janssen, P. M., Blanz, J., von Figura, K., Saftig, P. (2000) Accumulation of autophagic vacuoles and cardiomyopathy in LAMP-2-deficient mice. *Nature*, 406(6798): 902–6.

Teichgräber, V., Ulrich, M., Endlich, N., Riethmüller, J., Wilker, B., De Oliveira-Munding, C. C., van Heeckeren, A. M., Barr, M. L., von Kürthy, G., Schmid, K. W., Weller, M., Tümmler, B., Lang, F., Grassme, H., Döring, G., Gulbins, E. (2008) Ceramide accumulation mediates inflammation, cell death and infection susceptibility in cystic fibrosis. *Nat Med*, 14(4): 382–91.

Thompson, R. J., Akana, H. C., Finnigan, C., Howell, K. E., Caldwell, J. H. (2006) Anion channels transport ATP into the Golgi lumen. *Am J Physiol Cell Physiol*, 290(2): C499–514.

Thorens, B., Vassalli, P. (1986) Chloroquine and ammonium chloride prevent terminal glycosylation of immunoglobulins in plasma cells without affecting secretion. *Nature*, 321(6070): 618–20.

Toei, M., Saum, R., Forgac, M. (2010) Regulation and isoform function of the V-ATPases. *Biochemistry*, 49(23): 4715–23.

Toyomura, T., Murata, Y., Yamamoto, A., Oka, T., Sun-Wada, G. H., Wada, Y., Futai, M. (2003) From lysosomes to the plasma membrane: localization of vacuolar-type H^+-ATPase with the a3 isoform during osteoclast differentiation. *J Biol Chem*, 278(24): 22023–30.

Trombetta, E. S., Parodi, A. J. (2003) Quality control and protein folding in the secretory pathway. *Annu Rev Cell Dev Biol*, 19: 649–676.

Ueno, T., Komatsu, M. (2017) Autophagy in the liver: functions in health and disease. *Nat Rev Gastroenterol Hepatol*, 14(3): 170–184.

Vajro, P., Zielinska, K., Ng, B. G., Maccarana, M., Bengtson, P., Poeta, M., Mandato, C., D'Acunto, E., Freeze, H. H., Eklund, E. A. (2018) Three unreported cases of TMEM199-CDG, a rare genetic liver disease with abnormal glycosylation. *Orphanet J Rare Dis*, 13(1): 4.

Vance, J. E., Karten, B. (2014) Niemann-Pick C disease and mobilization of lysosomal cholesterol by cyclodextrin. *J Lipid Res*, 55(8): 1609–21.

Van Damme, T., Gardeitchik, T., Mohamed, M., Guerrero-Castillo, S., Freisinger, P., Guillemyn, B., Kariminejad, A., Dalloyaux, D., van Kraaij, S., Lefeber, D. J., Syx, D., Steyaert, W., De Rycke, R., Hoischen, A., Kamsteeg, E. J., Wong, S. Y., van Scherpenzeel, M., Jamali, P., Brandt, U., Nijtmans, L., Korenke, G. C., Chung, B. H. Y., Mak, C. C.

Y., Hausser, I., Kornak, U., Fischer-Zirnsak, B., Strom, T. M., Meitinger, T., Alanay, Y., Utine, G. E., Leung, P. K. C., Ghaderi-Sohi, S., Coucke, P., Symoens, S., De Paepe, A., Thiel, C., Haack, T. B., Malfait, F., Morava, E., Callewaert, B., Wevers, R. A. (2017) Mutations in ATP6V1E1 or ATP6V1A Cause Autosomal-Recessive Cutis Laxa. *Am J Hum Genet*, 100(2): 216–227.

Vargas-Poussou, R., Houillier, P., Le Pottier, N., Strompf, L., Loirat, C., Baudouin, V., Macher, M. A., Déchaux, M., Ulinski, T., Nobili, F., Eckart, P., Novo, R., Cailliez, M., Salomon, R., Nivet, H., Cochat, P., Tack, I., Fargeot, A., Bouissou, F., Kesler, G. R., Lorotte, S., Godefroid, N., Layet, V., Morin, G., Jeunemaître, X., Blanchard, A. (2006) Genetic investigation of autosomal recessive distal renal tubular acidosis: evidence for early sensorineural hearing loss associated with mutations in the ATP6V0A4 gene. *J Am Soc Nephrol*, 17(5):1437–43.

Villanova, M., Louboutin, J. P., Chateau, D., Eymard, B., Sagniez, M., Tomé, F. M., Fardeau, M. (1995) X-linked vacuolated myopathy: complement membrane attack complex on surface membrane of injured muscle fibers. *Ann Neurol*, 37(5): 637–45.

Villard, L., des Portes, V., Levy, N., Louboutin, J. P., Recan, D., Coquet, M., Chabrol, B., Figarella-Branger, D., Chelly, J., Pellissier, J. F., Fontes, M. (2000) Linkage of X-linked myopathy with excessive autophagy (XMEA) to Xq28. *Eur J Hum Genet*, 8(2): 125–9.

Vinson, C. R., Adler, P. N. (1987) Directional non-cell autonomy and the transmission of polarity information by the frizzled gene of Drosophila. *Nature*, 329(6139): 549–51.

Vitavska, O., Wieczorek, H., Merzendorfer, H. (2003) A novel role for subunit C in mediating binding of the H^+-V-ATPase to the actin cytoskeleton. *J Biol Chem*, 278(20): 18499–505.

von Schwarzenberg, K., Wiedmann, R. M., Oak, P., Schulz, S., Zischka, H., Wanner, G., Efferth, T., Trauner, D., Vollmar, A. M. (2013) Mode of cell death induction by pharmacological vacuolar H^+-ATPase (V-ATPase) inhibition. *J Biol Chem*, 288(2): 1385–96.

Wang, D., Epstein, D., Khalaf, O., Srinivasan, S., Williamson, W. R., Fayyazuddin, A., Quiocho, F. A., Hiesinger, P. R. (2014) Ca^{2+}-Calmodulin regulates SNARE assembly and spontaneous neurotransmitter release via V-ATPase subunit V0a1. *J Cell Biol*, 205(1): 21–31.

Wang, H., Kesinger, J. W., Zhou Q., Wren, J. D., Martin, G., Turner, S., Tang, Y., Frank, M. B., Centola, M. (2008) Identification and characterization of zebrafish ocular formation genes. *Genome*, 51(3): 222–235.

Wang, L., Chen, J., Ning, C., Lei, D., Ren, J. (2018) Endoplasmic Reticulum Stress Related Molecular Mechanisms in Nonalcoholic Fatty Liver Disease (NAFLD). *Curr Drug Targets*, 19(9): 1087–1094.

Wang, Y., Cipriano, D. J., Forgac, M. (2007) Arrangement of subunits in the proteolipid ring of the V-ATPase. *J Biol Chem*, 282(47): 34058c65.

Wang, Y., Inoue, T., Forgac, M. (2004) TM2 but not TM4 of subunit c" interacts with TM7 of subunit a of the yeast V-ATPase as defined by disulfide-mediated cross-linking. *J Biol Chem*, 279(43): 44628–38.

Watanabe, N., Bokuda, K., Fujiwara, T., Suzuki, T., Mito, A., Morimoto, S., Jwa, S. C., Egawa, M., Arai, Y., Suzuki, F., Sago, H., Ichihara, A. (2012) Soluble (pro)renin receptor and blood pressure during pregnancy: a prospective cohort study. *Hypertension*, 60(5): 1250–6.

Watanabe, N., Morimoto, S., Fujiwara, T., Suzuki, T., Taniguchi, K., Ando, T., Kimura, T., Sago, H., Ichihara, A. (2013a) Association between soluble (Pro)renin receptor concentration in cord blood and small for gestational age birth: a cross-sectional study. *PLoS One*, 8(3): e60036.

Watanabe, N., Morimoto, S., Fujiwara, T., Suzuki, T., Taniguchi, K., Mori, F., Ando, T., Watanabe, D., Kimura, T., Sago, H., Ichihara, A. (2013b) Prediction of gestational diabetes mellitus by soluble (pro)renin receptor during the first trimester. *J Clin Endocrinol Metab*, 98(6): 2528–35.

Webb, J. L., Ravikumar, B., Rubinsztein, D. C. (2004) Microtubule disruption inhibits autophagosome–lysosome fusion: implications for studying the roles of aggresomes in polyglutamine diseases. *Int J Biochem Cell Biol*, 36: 2541–2550.

Wei, Y., Pattingre, S., Sinha, S., Bassik, M., Levine, B. (2008) JNK1-mediated phosphorylation of Bcl-2 regulates starvation-induced autophagy. *Mol Cell*, 30(6): 678–88.

Weinert, S., Jabs, S., Supanchart, C., Schweizer, M., Gimber, N., Richter, M., Rademann, J., Stauber, T., Kornak, U., Jentsch, T. J. (2010) Lysosomal pathology and osteopetrosis upon loss of H^+-driven lysosomal Cl^- accumulation. *Science*, 328(5984): 1401–3.

Weisman, L. S., Bacallao, R., Wickner, W. (1987) Multiple methods of visualizing the yeast vacuole permit evaluation of its morphology and inheritance during the cell cycle. *J Cell Biol*, 105(4): 1539–47.

Weisz, O. A. (2003) Organelle acidification and disease. *Traffic*, 4(2): 57–64.

Welsh, L. M., Tong, A. H., Boone, C., Jensen, O. N., Otte, S. (2006) Genetic and molecular interactions of the Erv41p-Erv46p complex involved in transport between the endoplasmic reticulum and Golgi complex. *J Cell Sci*, 119(Pt 22): 4730–40.

Wendling, O., Champy, M. F., Jaubert, S., Pavlovic. G., Dubos, A., Lindner, L., Jacobs, H., Mark, M., Combe, R., Da Cruz, I. G., Luche, H., Mudgett, J. S., Rosahl, T., Sorg, T., Malissen, M., Reilly, P. T., Hérault, Y. (2017) Atp6ap2 ablation in adult mice impairs viability through multiple organ deficiencies. *Sci Rep*, 7(1): 9618.

Wilkens, S., Vasilyeva, E., Forgac, M. (1999) Structure of the vacuolar ATPase by electron microscopy. *J Biol Chem*, 274(45): 31804–10.

Wilkens, S., Forgac, M. (2001) Three-dimensional structure of the vacuolar ATPase proton channel by electron microscopy. *J Biol Chem*, 276(47): 44064–8.

Wilkinson-Berka, J. L., Heine, R., Tan, G., Cooper, M. E., Hatzopoulos, K. M., Fletcher, E. L., Binger, K. J., Campbell, D. J., Miller, A. G. (2010) RILLKKMPSV influences the vasculature, neurons and glia, and (pro)renin receptor expression in the retina. *Hypertension*, 55(6): 1454–60.

Williamson, W. R., Hiesinger, P. R. (2010) On the role of v-ATPase V0a1-dependent degradation in Alzheimer disease. *Commun Integr Biol*, 3(6): 604–7.

Wilson, D. W., Lewis, M. J., Pelham, H. R. (1993) pH-dependent binding of KDEL to its receptor in vitro. *J Biol Chem*, 268(10): 7465–8.

Wu, M. M., Llopis, J., Adams, S., McCaffery, J. M., Kulomaa, M. S., Machen, T. E., Moore, H. P., Tsien, R. Y. (2000) Organelle pH studies using targeted avidin and fluorescein-biotin. *Chem Biol*, 7(3): 197–209.

Wu, M. M., Grabe, M., Adams, S., Tsien, R. Y., Moore, H. P., Machen, T. E. (2001) Mechanisms of pH regulation in the regulated secretory pathway. *J Biol Chem*, 276(35): 33027–35.

Xie, Z., Klionsky, D. J. (2007) Autophagosome formation: core machinery and adaptations. *Nat Cell Biol*, 9(10): 1102–1109.

Xu, T., Forgac, M. (2001) Microtubules are involved in glucose-dependent dissociation of the yeast vacuolar [H+]-ATPase in vivo. *J Biol Chem*, 276(27): 24855–61.

Yamamoto, H., Komekado, H., Kikuchi, A. (2006) Caveolin is necessary for Wnt-3a-dependent internalization of LRP6 and accumulation of beta-catenin. *Dev Cell*, 11(2): 213–23.

Yamashiro, C. T., Kane, P. M., Wolczyk, D. F., Preston, R. A., Stevens, T. H. (1990) Role of vacuolar acidification in protein sorting and zymogen activation: a genetic analysis of the yeast vacuolar proton translocating ATPase. *Mol Cell Biol*, 10(7): 3737–3749.

Yanai, K., Saito, T., Kakinuma, Y., Kon, Y., Hirota, K., Taniguchi–Yanai, K., Nishijo, N., Shigematsu, Y., Horiguchi, H., Kasuya, Y., Sugiyama, F., Yagami, Ki., Murakami, K., Fukamizu, A. (2000) Renin-dependent cardiovascular functions and renin-independent blood-brain bar-

rier functions revealed by renin-deficient mice. *J Biol Chem*, 275: 5–8.

Yang, D. Q., Feng, S., Chen, W., Zhao, H., Paulson, C., Li, Y. P. (2012) V-ATPase subunit ATP6AP1 (Ac45) regulates osteoclast differentiation, extracellular acidification, lysosomal trafficking, and protease exocytosis in osteoclast-mediated bone resorption. *J Bone Miner Res*, 27(8): 1695–707.

Yla-Anttila, P., Vihinen, H., Jokitalo, E., Eskelinen, E. L. (2009) 3D tomography reveals connections between the phagophore and endoplasmic reticulum. *Autophagy*, 5(8): 1180–5.

Yoon, M. S., Choi, C. S. (2016) The role of amino acid-induced mammalian target of rapamycin complex 1(mTORC1) signaling in insulin resistance. *Exp Mol Med*, 48(1): e201.

Yoshikawa, A., Aizaki, Y., Kusano, K., Kishi, F., Susumu, T., Iida, S., Ishiura, S., Nishimura, S., Shichiri, M., Senbonmatsu, T. (2011) The (pro)renin receptor is cleaved by ADAM19 in the Golgi leading to its secretion into extracellular space. *Hypertens Res*, 34(5): 599–605.

Zhang, C. S., Jiang, B., Li, M., Zhu, M., Peng, Y., Zhang, Y. L., Wu, Y. Q., Li, T. Y., Liang, Y., Lu, Z., Lian, G., Liu, Q., Guo, H., Yin, Z., Ye, Z., Han, J., Wu, J. W., Yin, H., Lin, S. Y., Lin, S. C. (2014) The lysosomal v-ATPase-Ragulator complex is a common activator for AMPK and mTORC1, acting as a switch between catabolism and anabolism. *Cell Metab*, 20(3): 526–40.

Zhang, J., Noble, N. A., Border, W. A., Owens, R. T., Huang, Y. (2008) Receptor-dependent prorenin activation and induction of PAI-1 expression in vascular smooth muscle cells. *Am J Physiol Endocrinol Metab*, 295(4): E810–9.

Zhang, X., Zhang, K. (2012) Endoplasmic Reticulum Stress-Associated Lipid Droplet Formation and Type II Diabetes. *Biochem Res Int*, 2012: 247275.

Zhang, Y., Gao, X., Michael Garavito, R. (2011) Structural analysis of the intracellular domain of (pro)renin receptor fused to maltose-binding protein. *Biochem Biophys Res Commun*, 407(4): 674–9.

Zhang, Y., Zeng, X., Jin, S. (2012) Autophagy in adipose tissue biology. *Pharmacol Res*, 66(6): 505–12.

Zhang, Z., Singh, R., Aschner, M. (2016) Methods for the Detection of Autophagy in Mammalian Cells. *Curr Protoc Toxicol*, 69: 20.12.1–20.12.26.

Zhang, Z., Zheng, Y., Mazon, H., Milgrom, E., Kitagawa, N., Kish-Trier, E., Heck, A. J., Kane, P. M., Wilkens, S. (2008) Structure of the yeast vacuolar ATPase. *J Biol Chem*, 283(51): 35983–95.

Zhao, H., Wang, J., Wang, T. (2018) The V-ATPase V1 subunit A1 is required for rhodopsin anterograde trafficking in Drosophila. *Mol Biol Cell*, 29(13): 1640–1651.

Zhong, Y., Wang, Q. J., Li, X., Yan, Y., Backer, J. M., Chait, B. T., Heintz, N., Yue, Z. (2009) Distinct regulation of autophagic activity by Atg14L and Rubicon associated with Beclin 1-phosphatidylinositol-3-kinase complex. *Nat Cell Biol*, 11(4): 468–76.

Zhou, A., Carrell, R. W., Murphy, M.P., Wei, Z., Yan, Y., Stanley, P. L., Stein, P. E., Broughton Pipkin, F., Read, R. J. (2010) A redox switch in angiotensinogen modulates angiotensin release. *Nature*, 468: 108–11.

Zimmerberg, J. (2001) How can proteolipids be central players in membrane fusion? *Trends Cell Biol*, 11(6): 233–5.

Zoncu, R., Bar-Peled, L., Efeyan, A., Wang, S., Sancak, Y., Sabatini, D. M. (2011) mTORC1 senses lysosomal amino acids through an inside-out mechanism that requires the vacuolar H(+)-ATPase. *Science*, 334(6056): 678–83.

Acknowledgments

Acknowledgments

At the end of this amazing chapter of my life, the time has come to acknowledge all the people who have contributed to make special this journey and which allowed me to grow not only from a scientific point of view but also enriched me as person.

First, I would like to thank my mentor Matias Simons. Thank you for accepting me into your laboratory, giving me the opportunity to embark on this extraordinary journey. Thank you for guiding me through these years with passion and method, making me a better scientist. Thank you for all the scientific discussions and for always being there, encouraging me to give more and to do always better. Thank you for your constant patience, especially for the difficulties caused by the language, and for your kindness to me.

Furthermore, I would like to express my utmost appreciation to the reviewers of my thesis, Thomas Braulke and Frank Lafont, for generously sharing with me their time, showing interest for my work and giving me helpful advice. I extend my gratitude to the members of my thesis committee, Arnaud Bruneel, Fabienne Foufelle and Etienne Morel, who have agreed to evaluate my work.

To Maria Rujano, with whom I started working in the ATP6AP2 project and from whom I learned a lot and not only about the *Drosophila* brain. Thank you to encourage always me, also in the dark days, you've been my second mentor and a source of inspiration all these years. Thank you for sharing the musical choices, for all the concerts and the "pub trips" (there is no problem in the world that can not be solved with a beer!).

To Valentina Marchesin, the kindest and most altruistic person known in this lab. Thank you for all the moments of "cut and sew", thank you for the scientific and personal support. But above all, thank you for always being optimistic and for being able to give your serenity to those around you!

To Gwenn Le Meur, the craziest research engineer I've ever met: sharing the office with you during all these years has been both an exciting and shocking experience. Thank you for the singing moments and the cakes, for your patience (especially in the last few months). I promise, one day we will dance all night long!

To Zvoni Marelja, the alpha male of the wild bunch of flies. Thank you to bringing testosterone in the girlZ office, for all your jokes and for teaching me how to be eco-free. Thank you to be the official organizer of all our events!

To the old members of the Simons lab: Virginie Hauser, Hetvi Gandhi, Sara Gonçalves

and Laure Villoing-Gaudé... and to the more recent members of the lab: Albert Pérez Marti, Mathilda Bedin, Luigi De La Motte and Chiara Garsia: all of you touched my heart and enriched my knowledge in a way or another. All of you created a wonderful atmosphere, making work so much fun!!

To all my friends, here in Paris and all around the world. To the "Ajo core" Lina, Mario, Elena and Alessandro (thank you especially for teaching me the "art of LaTeX"): you have made even the most unbearable moments funny! To all the "Italians abroad", thank you for always making me feel like at home.... and to all my "old" friends, despite the distance, you are always present and your love means so much to me!!

To the greatest friend that this Parisian experience could give to me, Arianna, you have changed my way to think. Thank you for all the supportive dinners and for always being there for me, to listen to all my problems and to always encourage me to break out of conventionality. Great adventures and sunny days are waiting for us!

Lastly, to my family, my parents Carlo and Erminia, my brother Francesco and the little Charlotte: without your unconditional love, support and encouragement none of this work would have been possible. You have tolerated and supported me every day, even if you were far away.

To all the people who have walked through my life during these arduous PhD years, each of you has made this journey special.

To all of you, I dedicate my dissertation, with all of my love.